Novel Phospholipid Probes for Exploring Biomembrane Functions and Their Behavior in Model Membranes

(生体膜機能解明のためのリン脂質様プローブ分子の開発とモデル膜系での動態解析)

A dissertation
submitted to the Graduate School of Science
of Osaka University
in partial fulfillment of the requirements
for the degree of
Doctor of Philosophy

Jin Cui

2015

Abstract

Lipid rafts show a similar character to the lipid ordered (L_o) phase in artificial membranes, which are often represented by microdomains enriched with sphingolipids and cholesterol (chol). The physicochemical properties of the specific lipids are believed to be important for fulfilling the rafts' functions such as cellular signal transduction. To gain better insight into the role of lipid rafts in these processes, a direct optical visualization of these domains is essential. The Raman image can be generated by measuring a specific molecular vibration to locate the Raman-tagged molecules. Three Raman probes of sphingomyelin (SM) were synthesized and evaluated for their applicability to imaging experiments. One probe containing a hydroxymethyl-1,3-butadiyne moiety in the polar head group showed strong scattering. The solid-state deuterium nuclear magnetic resonance (^{2}H NMR) spectra of the probe revealed excellent compatibility with natural SM in phase behavior by indicating that the probe undergoes phase separation to form raft-like L_o domains in the raft-mimicking mixed bilayers.

Uncovering the behavior of individual lipids in membranes is necessary for a better understanding of the molecular mechanisms underlying the biomedical functions of lipid rafts. Dioleoylphosphatidylcholine (DOPC) is a typical liquid disordered (L_d) component in raft-model membranes, and has often been used to prepare a ternary mixture with SM and chol that forms L_o/L_d-co-existing bilayers. Although incorporation of unsaturated DOPC into L_d phases is energetically favorable, a small amount of DOPC is always found in L_o phases. However, this phase segregation is difficult to detect using a previously reported DOPC probe ([C11-$^2H_2$] DOPC). [C6-$^2H_2$] DOPC was designed based on molecular dynamics (MD) simulation and synthesized through a highly efficient synthetic route. [C6-$^2H_2$] DOPC shows clear phase separation and characteristic phase behavior at various temperatures. It was successfully utilized for the comparison of membrane properties between SM and dihydrosphingomyelin (DHSM) membranes.

It is of great biological significance to understand how the lipids and proteins interact in membranes. Bacteriorhodopsin (bR) is the only protein in the purple membrane (PM) of *Halobacterium halobium* and exits in trimer form with 6 lipids located within the trimer and 24 lipids surrounding the protein surface. Phosphatidylglycerophosphate methyl ester (PGP-Me) is the major phospholipid in PM. An analogue of PGP-Me with two simple straight side chains was selected to prepare the model membranes to mimic the native cellular environment for the *in situ* study of lipid-protein interactions. A stereoselective synthetic route to the analogue was developed using H-phosphonate chemistry. ^{2}H-labled PGP-Me analogue was synthesized and used as an isotope probe for a mesoscopic investigation of lipid-protein interactions in membranes. Solid-state ^{31}P NMR spectra suggested the formation of multiple phases using the analogue in bilayer preparation on glass plates. ^{2}H NMR spectra provided useful information of lipid-bR interactions in multilamellar dispersions.

Table of Contents

List of Abbreviations

Å	angstrom
Ac	acetyl
AFM	atomic force microscopy
ATRI	alkyne-tag Raman imaging
B_0	magnetic field
BCl_3	boron trichloride
Bn	benzyl
Bodipy	dipyrrometheneboron difluoride
BPG	archaeal cardiolipin
bR	bacteriorhodopsin
CARS	coherent anti-stokes Raman scattering
CHAPS	3-[(3-cholamidopropyl)dimethylammonio]-2-hydroxy- 1-propanesulfonate
chol	cholesterol
CoA	acyl-coenzyme A
CoQ	coenzyme Q
dbR	delipidated bR
DDQ	2,3-dichloro-5,6-dicyano-1,4-benzoquinone
DHSM	dihydrosphingomyelin
DLPC	1,2-Dilauroyl-sn-glycero-3-phosphocholine
DM	dodecyl-β-D- maltoside
DMAP	N,N-dimethylaminopyridine
DMF	N,N-dimethylformamide
DMPC	dimyristoylphosphatidylcholine
DMSO	dimethyl sulfoxide
DOPC	dioleoylphosphatidylcholine
DPPC	1,2-dihexadecanoyl-sn-glycero-3-phosphocholine
DRM	detergent-resistant membrane
DSC	differential scanning calorimetry
DSPC	1,2-distearoyl-sn-glycero-3-phosphocholine
e.e.	enantiomeric excess
E-CARS	epi-detected coherent anti-Stokes Raman scattering
EDCI	ethyl-3-(3-dimethylaminopropyl)carbodiimide hydrochloride
EdU	5-ethynyl-2′-deoxyuridine
eq	equivalent
ESI	electrogen fluoride
ESR	electron-spin resonance
Et	ethyl
G1P	sn-glycerol-1-phosphate
G3P	sn-glycerol-3-phosphate
GDNF	glial-cell-derived neurotrophic factor
GlyC	archaeal glycocardiolipin

GPCR	G-protein coupled receptor
GSL	glycosphingolipid
GUV	giant unilamellar vesicle
HIV	immunodeficiency Virus
HPLC	high performance liquid chromatography
Hz	hertz
i-	iso
IgE	immunoglobulin E
LB	Langmuir–Blodgett
L_d	liquid disordered
L_o	liquid ordered
LPC	lysophosphocholine
L_α	liquid crystalline
MD	molecular dynamics
MDCK	Madin-Darby canine kidney
Me	methyl
MLV	multilamellar vesicle
NBD	7-nitrobenz-2-oxa-1,3-diazole
NMR	nuclear magnetic resonance
p-	para
PA	phosphatidic acid
PC	phosphatidylcholine
PE	phosphatidylethanolamine
PG	phosphatidylglycerol
PGP-Me	phosphatidylglycerophosphate methyl ester
PI	phosphatidylinositol
PM	purple membrane
PMB	p-methoxybenzyl
POPC	palmitoyloleoylphosphatidylcholine
POPE	l-palmitoyl-2-oleoyl-sn-glycero- 3-phosphoethanolm
POPG	l-palmitoyl-2-oleoyl-sn-glycero-3-phosphoglycerol
ppm	parts per million
PS	phosphatidylserine
PSG	phosphatidylglycerol sulfate
PSM	palmitoylsphingomyelin
Pv	pivaloyl
quant	quantitative
rt	room temperature
S_{CD}	order parameter
SM	sphingomyelin
sn	stereochemical numbering
SSM	N-stearoyl sphingomyelin
S-TGA-1	sulfated triglycoside lipid
STM-TERS	STM-tip enhanced Raman spectroscopy

t-	tertiary
TBAF	tetra-n-butylammonium fluoride
TBAI	tertrabutylammonium iodide
TBDPS	*t*-butyldiphenylsilyl
TBS	*t*-butyldimethylsilyl
TF	TopFluor
TFA	trifluoroacetic acid
THF	tetrahydronfuran
TLC	thin layer chromatography
TMEDA	tetramethylethylenediamine
TrCl	tritylchloride
Ts	*p*-toluenesulfonyl
$\Delta\nu_Q$	quadrupole splitting

Chapter 1

Introduction

1.1 Cell Membranes

All prokaryotic or eukaryotic cells are surrounded by a thin (~30 Å) and flexible plasma membrane which protects and organizes cells. The outer plasma membrane in cells controls not only what enters the cell, but also how much of any certain substance comes in. In eukaryotic cells, the internal membranes encase the organelles and regulate the exchange of essential cell components.

1.2 Membrane Lipids

In cell membranes, there are hundreds of lipids which account for about half the mass of cell membranes, into which different proteins are embedded. Lipids can be defined as hydrophobic or amphipathic small molecules that may be generated partly or entirely by carbanion-based condensations of thioesters (fatty acyls, glycerolipids, glycerophospholipids, sphingolipids, saccharolipids, and polyketides) and/or by carbocation-based condensations of isoprene units (prenol lipids and sterol lipids).[1,2)]

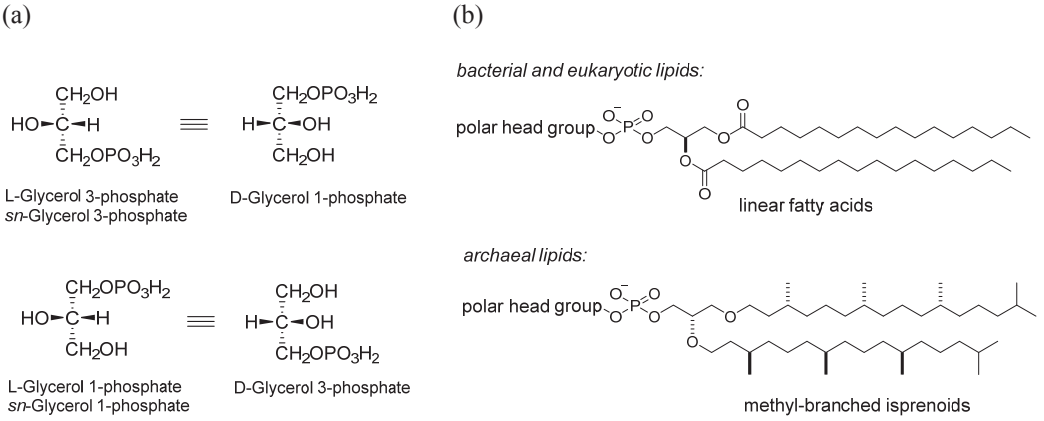

Figure 1-1. (a) Fischer projection of glycerol phosphate and the nomenclature using new stereochemical numbering (*sn*) system. (b) Chemical structure difference between bacterial/eukaryotic lipids and archaeal lipids.

In bacteria and eukaryotes, *sn*-glycerol-3-phosphate (G3P) is bound to fatty acids by ester linkages. (Figure 1-1) In contrast, in archaea, the phospholipid backbone is built on the opposite

glycerol stereoisomer, *sn*-glycerol-1-phosphate (G1P), the side chains (isoprenoid derivatives) are bound to G1P by ether linkages.[3,4] The major structural lipid in bacterial and eukaryotic membranes is glycerophospholipid composed of glycerol backbone, a polar hydrophilic phosphate group, and two hydrophobic fatty acid chains. Its family contains phosphatidylcholine (PC), phosphatidylethanolamine (PE), phosphatidylserine (PS), phosphatidylinositol (PI), and phosphatidic acid (PA). In most eukaryotic membrane, PC accounts for more than half of the phospholipids.[5] The sphingolipids are another important class of structural lipids. They have been isolated for the first time from brain tissue in the late 1880s by Johann L.W. Thudichum.[6] In sphingolipids, the sphingoid base backbone is synthesized *de novo* from serine and a long chain fatty acyl-coenzyme A (CoA), then converted into ceramides, phosphosphingolipids, glycosphingolipids (GSLs), and other derivatives.[7,8] Sphingomyelin (SM) is the most abundant sphingolipid in eukaryotic cells. It is composed of a phosphocholine head group, a sphingosine, and a fatty acid.[9] The acyl side chains in natural SMs are usually highly saturated and differ in length from 16:0 to 24:1. In mammalian tissues, SMs account for 2–15% of the total organ phospholipids.[9] They are found at particularly high concentrations in certain tissues such as brain, peripheral nervous tissue, and ocular lenses.[9,10] Dihydrosphingomyelin (DHSM) is the major phospholipid of human lens membranes. Cholesterol (chol) is another one of the most basic lipids in mammalian cell membranes. It interacts with sphingolipids to form particular phases said to be responsible for a variety of biological processes. The hydroxy group on chol interacts with the polar head groups of sphingolipids, while the hydrophobic steroid and the hydrocarbon chain are embedded in the membranes. It modulates membrane rigidity or/and fluidity over the range of physiological temperatures.[11-13]

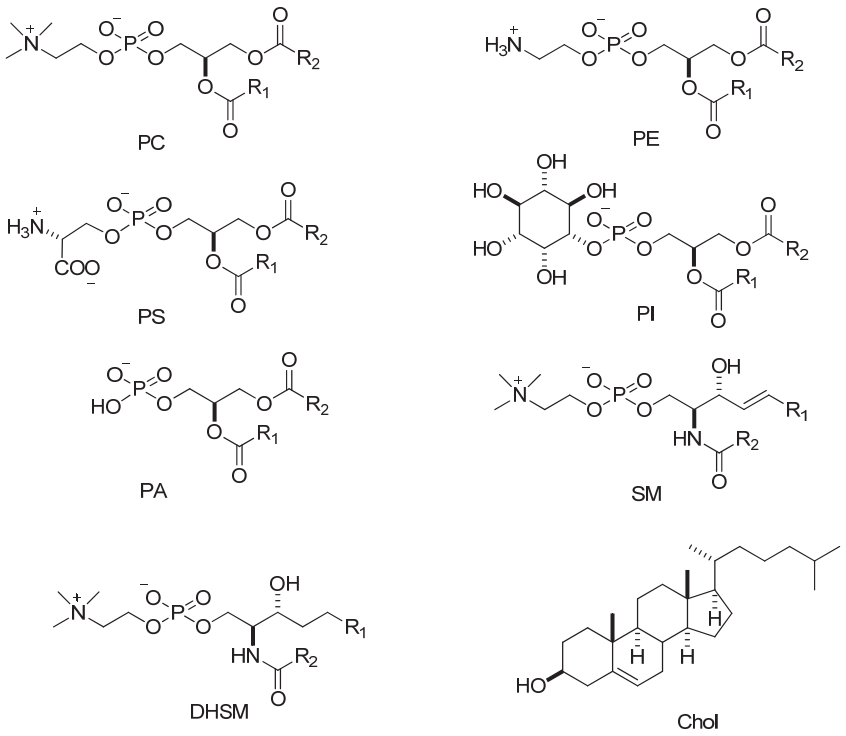

Figure 1-2. Chemical structure of lipids in bacterial/eukaryotic membranes. The side chain R_1 or R_2 in fatty acid differ in length and/or the presence or absence of double bonds.

1.3 Lipid Organization in Membranes

1.3.1 Membrane Structure

When mixed lipids with water, the tendency of the hydrophobic side chains to self-associate driven by entropy, and the propensity of the hydrophilic moieties to interact with aqueous environments, causes them to aggregate into bilayers without any energy input. Lipid bilayer is the basic structure of all cell membranes, and this concept became the basis for future models of membrane structure.[14] The first clues to bilayer structure in cellular membrane came from the experiment with red blood cell membranes performed by Gortner and Grendel in 1925.[15] Lipid bilayer structure was further observed using electron microscopy experiments at high resolution by Stoeckenius in 1962.[16] The development of the "fluid mosaic model" by Singer and Nicholson in 1972 represents an influential step in the study of membranes.[17] (Figure 1-3) Recent biochemical and biophysical findings have provided a detailed model of the structure and composition of plasma membrane. Different lipid compositions are asymmetrically distributed over the exoplasmic and cytoplasmic leaflets of the membrane.[18] An updated version of membrane

structure further suggested that "membranes are patchy, with segregated regions of structure and function, that lipid regions vary in thickness and composition, and that crowding and ectodomains limit exposure of lipid to the adjacent aqueous regions."[19)]

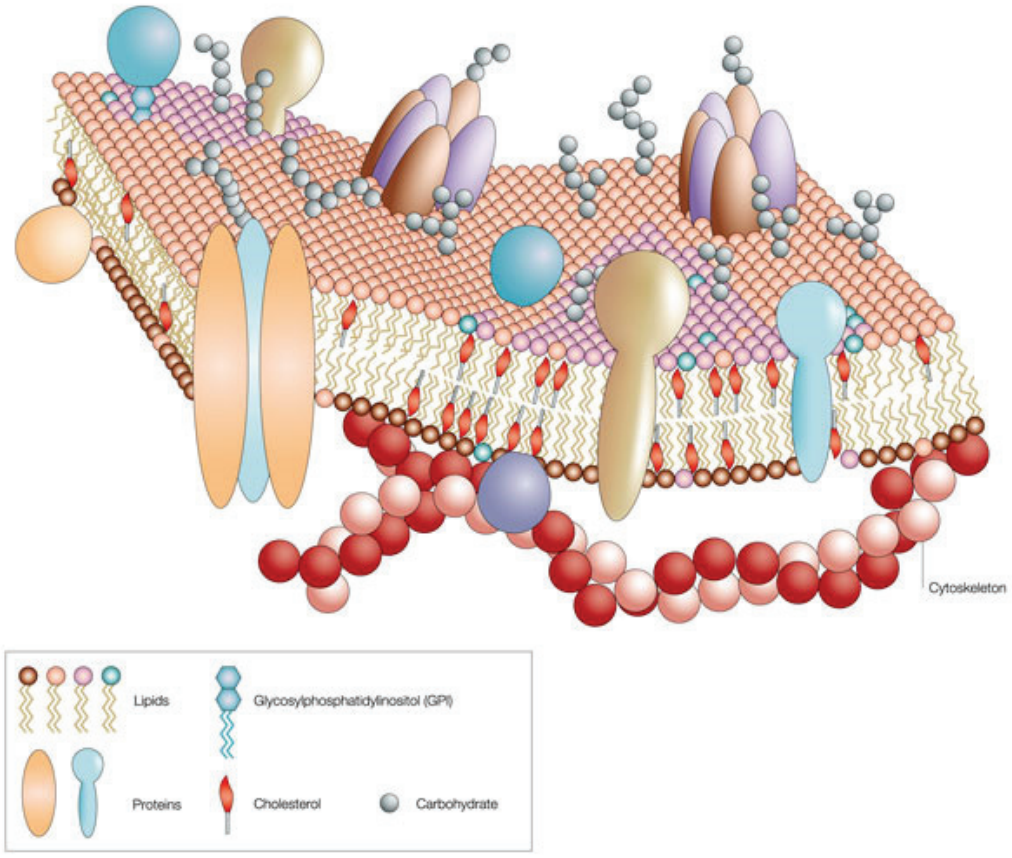

Figure 1-3. The fluid-mosaic model of the cell membrane. Reprinted with permission from *Horizon Symposia: Living Frontier*, **2004**, 1–4. © 2004 Nature Publishing Group.

1.3.2 Lipid Raft Concept

Earlier research considered that lipid molecules in membranes function as a passive and fluid solvent for proteins which participate in various biological processes. The raft concept brought lipids back into the picture by giving them a function and by introducing chemical specificity into the lateral heterogeneity of membranes.[20a)] The existence of lipid rafts was first hypothesised by Simons and Ikonen in 1988.[20b)] This hypothesis proposes that preferential interactions between lipids generate domains containing particular lipid molecules to drive the sorting of membrane

proteins.[20b,21] The raft concept originated from studies on epithelial cell polarity.[20b] The plasma membranes in epithelial cells are polarized into apical and basolateral domains. The former is enriched in sphingolipids (glycosphingolipids and sphingomyelin) and the latter in glycerolipid (phosphatidylcholine). In epithelial Madin-Darby canine kidney (MDCK) cells, glycosphingolipids, glucosylceramides were preferentially transported to the apical membrane. It was proposed that within the exoplasmic leaflet of the Golgi membrane, glycosphingolipid clusters together to form microdomains which serve as sorting centres for proteins responsible for delivery to the apical plasma membrane.[20b,21] Further study found that GPI-anchored proteins and influenza haemagglutinin form large complexes with sphingolipids and chol after Triton X-100 extraction, creating detergent-resistant membranes (DRMs) complexes, which possess specific properties.[22-24] This method provided a simple way for identifying raft components and contribute to the understanding for rafts as functional domains. Presently, lipid raft was defined as follows: "Membrane rafts are small (10–200 nm), heterogeneous, highly dynamic, sterol- and sphingolipid-enriched domains that compartmentalize cellular processes. Small rafts can sometimes be stabilized to form larger platforms through protein-protein and protein-lipid interactions."[25] Scientists have been making efforts to develop new technologies to characterize raft composition, size, and behavior. Although the existence of lipid rafts in cell has gained general acceptance, it has been proven difficult to pin down their size and life span on a cell membrane.[26]

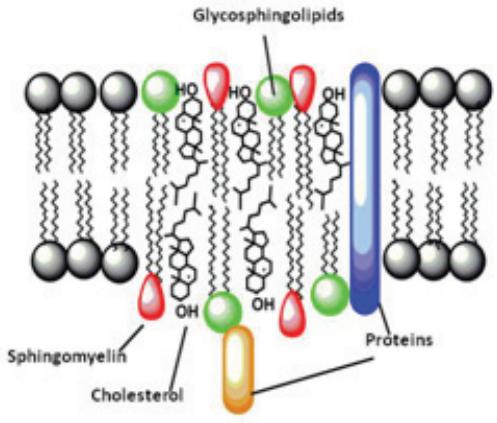

Figure 1-4. Lipid rafts in cell membranes.

Lipid rafts play an important role in many biological processes at the cell surface, such as

immunoglobulin E (IgE) signaling,[27,28] which convincingly demonstrated that lipid rafts are involved in signaling process. Other signal transduction processes shown to involve lipid rafts were T-cell antigen receptor signaling,[29,30] glial-cell-derived neurotrophic factor (GDNF) signaling,[31] Ras signaling[32] and Hedgehog signaling.[33,34] Lipid rafts are also involved in virus entry and assembly. Some viruses are now believed to bud from lipid rafts, including Human Immunodeficiency Virus (HIV) and influenza, which organize a lipid raft domain around their nucleocapsid that includes viral glycoproteins and excludes most host cell surface proteins from the budding viral envelope.[35,36]

1.3.3 Lipid Phases in Membranes

The lipids in membranes can exist in multiple possible phase states. At low temperature, the pure saturated lipid molecules can form a crystalline, solid gel-like phase (S_o or L_β).[37] The lateral mobility of the lipids is highly restricted. The bilayer can converts to a liquid-crystalline, fluid phase (L_α or L_d) beyond a certain temperature (melting temperature). The incorporation of chol can modulate the phase behavior. The tight packing between chol and saturated acyl chains causing the methylene groups to adopt an extended conformation, and a third phase (liquid ordered (L_o)) is possible to form.[38,39] In this phases, there is a high degree of fatty acid chain ordering, which is a typical feature in L_β phase, but with the translational disorder that is characteristic of the L_α phase.[40] The possible phase states at thermodynamic equilibrium in the model can be revealed in the lipid phase diagrams (Figure 1-5), which can be provided from thermodynamic data obtained by differential scanning calorimetry (DSC) or from spectroscopic methods such as NMR, electron-spin resonance (ESR), or fluorescence.

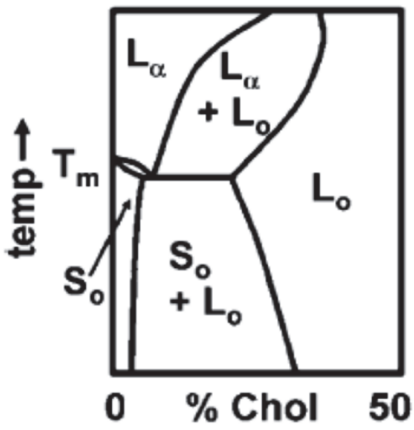

Figure 1-5. Phase diagrams for bilayer membranes containing phospholipids and chol. Reprinted with permission from *Biochem. Biophys. Acta* **2005**, 1746, 172–185. Copyright © (2005) Elsevier

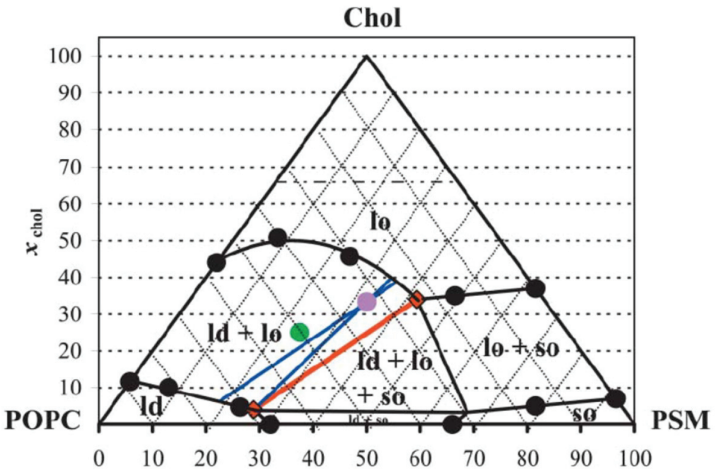

Figure 1-6. Phase diagram of PSM/POPC/chol at 23ºC. The circles are experimental points. The red (quasi) tie-line on the tietriangle describes the lo/ld composition at the right of which there is also so phase. The blue tie-lines are the interval for the possible tie-lines that contain the 1:1:1 composition. The purple point marks the 1:1:1 composition and the green point marks the 2:1:1 composition. The dashed horizontal line for $X_{chol} = 0.66$ represents the chol solubility limit on the lipid bilayer. Reprinted with permission from *Biophys. J.* **2003**, 85, 2406–2416. Copyright © (2003) the Biophysical Society

Ternary palmitoylsphingomyelin (PSM)/palmitoyloleoylphosphatidylcholine (POPC)/chol or

PSM/dioleoylphosphatidylcholine (DOPC)/chol mixture has been often used as a model to mimic the raft-like membranes.[41] Figure 1-6 shows the phase diagram of PSM/POPC/chol at 23 ºC. The main features are a broad L_o/L_d phase coexistence region in the diagram. In the diagram, the L_o/L_d phase separation disappeared when the content of chol reduced. A high content of PSM in the membranes will give rise to the formation of the solid gel-like S_o phase. The purple point marks the PSM/POPC/chol 1:1:1 composition. From this point, as chol was added, the topology of the domains was changed, and eventually L_o/L_d phase separation disappeared at high chol fractions. The membranes exist as a unique L_o phase.[42]

1.3.4 Imaging Methods for Studying Lipid Organization in Membranes

Lipid rafts may exist in cells came from the observation that cell membranes are not fully solubilized by non-ionic detergents at low temperatures. It has been argued that DRMs that are derived from cells do not reflect membrane substructures in living cells. Because the detergents used in this technique may disrupt specific associations of lipids and/or affect the partitioning of membrane proteins into a specific phase.[43-45] It is unlikely that DRMs reflect some preexisting structure or organization of the membrane.[46] Thus, various methods for studying the phase behavior of raft-mimic model membranes or native membranes in situ have been developed.

Optical techniques remain significant in lipid rafts studies.[47] Fluorescent microscopy has been recognized as a common method for in situ study of lipid rafts in living system. This method allows imaging at tens of nanometers with high sensitivity. However, it has inherent limitations. It requires the use of large fluorescent probes which possess distinct physical properties from the small lipid molecules and usually alter the physical properties of membranes. The fluorescent probes include cholestatrienol, 7-nitrobenz-2-oxa-1,3-diazole (NBD)-chol and TopFluor (TF)-chol, and acyl chain or head group modified phospholipids.[47] The chemical modification of a lipid molecule with a fluorescent moiety usually results in an inconsistent or even diametrically opposite distribution tendency in membrane phases.[47] Recent study has shown that the lipid-lipid interaction can be easily disturbed by trace amount of extrinsic fluorescent lipids.[48] The chemical modification of the side chain or polar head group of SM with NBD, dipyrromethene boron difluoride (Bodipy), Atto647N and Atto532 have been reported and used in raft imaging in giant unilamellar vesicles (GUVs). (Figure 1-7)[49-51] Although SM is the major lipids in raft-like L_o

phases, these probes largely prefer to L_d phases rather than L_o phases. It is considered that the bulky fluorescent groups on the acyl chains or head groups can generate unfavorable effect on lipid-lipid packing in L_o phases. Thus, the large probes can be easily depleted from the tightly packed L_o domains.[47)]

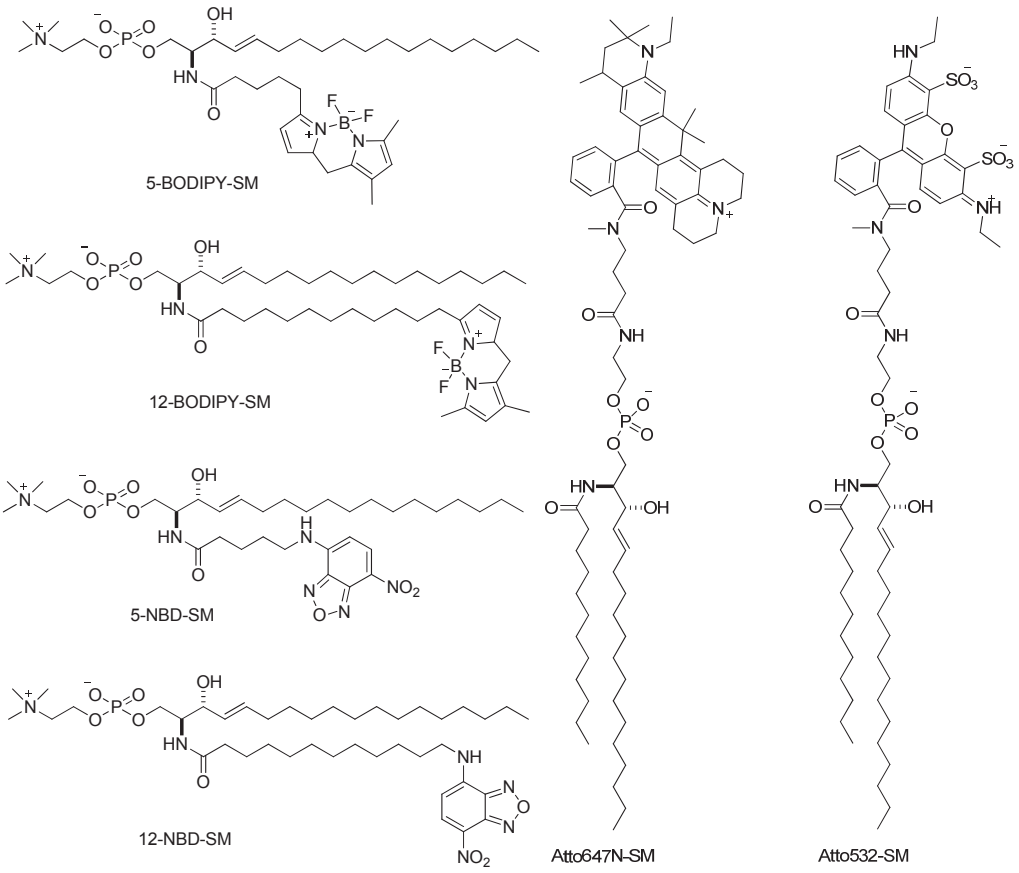

Figure 1-7. Chemical structure of fluorescent SMs.

Atomic force microscopy (AFM) provides a nano-scale resolution for membrane imaging, and can distinguish L_o or L_d phases based on their characteristic membrane thickness.[52,53)] L_o phase is thicker by 0.5 nm as compared to the L_d phase. However, AFM technique is only suitable for model or isolated native membranes immobilized on surfaces. The distribution and dynamics of specific lipid cannot be obtained by AFM. Recently ion mass microscopy has been applied to ^{2}H-1,2-Distearoyl-sn-glycero-3-phosphocholine (DSPC)/^{15}N-1,2-Dilauroyl-sn-glycero-3-phosphocholine (DLPC)/chol and ^{2}H-PSM/^{15}N-DOPC/^{13}C-chol/18-F-G_{M1} artificial membranes.[54)]

The heterogeneous distribution of lipid components has been observed by detecting isotope-labeled secondary ions. However, this technique is invasive. It needs freeze-dried sample and works under ultra-high vacuum.

Raman microscopy is a powerful technique that combines vibrational spectroscopy technique with optical microscopy.[55] It can detect specific vibrational signals of biomolecules and has been used for cell imaging.[56-58] Raman microscopy can detect molecules without labeling. However, the Raman signals of most endogenous molecules share the similar chemical groups that make it difficult to distinguish from each other. Alkyne, nitrile, azide, and deuterium, are expected to be potentially useful Raman tags as their Raman peaks are located in the cellular silent region. Among these groups, deuterium is a promising Raman tag due to its small size and good biocompatibility. Side chain-perdeuterated 1,2-dihexadecanoyl-sn-glycero-3-phosphocholine (DPPC) or DSPC has been used as Raman spectroscopic probes for Raman imaging of model membranes.[59]

Using perdeuterated DSPC, lipid phase separation in binary GUVs can be directly observed by coherent anti-stokes Raman scattering (CARS). (Figure 1-8)

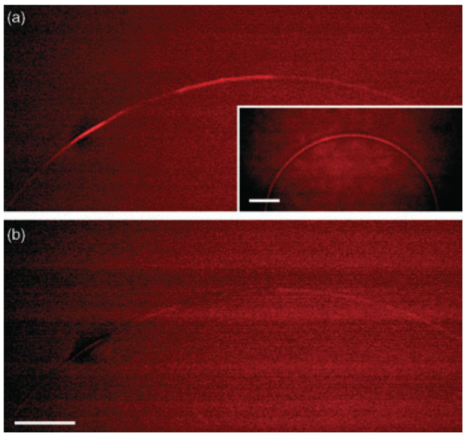

Figure 1-8. CARS images of part of an unstained GUV of binary mixture 1:1 DOPC/DSPC-d_{70}. a) On resonance with DSPC-d_{70} at 2090 cm^{-1} showing a sharp phase segregation of the lipids. Inset shows a vesicle of 1:1 DOPC/DSPC-d_{70} with 10% chol, in which the clear pattern is absent. b) Similar vesicle as in (a) recorded off-resonance with DSPC at 2140 cm^{-1}. Scale bars are 5 mm. Reprinted with permission from *Chem. Phys. Chem* **2005**, *6*, 77–79. Copyright © (2005) WILEY-VCH Verlag GmbH & Co. KGaA, Weinheim

The translation and undulation motions of GUVs might hamper the quantitative CARS imaging measurements. Thus, supported bilayers have been prepared by rupturing GUVs to a coverslip to form bilayer patches for Raman imaging. Figure 1-9 shows an imaging study of the planar bilayers of DOPC/DPPC-d_{62} (1/1 mol) mixtures containing 0, 10, 20, 30, and 40% (molar percentage) chol. With 10% chol added to the DOPC/DPPC-d_{62}mixture, no domains have been observed. The bilayer is in a fluid ordered phase. The addition of 20% chol causes the formation of percolating L_d and circular L_o domains. DPPC-d_{62} is suggested to be enriched in the L_o domains. When the content of chol is increased to 30%, the bilayer is homogeneously mixed. No phase separation can be observed. (Figure 1-9)

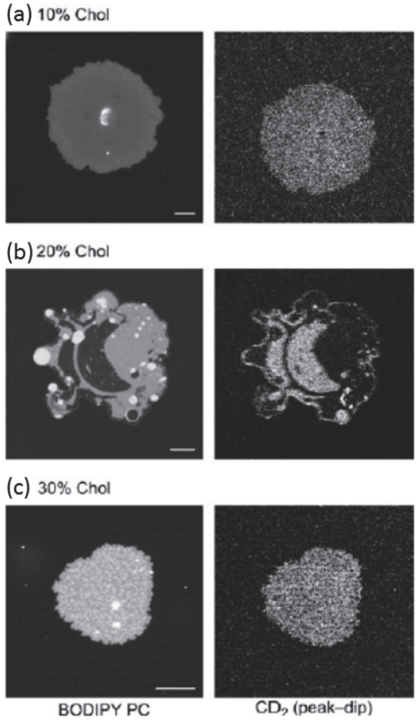

Figure 1-9. The epi-detected coherent anti-Stokes Raman scattering (E-CARS) (right) and fluorescence (left) images of the DOPC/DPPC-d_{62} (1:1) bilayer patches. The E-CARS images are difference images obtained by subtracting the image taken at 2125 cm^{-1} from the image taken at 2080 cm^{-1}. Bar length = 10 μm. Reprinted with permission from *Biophys. J.* **2005**, 89, 3480–3490. Copyright © (2005) the Biophysical Society

Figure 1-10 shows the Raman imaging of DPPC-d_{62}/DOPC binary monolayer prepared by

Langmuir–Blodgett (LB) technique, an alternative technique of creating model membranes on surfaces. The bright pixels exhibit the distribution of DPPC-d_{62} molecules underneath the tip.

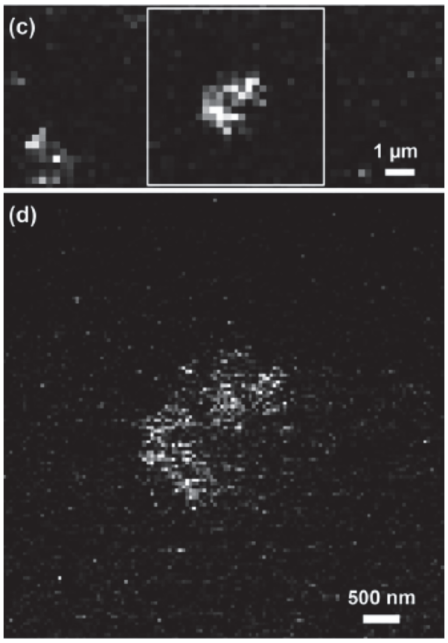

Figure 1-10. STM-tip enhanced Raman spectroscopy (STM-TERS) images of DPPC-d_{62}/DOPC binary monolayer of 26×64 pixels (c) and 128×128 pixels (d) from two consecutive raster scans in the same region (the area of (d) is indicated in (c) with a white box on a mixed monolayer on template-stripped gold reveal a micron-sized structure. Reprinted with permission from *Phys. Chem. Chem. Phys.* **2011**, 13, 9978–9981 Copyright © (2011) Royal Society of Chemistry

Although the abundant C-D bonds in these lipids give rise to strong Raman intensity, there is a small but significant difference in thermodynamics between the perdeuterated probe and the no-deuterium lipid, indicating the acyl chain behavior was perturbed by deuteration. This may hamper the elucidating the precise phase properties of the original lipid.

Recently alkyne-tagged biomolecules have been developed and used alkyne-tag Raman imaging (ATRI) in living cells.[56,57)] The alkyne moiety shows a specific and strong Raman scattering peak in a cellular Raman-silent region (1800~2800 cm^{-1}) where most endogenous molecules in cell have no Raman peak. The relative Raman shift/intensity various types of alkynes have been

measured in order to find optimum tag molecules for ATRI.[57] (Figure 1-11)

a)

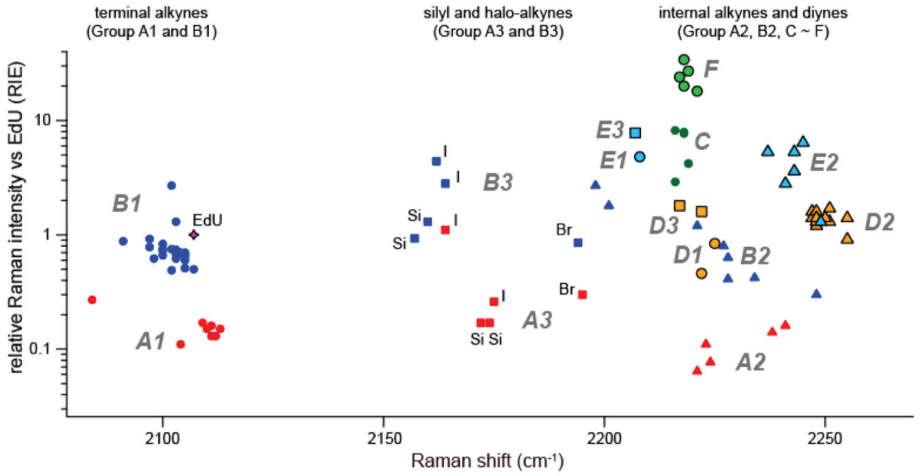

b)

Group	R: alkyl, alkenyl, acyl etc. Ar: aryl, X: $SiMe_3$, Br, or I	number of compounds	average RIE	Raman shift (cm^{-1})	representative example	RIE	Raman shift (cm^{-1})
A1	R—≡—H	8	0.16	2084 ~ 2113	HO—≡	0.16	2111
A2	R—≡—R	5	0.11	2221 ~ 2241	HO—≡—$(CH_2)CH_3$	0.11	2223
A3	R—≡—X	5	0.40	2164 ~ 2195	HO—≡—$SiMe_3$	0.17	2172
B1	Ar—≡—H	22	0.81	2091 ~ 2107	Ph—≡	0.49	2102
B2	Ar—≡—R	8	1.0	2198 ~ 2248	Ph—≡—$(CH_2)_3CO_2Me$	0.63	2228
B3	Ar—≡—X	5	2.1	2157 ~ 2194	Ph—≡—$SiMe_3$	0.93	2157
C	Ar—≡—Ar	5	6.2	2216 ~ 2219	Ph—≡—Ph	4.2	2219
D1	R—≡—≡—H	2	0.65	2222 ~ 2225	HO—≡—≡	0.84	2225
D2	R—≡—≡—R	13	1.4	2247 ~ 2255	HO—≡—≡—CMe_3	1.7	2251
D3	R—≡—≡—X	2	1.7	2217 ~ 2222	HO—≡—≡—$SiMe_3$	1.6	2222
E1	Ar—≡—≡—H	1	4.8	2208	Ph—≡—≡	4.8	2208
E2	Ar—≡—≡—R	6	4.1	2237 ~ 2249	Ph—≡—≡—CMe_3	5.3	2237
E3	Ar—≡—≡—X	1	7.8	2207	Ph—≡—≡—$SiMe_3$	7.8	2207
F	Ar—≡—≡—Ar	5	25	2217 ~ 2221	Ph—≡—≡—Ph	27	2219

Other examples of B1 and B3

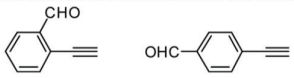

RIE / Raman shift (cm^{-1})	0.73 / 2100	1.3 / 2103	Ph—≡—Br 0.85 / 2194	Ph—≡—I 2.8 / 2164

Figure 1-11. Structure-Raman shift/intensity relationship of alkynes. (a) Plot of relative Raman intensity versus EdU (RIE) and Raman shift of various types of alkynes. (b) Alkynes are divided into 14 groups according to the substitution pattern. Average RIE, range of Raman shift, and representative alkynes of each group are shown. Reprinted with permission from *J Am Chem Soc.* **2012**, *134*, 20681–20689. Copyright © (2011) American Chemical Society.

In Figure 1-11, substituted alkynes were divided into 14 groups. The results indicated that aromatic ring conjugated alkynes give rise to very strong Raman intensity (RIE, group A < B < C). Raman shift/intensity of alkyne changed with the type and position of the substituent. The conjugated diynes, particularly 1,4-disubstituted diynes, (groups D−F) have been considered as promising Raman tags due to the high Raman intensity. They showed higher wavenumbers compared to simple alkynes (groups A vs D, B vs E, and C vs F). Conjugation of the diyne to an aromatic ring resulted in enhanced Raman intensity (RIE, group D < E< F).[57] Recent study achieved the Raman imaging of Alkyne-tagged 5-ethynyl-2′-deoxyuridine (EdU) and diyne-tagged AltQ2 in cells. The Raman image clearly showed that alkyne-tagged EdU was localized in the nucleus, whereas diyne-tagged AltQ2 was localized in the cytoplasm.[57]

1.3.5 Solid-State Deuterium NMR Study of Membranes

Solid state ^{2}H NMR is a versatile method for the investigation of the physical properties of model membranes in a noninvasive manner. In membranes, the molecular motions of lipids are hindered due to the parallel packing of the lipid molecules. In many cases, membranes behave like uniaxial liquid crystals. The molecular movements exhibit rotational symmetry with respect to the axis. ^{2}H NMR spectroscopy provides information of the ordering of the deuterated lipid molecules, the angular fluctuations of the lipids around the optical axis as well as the rate of the segmental reorientations.[60]

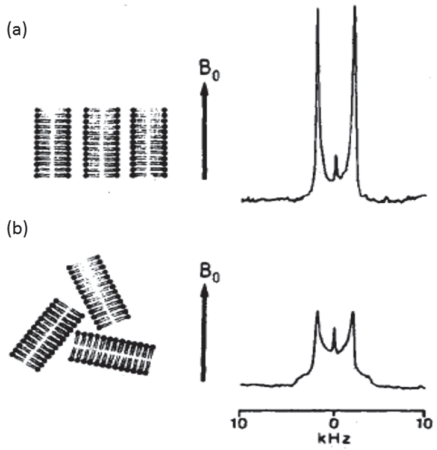

Figure 1-12. ^{2}H NMR spectra of a mixture of l-palmitoyl-2-oleoyl-sn-glycero-3-phosphoethanolm (POPE)/l-palmitoyl-2-oleoyl-sn-glycero-3-phosphoglycerol (POPG) (83/17). POPG was deuteriated at the *sn*-2´-position of the glycerol headgroup. Spectrum A demonstrates the orientation of the lipid bilayer by the magnetic field while spectrum B results from vortexing the sample. The orientational distribution of lipid bilayers with respect to the magnetic field Bo is shown schematically on the left. Reprinted with permission from *Acc. Chem. Res.* **1987**, *20*, 221–228. Copyright © (1987) American Chemical Society.

Figure 1-12 shows the ^{2}H NMR spectrum of deuteriated phosphatidylglycerol. The bilayer normal is perpendicular to the magnetic field (B_0). This kind of macroscopically oriented membranes can be easily prepared by spreading lipid solution on the flat glass plates.[61] The ^{2}H NMR spectrum is characterized by two sharp peaks corresponding to the two allowed NMR transitions of the deuterium nucleus (I = 1). The quadrupole splitting ($\Delta\nu_Q$) is given by the separation between the two resonances. It provides information about the average orientation and the fluctuations of the C-D bond vector which is usually expressed in terms of molecular order parameter (S_{CD}).[62]

Figure 1-12 **b** shows the ^{2}H MMR spectrum of a non-oriented sample. Since all orientations of the bilayers relative to B_0 exist simultaneously, the signal becomes powder-type spectra, the peak becomes broad and the intensity reduced. The separation of the two maxima is equal to the quadrupole splitting observed in the oriented membranes. Compared with non-oriented sample, the spectrum obtained from macroscopic alignment membranes has improved spectral resolution and excellent sensitivity for phase transitions.[61]

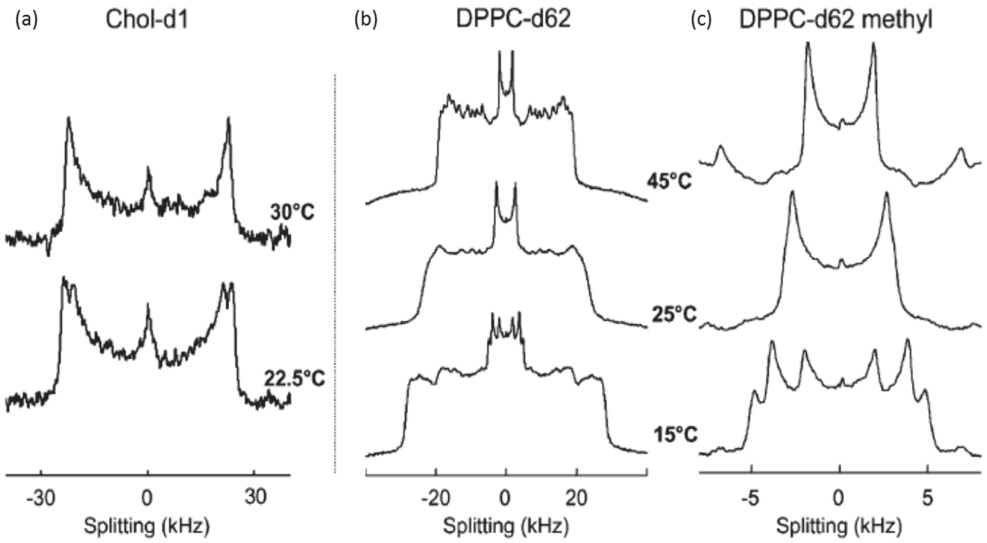

Figure 1-13. ^{2}H NMR spectra for multilamellar vesicles (MLVs). (a) 1:1 DOPC/DPPC + 30% *d*-chol (chol-d1) and (b,c) 1:1 DOPC/DPPC-d_{62} + 30% chol. Spectra in c are an expanded view of the terminal methyl splitting in b. At low temperature (22.5ºC in a and 15ºC in b,c), multiple splittings are present in both chol-d1 and in the methyl region of DPPC-d62 indicating that large-scale (160 nm) phase separation has occurred. Reprinted with permission from *Biophys. J.* **2004**, 86, 2910–2922. Copyright © (2004) the Biophysical Society

^{2}H NMR can be used to detect immiscibility of ternary membranes and for quantitatively determine the lateral distribution of lipid in different phases.[63,64] Figure 1-13 shows the ^{2}H NMR spectra of ternary membranes labeled with 3-α-*d*-chol (*d*-chol) or side chain-perdeuterated DPPC (DPPC-d_{62}).[63] In Figure 1-13 **a**, *d*-chol shows two pair of peaks at 22.5 ºC, suggesting two types of liquid environments exist in the mixture. The outer splitting corresponding to the more ordered L_o phase with larger integrated intensity, indicating that most of the chol-d1 is in this phase. DPPC-d_{62} behaves similarly as shown in Figure 1-13 **b**. The peak from the methyl group splits into three peaks. The inner peak is due to DPPC-d_{62} in the less ordered liquid crystalline (L_α) phase. The two outer splittings stem from nonequivalence of the terminal methyl groups of the *sn*-1 and *sn*-2 chains. They are in the same liquid-ordered state. At high temperature, the phase separation disappeared, suggesting a homogeneous L_α phase.[63]

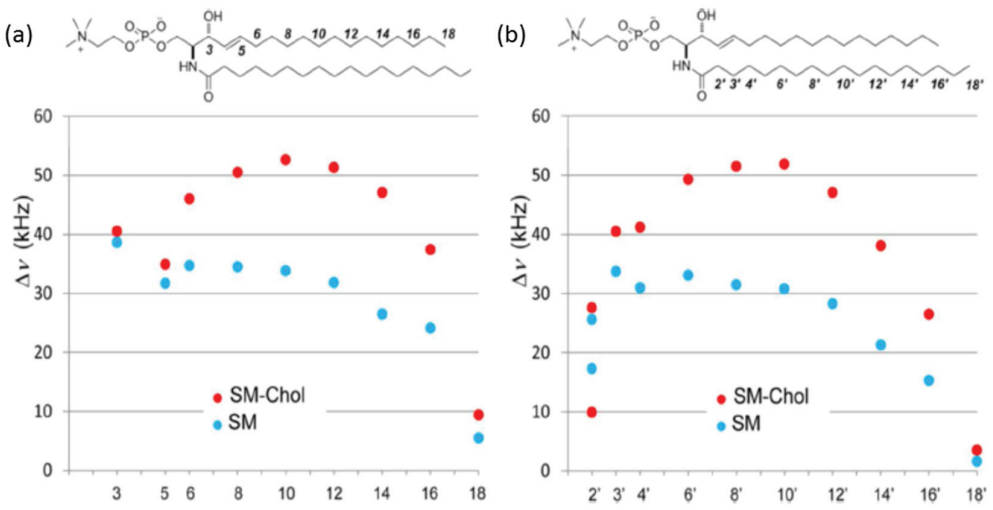

Figure 1-14. Quadrupole splitting profiles obtained from SSM that has been site-specifically deuterium-labeled on the sphingosine (a) and (b) stearoyl chains. Data were obtained in the absence (blue circles) and presence (red ones) of 50 mol % chol at 45 °C. Reprinted with permission from *Biochemistry* **2012**, *51*, 8363–8370. Copyright © (2012) American Chemical Society.

One inherent disadvantage with perdeuterated acyl chains is that it will cause overlapping of quadrupole splittings, which can lead to the misassignment of deuterium signals.[65] In addition, the multideuterated lipids can alter the physical properties of lipid bilayers significantly by the accumulated deuterium isotope effects as mentioned above. Thus site-specifically deuterated lipid can be used to gain accurate dynamics information on the lipid molecule. Recently, the comprehensive molecular motion capture of SM has been achieved using site-specifically labeled SM.[66] The order profiles revealed a reasonable model for the mechanism of raft formation. In binary liposomes, chol enhances orders of the middle region of hydrocarbon chains more efficiently than other positions. (Figure 1-14) The observed quadrupole splitting profiles are distinct from those reported from perdeuterated sphingomyelins. The site-selectively labeled SMs can be used in more complex membrane systems to study lipid rafts organization.[66]

1.4 Lipid-Protein Interactions in Membranes

1.4.1 Integral and Peripheral Membrane Proteins

There is a high content of proteins in cell membranes. These proteins are important for the function of a cell.[67] Membrane proteins include integral (or intrinsic) membrane proteins and peripheral (or extrinsic) membrane proteins. Integral membrane proteins are embedded in the phospholipid bilayer and can span the whole hydrophobic core of phospholipid bilayer in membrane at least once. To transfer a peptide bond from water into a non-polar region is highly energetically unfavorable. Thus, the formation of peptide hydrogen bonds will drastically reduce the energy cost. The membrane spanning regions adopt either α-helical or β-sheet structures to generate the maximum number of peptide hydrogen bonds.[68] The hydrophobic residues in the proteins interact with fatty acyl groups of phospholipids, thus anchoring the protein to the membrane. For integral monotopic proteins, they do not span across the membrane and are anchored to one leaflet of membrane by covalently bound fatty acids.

The function of integral membrane protein is closely related to the membrane environment, and cannot function when the protein is not embedded within the membrane. The integral membrane proteins can be removed from the membrane with specific chemical treatment. As the hydrophobic regions of the protein are protected by the phospholipid bilayers, detergents, denaturing solvents, and nonpolar solvents can be used to disrupt the phospholipid bilayer and extract the integral membrane protein.[69] The examples of integral transmembrane proteins includes G-protein coupled receptors (GPCRs) which are involved in a broad range of biological processes[70] and voltage-gated ion channels such as those which transport potassium, sodium or calcium ions across cells.[71]

Peripheral membrane proteins are associated with membranes but do not interact with the hydrophobic core of the lipid bilayer.[72,73] They are often found in association with integral membrane proteins or lipid polar head groups. Some peripheral membrane proteins are bound to cytosolic face of the plasma membrane, including cytoskeletal proteins spectrin, actin in erythrocytes and the enzyme proteinkinase C.[74] The peripheral membrane proteins can also be found to localize to the exoplasmic surface of the plasma membrane. In contrast to integral membrane proteins, peripheral membrane proteins tend to locate in the water soluble fractions during a protein purification procedure.[75]

1.4.2 Annular and Non-annular Lipids in Membranes

Lipids interact with integral membrane proteins in different manner. Generally two types of binding modes can be found for the lipid-protein interactions. a) Boundary lipids or annular lipids can form an annular shell of lipid around the protein surface.[76] Annular lipids interact with the protein relatively non-specifically. The rate of exchange of lipid molecules between the annular shell around a membrane protein and the bulk phase is generally around $1-2\ 10^7\ s^{-1}$ at 37 ºC. b) Non-annular lipids or co-factor lipids can bound at protein–protein interfaces in multisubunit proteins or are immersed in cavities and clefts of protein inside.[77] Some of these lipids play an important role in folding and assembly of membrane proteins. Compared with annular lipids, the rate of exchange of non-annular lipid with bulk lipid should be relatively slow due to the high specific interaction with proteins. The high-resolution crystal structures of membrane proteins usually contain lipid molecules which are likely to be non-annular lipids because of the strong binding to protein which lead to the immobilization of at least part of the lipid molecules.[78] The annular/non-annular lipid molecules identified in the crystal structures of membrane proteins have been summarized in Table 1-1.

Table 1-1. Lipid molecules identified in crystal structures of α-helical membrane proteins

Protein	PDB[a] code	Annular lipids	Non-annular lipids	
			Between helices[b]	Between subunits[b]
Bacteriorhodopsin	1QHJ	6		2
Rhodopsin	1GZM	1		
Bacterial Photosynthetic Reaction centres				
Rhodobacter sphaeroides	1QOV			1
	1OGV			
	1M3X	1?	1?	1
Thermochromatium tepidum	1EYS			1
Photosytem 1 from *Synechococcus elongates*	1JB0	1	2	1
Light-harvesting complex from spinach	1RWT			2
Cytochrome c oxidase from *Paracoccus denitrificans*	1QLE		1	1
Cytochrome bc_1 from Saccharomyces cerevisiae	1KB9		1	4
Cytochrome b_6f from *Chlamydomonas reinhardtii*	1Q90			2
Succinate dehydrogenase from E. *coli*	1NEK	1		1
Nitrate reductase	1Q16			1
ADP/ATP carrier from mitochondria	1OKC	7		
Potassium channel KcsA	1K4C			1

[a] Protein data bank [b] Non-annular lipids are classified as either being located between transmembrane a-helices within a monomer or between subunits in a multimeric complex. *Biochim. Biophys. Acta* **2004**, 1666, 62–87

1.4.3 Hydrophobic Matching

A basic model of lipid-protein interactions is hydrophobic matching (Figure 1-15), which means the hydrophobic thickness of the lipid bilayer match well the hydrophobic length of the trans-membrane domain of protein in the lipid bilayer. There is high cost of exposing either lipid side chains or hydrophobic amino acids residues to the water phase.

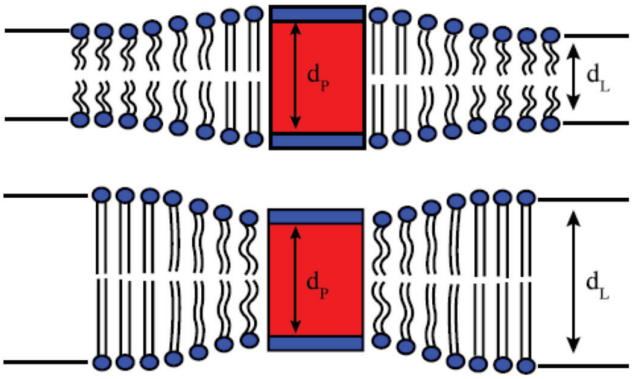

Figure 1-15. Schematic illustration of the concept of hydrophobic matching between the hydrophobic length of the trans-membrane domain of protein and the hydrophobic thickness lipid bilayer. Reprinted with permission from *Biochim. Biophys. Acta* **2004**, 29, 469–477. Copyright © (2004) Elsevier.

Hydrophobic matching suggests that the acyl chains of lipids in the vicinity of a membrane protein change their length to match the hydrophobic thickness of the protein.[79] When the hydrophobic thickness of the bilayer is less than the hydrophobic length of the protein, the acyl chains will stretch to increase the bilayer thickness. Conversely, the side chains will compress to form a thinner bilayer when the hydrophobic thickness of the bilayer is greater than the hydrophobic length of the trans-membrane domain in protein. A Recent study provided a novel view of the hydrophobic matching.[80] An increase in helical content of rhodopsin, the mammalian dim-light photoreceptor and the best characterized GPCR, with increasing bilayer thickness was observed, indicating proteins can change their structure to adapt the change of hydrophobic thickness in bilayers.[80]

1.4.4 Bacteriorhodopsin and Lipids in Purple Membranes

Bacteriorhodopsin (bR) is a retinal-binding integral membrane protein that functions as a light-driven proton pump in the purple membrane (PM) of *Halobacterium halobium*.[81] It is a small protein with 26 kDa (248 amino acid residues) of seven transmembrane helices with short interhelical loops and extramembrane N- and C-termini. The retinaldehyde within bR is covalently bound to a lysine residue (K216) in helix G. (Figure 1-16)

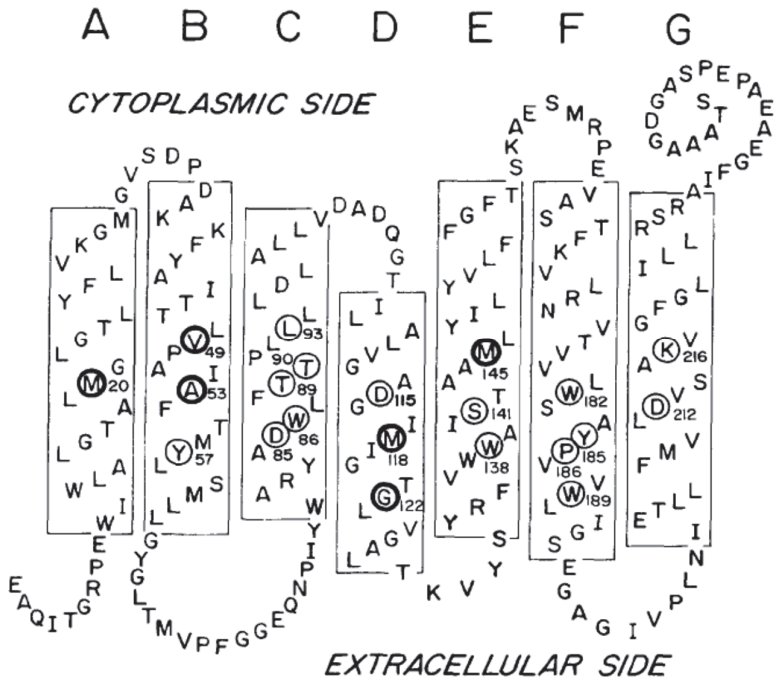

Figure 1-16. Secondary structure model of bR Boxes A-G represent the seven transmembrane α-helical segments. The region of the D-E loop was modified according to spin labeling experiments. The residues proposed to constitute the retinal-binding pocket are circled. The residues reported here are emphasized in boldface type. Reprinted with permission from *J. Biol. Chem.,* **1993**, *268*, 20305–20311. Copyright © (1993) the American Society for Biochemistry and Molecular Biology

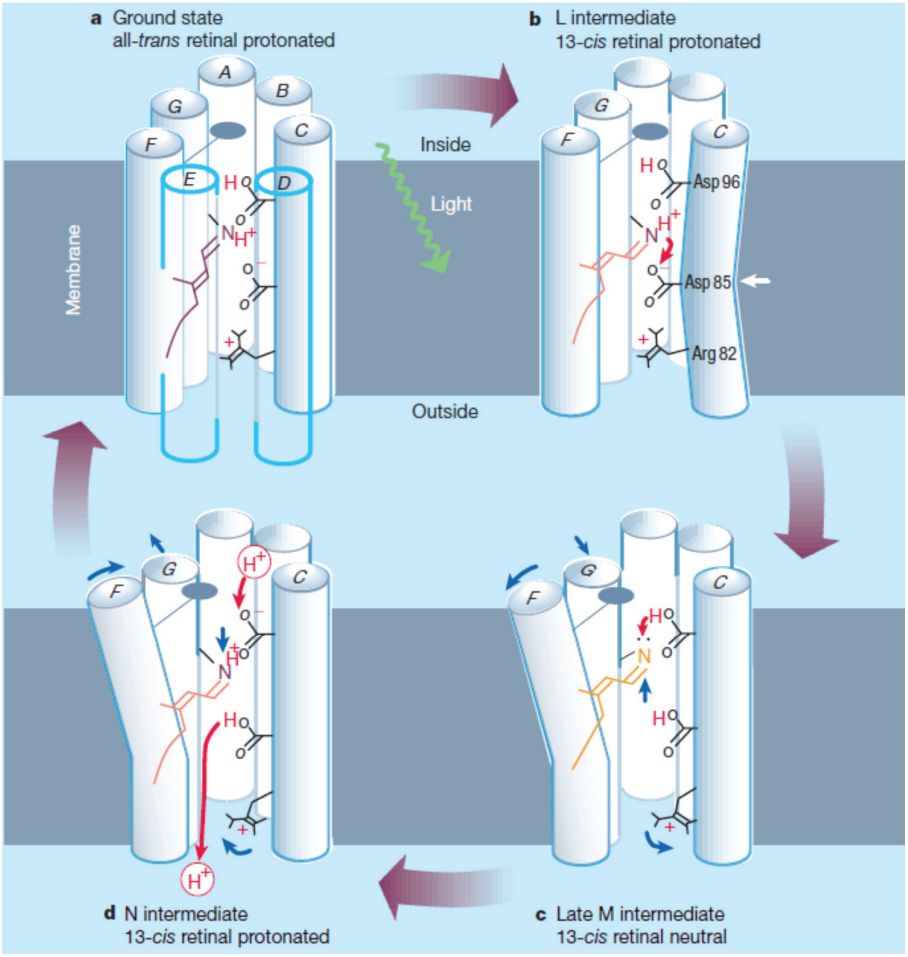

Figure 1-17. Molecular mechanism of proton (H^+) pumping in bR. Red arrows, proton movements; blue arrows, movements by groups of atoms. Helices D and E are omitted in b–d for clarity. Reprinted with permission from *Nature* **2000**, *406*, 569–570. Copyright © (2000) Nature Publishing Group

The proton pumping cycles in bR yield the proton gradient which powers the synthesis of adenosine triphosphate (ATP) by an ATP synthase.[82] The cycles rely on a pigment that can also be found in human being, retinal or vitamin A. The retinal in bR is covalently attached to a K216 in helix G, and is bound in the space between the seven transmembrane helices (A to G). Figure 1-17 shows the main events in the proton pumping cycles.[83] From (a) to (b), light-induced protonated retinal isomerization from all-trans (purple) to 13-cis (pink) triggers the transfer of the proton from the Schiff's base to aspartate (Asp) 85. This transfer is helped by a slight movement of Asp 85 in helix C towards the nitrogen atom in L intermediate. In the M state (c), the

deprotonated retinal (yellow) straightens and pushes away the upper half of helix F causing it to tilt, while the top of helix G moves partly into its place. This movement lets the deprotonated retinal close to Asp 96 in helix C, from which it abstracts a proton. The tilting of helixs F and G opens a channel on the cytoplasmic side of the membrane through which Asp 96 is reprotonated (d). In N intermediate, the proton at Asp 85 travels via a network of hydrogen bonds and water molecules to the outside medium, past Arg 82 from helix C, which has moved slightly.[84)]

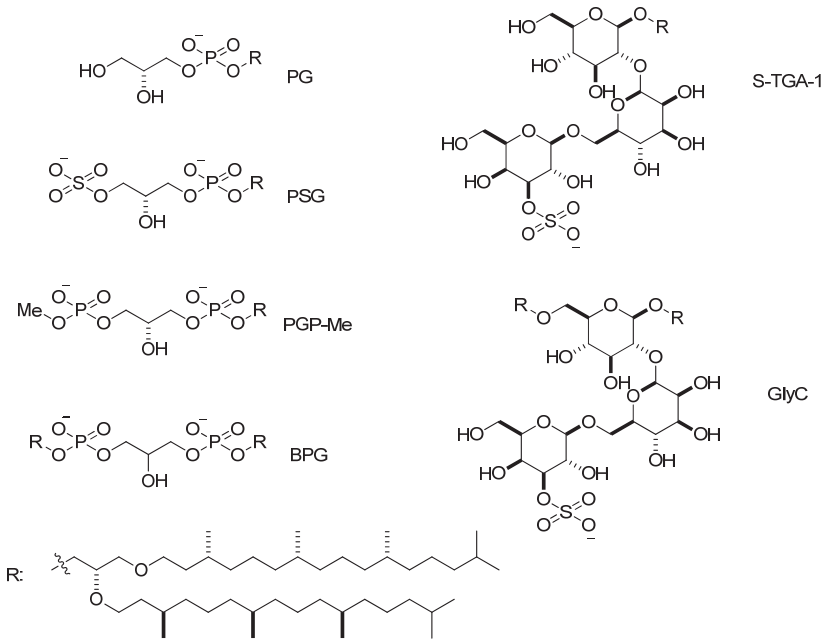

Figure 1-18. Chemical structure of polar lipids in purple membranes.

BR account for 75% of the membrane mass. In PM, bR is organized in trimmers with 30 lipid molecules associated with each trimer: 6 lipids located within the trimer and 24 surrounding the protein surface.[85)] Most of PM lipids are polar lipids (90%) with 10% neutral lipids which are mainly squalene. The polar lipids include 2,3-di-*O*-phytanyl-*sn*-glycerol phosphatidylglycerol (PG), phosphatidylglycerol sulfate (PSG), phosphatidylglycerophosphate methyl ester (PGP-Me), archaeal cardiolipin (BPG), sulfated triglycoside lipid (S-TGA-1) and archaeal glycocardiolipin (GlyC). The major polar lipid was found to be the PGP-Me by quantitative analysis of the lipid extract of the purple membrane.[86)]

Usually, the annular lipids will be too disordered to appear in high-resolution structures.

However, these lipids have been resolved on the surface of bR trimer by X-ray diffraction. (Figure 1-19) The lipid head groups are disordered and not resolved but the fatty acyl chains are well resolved. The lipid side chains bound in distinct grooves on the surface of the protein.[85] These situations suggest that strong, specific or functionally significant lipid-bR interactions may take place in the membranes.

(a) (b)

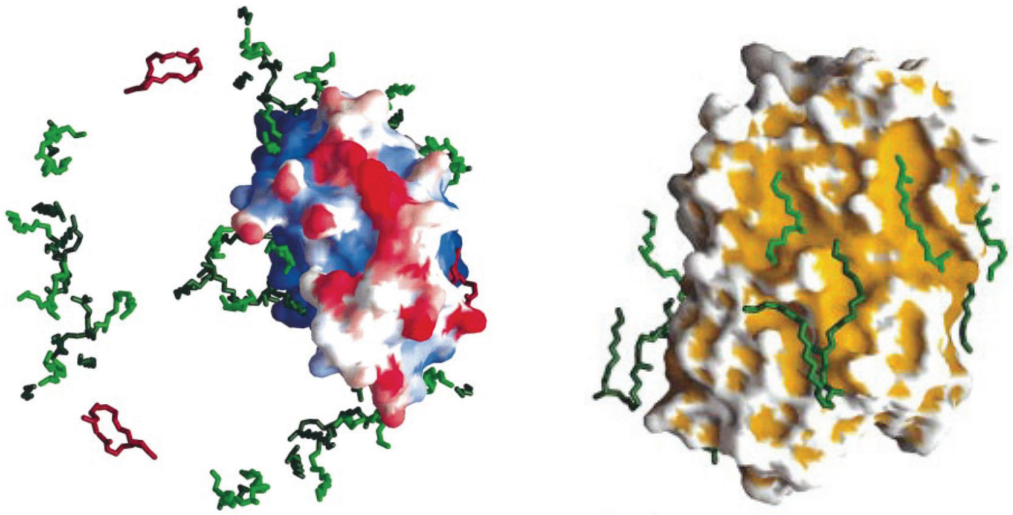

Figure 1-19. X-ray diffraction of bR trimer. (a) View of a bR trimer perpendicular to the bilayer plane. The remaining lipids form an annulus around the protein surface (b) Side-view of the protein and ordered lipids. The head groups of lipids are not resolved but the fatty acyl chains are well resolved. Reprinted with permission from *J Mol Biol.,* **1993**, 291, 899–911. Copyright © (1993) Elsevier

1.4.5 Bacteriorhodopsin-Lipids Interactions

BR interacts with PM lipids by hydrogen bond, salt bridge, and van del Waals contact.[87] Recent studies suggest that the PM lipids play an important role in the physiological activities of bR, which can be evident from significant changes in the photochemical cycle kinetics.[88,89] When natural membrane lipids are partly or completely replaced with detergents, the local conformation and dynamics of bR can be altered.[90] The peculiar homogeneous structure of purple membrane alkyl chain lipids is likely to be an essential requirement for maintenance of the native structure of

bR over a wide pH range.[91] In PM membranes, bR forms trimeric units that are arranged as a two-dimensional hexagonal lattice. In the arrangement of bR trimer, there are ten lipids per bR monomer, including six to seven phospholipids, two to three sulfoglycolipids and one squalene fill the space between the proteins.[92,93] The importance of these endogeneous lipids for the lattice assembly of bR can be realized when one attempts to regenerate it by incorporation into dimyristoylphosphatidylcholine (DMPC) bilayers.[94]

1.5 Aim of the Projects

Synthesis of Raman-tagged Sphingomyelin and Elucidation of Lipid Organization in Raft-like Domains

Due to the interesting functions of lipid rafts in biological processes, the original aim of this PhD thesis was to develop a useful probe to dye raft-like regions in membranes. Considering that the polar head group region of phospholipids in membrane is relatively loosely packed, the modification of SM head group may generate a minimal impact on lipid packing. Thus, in this PhD work, three Raman probes have been designed based on N-stearoyl sphingomyelin (SSM), where the polar head group was tagged with alkyne, diyne and $(CD_3)_3$, respectively. (Figure 1-20) To find the best candidate probe, the relative Raman shift and intensity of these Raman groups should be compared. It was assumed that the alkyne and diyne moieties on the polar head group of SM might generate unfavorable effect on lipid-lipid packing. Thus the phase behavior similarity of alkyne-SM **1** and diyne-SM **2** *vs* native SM should be evaluated. In addition, the raft-like domains selectivity of the developed probe is an interesting question that was going to be explored in this PhD work.

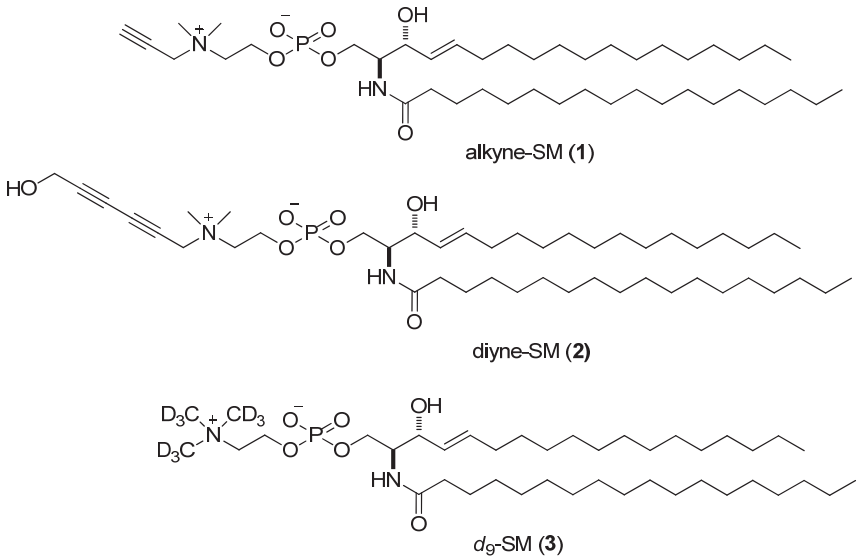

Figure 1-20. Chemical structure of alkyne-SM (**1**), diyne-SM (**2**) and d_9-SM (**3**).

To set these into practice, the first task was to achieve the synthesis of these probes. A suitable synthetic route including a common intermediate of all the target molecules should be developed. Second, the relative Raman shift/intensity of the obtained probes should be compared. Third, ^{2}H NMR measurement was planned to evaluate the raft-formation of the candidate probe. In ^{2}H NMR spectra, quantitative distribution of interested lipid in raft-like domains would be provided. To do so, several site-specifically deuterated lipids would be synthesized and used for ^{2}H NMR measurements. (Figure 1-21)

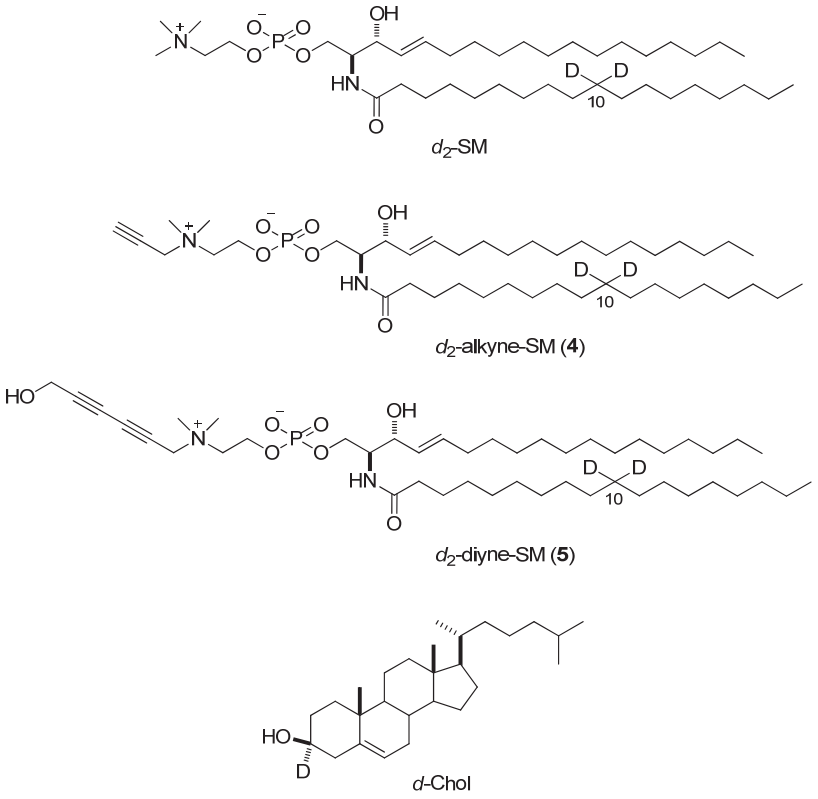

Figure 1-21. Chemical structure of d_2-SM, d_2-alkyne-SM (**4**), d_2-diyne-SM (**5**) and *d*-chol.

Synthesis of Deuterated Dioleoylphosphatidylcholine for Investigation of Membrane Properties.

The original aim of this Chapter was to develop a useful ^{2}H NMR probe for studying lipid organization in raft-like membranes. DOPC is a typical L_d component in raft-model membranes, and has often been used to prepare a ternary L_o/L_d-co-existing mixture with SM and chol. Although incorporation of unsaturated DOPC into L_o phases is energetically unfavorable, a small amount of DOPC is always found in these phases. However, the phase distribution in L_o phases is difficult to detect using a previously reported DOPC probe [C11-$^2H_2$] DOPC due to the inappropriate deuterated position. Based on molecular dynamics (MD) simulation, [C6-$^2H_2$] DOPC **7** has been rationally designed as a useful ^{2}H NMR probe. (Figure 1-22)

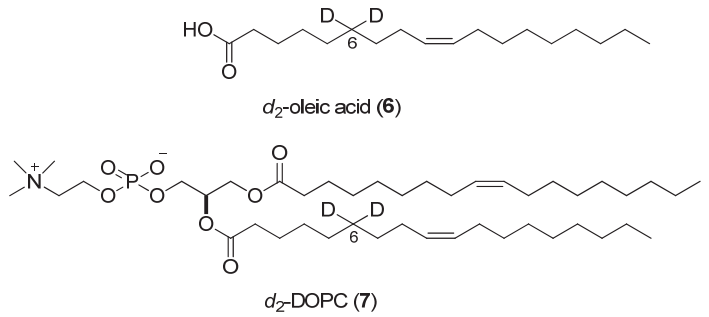

Figure 1-22. Chemical structure of d_2-oleic acid (**6**) and d_2-DOPC (**7**).

The first task was to achieve the synthesis of compound **7**. The only known synthetic route to [C6-$^2H_2$] oleic acid **6**, the key precursor for the synthesis of target molecule, is a long linear (14 steps) sequence. Thus an efficient synthetic route to this intermediate would be developed. Then, compound **7** obtained from **6** would be used for investigation of the behavior in raft-like membranes by ^{2}H NMR.

Stereoselective Synthesis of Phosphatidylglycerophosphate Methyl Ester Analogues towards Evaluation of Bacteriorhodopsin-Lipids Interactions in Membranes

It is of great biological significance to understand how the lipids and proteins interact in membranes. To provide a deep insight into the lipid-protein interactions, in this Chapter, bR was opted as a model protein, and an analogue retain the head group structure of PGP-Me bearing two unbranched side chains was designed. It will be used to prepare the model membranes to mimic the native cellular environment for *in situ* study of lipid-bR interactions.

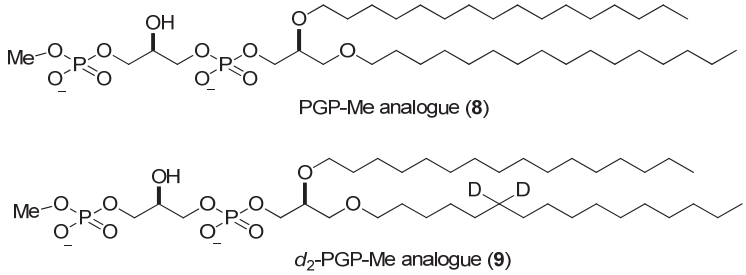

Figure 1-23. Chemical structure of PGP-Me analogue (**8**) and d_2-PGP-analogue (**9**).

PGP-Me is a diacidic phospholipid comprising a chiral polar diphosphoric head group and two hydrophobic side chains which are bound to the chiral glycerol backbone by ether linkages. The stereoselective synthetic method for PGP-Me or its analogue has not yet been reported. Thus, the first task in this section was to design a novel and rational synthetic route to the target molecule. Then, a site-specifically deuterated analogue will be synthesized for solid-state ^{2}H NMR measurements, by which useful information about lipid-bR interactions will be provided. (Figure 1-23)

There are several type of commercial lipids with different polar heads, such as PC, PG, PE, PS, and PA, which have the similar side chain structure with the analogue. Thus, further physicochemical analytic result of the developed analogue would be useful for selectively evaluation of the importance of head group of PGP-Me in sustaining structural and functional integrity of protein in membranes.

References

1) Fahy, E.; Subramaniam, S.; Brown, H. A.; Glass, C. K.; Merrill, A. H., Jr.; Murphy, R. C.; Raetz, C. R.; Russell, D. W.; Seyama, Y.; Shaw, W.; Shimizu, T.; Spener, F.; van Meer, G.; VanNieuwenhze, M. S.; White, S. H.; Witztum, J. L.; Dennis, E. A. *J. Lipid Res.* **2005**, *46*, 839-861.

2) Fahy, E.; Subramaniam, S.; Murphy, R. C.; Nishijima, M.; Raetz, C. R.; Shimizu, T.; Spener, F.; van Meer, G.; Wakelam, M. J.; Dennis, E. A. *J. Lipid Res.* **2009**, *50* Suppl, S9-14.

3) Lombard, J.; Lopez-Garcia, P.; Moreira, D. *Nat. Rev. Microbiol.* **2012**, *10*, 507-515.

4) Pereto, J.; Lopez-Garcia, P.; Moreira, D. *Trends Biochem. Sci.* **2004**, *29*, 469-477.

5) van Meer, G.; Voelker, D. R.; Feigenson, G. W. *Nat. Rev. Mol. Cell Biol.* **2008**, *9*, 112-124.

6) Thudicum, J. L. W.*A Treatise on the Chemical Composition of Brain.* London: Bailliere, Tindall and Cox, **1884**.

7) Lahiri, S.; Futerman, A. H. *Cell Mol. Life Sci.* **2007**, *64*, 2270-2284.

8) Merrill Jr, A. H.; Sullards, M. C.; Allegood, J. C.; Kelly, S.; Wang, E. *Methods.* **2005**, *36*, 207-224.

9) Koval, M.; Pagano, R. E. *Biochim. Biophys. Acta.* **1991**, *1082*, 113-125.

10) Barenholz, Y.; Thompson, T. E. *Chem. Phys. Lipids.* **1999**, *102*, 29-34.

11) Bloch, K. E. *CRC Crit. Rev. Biochem.* **1983**, *14*, 47-92.

12) Xu, F.; Rychnovsky, S. D.; Belani, J. D.; Hobbs, H. H.; Cohen, J. C.;Rawson, R. B. *Proc. Natl. Acad. Sci. U. S. A.* **2005**, *102*, 14551-14556.

13) Bhattacharya, S.; Haldar, S. *Biochim. Biophys. Acta.* **2000**, *1467*, 39-53.

14) Sadava, D. E. *Cell biology : organelle structure and function.* Boston [etc.]: Jones and Bartlett publishers, **1993**.

15) Gorter, E.; Grendel, F. *J. Exp. Med.* **1925**, *41*, 439-443.

16) Stoeckenius, W. *Circulation.* **1962**, *26*, 1066-1069.

17) Singer, S. J.; Nicolson, G. L. *Science.* **1972**, *175*, 720-731.

18) van Meer, G. *Annu. Rev. Cell Biol.* **1989**, *5*, 247-275.

19) Engelman, D. M. *Nature.* **2005**, *438*, 578-580.

20) (a) Simons, K.; Gerl, M. J. *Nat. Rev. Mol. Cell Biol.* **2010**, *11*, 688-699; (b) Simons, K.; van Meer, G. *Biochemistry.* **1988**, *27*, 6197-6202.

21) Simons, K.; Ikonen, E. *Nature.* **1997**, *387*, 569-572.

22) Brown, D. A.; Rose, J. K. *Cell.* **1992**, *68*, 533-544.

23) Brown, D. *Braz. J. Med. Biol. Res.* **1994**, *27*, 309-315.

24) Hooper, N. M. *Mol. Membr. Biol.* **1999**, *16*, 145-156.

25) Pike, L. J. *J. Lipid Res.* **2006**, *47*, 1597-1598.

26) Travis, J. *Science.* **2011**, *334*, 1046.

27) Dykstra, M.; Cherukuri, A.; Pierce, S. K. *J. Leukoc. Biol.* **2001**, *70*, 699-707.

28) Wu, L. C. *J. Biol. Chem.* **2011**, *286*, 32891-32897.

29) Janes, P. W.; Ley, S. C.; Magee, A. I.; Kabouridis, P. S. *Semin. Immunol.* **2000**, *12*, 23-34.

30) Janes, P. W.; Ley, S. C.; Magee, A. I. *J. Cell. Biol.* **1999**, *147*, 447-461.

31) Pierchala, B. A.; Milbrandt, J.; Johnson, E. M., Jr. *J. Neurosci.* **2006**, *26*, 2777-2787.

32) Roy, S.; Wyse, B.; Hancock, J. F. *Mol. Cell. Biol.* **2002**, *22*, 5128-5140.

33) Filmus, J.; Capurro, M. *Matrix Biol.* **2014**, *35*, 248-252.

34) Zhuang, L.; Kim, J.; Adam, R. M.; Solomon, K. R.; Freeman, M. R. *J. Clin. Invest.* **2005**, *115*, 959-968.

35) Waheed, A. A.; Freed, E. O. *Virus Res.* **2009**, *143*, 162-176.

36) Scheiffele, P.; Rietveld, A.; Wilk, T.; Simons, K. *J. Biol. Chem.* **1999**, *274*, 2038-2044.

37) Hancock, J. F. *Nat. Rev. Mol. Cell Biol.* **2006**, *7*, 456-462.

38) Vist, M. R.; Davis, J. H. *Biochemistry.* **1990**, *29*, 451-464.

39) Ipsen, J. H.; Karlstrom, G.; Mouritsen, O. G.; Wennerstrom, H.; Zuckermann, M. J. *Biochim. Biophys. Acta.* **1987**, *905*, 162-172.

40) McIntosh, T. J. *Biochim. Biophys. Acta.* **1978**, *513*, 43-58.

41) de Almeida, R. F.; Fedorov, A.; Prieto, M. *Biophys. J.* **2003**, *85*, 2406-2416.

42) Veatch, S. L.; Keller, S. L. *Phys. Rev. Lett.* **2002**, *89*, 268101.

43) Simons, K.; Vaz, W. L. *Annu. Rev. Biophys. Biomol. Struct.* **2004**, *33*, 269-295.

44) Lichtenberg, D.; Goni, F. M.; Heerklotz, H. *Trends Biochem. Sci.* **2005**, *30*, 430-436.

45) Sot, J.; Bagatolli, L. A.; Goni, F. M.; Alonso, A. *Biophys. J.* **2006**, *90*, 903-914.

46) Zurzolo, C.; van Meer, G.; Mayor, S. *EMBO Rep.* **2003**, *4*, 1117-1121.

47) Klymchenko, A. S.; Kreder, R. *Chem. Biol.* **2014**, *21*, 97-113.

48) Cruz, A.; Vazquez, L.; Velez, M.; Perez-Gil, J. *Langmuir.* **2005**, *21*, 5349-5355.

49) Baumgart, T.; Hunt, G.; Farkas, E. R.; Webb, W. W.; Feigenson, G. W. *Biochim. Biophys. Acta.* **2007**, *1768*, 2182-2194.

50) Sengupta, P.; Hammond, A.; Holowka, D.; Baird, B. *Biochim. Biophys. Acta.* **2008**, *1778*, 20-32.

51) Sezgin, E.; Levental, I.; Grzybek, M.; Schwarzmann, G.; Mueller, V.; Honigmann, A.; Belov, V. N.; Eggeling, C.; Coskun, U.; Simons, K.; Schwille, P. *Biochim. Biophys. Acta.* **2012**, *1818*, 1777-1784.

52) Chiantia, S.; Ries, J.; Kahya, N.; Schwille, P. *Chem. Phys. Chem.* **2006**, *7*, 2409-2418.

53) Chiantia, S.; Kahya, N.; Schwille, P. *Langmuir.* **2007**, *23*, 7659-7665.

54) Lozano, M. M.; Liu, Z.; Sunnick, E.; Janshoff, A.; Kumar, K.; Boxer, S. G. *J. Am. Chem. Soc.* **2013**, *135*, 5620-5630.

55) Fujita, K.; Smith, N. I. *Mol. Cells.* **2008**, *26*, 530-535.

56) Yamakoshi, H.; Dodo, K.; Okada, M.; Ando, J.; Palonpon, A.; Fujita, K.; Kawata, S.; Sodeoka, M. *J. Am. Chem. Soc.* **2011**, *133*, 6102-6105.

57) Yamakoshi, H.; Dodo, K.; Palonpon, A.; Ando, J.; Fujita, K.; Kawata, S.; Sodeoka, M. *J. Am. Chem. Soc.* **2012**, *134*, 20681-20689.

58) Wei, L.; Hu, F.; Shen, Y.; Chen, Z.; Yu, Y.; Lin, C. C.; Wang, M. C.; Min, W. *Nat. Methods.* **2014**, *11*, 410-412.

59) Mendelsohn, R.; Koch, C. C. *Biochim. Biophys. Acta.* **1980**, *598*, 260-271.

60) Seelig, J.; Macdonald, P. M. *Acc. Chem. Res.* **1987**, *20*, 221-228.

61) Steinbauer, B.; Mehnert, T.; Beyer, K. *Biophys. J.* **2003**, *85*, 1013-1024.

62) Oldfield, E.; Meadows, M.; Rice, D.; Jacobs, R. *Biochemistry.* **1978**, *17*, 2727-2740.

63) Veatch, S. L.; Polozov, I. V.; Gawrisch, K.; Keller, S. L. *Biophys. J.* **2004**, *86*, 2910-2922.

64) Bartels, T.; Lankalapalli, R. S.; Bittman, R.; Beyer, K.; Brown, M. F. *J. Am. Chem. Soc.* **2008**, *130*, 14521-14532.

65) Mehnert, T.; Jacob, K.; Bittman, R.; Beyer, K. *Biophys. J.* **2006**, *90*, 939-946.

66) Matsumori, N.; Yasuda, T.; Okazaki, H.; Suzuki, T.; Yamaguchi, T.; Tsuchikawa, H.; Doi, M.; Oishi, T.; Murata, M. *Biochemistry.* **2012**, *51*, 8363-8370.

67) Krogh, A.; Larsson, B.; von Heijne, G.; Sonnhammer, E. L. *J Mol Biol.* **2001**, 305, 567-580.

68) Lee, A. G. *Mol. Biosyst.* **2005**, *1*, 203-212.

69) Seddon, A. M.; Curnow, P.; Booth, P. J. *Biochim. Biophys. Acta.* **2004**, *1666*, 105-117.

70) Wettschureck, N.; Offermanns, S. *Physiol. Rev.* **2005**, *85*, 1159-1204.

71) Long, S. B.; Tao, X.; Campbell, E. B.; MacKinnon, R. *Nature.* **2007**, *450*, 376-382.

72) Resh, M. D. *Nat. Chem. Biol.* **2006**, *2*, 584-590.

73) Bhatnagar, R. S.; Gordon, J. I. *Trends Cell Biol.* **1997**, *7*, 14-20.

74) Xu, K.; Zhong, G.; Zhuang, X. *Science.* **2013**, *339*, 452-456.

75) Smith, S. M. *Methods Mol. Biol.* **2011**, *681*, 485-496.

76) Lee, A. G. *Biochim. Biophys. Acta.* **2003**, *1612*, 1-40.

77) Simmonds, A. C.; East, J. M.; Jones, O. T.; Rooney, E. K.; McWhirter, J.; Lee, A. G. *Biochim. Biophys. Acta.* **1982**, *693*, 398-406.

78) Palsdottir, H.; Hunte, C. *Biochim. Biophys. Acta.* **2004**, *1666*, 2-18.

79) Nielsen, C.; Goulian, M.; Andersen, O. S. *Biophys. J.* **1998**, *74*, 1966-1983.

80) Soubias, O.; Niu, S. L.; Mitchell, D. C.; Gawrisch, K. *J. Am. Chem. Soc.* **2008**, *130*, 12465-12471.

81) Stoeckenius, W.; Lozier, R. H.; Bogomolni, R. A. *Biochim. Biophys. Acta.* **1979**, *505*, 215-278.

82) Freisleben, H. J.; Zwicker, K.; Jezek, P.; John, G.; Bettin-Bogutzki, A.; Ring, K.; Nawroth, T. *Chem. Phys. Lipids.* **1995**, *78*, 137-147.

83) Kuhlbrandt, W. *Nature.* **2000**, *406*, 569-570.

84) Lanyi, J. K. *Biochim. Biophys. Acta.* **2006**, *1757*, 1012-1018.

85) Luecke, H.; Schobert, B.; Richter, H. T.; Cartailler, J. P.; Lanyi, J. K. *J. Mol. Biol.* **1999**, *291*, 899-911.

86) Corcelli, A.; Lattanzio, V. M.; Mascolo, G.; Papadia, P.; Fanizzi, F. *J. Lipid Res.* **2002**, *43*, 132-140.

87) Cartailler, J. P.; Luecke, H. *Annu. Rev. Biophys. Biomol. Struct.* **2003**, *32*, 285-310.

88) Mukhopadhyay, A. K.; Bose, S.; Hendler, R. W. *Biochemistry.* **1994**, *33*, 10889-10895.

89) Dracheva, S.; Bose, S.; Hendler, R. W. *FEBS Lett.* **1996**, *382*, 209-212.

90) Tanio, M.; Tuzi, S.; Yamaguchi, S.; Konishi, H.; Naito, A.; Needleman, R.; Lanyi, J. K.; Saito, H. *Biochim. Biophys. Acta.* **1998**, *1375*, 84-92.

91) Pomerleau, V.; Harvey-Girard, E.; Boucher, F. *Biochim. Biophys. Acta.* **1995**, *1234*, 221-224.

92) Kates, M.; Moldoveanu, N.; Stewart, L. C. *Biochim. Biophys. Acta.* **1993**, *1169*, 46-53.

93) Grigorieff, N.; Beckmann, E.; Zemlin, F. *J. Mol. Biol.* **1995**, *254*, 404-415.

94) Sternberg, B.; L'Hostis, C.; Whiteway, C. A.; Watts, A. *Biochim. Biophys. Acta.* **1992**, *1108*, 21-30.

Chapter 2

Synthesis of Raman-tagged Sphingomyelin and Elucidation of Lipid Organization in Raft-like Domains

2.1 Introduction

Lipid rafts show a similar character to the lipid ordered (L_o) phase in artificial membranes, which are often represented by microdomains enriched with sphingolipids and chol. The physicochemical properties of the specific lipids are believed to be important for fulfilling the rafts' functions such as cellular signal transduction.[1)] To gain better insight into the role of lipid rafts in these processes, a direct optical visualization of such domains is essential. However, the task in raft imaging has not been truly achieved due to the lack of a suitable raft-specific probe. Fluorescent microscopy is the most common method to obtain information on molecular localization. This method usually requires doping of the membranes with fluorescently labeled lipids. However, the probes attached with a relatively large fluorophore possess physical properties that are distinct from the small lipid molecules, and usually alter the membrane properties.[2)] In model membranes, the chemical modification of a lipid molecule with a fluorescent moiety usually results in an inconsistent, or even completely opposite, distribution tendency in the membrane phases.[3)]

In contrast, Raman-active moieties are considered to have less influence on the membrane properties due to their small size. Over the last several years, cellular imaging by Raman spectroscopy has attracted much attention. The Raman image can be generated by measuring a specific molecular vibration to locate the Raman-tagged molecules.[4)] Raman-active alkyne, diyne, azide, deuterium, and nitrile groups give rise to Raman scattering bands in the cellular silent region (1800–2800 cm^{-1}), in which most endogenous biomolecules do not exhibit a signal. This indicates the potential value of the incorporation of these groups into small molecules as Raman tags. [5)] Alkyne-tagged coenzyme Q (CoQ) and 5-ethynyl-2′-deoxyuridine (EdU) analogs have been recently used for imaging microscopy in living HeLa cells.[5)] The most significant features of this tag are its suitable wavenumber of the Raman band and strong scattering intensity, which allow high-contrast Raman imaging. Deuterium is expected to be another promising candidate due to its small size and good physical compatibility. Although the Raman intensity derived from the C–D bond is relatively week, multiple-deuterated methylene or methyl groups may generate

relatively strong Raman signals. Thus, these tags could be further applied in raft-specific lipids to mark raft-like domains.

In order to observe domain formation by Raman microscopy, previous studies have adopted acyl-labeled Raman probes such as DPPC-d_{62} or DSPC-d_{70}, in which the glycerophospholipid was labeled with perdeuterated fatty acids.[6)] Although the acyl deuterated probes are believed to have excellent compatibility with the natural lipids, the hydrocarbon packing in membrane are slightly different between highly deuterated and non-deuterated acyl chains.[6a,7)] The lipid rafts are best characterized by the highly packed acyl chains, as is the case with the L_o phase in artificial membranes. A small but significant perturbation in the acyl chains behavior caused by full deuteration may disturb the elucidating of the precise phase properties of the original lipid.

In contract, since the polar head of phospholipids is relatively loosely packed even in the L_o-phase, this portion is occasionally more suitable for chemical modifications. Thus, for investigating the atomistic mechanism underlying formation of the raft-mimicking L_o phase, besides acyl chain-tagged Raman probes, those with a small tag on the head group can be complimentarily used in the imaging of membrane domains.

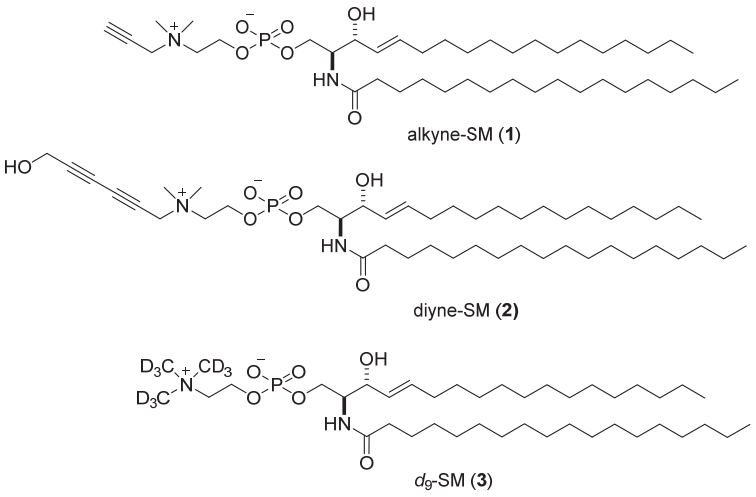

In this Chapter, three polar head modified Raman-tagged SMs (**1**, **2** and **3**) have been designed and synthesized. Their Raman spectra have been measured in a monolayer form. Membrane behaviors of the promising candidates have been evaluated using solid-state ^{2}H NMR. Two probes possess terminal alkyne and hydroxymethyl-1,3-butadiyne groups, respectively; The third probe is

labeled with nine deuterium atoms at the trimethyl ammonium moiety, which encompasses the largest number of chemically equivalent C-D bonds in the polar head of SM. All of the probes possess a stearoyl (C18:0) moiety since stearic acid is one of the common acyl groups in SMs, particularly in those of bovine brain.[8)]

2.2 Results and Discussion

2.2.1 Synthesis of Alkyne-SM, Diyne-SM, and d_9-SM

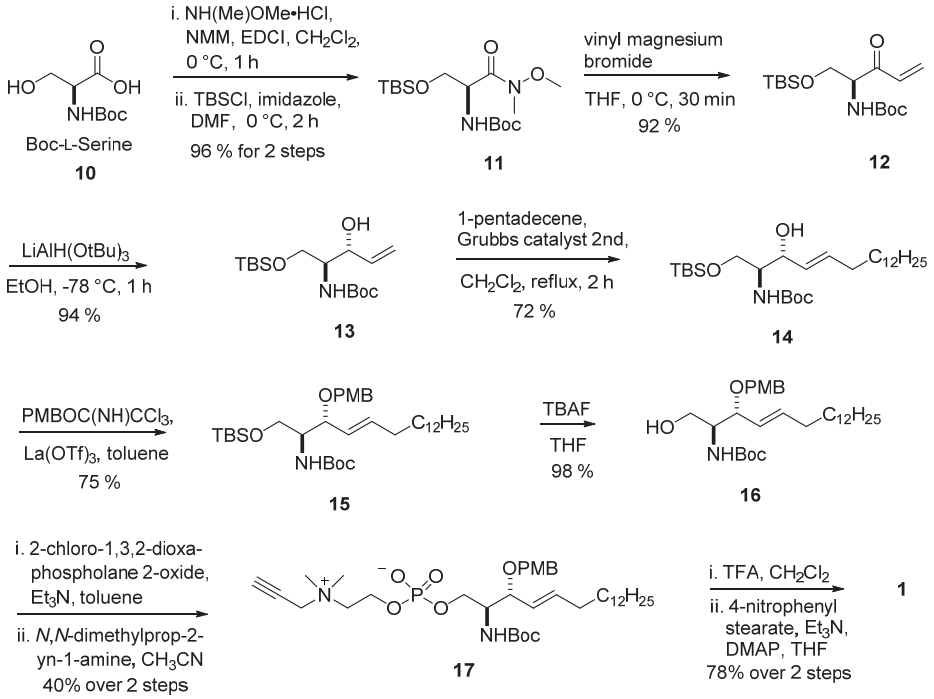

Scheme 2-1. Synthesis of alkyne-SM **1**.

As shown in Scheme 2-1, alkyne-SM **1** was synthesized from Boc-L-serine through a protected sphingosine using a partially modified procedure from those in previous reports.[9,10] The reaction mechanism of the selected steps in this sequence will be described in the following sections.

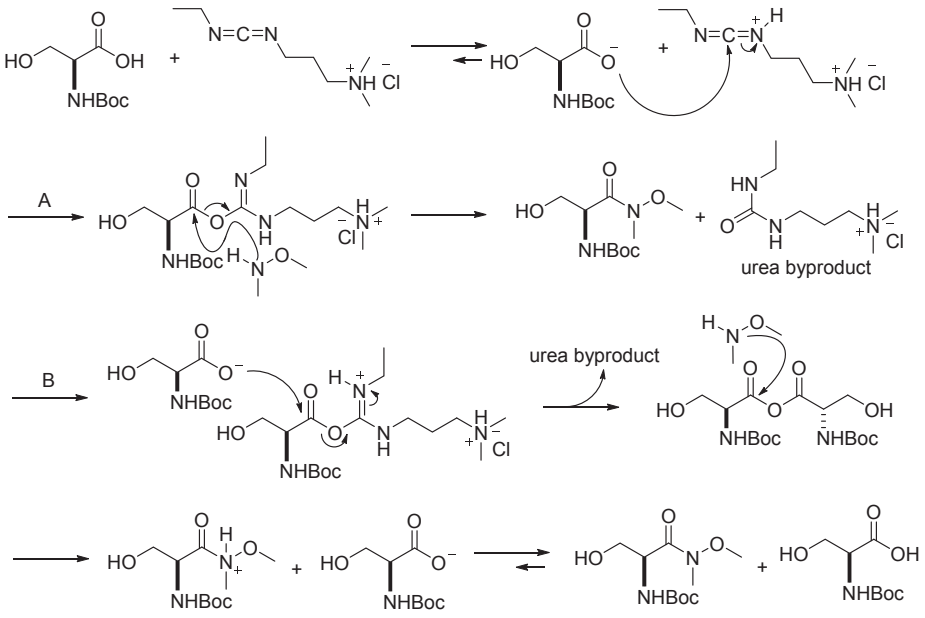

Scheme 2-2. Condensation reaction.

In the condensation reaction, 1-ethyl-3-(3-dimethylaminopropyl)carbodiimide hydrochloride (EDCI) was used to active the carboxylic acid for crosslinking. The detailed mechanism is shown in Scheme 2-2. There are two possible routes (A and B) for generating the desired Weinreb amide.[11a)]

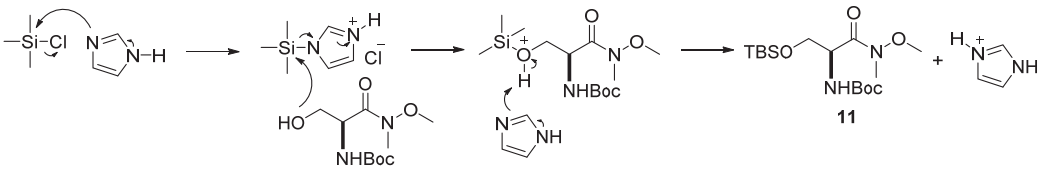

Scheme 2-3. TBS protection of Weinreb amide.

Using imidazole as catalyst, the primary alcohol of the Weinreb amide was protected with *t*-butyldimethylsilyl (TBS) ether. (Scheme 2-3)

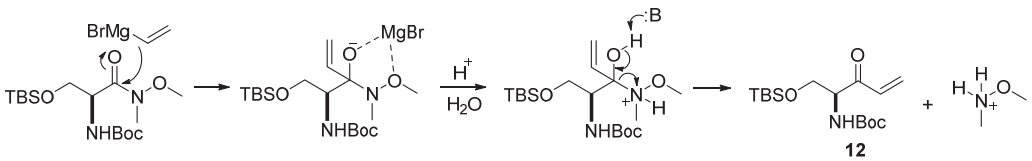

Scheme 2-4. Synthesis of olefin ketone **12**.

For the reaction of organometallic reagents with acid derivatives, such as ester and acid chloride, the substrate will add two equivalents of organometallic compound. For the Weinreb amide, the organometallic adduct of this compound is able to form a stable chelate, and it will not regenerate an electrophilic carbonyl group in situ for further reaction. Acidic aqueous work up liberates the desired ketone **12** from this chelate.[11b] (Scheme 2-4)

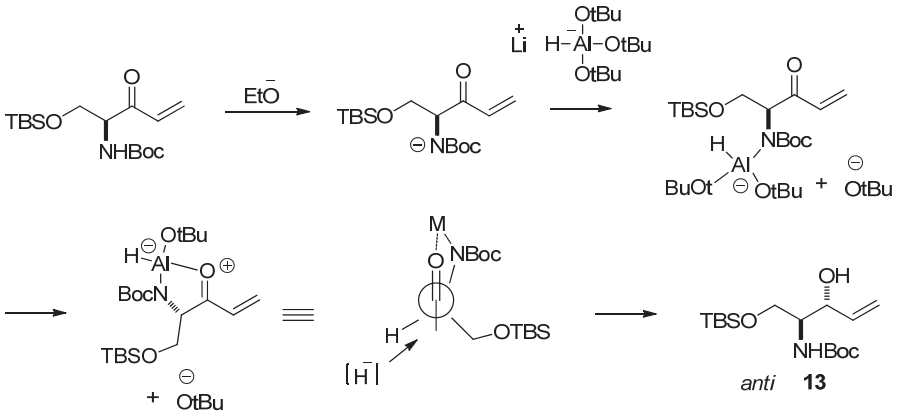

Scheme 2-5. Selective reduction of olefin ketone **13**.

The selective reduction of olefin ketone has been established using aluminum which can form only weak complexes with neutral species but much stronger complexes with anionic species.[12,13] (Scheme 2-5) The ethoxide generated in the reaction condition deprotonates the NHBoc to initiate a complex formation and a chelate formation. The Boc-protected amino ketone is converted to a deprotonated carbamate, which could bind to aluminum through nitrogen, followed by chelate formation to the carbonyl oxygen. Stereoselective reduction of the chelated amino ketone can give desired amino alcohol due to steric hindrance by using chelation control which enforces a syn-periplanar relationship between the amine and ketone groups, and leads to the formation of the anti-amino alcohol with high yields.[14]

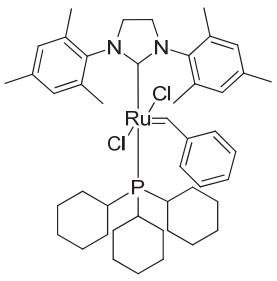

Figure 2-1. Chemical structure of Grubbs catalyst 2nd.

Next, using reported method, substrate **13** was stirred with 4 equiv of olefin and catalytic amount of Grubbs catalyst second generation (Figure 2-1) in dichloromethane at reflux. The reaction proceeded smoothly, and desired product was obtained as sole (*E*)-stereoisomer in good yield.

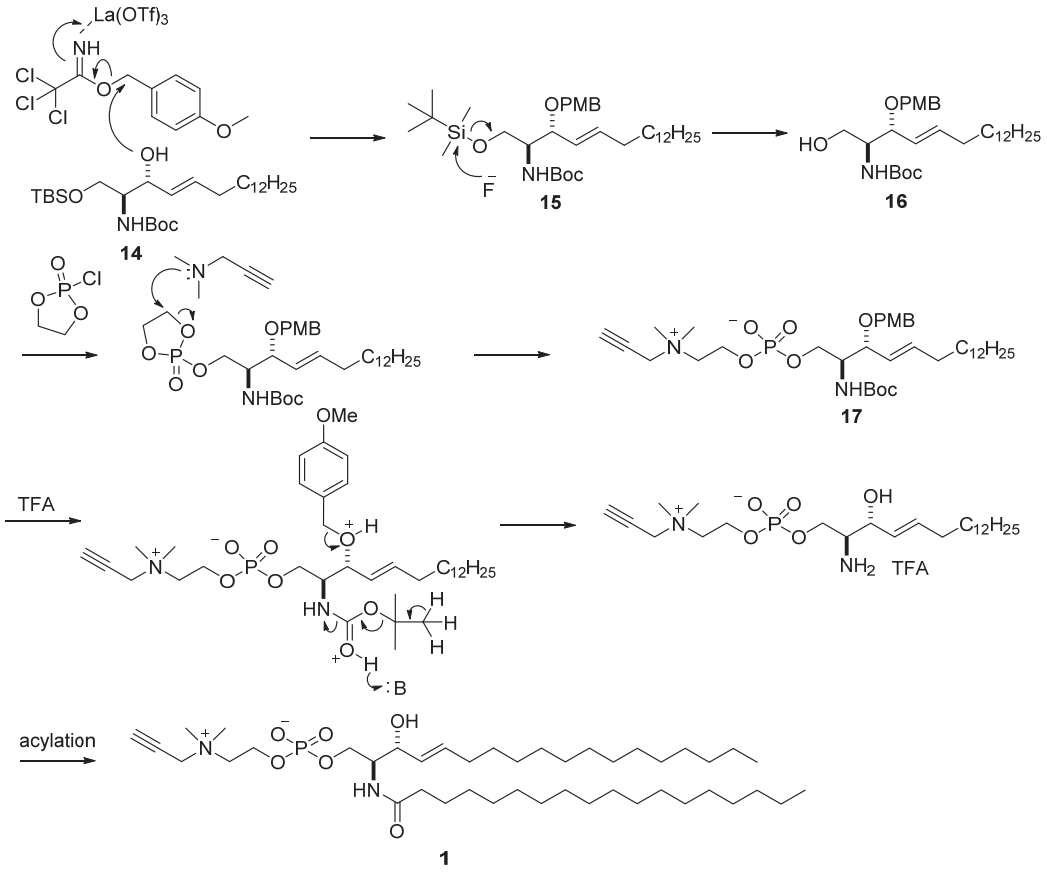

Scheme 2-6. Synthesis of alkyne SM **1**.

Protection of the secondary OH of **14** catalyzed by Lanthanum (III) triflate ($La(OTf)_3$) afforded intermediate **15**. The cleavage of silyl ether in **15** with *tetra*-n-butylammonium fluoride (TBAF) in THF yielded alcohol **16**. The alkynyl intermediate **17** was synthesized by the treatment of cyclic phospholane with *N,N*-dimethylprop-2-yn-1-amine in acetonitrile.[10] Simultaneous removal of PMB and Boc groups using trifluoroacetic acid followed by acylation with 4-nitrophenyl stearate furnished alkyne SM **1**. (Scheme 2-6)

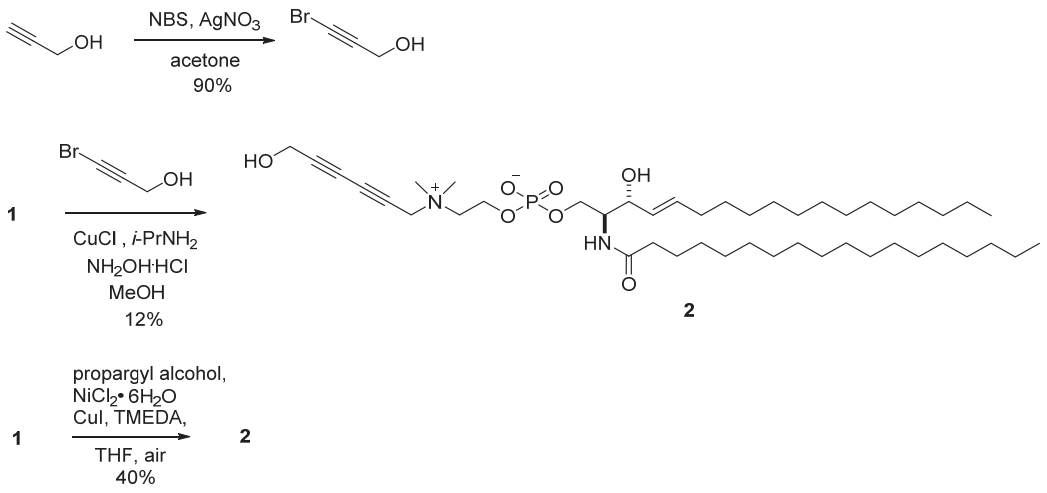

Scheme 2-7. Synthesis of diyne-SM **2**.

Initially, Cadiot–Chodkiewicz coupling was opted to synthesize the diyne probe using 3-bromoprop-2-yn-1-ol as the coupling partner under the classical coupling conditions (copper (I) chloride, 5 mol %; hydroxylamine, 30 mol %; *i*-$PrNH_2$ in aqueous methanol). (Scheme 2-7)[15] Unfortunately, it was difficult to drive the coupling to completion and only a modest conversion was achieved, as judged by ^1H NMR. Furthermore, the remaining alkyne **1** was hardly separable from compound **2** due to their similar polarities. The Lei group reported a mild Ni/Cu-cocatalyzed oxidative coupling reaction, by which the C_{sp}–C_{sp} coupling was performed in a manner favoring the formation of the heterocoupled product over the homocoupled products by increasing the molar ratio of the two terminal alkynes.[16] Based on their conditions, the coupling of **1** with a large excess of propargyl alcohol enabled selective conversion to **2**, which was easily separated by flash chromatography, although the isolated yield was modest (40%). (Scheme 2-7)

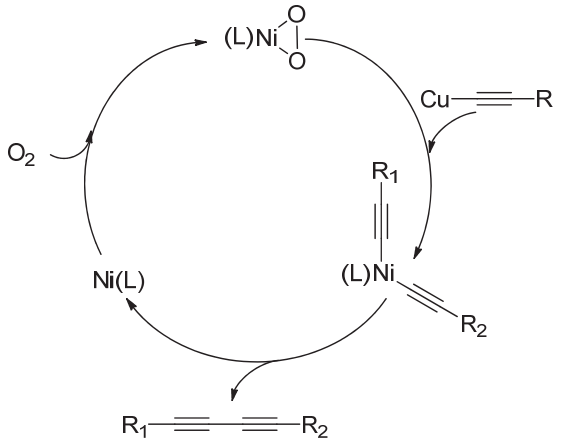

Figure 2-2. Proposed reaction pathways of alkyne cross-couplings.

As described in the reported paper[16], the reaction is proposed to start from oxidation of the Nickel complex by oxygen to generate a Ni(O_2) intermediate, which is transmetalated with an copper alkynyl reactive specie to generate a dialkynyl-Ni intermediate. The reductive elimination release the crosss-coupled product and regenerate the Ni(0) complex. (Figure 2-2)

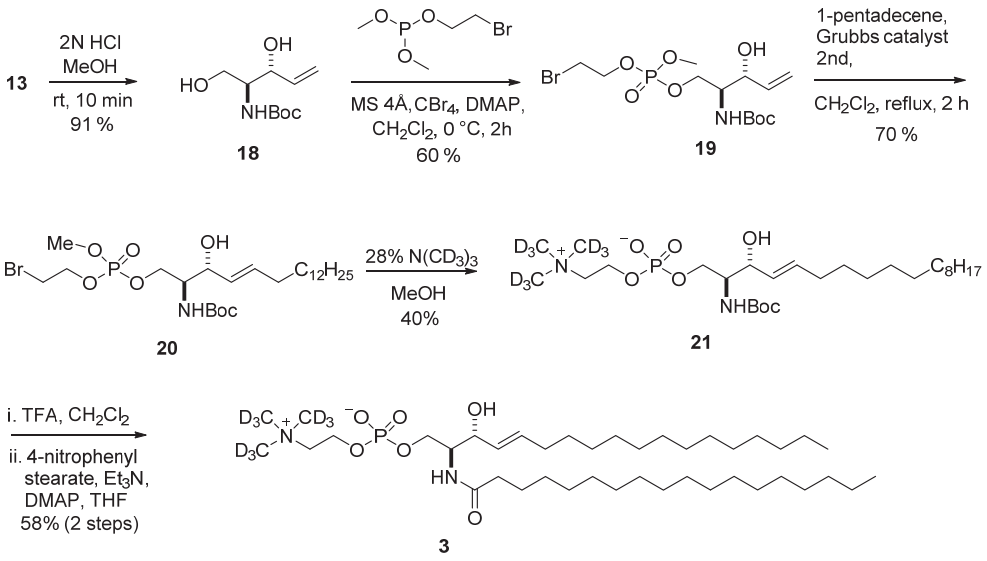

Scheme 2-8. Synthesis of d_9-SM **3**.

As shown in Scheme 2-8, TBS deprotection of **13** followed by phosphorylation and olefination yields compound **19**, which is treated with 28% $N(CD_3)_3$ solution in MeOH furnished **21** in a modest yield.[9] Boc deprotection by TFA, followed by acylation with *p*-nitrophenyl stearate, produced the desired compound **3**.

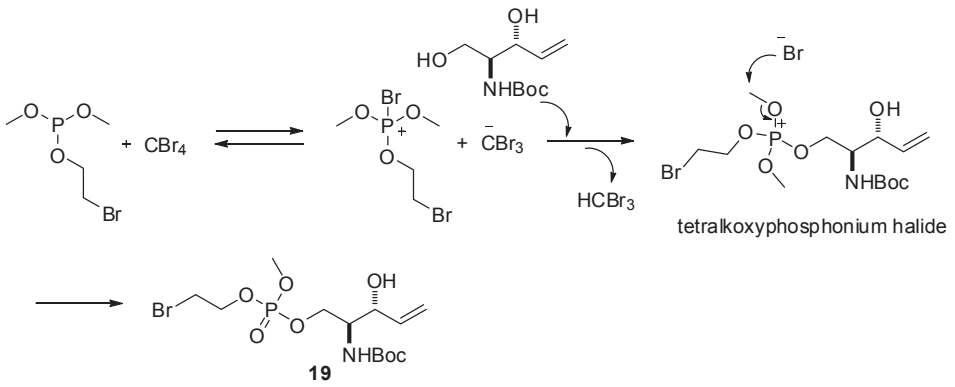

Scheme 2-9. Reaction mechanism of phosphorylation.

As shown in Scheme 2-9, the phosphorylation procedure includes the oxidation of phosphites by carbon tetrahalides in the presence of alcohols, which was first reported by Burn and Cadogan.[17] The reaction was used for synthesizing protected phosphate esters from alcohols.[18] The preparation of 2-bromoethyl dimethyl phosphite was reported by Katsumura *et al*.[19]

2.2.2 Relative Raman Shift and Intensity of Alkyne-SM, Diyne-SM, and d_9-SM

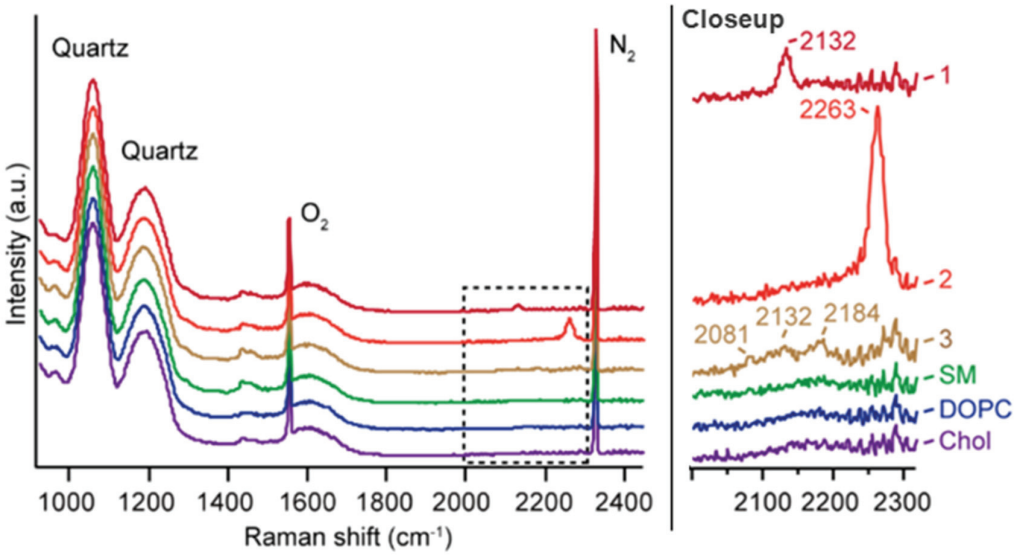

Figure 2-3. Raman spectra of pure alkyne-SM **1**, diyne-SM **2**, SM-d_9 **3**, SM, DOPC, and chol in quartz supported monolayers. Exposure time was 6 s. Raman measurements were performed for 30 times per sample. Averaged Raman spectra are displayed in the image.

The relative Raman shift and intensity of these Raman probes have been compared using their

monolayer systems prepared by the Langmuir–Blodgett (LB) technique. As shown in Figure 2-3, the signals from diynes, alkynes, and C–D bonds, are observed in the cellular silent region, where no Raman band occurs from non-labeled SM, 1,2-dioleoyl-sn-glycero-3-phosphocholine (DOPC) or chol; these three lipids are the constituents of raft-model membranes. The triple bond in alkyne-SM **1** shows a single Raman peak at 2132 cm^{-1}. The conjugated triple bonds in diyne-SM **2** show a significantly enhanced intensity and peak shifts to longer wavelengths at 2263 cm^{-1} and give rise to an approximately five-fold greater peak height than does the alkyne in **1**. Thus, the strong Raman peak of the diyne group facilitated clear imaging of **2** in artificial membranes, whereas the imaging from **1** was obscure due to its weak Raman signal. In the case of SM-d_9 **3**, the observed peaks can be assigned to symmetric CD_3 stretching at 2184 cm^{-1}, and Fermi resonance multiplets at 2132^{-1} and 2081 cm^{-1} with overtone or combination tone of CD_3 deformation. The apparent Raman intensity of the deuterated methyl groups is lower than that of alkyne **1**.

2.2.3 Differential Scanning Calorimetry Study

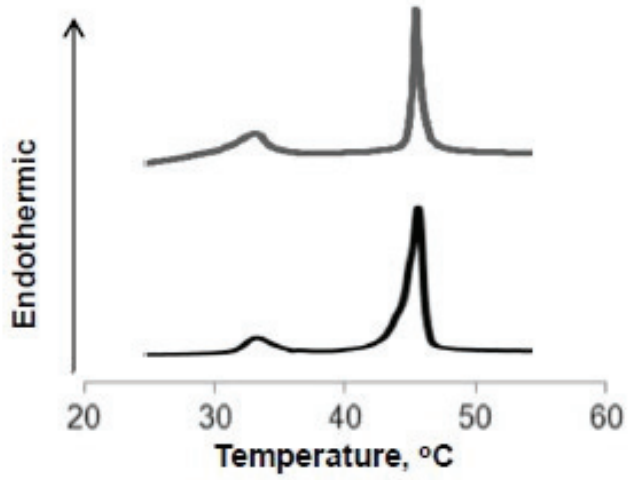

Figure 2-4. Differential scanning calorimeter (DSC) curve of compound **3** (top) and native SM (bottom).

A differential scanning calorimeter (DSC) study of compound **3** showed that its phase transition temperature is 44.5 ºC (Figure 2-4), which is the same as that of native SM, indicating it should

have phase behavior similar to that of SM. However, this probe did not give rise to intense Raman bands. Thus, the compatibility of **1** and **2** with natural SM has been evaluated.

2.2.4 Preparation of Oriented Membranes

The macroscopically aligned membranes, in which the bilayer normal is perpendicular to the magnetic field direction, have improved spectral resolution and sensitivity compared to powder pattern samples. The theromdynamics of the candidate probes have been studied in such an oriented membrane system. A sample preparation procedure is shown in Figure 2-5. Compared with the preparation of liposome, the amount of sample needed for the formation of oriented membrane is reduced. Totally 2 mg of lipids were deposited on 14 glass slides, and each slide contains around one thousand lipid bilayers aligned mechanically between each pair of glass surfaces. Once the organic solvent was completely removed, the slides were stacked and hydrated with K_2SO_4-saturated deuterium-depleted water at 96% relative humidity and 40 °C for 3 days before inserting into an open-ended NMR tube. The tube was sealed after rehydration for ~12h. The final sample should be clear.

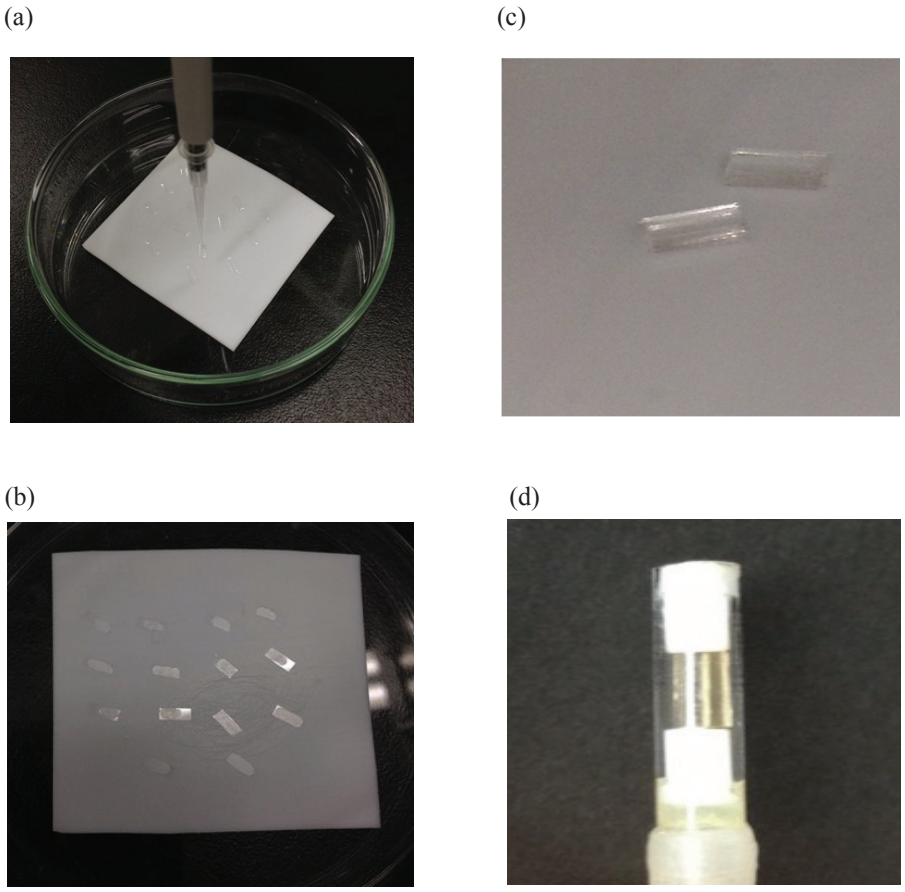

Figure 2-5. Sample preparation for oriented multibilayers formed on glass plates. (a) Lipids in organic solvent were deposited on the glass slides. (b) The organic solvent was completely removed under vacuum. (c) The slides were stacked and hydrated. (d) The slides were transferred into a NMR tube.

2.2.5 ^{2}H NMR Study of *d*-Chol in Oriented Membranes

By using ^{2}H NMR of 3α-deuterated chol (*d*-chol),[20] it is possible to quantify the molecular ordering of chol in the host lipid bilayers and to quantitatively characterize the physicochemical properties of the mixed lipid membranes.[21] As shown in Figure 2-6, the ^{2}H NMR spectra of *d*-chol provided a sharp quadrupolar doublet (45.3 kHz), which was assigned to *d*-chol embedded in the DOPC bilayers.[22] Among artificial membranes, ternary SM/chol/DOPC bilayers are often used as a model to mimic raft-like domains. In this system (Figure 2-6, **b**), a second set of more ordered peaks appeared, indicating that the raft-like liquid ordered (L_o) domains was formed. The inner

shoulders correspond to the DOPC-rich L_d phases as indicated by the same splitting width as that of the DOPC-chol membrane. The major fraction of *d*-chol was partitioned to the L_o phases, as shown by the higher intensity of the outer quadrupole splitting. This uneven distribution of *d*-chol demonstrates direct experimental evidence in support of the preferential affinity of chol for SM over DOPC. The L_o-liquid/L_d-liquid immiscibility was also observed in the **1**/*d*-chol/DOPC (1/1/1 mol) and **2**/*d*-chol/DOPC (1/1/1 mol) mixtures (Figure 2-6, **b** and **c**). Similarly, the preference of chol by **1** and **2** was revealed by the presence of the larger outer doublet. The intensity of the inner peak of **1** is comparable to that of the SM mixture; the inner doublet peak of the **2**-containing mixture was slightly higher than that of the SM and **1** systems. Since the quadrupolar splitting magnitude $\Delta\nu_Q$ is not dependent on the orientation of a chol molecule in membranes but mostly on the ordering of phospholipid/chol mixed domains under present conditions,[21,23] the observed $\Delta\nu_Q$ values, which are usually expressed in terms of the molecular order parameter (S_{CD}), largely represents the wobbling motion of the rigid skeleton of chol in the L_o and L_d phases. For each phase, the almost identical S_{CD} values are observed for the SM, **1**, and **2** mixtures, indicating that the membrane rigidity and/or fluidity for the **1** and **2** mixtures are very similar to those of SM. A comparation of $\Delta\nu_Q$ and S_{CD} is shown in Table 2-1.

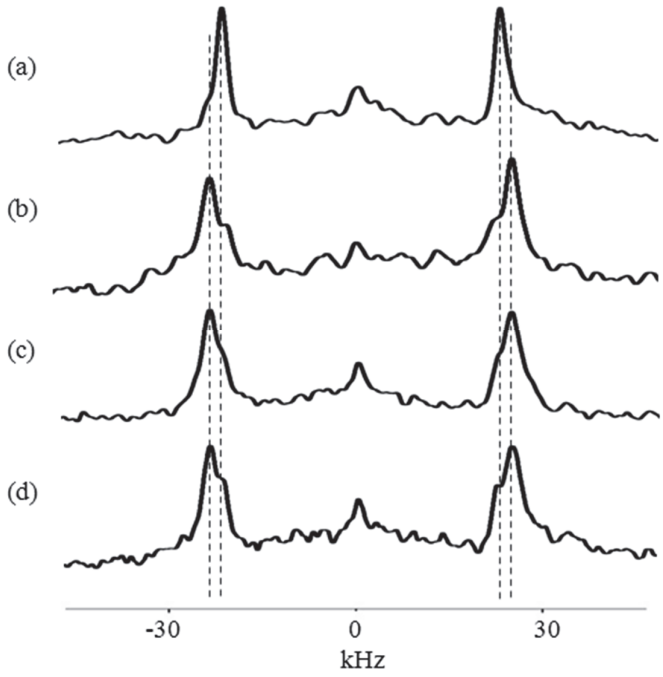

Figure 2-6. ^{2}H NMR spectra from oriented multi-bilayers. (a) *d*-chol/DOPC (1/1 mol), (b) SM/*d*-chol/DOPC (1/1/1 mol), (c) **1**/*d*-chol/DOPC (1/1/1 mol) and (d) **2**/*d*-chol/DOPC (1/1/1 mol) at 25 °C.

Table 2-1. Molecular ordering of chol-*d* in SM, **1** and **2** membranes determined by ^{2}H NMR at 25 °C

	SM/*d*-chol/DOPC (1/1/1 mol)	**1**/*d*-chol/DOPC (1/1/1 mol)	**2**/*d*-chol/DOPC (1/1/1 mol)
$\Delta\nu_Q$[a](L_o)	48.2 kHz	47.7 kHz	47.8 kHz
$\Delta\nu_Q$ (L_d)	43.1 kHz	43.9 kHz	43.7 kHz
S_{CD}[b](L_o)	0.38	0.38	0.38
S_{CD} (L_d)	0.34	0.35	0.35

[a] Quadrupolar splitting.

[b] Order parameter, describing the motion of the C–D bond with respect to the bilayer normal. This value can be calculated via the following equation: $\Delta\nu_Q = (3/4)\,(e^2qQ/h)\,|S_{CD}|$, where e^2qQ/h = 168 kHz is the static quadrupolar coupling constant.

To further assess their similarity to SM in phase behaviour, the lateral distribution and ordering

using oriented multi-bilayers containing selectively deuterated SM (d_2-SM),[24] deuterated alkyne-SM **4** and diyne-SM **5** have been examined. Herein, the oriented membrane containing selectively ^{2}H-labeled acyl chains was adopted to avoid overlapping of quadrupole doublet signals[25] and to observe the minor signals in the L_d phase. Another unfavorable effect from perdeuterated lipids is that they can alter the physical properties of lipid bilayers as described above.[26] Previous study indicated that chol enhances the order of the C10 position more effectively than other positions in the acyl chains of SM,[24] implying that the ^{2}H NMR spectrum should show clearly separated signals for the L_o and L_d phases.

2.2.6 Synthesis of d_2-SM, d_2-Alkyne-SM, and d_2-Diyne-SM

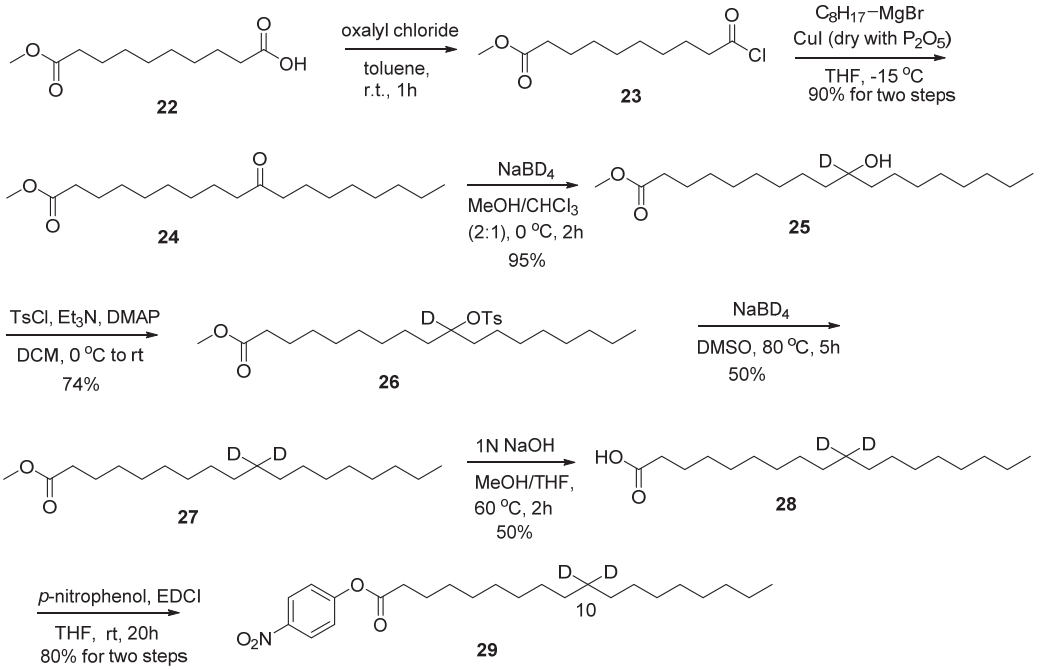

Scheme 2-10. Synthesis of C10-deuterated acyl chain.

The synthetic method of C10-deuterated acyl chain is shown in Scheme 2-10. The key step is the coupling reaction between acyl chloride and Grignard reagent using copper(I) iodide as catalyst. To obtain a high yield, one equivalent of butylmagnesium bromide was used and was added slowly in the mixture of acyl chloride and dry CuI in THF over 1 h.

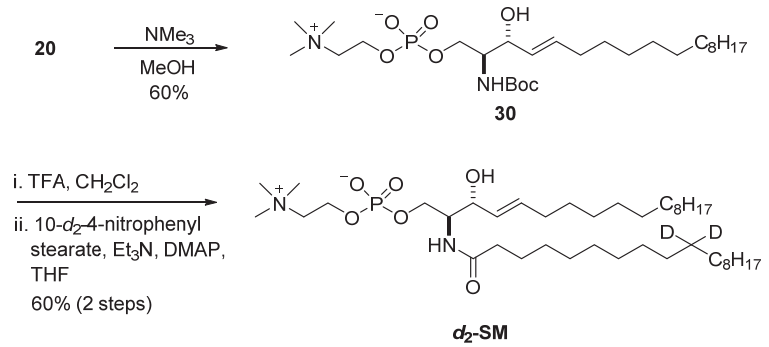

Scheme 2-11. Synthesis of d_2-SM.

d_2-SM was synthesized based on the synthetic method [9] described in Scheme 2-11, and used as a control for ^{2}N NMR measurements.

An alternate synthetic route to the deuterated acyl chain for synthesizing deuterium-labled lipids has been developed in this work. (Scheme 2-12) Compare to the method in Scheme 2-10, the alternate route is more efficient. The key step in the sequence is a copper-catalyzed Kumada–Corriu coupling.

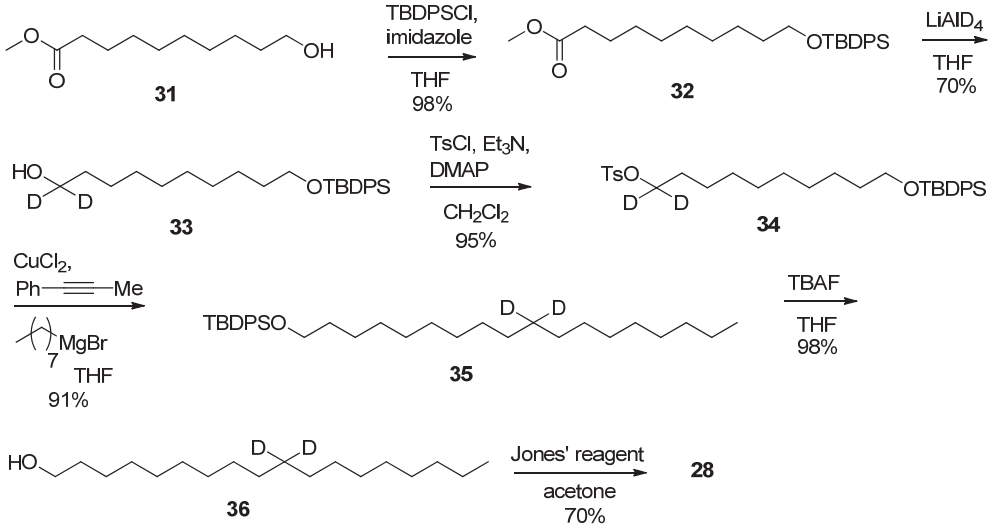

Scheme 2-12. An alternate synthetic route to C10-deuterated acyl chain **28**.

Protection of the primary alcohol group of **31** afforded compound **32**. Reduction of the ester with $LiAlD_4$, followed by tosylation, provided deuterated intermediate **34**. The tosylated precursor has been recently considered as a more suitable coupling partner than the brominated one for C_{sp3}-C_{sp3} Kumada–Corriu coupling.[27] Compound **34** was subsequently coupled with a Grignard

reagent to afford **35** in excellent yield (91%). Removal of *t*-butyldiphenylsilyl (TBDPS), followed by Jones' oxidation, led to **28**, which was then converted into the corresponding active ester **29** by a condensation reaction with *p*-nitrophenol. Using the same synthetic method as for compound **1** and **2**, the deuterated Raman probes **4** and **5** were synthesized.

2.2.7 ^{2}H NMR Measurements of d_2-SM, d_2-Alkyne-SM, and d_2-Diyne-SM

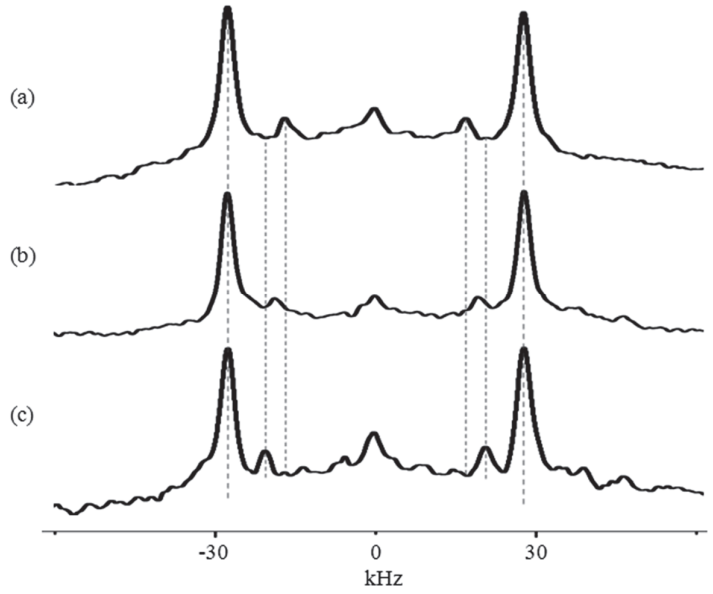

Figure 2-7. ^{2}H NMR spectra from oriented multi-bilayers. (a) d_2-SM/DOPC/ chol (1/1/1 mol), (b) **4**/DOPC/chol (1/1/1 mol) and (c) **5**/DOPC/chol (1/1/1 mol) at 25 °C.

Figure 2-7 shows the ^{2}H NMR spectra of d_2-SM/chol/DOPC (1/1/1 mol), **4**/chol/DOPC (1/1/1 mol), and **5**/chol/DOPC (1/1/1 mol). Two pairs of resolved doublets are displayed for d_2-SM /chol/DOPC, indicating the presence of two immiscible liquid phases with different lipid components, which confirmed the observed raft formation in the SM/*d*-chol/DOPC mixtures. A large majority of d_2-SM is found in the L_o phases with a quadrupolar splitting of 55.3 kHz (S_{CD} = 0.44), while a small fraction pertains to the L_d phases, as characterized by a splitting at 34.1 kHz (S_{CD} = 0.27). Coupled with the phase distribution of chol-*d* in L_o/L_d phases, this result reflects that, in the L_o phase, the molar ratio of SM to chol will be more than 1/1.

A comparison of the spectra of **4** and **5** with that of d_2-SM shows a high degree of conformity in

phase redistribution. Excellent preferences of **4** and **5** for the L_o phase were observed (Figure 2-7, **b** and **c**), although the inner peak intensity of **5** is slightly larger than those of the other two membranes. The quadrupolar splitting magnitudes of **4** and **5** in the L_o phase are $\Delta\nu_Q$ = 55.2 kHz (S_{CD}, 0.44), and $\Delta\nu_Q$ = 55.4 kHz (S_{CD}, 0.44), respectively. The S_{CD} values are the same as that obtained from d_2-SM, and are close to the maximum value, 0.5, indicating that the ternary mixtures show a typical characteristic of the L_o phases.[28] These results revealed that the molecular orientation and mobility in the raft-like L_o domains are minimally affected by the alkyne and diyne head groups. Interestingly, these analogues showed increased quadrupolar splitting of the inner peaks compared with that of d_2-SM. In the L_d phases, the $\Delta\nu_Q/S_{CD}$ of d_2-SM, **4** and **5** is 34.1 kHz/0.27, 38.3 kHz/0.30 and 41.0 kHz/0.33, respectively. The increase in order is accompanied by an increase of head group size. It is worth noting that a similar tendency appeared with respect to the intensity of the inner peak of chol. Thus, the ordering effect of chol may be slightly enhanced in the L_d phases of **4** and **5**.

2.2.8 Raman Microscopy

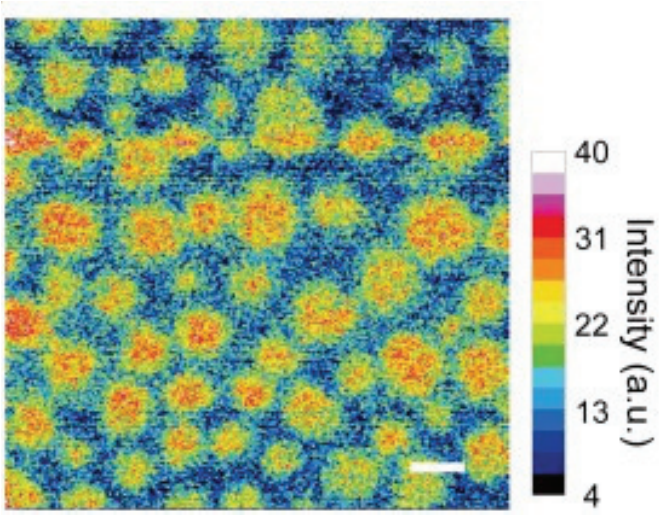

Figure 2-8. Slit-scanning Raman microscopy of a **2**/DOPC/chol (1/1/1 mol) monolayer. The image was reconstructed using the diyne peak intensity at 2262 cm^{-1}. Exposure time and laser power were 100 sec/line and 10.5 $mW/\mu m^2$. The image is shown in a 16-color display. The images consist of 412 x 400 pixels. Scale bar is10 μm.

Finally, Raman microscopic observation of a raft like **2**/DOPC/chol ternary membrane was performed.[29] (Figure 2-8) A heterogeneous distribution of the probe has been visualized. Interestingly, it was enriched in the central region of raft domains compared with the peripheral area. The presence of central region, peripheral area and no-raft phase (L_d phase) suggested a "three phase" distribution. The observed model is incompatible with the generally accepted raft model, in which the raft-containing membranes show a clear biphasic separation.[29] It is speculated that there is a gradual change of SM concentration between the raft center and no raft regions in order to minimize energetically unfavorable hydrophobic mismatch.

This Chapter showed the rational design and preparation of three Raman-active SMs (**1**-**3**) bearing alkyne, diyne and multiple C–D bonds on the polar head group.[30] In a supported monolayer-membrane, they generated characteristic Raman peaks in the cellular silent region. Current results indicate that diyne SM **2** is the best candidate for the high contrast observation of raft-like domains over a reasonable time frame. Firstly, it gives rise to a strong and sharp Raman peak compared with **1** and **3**. Secondly, the ^{2}H NMR spectra highlight the similarity in raft-like domain formation between this probe and natural SM. In addition, the probe has a clear preference to partitioning into L_o phases.[30] Raman microscopic using the developed probe in monolayer provided a "three phase" distribution of raft-like membranes.[29]

References

1) (a) Simons, K.; Ikonen, E. *Nature.* **1997**, *387*, 569-572; (b) Simons, K.; Toomre, D. *Nat. Rev. Mol. Cell Biol.* **2000**, *1*, 31-39; (c) Brown, D. A.; Rose, J. K. *Cell.* **1992**, *68*, 533-544; (d) Lingwood, D.; Simons, K. *Science.* **2010**, *327*, 46-50.

2) Cruz, A.; Vazquez, L.; Velez, M.; Perez-Gil, J. *Langmuir.* **2005**, *21*, 5349-5355.

3) (a) Baumgart, T.; Hunt, G.; Farkas, E. R.; Webb, W. W.; Feigenson, G. W. *Biochim. Biophys. Acta.* **2007**, *1768*, 2182-2194; (b) Sezgin, E.; Levental, I.; Grzybek, M.; Schwarzmann, G.; Mueller, V.; Honigmann, A.; Belov, V. N.; Eggeling, C.; Coskun, U.; Simons, K.; Schwille, P. *Biochim. Biophys. Acta.* **2012**, *1818*, 1777-1784; (c) Klymchenko, A. S.; Kreder, R. *Chem. Biol.* **2014**, *21*, 97-113.

4) (a) Fujita, K.; Smith, N. I. *Mol. Cells.* **2008**, *26*, 530-535; (b) Yamakoshi, H.; Dodo, K.; Okada, M.; Ando, J.; Palonpon, A.; Fujita, K.; Kawata, S.; Sodeoka, M. *J. Am. Chem. Soc.* **2011**, *133*, 6102-6105.

5) Yamakoshi, H.; Dodo, K.; Palonpon, A.; Ando, J.; Fujita, K.; Kawata, S.; Sodeoka, M. *J. Am. Chem. Soc.* **2012**, *134*, 20681-20689.

6) (a) Mendelsohn, R.; Koch, C. C. *Biochim. Biophys. Acta.* **1980**, *598*, 260-271; (b) Li, L.; Wang, H.; Cheng, J. X. *Biophys. J.* **2005**, *89*, 3480-3490; (c) Potma, E. O.; Xie, X. S. *Chem. Phys. Chem.* **2005**, *6*, 77-79; (d) Opilik, L.; Bauer, T.; Schmid, T.; Stadler, J.; Zenobi, R. *Phys. Chem. Chem. Phys.* **2011**, *13*, 9978-9981.

7) Guard-Friar, D.; Chen, C. H.; Engle, A. S. *J. Phys. Chem.* **1985**, *89*, 1810-1813.

8) Garner, A. E.; Smith, D. A.; Hooper, N. M. *Mol. Membr. Biol.* **2007**, *24*, 233-242.

9) Yamamoto, T.; Hasegawa, H.; Hakogi, T.; Katsumura, S. *Org. Lett.* **2006**, *8*, 5569-5572.

10) (a) Sandbhor, M. S.; Key, J. A.; Strelkov, I. S.;Cairo, C. W. *J. Org. Chem.* **2009**, 74, 8669-8674; (b) Goretta, S. A.; Kinoshita, M.; Mori, S.; Tsuchikawa, H.; Matsumori, N.; Murata, M. *Bioorg. Med. Chem.* **2012**, *20*, 4012-4019.

11) (a) Montalbetti, C. A. G. N.; Falque, V. *Tetrahedron.* **2005**, 61, 10827-10852; (b) Nahm, S.; Weinreb, S. M. *Tetrahedron Lett.* **1981**, *22*, 3815-3818.

12) Pohlmeier, A.; Knoche, W. *Int. J. Chem. Kinet.* **1996**, *28*, 125-136.

13) Healy, M. D.; Power, M. B.; Barron, A. R. *Coord. Chem. Rev.* **1994**, *130*, 63-135.

14) Kitagawa, F.; Murase, M.; Kitamura, N. *J. Org. Chem.* **2002**, *67*, 2524-2531.

15) Cadiot, P.; Chodkiewicz, W. in Chemistry of Acetylenes; Viehe, H. G., Ed.; Marcel Dekker, New York, **1969**; pp 597–647.

16) Yin, W.; He, C.; Chen, M.; Zhang, H.; Lei, *A. Org. Lett*. **2009**, *11*, 709-712.

17) Burn, A. J.; Cadogan, J. I. G. Chem. Ind. (London) **1963**, 736.

18) Oza, V. B.; Corcoran, R. C. *J. Org. Chem.* **1995**, *60*, 3680-3684.

19) Yamamoto, T.; Hasegawa, H.; Ishii, S.; Kaji, S.; Masuyama, T.; Harada, S.; Katsumura, S. *Tetrahedron.* **2008**, *64*, 11647-11660.

20) *d*-Chol was synthesized from commercial 5-cholesten-3-on by reduction using deuterated reducing reagent NaBD4.

21) (a) Guo, W.; Kurze, V.; Huber, T.; Afdhal, N. H.; Beyer, K.; Hamilton, J. A. *Biophys. J.* **2002**, *83*, 1465-1478; (b) Murari, R.; Murari, M. P.; Baumann, W. J. *Biochemistry.* **1986**, *25*, 1062-1067.

22) Brzustowicz, M. R.; Cherezov, V.; Caffrey, M.; Stillwell, W.; Wassall, S. R. *Biophys. J.* **2002**, *82*, 285-298.

23) Matsumori, N.; Kasai, Y.; Oishi, T.; Murata, M.; Nomura, K. *J. Am. Chem. Soc.* **2008**, *130*, 4757-4766.

24) Matsumori, N.; Yasuda, T.; Okazaki, H.; Suzuki, T.; Yamaguchi, T.; Tsuchikawa, H.; Doi, M.; Oishi, T.; Murata, M. *Biochemistry.* **2012**, *51*, 8363-8370.

25) Mehnert, T.; Jacob, K.; Bittman, R.; Beyer, K. *Biophys. J.* **2006**, *90*, 939-946.

26) Calhoun, W. I.; Shipley, G. G. *Biochim. Biophys. Acta.* **1979**, *555*, 436-441.

27) Lethu, S.; Matsuoka, S.; Murata, M. *Org. Lett.* **2014**, *16*, 844-847.

28) Bartels, T.; Lankalapalli, R. S.; Bittman, R.; Beyer, K.; Brown, M. F. *J. Am. Chem. Soc.* **2008**, *130*, 14521-14532.

29) Sphingomyelin Distribution in Lipid Rafts of Artificial Monolayer Membranes Visualized by Raman Microscopy. Ando, J.; Kinoshita, M.; Cui, J.; Yamakoshi, H.; Dodo, K.; Fujita, K.; Murata, M.; Sodeoka, M. **2015** (submitted)

30) Raman-Tagged Sphingomyelin that Closely Mimics Original Raft-Forming Behavior. Cui, J.; Ando, J.; Kinoshita, M.; Sato F.; Sodeoka, M.; Murata, M. (to be submitted)

Chapter 3

Synthesis of Deuterated Dioleoylphosphatidylcholine for Investigation of Membrane Properties.

3.1 Introduction

Lipid organization has been at the center of research on lipid rafts. The rigid chol enhances the ordering of sphingolipids and induces the formation of the liquid ordered (L_o) phase, which has distinct physical properties from that of liquid disordered (L_d) phase.[1,2] Lipid rafts show behavior similar to that of a liquid-ordered (L_o) phase. Raft formation is thought to be caused by the L_o/L_d phase separation process.[3-5] Uncovering the behavior of individual lipids in these phases is necessary for a better understanding of the molecular mechanisms underlying the biomedical functions of lipid rafts.

Dioleoylphosphatidylcholine (DOPC) is a typical L_d component in raft-model membranes, and has often been used to prepare a ternary mixture with sphingomyelin (SM) and chol that forms L_o/L_d-co-existing bilayers. Although incorporation of unsaturated DOPC into L_d phases is energetically favorable,[6] a small amount of DOPC is always found in L_o phases. However, this phase segregation is difficult to detect using a previously reported DOPC probe [C11-$^2H_2$] DOPC.[7,8] In fact, the allylic C11 of oleic acid is not the best position for ^{2}H-labeling since the C9-C10 double bond forces the orientation of the C11-H bonds not to be perpendicular to the membrane normal unlike the orientation of other C-H moieties apart from the C9-C10 double bond. This particular situation of C11 (and C8) results in the smaller magnitude in quadrupolar coupling of the CD_2 moiety, which hampers the observation of the clearly separated ^{2}H signals between L_o and L_d phases. In particular, it becomes more difficult to examine the phase behavior of the L_o domains that contains a small amount of DOPC.

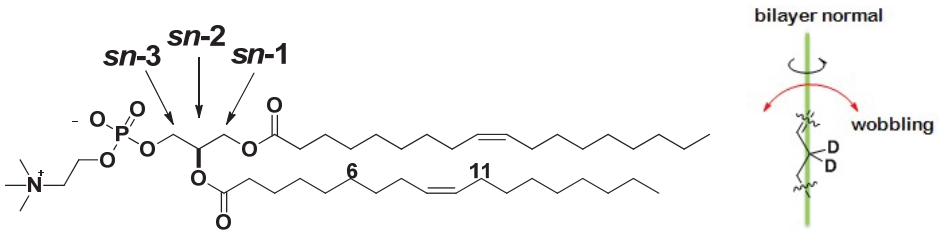

Figure 3-1. Chemical structure of DOPC and the wobbling motion of allylic C11.

Recent molecular dynamics (MD) simulations suggest that, in DOPC/chol bilayers, chol enhances the order of C6 methylene of an oleoyl group more effectively than that of other carbons in the *sn*-2 acyl chain of DOPC.[9] (Figure 3-2) Thus, in ternary SM/chol/DOPC membranes, [C6-$^2H_2$] DOPC should show clear separated signals of DOPC in the L_o phase.

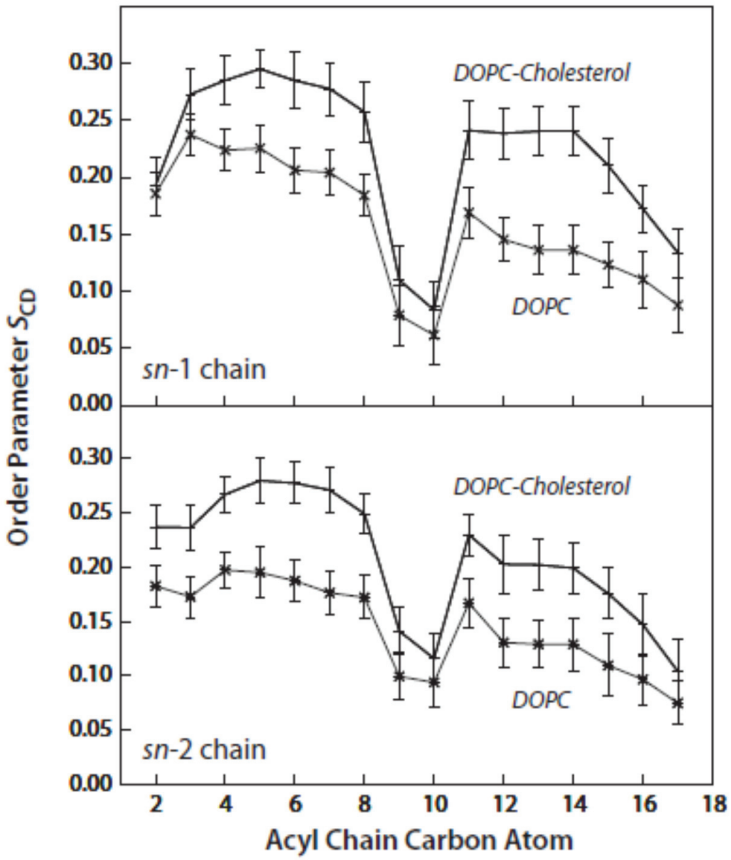

Figure 3-2. Order-parameter profiles for the acyl chains of DOPC in the absence and presence chol (2:1 DOPC/chol) determined from MD simulations. Reprinted with permission from *Biophys. J.* **2011**, 100, 1455–1462. Copyright © (2011) the Biophysical Society

However, the only one synthetic method of [C6-$^2H_2$] oleic acid, the key precursor for the synthesis of [C6-$^2H_2$] DOPC, is a linear 14-step sequence including a classical malonate extension process. Thus, a more efficient synthetic method is highly desirable, although the reported method is suitable for large-scale industrial synthesis. The reported scheme has been summarized in Scheme 3-1 for reference.

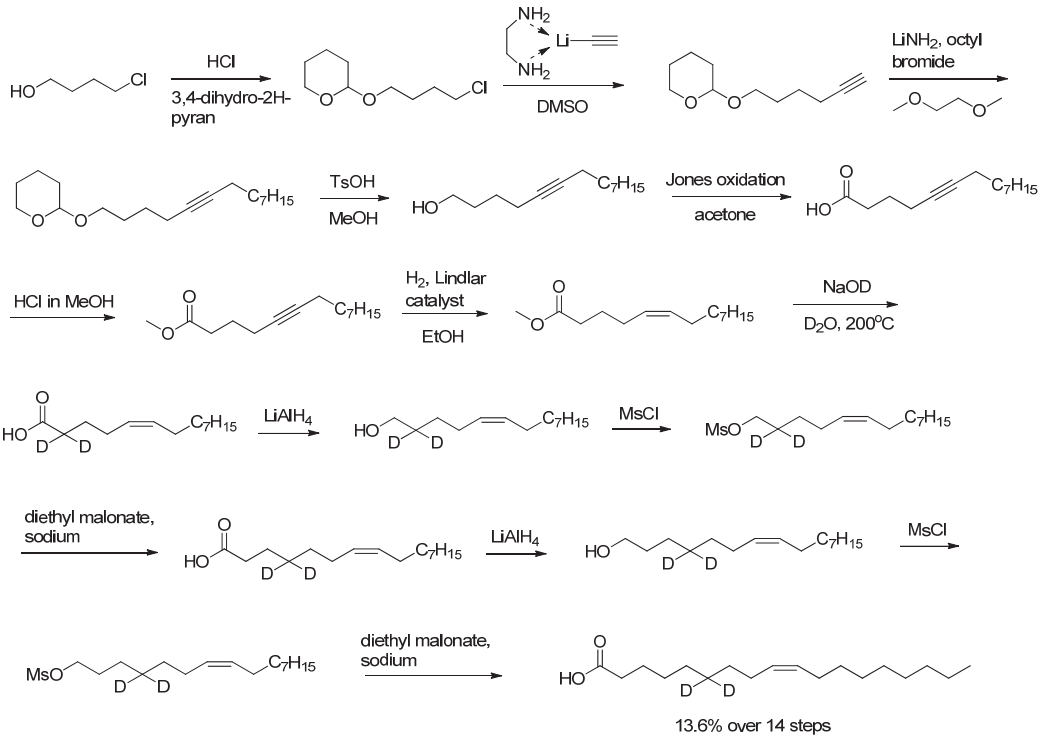

Scheme 3-1. The known method for making [C6-$^2H_2$] oleic acid. Reported in A.P. Tulloch, *Chemistry and Physics of Lipids* **1979**, *25*, 225.

3.2 Results and Discussion

3.2.1 Synthesis of [C6-$^2H_2$] Oleic Acid and [C6-$^2H_2$] DOPC

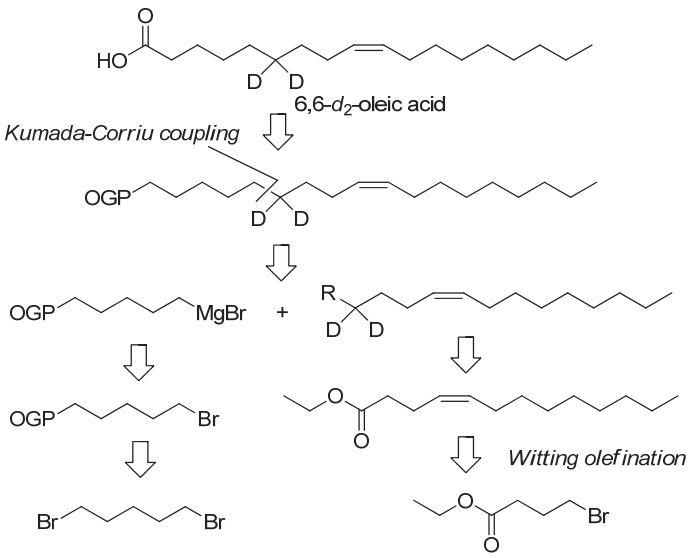

Scheme 3-2. Retrosynthesis of [C6-$^2H_2$] oleic acid.

An efficient synthetic method has been firstly developed.[10] The retrosynthetic analysis is shown in Scheme 3-2. The target molecule would be formed through alcohol deprotection followed by oxidation reaction of a protected precursor, which would be prepared by two fragments via a C_{sp3}-C_{sp3} cross coupling. The deuterium in the olefin would be introduced by lithium aluminum deuteride ($LiAlD_4$) reduction of an ester, which could be derived from a commercial bromide through a Wittig olefination.

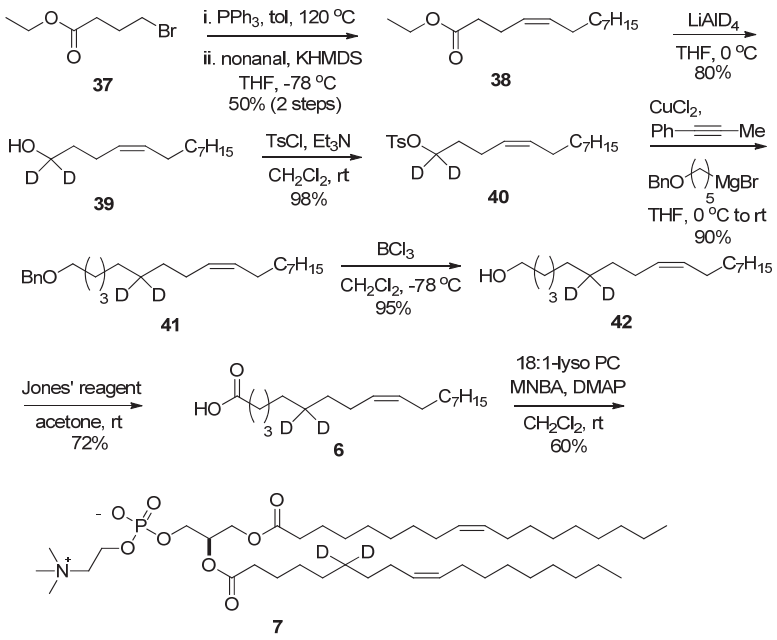

Scheme 3-3. Synthesis of [C6-$^2H_2$] oleic acid **6** and [C6-$^2H_2$] DOPC **7**.

The improved synthesis began with the preparation of phosphonium salt from brominated ester **37**, followed by Wittig olefination to give pure *cis*-olefin **2**. (Scheme 3-3) Subsequent reduction of the ester with $LiAlD_4$ afforded deuterated alcohol **39**, which was tosylated to give the deuterated intermediate **40**. A recent study suggested that the tosylated precursor is a more suitable coupling partner than the brominated one for C_{sp3}-C_{sp3} Kumada−Corriu coupling. Compound **40** was subsequently coupled with a Grignard reagent prepared from the commercial benzyloxypentyl bromide to afford cross-coupled product **41** in high yield. Benzyl deprotection by boron trichloride followed by Jones' oxidation led to the desired [C6-$^2H_2$] oleic acid **6** in 24% overall yield after 7 steps. Finally, [C6-$^2H_2$] DOPC **7** was prepared using 18:1-lyso PC under typical condensation conditions.[10)]

3.2.2 ^{2}H NMR Measurements

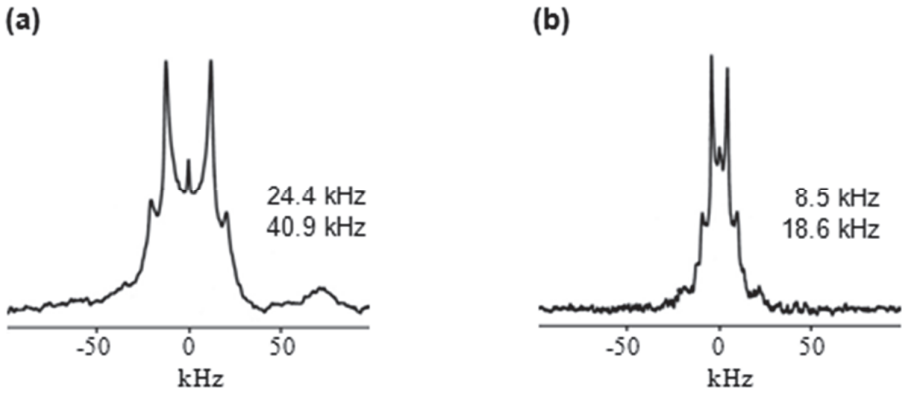

Figure 3-3. ^{2}H NMR spectra of 50 wt% aqueous multilammellar dispersions at 30 °C. (**a**) **7**/SM/chol (1/1/1 mol) and (**b**) [C11-$^2H_2$] DOPC/SM/chol (1/1/1 mol).

Firstly, the ^{2}H NMR of powder-type hydrated membrane has been measured. The standard wideline spectra were recorded as shown in Figure 3-3. As expected, **7** generates much more clearly separated peaks than [C11-$^2H_2$] DOPC does. The two doublet peaks in each spectra corresponding to the L_o and L_d phase, respectively, the major fraction of DOPC is in the L_d phase as shown by the larger integrated intensity of the inner doublet. Notably, the peak distance between inner and outer splittings in **7**/SM/chol membranes increased by 1.6 fold compared to [C11-$^2H_2$] DOPC-containing mixtures. The above data confirms that **7** is the better probe appropriate for the L_o/L_d-separated systems.[10)]

As the macroscopically aligned membranes have improved spectral resolution and sensitivity compared to powder pattern samples, the ^{2}H NMR of **7** was then recorded in such an oriented membrane system.

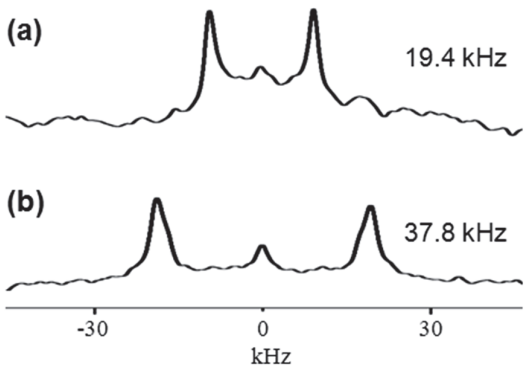

Figure 3-4. ^{2}H NMR spectra and quadrupolar splitting of oriented multi-bilayers. (a) pure **7** and (b) chol/**7** (1/1 mol) at 30°C.

The ^{2}H NMR spectra of **7** was recorded in oriented membranes form in the absence and presence of 50 mol % chol. In Figure 3-4 **a**, the ^{2}H NMR spectra of pure **7** membranes provided a pair of sharp quadrupolar splitting, corresponding to the rapid and disordered motions in the acyl chains. In Figure 3-4 **b**, the incorporation of chol into pure **7** membranes leads to the appearance of a set of more ordered peak. In bilayers, the methylenes in the side chains of DOPC undergo rapid *gauche-trans* isomerization, and such increased chain order correlated with the increased *trans* polulations of the C-C bonds due to the ordering effect of chol. The broadening of doublets is due to the fast lipid diffusion in different domains on ^{2}H NMR timescale.

Next, the ^{2}H NMR spectra of **7** was measured in raft-like ternary membranes. (Figure 3-5 **a**) In the bottom trace of Figure 3-5 **a**, the ^{2}H NMR spectrum of oriented **7**/SM/chol bilayers at 30 °C provided completely separated doublets with even higher resolution than the powder-type ^{2}H NMR spectra. It is clear to see that small fraction of **7** is in the L_o phase, while major fraction pertains to the L_d phase. The integration area ratio of the outer doublet peak to the inner doublet peak is 28/72. As temperature rose, the order of **7** in L_o phase decreased while that in L_d phase increased, and the phase separation was poorly observed at 40 °C. Then, at 45 °C, the spectra gave completely fused signals, and the peak became sharp and less ordered at 50 °C, indicating the membranes were uniformly mixed. The ^{2}H NMR spectra also shows isotropic components as shown by the central peak. Although the sample contains a small amount of HDO in the water, the isotropic signal is most likely due to the presence of non-oriented structures (such as micelles)

tumbling rapidly in water. As temperature rose, more amounts of isotropic non-oriented phases were formed.[10)]

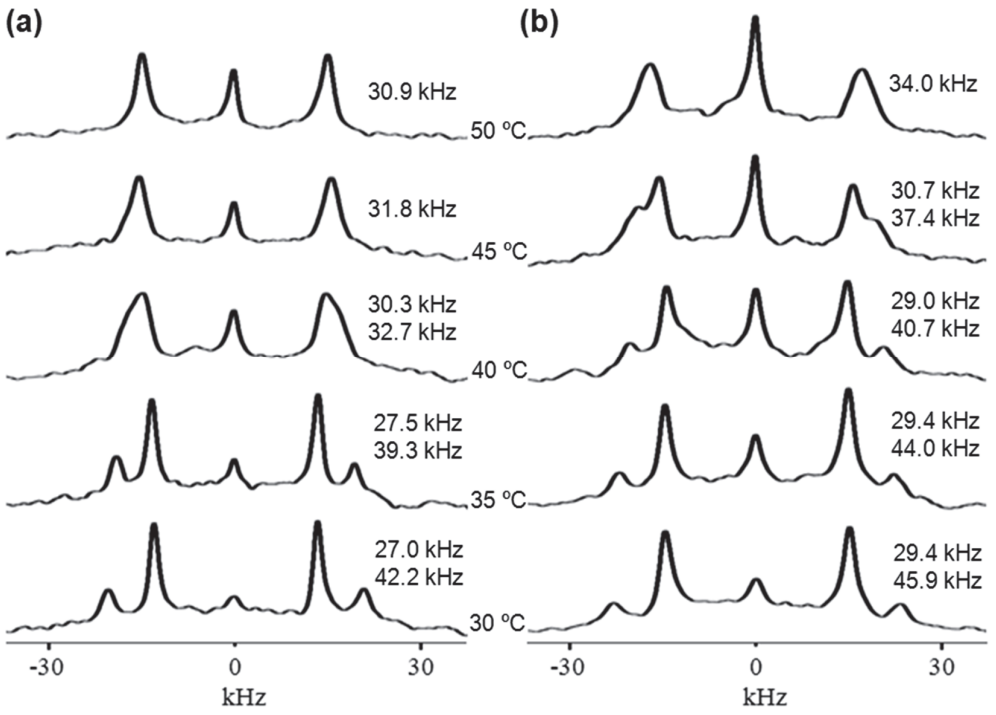

Figure 3-5. Temperature dependence of ^{2}H NMR spectra and quadrupolar splitting of oriented multi-bilayers formed on glass plates. (**a**) **7**/SM/chol (1/1/1 mol) and (**b**) **7**/DHSM/chol (1/1/1 mol). The angle between the bilayer normal and the magnetic field is set at 90°.

Due to the superior performance of **7** with regard to the clear L_o/L_d phase separation and high sensitivity for phase transitions, it is convinced that this molecule could be further applied to probe the membrane property alteration, which was thought to be closely related to cellular functions. Dihydrosphingomyelin (DHSM) is the major phospholipid of human lens membranes, whereas being a rather minor constituent in other tissues.[11)] However, an enrichment of DHSM was found in the HIV-1 membrane, produced from the host cell through viral release.[12)] Recent studies indicated that DHSM is important for HIV-1 gp41-mediated fusion.[13,14)] The role of DHSM in regulating membrane properties can be speculated by previous study that DHSM tends to form rigid domains due to the lack of *trans* double bond in the ceramide backbone.[15)] To further

examine the relevance of DHSM in domain formation, compound **7** was applied to the DHSM-containing ternary system.

As compared with **7**/SM/chol mixtures, less fraction of **7** should be partition to the highly ordered DHSM-enriched phase. Fortunately, small but clearly visible distribution of **7** in L_o phase was detected as shown by the outer doublet in the bottom spectra in Figure 3-5 **b**. At 30 °C, the integration area ratio of the outer doublet peak to the inner doublet peak drops to 16/84, much lower than that in the SM ternary mixtures, revealing that the greater amount of DOPC is excluded from the DHSM-enriched phase. As temperature rose, the order of **7** in L_o phases decreased slower than that in the SM mixture, and the apparent phase separation was clearly observed even at 45 °C, at which only one doublet appeared in the SM mixtures, implying the thermostability of the L_o domains was obviously enhanced in the DHSM mixture. These results are in agreement with recent finding in binary DHSM/DOPC bilayers, in which the DHSM prompts the formation of rigid and stable DHSM-rich domains.[16] Moreover, it is interesting to observe that the order of **7** in both L_o and L_d phases of the DHSM mixture dramatically increased as compared with the SM mixture (Figure 3-6), indicating that DHSM enhanced the rigidity not only of DHSM-rich L_o phases, but of DHSM-poor L_d phases. It is speculated that DHSM with saturated C_4-C_5 bond increases the accessibility of neighboring lipid molecules, thus leading to an enhanced intermolecular interaction by lipid packing in cellular membranes. The ^{2}H NMR spectra of **7**/DHSM/chol mixtures show larger isotropic components compared to SM mixtures, revealing more amounts of **7**-containing non-oriented structures were formed in DHSM membranes. This result indicates the embedding of unsaturated lipids into DHSM-containing membranes become difficult due to the increased membrane rigidity. The distinct differences observed in the ^{2}H NMR spectra of **7** between SM and DHSM ternary mixtures evidently demonstrates the versatility of this DOPC probe for sensing of change in membrane properties.[10]

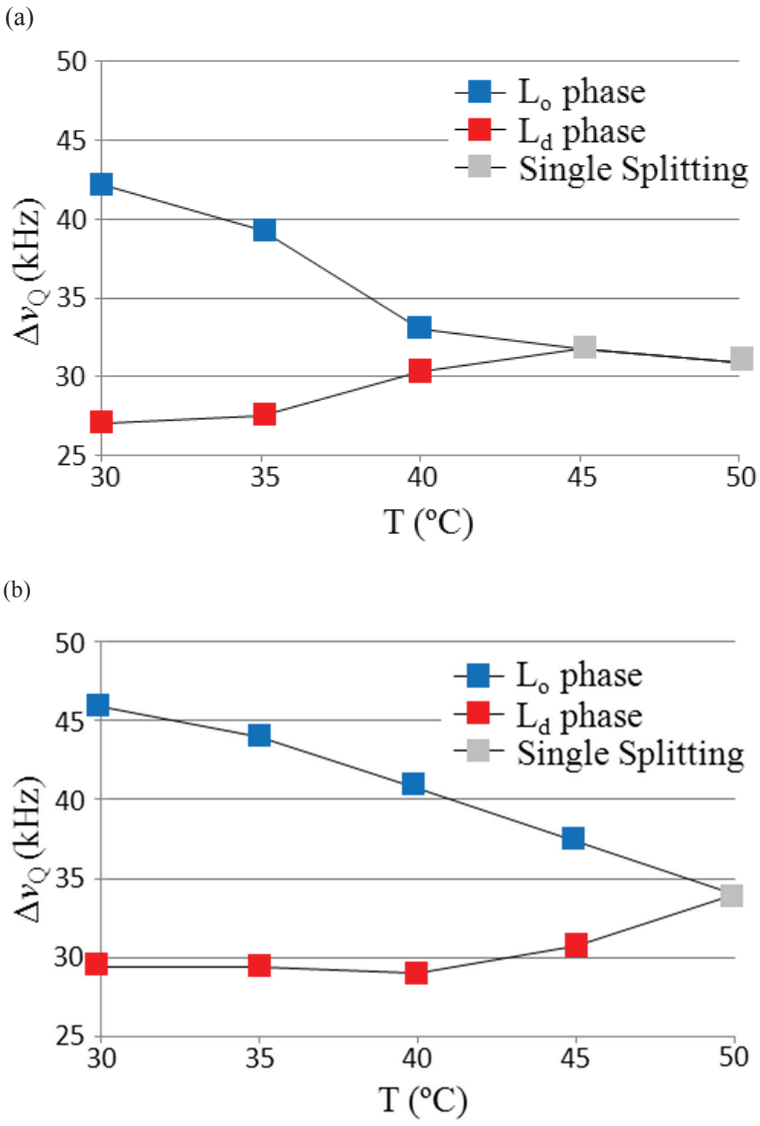

Figure 3-6. Magnitude of **7** splitting: (**a**) **7**/SM/chol (1/1/1 mol) and (**b**) **7**/DHSM/chol (1/1/1 mol).

In this Chapter, a highly efficient synthetic route to [C6-$^2H_2$] oleic acid has been established. Using this intermediate, [C6-$^2H_2$] DOPC was synthesized as a useful ^{2}H NMR probe to investigate the behavior of lipids in raft-like membranes. Owing to the reasonable deuterated position as well as an appropriate sample preparation of mechanically oriented membranes, the probe exhibits completely separated and well-resolved ^{2}H NMR signals stem from both L_o and L_d phases. With these advantages, the probe was successfully applied to examine the difference in membrane

properties between SM and DHSM. Their phase behavior between L_o and L_d phases could be easily distinguished.

References

1) Simons, K.; Toomre, D. *Nat. Rev. Mol. Cell Biol.* **2000**, *1*, 31-39.

2) de Almeida, R. F.; Fedorov, A.; Prieto, M. *Biophys. J.* **2003**, 85, 2406-2416.

3) Campbell, S. M.; Crowe, S. M.; Mak, J. *J. Clin. Virol.* **2001**, *22*, 217-227.

4) Fittipaldi, A.; Ferrari, A.; Zoppe, M.; Arcangeli, C.; Pellegrini, V.; Beltram, F.; Giacca, M. *J. Biol. Chem.* **2003**, *278*, 34141-34149.

5) Zaas, D. W.; Duncan, M.; Rae Wright, J.; Abraham, S. N. *Biochim. Biophys. Acta.* **2005**, *1746*, 305-313.

6) Bezlyepkina, N.; Gracia, R. S.; Shchelokovskyy, P.; Lipowsky, R.; Dimova, R. *Biophys J.* **2013**, *104*, 1456-1464.

7) Chupin, V.; Killian, J. A.; de Kruijff, B. *Biophys. J.* **1987**, *51*, 395-405.

8) van Duyl, B. Y.; Ganchev, D.; Chupin, V.; de Kruijff, B.; Killian, J. A. *FEBS Lett.* **2003**, *547*, 101-106.

9) Mihailescu, M.; Vaswani, R. G.; Jardon-Valadez, E.; Castro-Roman, F.; Freites, J. A.; Worcester, D. L.; Chamberlin, A. R.; Tobias, D. J.; White, S. H. *Biophys. J.* **2011**, *100*, 1455-1462.

10) Cui, J.; Lethu, S.; Yasuda, T.; Matsuoka, S.; Matsumori, N.; Sato, F.; Murata, M. *Bioorg. Med. Chem. Lett.* **2015**, *25*, 203-206.

11) Nyholm, T.; Nylund, M.; Soderholm, A.; Slotte, J. P. *Biophys. J.* **2003**, *84*, 987-997.

12) Brugger, B.; Glass, B.; Haberkant, P.; Leibrecht, I.; Wieland, F. T.; Krausslich, H. G. *Proc. Natl. Acad. Sci. U. S. A.* **2006**, *103*, 2641-2646.

13) Vieira, C. R.; Munoz-Olaya, J. M.; Sot, J.; Jimenez-Baranda, S.; Izquierdo-Useros, N.; Abad, J. L.; Apellaniz, B.; Delgado, R.; Martinez-Picado, J.; Alonso, A.; Casas, J.; Nieva, J. L.; Fabrias, G.; Manes, S.; Goni, F. M. *Chem. Biol.* **2010**, *17*, 766-775.

14) Klug, Y. A.; Ashkenazi, A.; Viard, M.; Porat, Z.; Blumenthal, R.; Shai, Y. *Biochem. J.* **2014**, *461*, 213-222.

15) Epand, R. M. *Biophys. J.* **2003**, *84*, 3102-3110.

16) Kinoshita, M.; Matsumori, N.; Murata, M. *Biochim. Biophys. Acta.* **2014**, *1838*, 1372-1381.

Chapter 4

Stereoselective Synthesis of Phosphatidylglycerophosphate Methyl Ester Analogues towards Evaluation of Bacteriorhodopsin-Lipids Interactions in Membranes

4.1 Introduction

Bacteriorhodopsin (bR) is the only protein in the purple membrane (PM) of *Halobacterium halobium*.[1] It functions as a light-driven proton pump and exits in a trimer form with 6 lipids located within the trimer and 24 surrounding the protein surface.[2] Polar lipids account for 90% of the total lipids in PM, including 2,3-di-*O*-phytanyl-*sn*-glycerol phosphatidylglycerol (PG), phosphatidylglycerol sulfate (PSG), phosphatidylglycerophosphate methyl ester (PGP-Me), archaeal cardiolipin (BPG), sulfated triglycoside lipid (S-TGA-1) and archaeal glycocardiolipin (GlyC), among which PGP-Me is the major lipid according to quantitative analysis of the lipid extract of PM.[3]

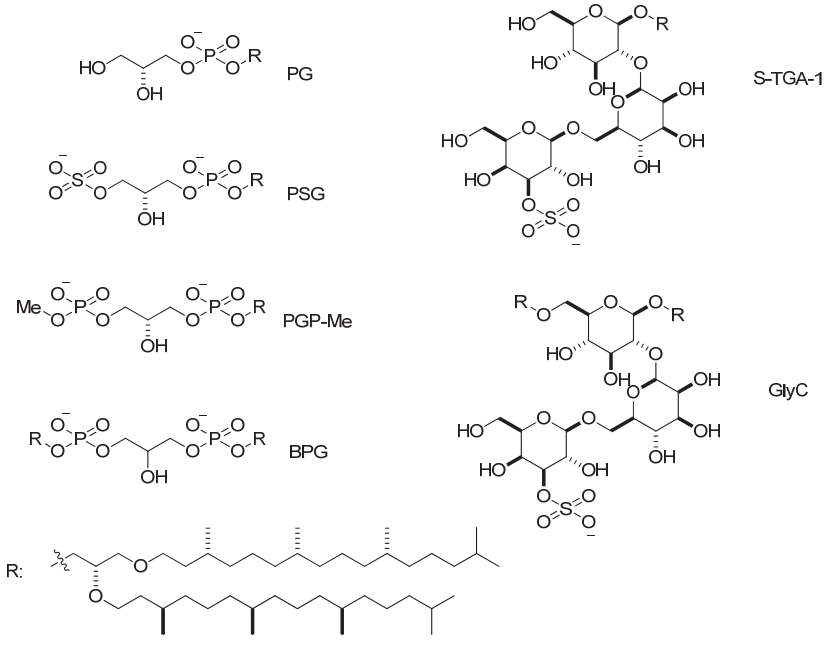

PGP-Me is a diacidic phospholipid comprising a chiral polar head group of bisphosphate ester and two hydrophobic side chains, which are bound to the chiral glycerol backbone by ether linkages. In this Chapter, a PGP-Me analogue (**8**) retained the head group in the native PGP-Me

moiety bearing two simple straight side chains was selected and used to mimic the native membrane-like environment for the *in situ* study of lipid-protein interactions.

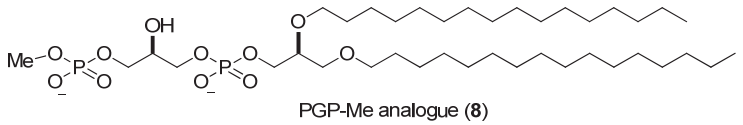

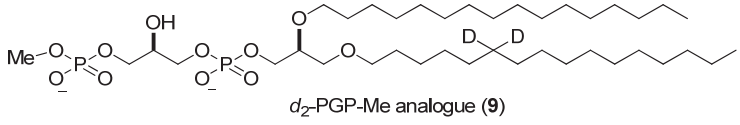

Molecular geometry of a lipid molecule is closely associated with the morphology and physical properties of membranes. The concept of packing parameter P ($P = V/al$, where V is the specific volume occupied by the tails, a is the area per lipid molecule in the dividing surface, and l is the effective length of the tails' region) can be used to characterize the propoperties of a lipid self-assembly.[4] Cylinder-shaped lipids (e.g., DOPC) have similar cross-sectional areas for the polar head and hydrophobic region, thus leading the P value to be around 1, and the formation of lamellar phases. Cone-shaped lipids (e.g., DOPE) with $P > 1$, which have a small polar head, favor the organization of membranes into inverted micelles (HII phases) or cubic (bicontinuous) structures. Invert cone-shaped lipids (e.g., lysophosphocholine (LPC)) with $P < 1$, which have a bulky polar head, favor the formation of tubular (HI) or spheric micelles.[5,6] The native PM lipids are known to form a lamellar structure.[7]

The most common technique used to detect lipid polymorphism is phosphorus nuclear magnetic resonance (^{31}P NMR).[8] Oriented and unoriented samples show different ^{31}P NMR lineshape.[9] Liposomal lipid dispersions where molecules are oriented to every direction result in a powder-like pattern spectrum with a narrower signal width, showing a low field shoulder and high field peak. The high field peak has been found to correspond with lipid molecules with their molecular axes perpendicular to the magnetic field, whereas the shoulder resonance position corresponding to those with a parallel orientation.[6] For the hexagonal H_{II} phase, lateral diffusion of the lipid molecules around the cylinders display an additional spectral pattern.[9] Lipids in micellar, inverted micellar, cubic or rhombic configurations allow effectively isotropic motion to

occur, resulting in a narrow symmetrical lineshape.[9] The isotropic structures include lipid bilayer vesicles with small radii. When a bilayer sample is perfectly aligned with the magnetic field, a single sharp resonance appears. Rotation of the oriented bilayers in the magnetic field gives rise to individual narrow resonances with different chemical shift.[6]

In this Chapter, a stereoselective synthetic route to the analogue (**8**) was developed using H-phosphonate chemistry. Based on the developed method, a site-specifically deuterated analogue (**9**) was synthesized for solid-state ^{2}H NMR measurements. Static ^{31}P NMR was first measured to evaluate the formation of oriented membranes constituted by the analogue. Lipid-bR interactions in membranes was further studied by ^{2}H NMR.

4.2 Results and Discussion

4.2.1 Synthesis of PGP-Me Analogue

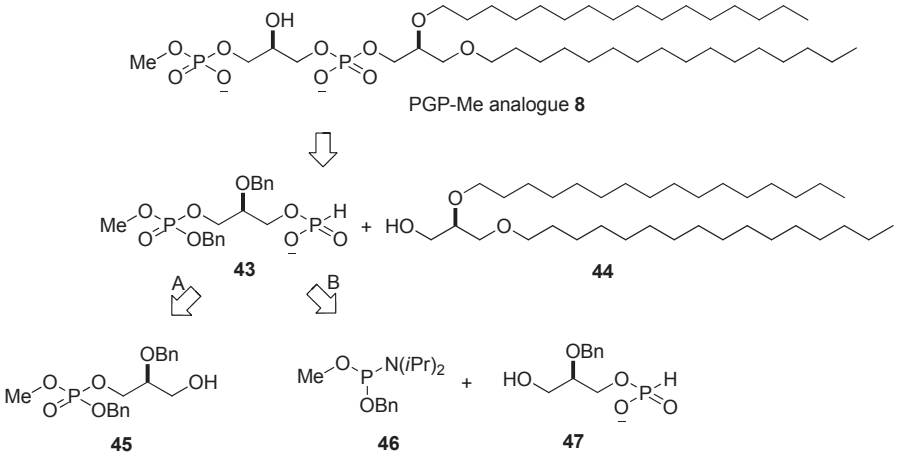

Scheme 4-1. Retrosynthetic analysis.

Retrosynthetically, compound **8** would be constructed by H-phosphonate coupling between **43** and **44**. The compound **43** could be obtained via phosphorylation either from phosphate ester **45** (Route A), or from H-phosphonate **47** (Route B). (Scheme 4-1)

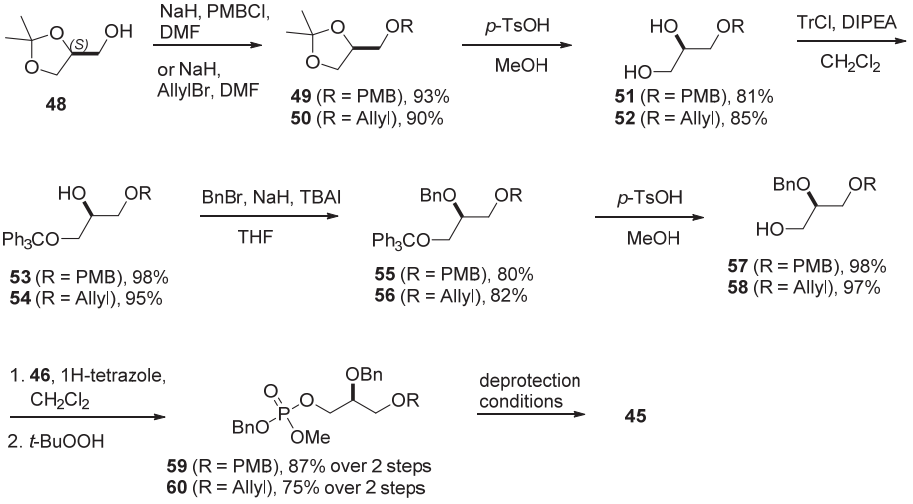

Scheme 4-2. Synthesis of **45**.

As shown in Scheme 4-2, the protected glycerols **57** and **58** were synthesized from commercially available (*S*)-solketal **48** using a partially modified procedure from those in previous reports.[10] Based on Route A (Figure 4-1), the primary alcohol in **57** and **58** was phosphorylated using phosphoramidite/1H-tetrazole followed by oxidation with *tert*-butyl hydroperoxide (*t*-BuOOH) to provide phosphotriester **59** and **60**, respectively. The ^{1}H NMR spectra indicated a mixture of diastereoisomers with d.r. ~ 2:1 according to the methylene proton peaks of benzyl phosphonate ester.

Table 4-1. Deprotection conditions for the synthesis of **45**.

entry	substrate	condition	yield
1	**59**	DDQ, CH_2Cl_2, rt, 2h	45.7%
2	**59**	CAN,CH_3CN/H_2O, rt, 2h	66%
3	**59**	Bobbitt′s salt, CH_3CN/H_2O, rt, 1h	ND
4	**60**	5% [Ru]/L[a], MeOH, rt, 5h	20%
5	**60**	8% [Ru]/L[a], MeOH, 35 °C, 30 min	87%
6	**60**	8% [Ru]/L[a], MeOH, rt 30min then 35 °C 1.5h	37%

[a] $[CpRu(CH_3CN)_3]$-PF_6/2-quinolinecarboxylic (1/1 mol)

To introduce the second phosphorus, the R group in **59** and **60** should be removed. Table 4-1

shows the deprotection conditions. Interestingly, the benzyl methylene protons in **45** show two pairs of doublets in a different ratio from that of the substrate. It is assumed that an isomerization reaction took place during deprotection or/and purification by the intramolecular nucleophilic attack of the phosphotriester by hydroxide via a phosphorane intermediate,[11] which would result in racemization of the chiral carbon atom in **45**. (Scheme 4-3)

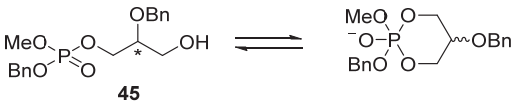

Scheme 4-3. Isomerization reaction of **45**.

In order to avoid the isomerization, as shown in Scheme 4-4, an alternative approach to the formation of the diphosphate **43** has been developed based on Route B. Compound **61** was obtained from (*R*)-solketal using the similar synthetic method described in Scheme 4-2. The primary alcohol in **61** was phosphorylated using 2-chloro-4H-benzo[*d*][1,3,2]dioxaphosphinin-4-one in pyridine followed by hydrolysis to provide H-phosphonate **62**, in which the PMB group was removed by TFA to give **47**, which was phosphorylated using phosphoramidite/1H-tetrazole followed by oxidation with *t*-BuOOH to provide **43**.

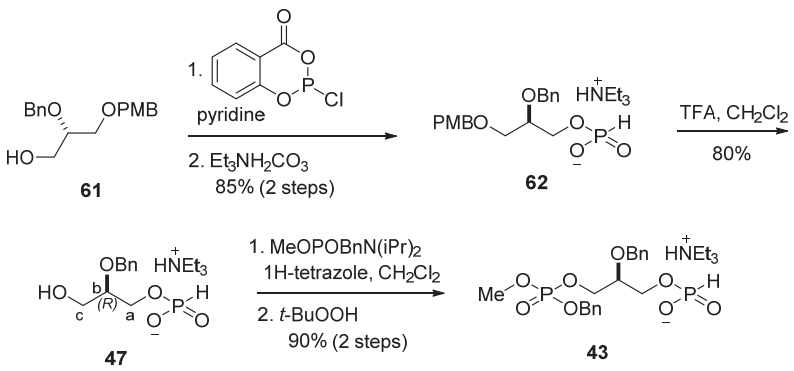

Scheme 4-4. Synthesis of **43**.

The determination of enantiomeric excess (e.e.) of compound **47** was achieved by ^{1}H NMR using Chirabite-AR[12] as a chemical shift reagent. (Figure 4-1)

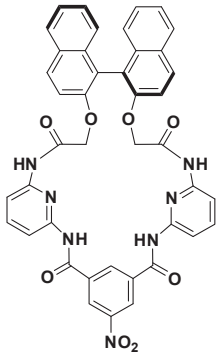

Figure 4-1. Chemical structure of Chirabite-AR.

Chirabite-AR is a bifunctional macrocycle with C_2 symmetry and is highly effective for a wide range of chiral molecules bearing a carboxylic acid, oxazolidinone, lactone, alcohol, sulfoxide, sulfoximine, isocyanate, or epoxide group. [12)]

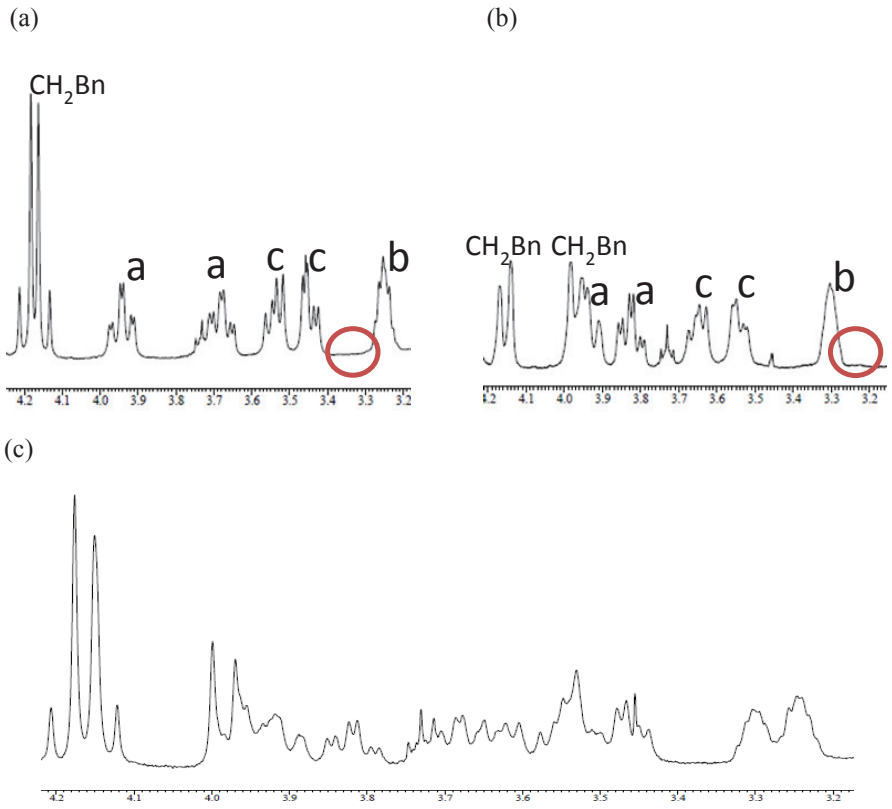

Figure 4-2. Determination of enantiomeric excess of **47** by ^{1}H NMR using Chirabite-AR. Partial enlarged ^{1}H NMR of (**a**) Chirabite-AR/(R)-**47** (1/1 mol), (**b**) Chirabite-AR/(S)-**47** (1/1 mol), and (**c**) Chirabite-AR/(R)-**47**/(S)-**47** (1/1/1 mol) in $CDCl_3$.

The ^{1}H NMR of Chirabite-AR/(R)-**47** and Chirabite-AR/(S)-**47** mixtures show a set of NMR peak, respectively. (Figure 4-2) The CH (Hb) signal of (R)-**47** or (S)-**47** shows resonance at 3.29 ppm. The proton signal appears at 3.25 ppm and 3.30 ppm in Chirabite-AR/(R)-**47** and Chirabite-AR/(S)-**47** mixtures, respectively. The signal of (R)-**47** shifted highfield by 0.04 ppm when 1 equiv of Chirabite-AR was added. In the case of (S)-**47**, the signal shifted downfield by 0.01 ppm. Distinguishable enantiomeric discrimination ($\Delta\Delta\delta$ = 0.06 ppm) was observed in Chirabite-AR/ (R)-**47**/(S)-**47** mixtures. ^{1}H NMR spectra suggest that the e.e. of compound **47** is more than 95% as indicated by the absence of NMR peak in the red circle.

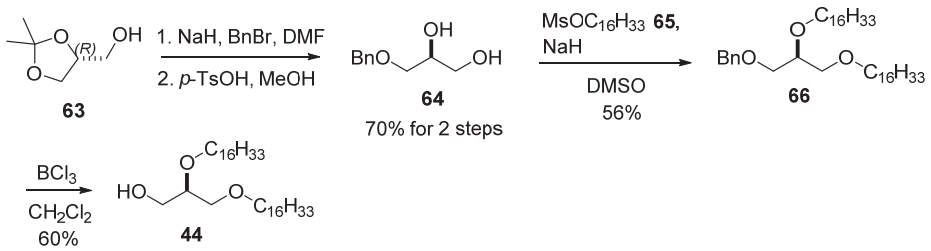

Scheme 4-5. Synthesis of **44**.

The synthesis of **44** began with the Bn protection of the primary OH of (R)-solketal **63**, followed by transacetalization using *p*-TsOH in methanol to give the 1,2-diol **64** in 70% isolated yield over two steps. Hexadecyl methanesulfonate **65** was synthesized from hexadecan-1-ol and used for the preparation of bisether **66** by the etheration with NaH as base. Benzyl deprotection by boron trichloride (BCl_3) led to the desired alcohol **44**. (Scheme 4-5)

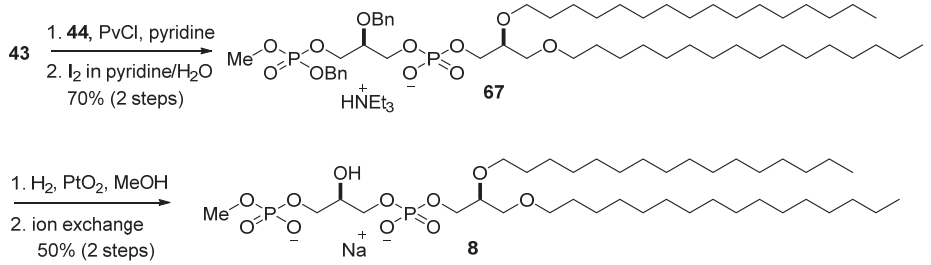

Scheme 4-6. Synthesis of **8**.

The synthesis of target molecule **8** is shown in Scheme 4-6. Using pivaloyl chloride (PvCl) as a

condensing agent, **43** was completely converted into a phosphite which was oxidized with iodine followed by hydrolysis with water to give **67**.[13,14] Deprotection of Bn ethers in the presence of Adams' catalyst followed by ion exchange produced **8** in 50% isolated yield over two steps.

4.2.2 Synthesis of ^{2}H-labled PGP-Me Analogue

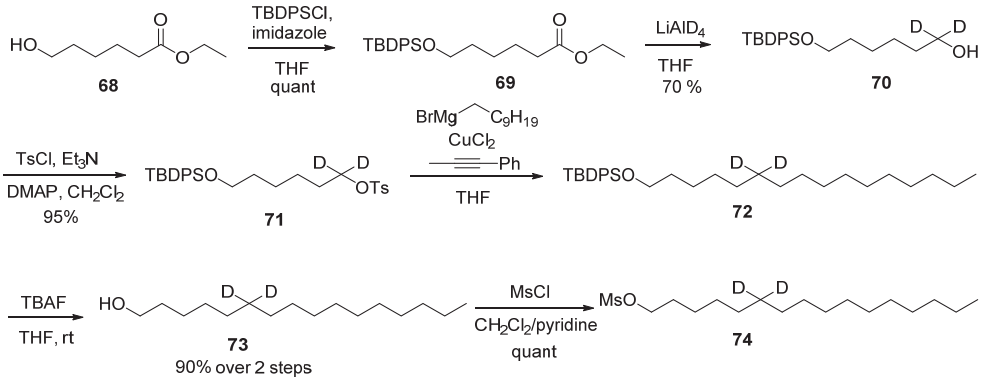

Scheme 4-7. Synthesis of **74**.

The deuterated PGP-Me analogue will be synthesized for ^{2}H NMR measurements. Thus, the synthetic route to the site-specifically deuterated side chain has been established. As shown in Scheme 4-7, TBDPS protection of the primary alcohol of **68** afforded compound **69**. Reduction of the ester with $LiAlD_4$, followed by tosylation, provided deuterated intermediate **71** for C_{sp3}-C_{sp3} Kumada–Corriu coupling.[15] Compound **71** was subsequently coupled with a Grignard reagent to afford **72**. Removal of TBDPS, followed by mesylation, led to compound **74**.

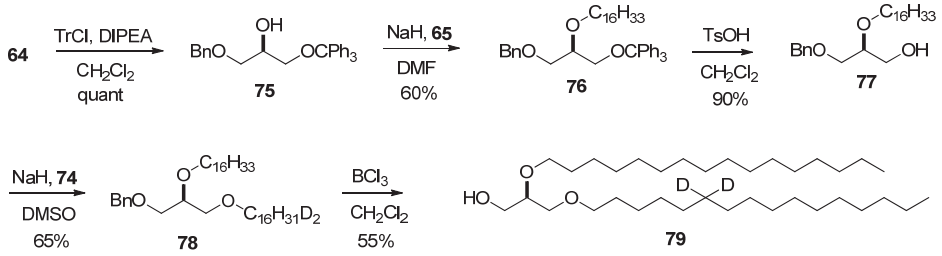

Scheme 4-8. Synthesis of **79**.

As shown in Scheme 4-8, selective protection of primary alcohol of **64** with tritylchloride (TrCl) afforded **75**, followed by etheration and deprotection, provided **77**. Compound **78** was then prepared using the deuterated hexadecyl methanesulfonate **74**, followed by Bn deprotection yielded **79**. Using the same synthetic method as for compound **8** (Scheme 4-6), the deuterated sample **9** was synthesized. (Scheme 4-9)

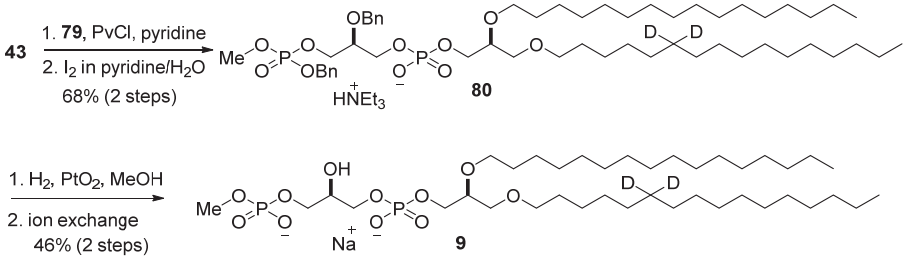

Scheme 4-9. Synthesis of **9**.

4.2.3 Formation of Oriented Membranes

Lipid molecules can self-assemble in an aligned fashion, which allows dynamic analysis in an environment that closely mimics the biological membrane. Aligning the lipid membrane in a single specific orientation in magnetic field allows improvement of spectra resolution.[16] This method provides unique insight into protein-lipid interactions based on solid-state ^{2}H NMR.[17] The PGP-Me analogue **8** has the different side chain structure and volume from the native PGP-Me. Thus, oriented membrane formation has first been examined by ^{31}P NMR, which is generally used for characterizing the orientation and morphology of lipid bilayers.

In preparation of an oriented membrane preparation, the hydration of pure **8** membrane was found to be difficult, and the total hydration time was extended to 10 days while membrane hydration was carried out for 4 days in usual procedures.[18] The ^{31}P NMR spectra of pure **8** membranes has been measured at 40 ºC, 50 ºC and 60 ºC, and the spectra recorded at 50 ºC generated the best spectral resolution. A DSC study shows that the phase transition temperature of **8** is 42 ºC. (data not shown) Thus all the samples has been recorded at 50 ºC.

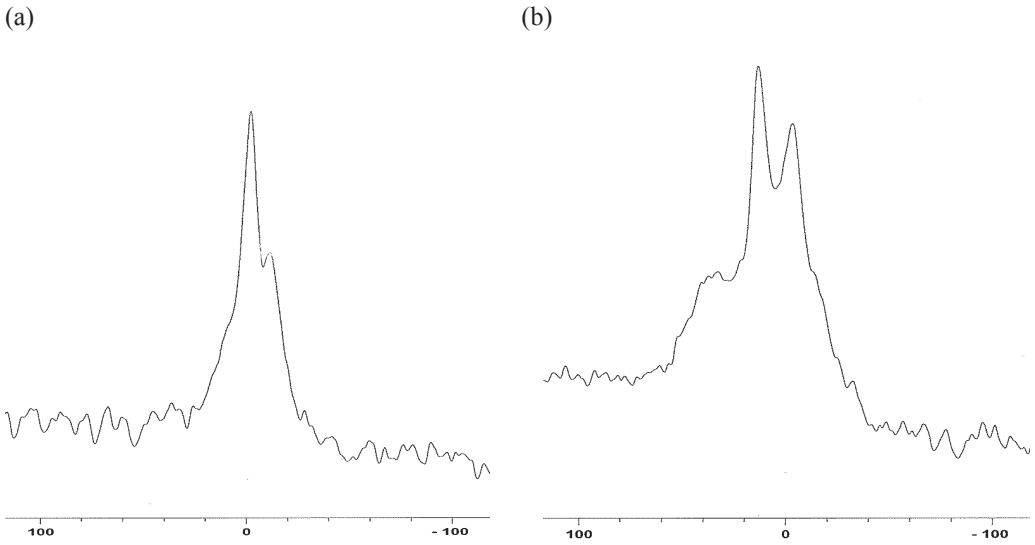

Figure 4-3. ^{31}P NMR spectra of pure **8** on coverslips. The angle between the normal of coverslips and the magnetic field is set at 90º (a) and at 0º (b), respectively.

Figure 4-3 shows the ^{31}P NMR spectra of pure **8** membranes. Two signal resonances were observed when the angle between the bilayer normal and the magnetic field was set at 90º (Figure 4-3 **a**). To assign the peak, the angle is adjusted to 0º. (Figure 4-3 **b**) Thus, the resonances from that oriented structures was shifted downfield. The peaks at ~25 ppm and ~13 ppm can be attributed to the oriented structures of **8**, whereas the resonances at -3.1 ppm and -8.0 ppm suggest possible vesicle formation. The sharp peaks at ~13 ppm in both of the spectra correspond to the terminal phosphate group due to the high degrees of freedom.

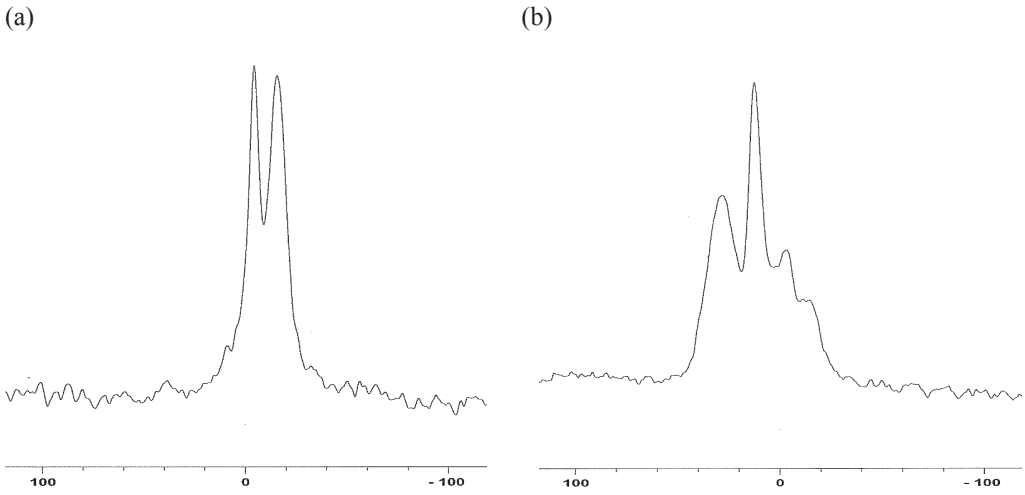

Figure 4-4. ^{31}P NMR of **8**/DMPC (1/2 mol) on coverslips. The angle between the bilayer normal and the magnetic field is set at 90º (a) and at 0º (b), respectively.

Figure 4-4 shows the ^{31}P NMR spectra of **8**/dimyristoylphosphatidylcholine (DMPC) mixtures. The spectra indicated that the addition of DMPC increased the proportion of oriented structures as shown by the reduced resonance intensity at -3.1 ppm and -8.0 ppm as shown in Figure 4-4 **b** compared with Figure 4-3 **b**. In Figure 4-4 **b**, the peak at ~25 ppm is inferred to be the superposition of head groups of **8** and DMPC.

The NMR results indicated that the adding of DMPC promoted the oriented alignment of lipid molecules. It was deduced that further dilution of **8** with DMPC would result in an increased proportion of oriented structures. However it would make the detection of NMR signal difficult due to the dilution of NMR signals of interest, ^{31}P in **8** and ^{2}H in **9**.

4.2.4 ^{2}H NMR Measurements

The ^{2}H NMR spectra of **9** has been measured in multilamellar dispersions form in the absence and presence of delipidated bR (dbR), which was purified from *Halobacterium halobium* according to the reported method.[19] Because the phase transition temperature of a pure membrane of the non-deuterated analogue **8** is 42 °C, the measurements were carried out at 50 °C.

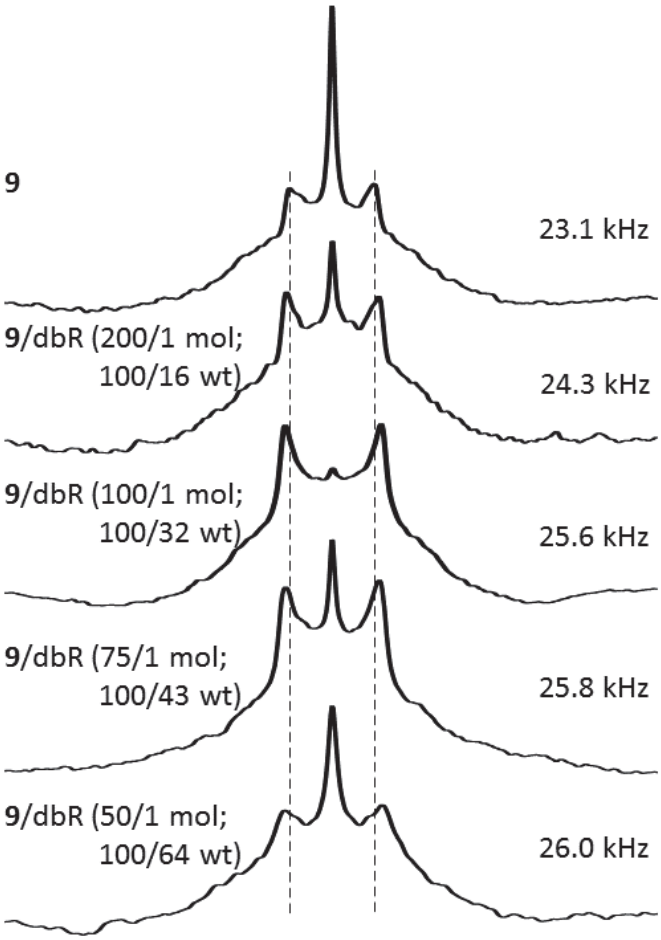

Figure 4-5. ^{2}H NMR spectra of 60 wt% aqueous multilamellar dispersions at 50 °C of pure **9** and **9**/dbR mixtures with different molar/weight ratios.

As shown in Figure 4-5, the ^{2}H NMR of pure **9** dispersion provided a pair of quadrupolar splitting with a powder pattern lineshape. It is worth noting that a strong isotropic signal was observed; which was likely due to the formation of micelles tumbling rapidly in water, although a trace amount of HDO in the sample might contribute a small portion of the singlet. Compared with native PGP-Me, the side chains of compound **9** has been largely reduced in size due to the lack to branched methyl groups. Thus the analogue has the shape of an inverted cone with packing parameter $P < 1$ and it favors the formation of micelles.

The addition of dbR altered the ^{2}H NMR spectra dramatically. The ^{2}H NMR spectra of **9**/dbR (200/1 mol) shows enhanced magnitude in quadrupolar splitting (24.3 kHz) compared to pure **9** sample (23.1 kHz) due to the restricted motion of side chains of **9** caused by hydrophobic

interactions with the protein. As the rate of exchange of annular lipids with bulk lipids is fast on the NMR time scale, only one pair of splitting was observed in the spectra. Interestingly, the intensity of isotropic peak decreased drastically, indicating the proportion of micelle structures is largely reduced in the mixture. At higher content of dbR (**9**/dbR with 100/1 mol), the side chain of **9** becomes more ordered and the isotropic peak is hardly observed. Meanwhile, the lack of micelle/liposome transition suppressed peak broadening and increased spectral resolution. Further addition of dbR change the lineshape of NMR spectra significantly. The central isotropic peak reappeared/increased and the spectra becomes poorly resolved accompanied by increasing the content of dbR.

In protein purification, most of PM lipids have been removed by detergent; however, a little amount of lipids remains around bR, including PGP-Me, PGS, and trace amount of PS. The molar ratio of dbR to these PM lipids is one to three. Thus, a mixture of **9**/PM lipids was subjected to ^{2}H NMR measurements in order to evaluate the contribution of protein in altering the behavior and morphology of **9** observed in the presence of dbR.

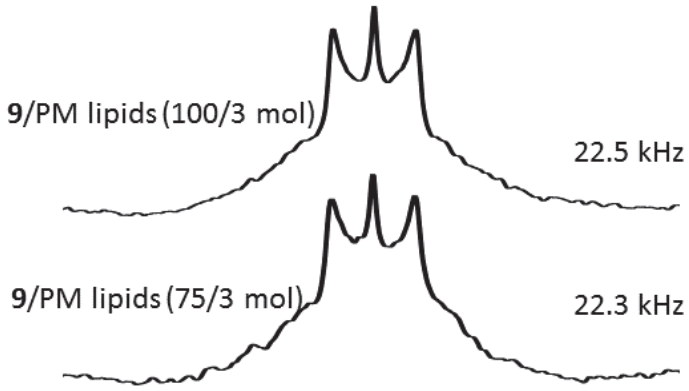

Figure 4-6. ^{2}H NMR spectra of 60 wt% aqueous multilamellar dispersions at 50 °C of **9**/PM lipids (100/3 mol) and **9**/PM lipids (75/3 mol)

As shown in Figure 4-6, the addition of PM lipids in **9** decreased the order of side chains compared to the spectra of pure **9** (Figure 4-5), thereby supporting that the observed ordering effect in **9**/dbR mixtures is due to lipid-protein interactions rather than lipid-lipid interactions. It is interesting that the isotropic signal exhibits significant difference in intensity between **9**/PM lipids (100/3 mol) and **9**/dbR (100/1 mol) mixtures. The observation of the strong isotropic peak in **9**/PM

lipids dispersion indicate that there remains significant amount of micelles in water. However, these structures can be hardly observed in **9**/dbR (100/1 mol) mixtures, indicating that bR can promote formation of liposomes in the mixture. The spectra of **9**/PM lipids (75/3 mol) dispersions provided similar lineshape as that of **9**/PM lipids (100/1 mol) mixtures.

References

1) Stoeckenius, W.; Lozier, R. H.; Bogomolni, R. A. *Biochim. Biophys. Acta.* **1979**, *505*, 215-278.

2) Luecke, H.; Schobert, B.; Richter, H. T.; Cartailler, J. P.;Lanyi, J. K. *J. Mol. Biol.* **1999**, *291*, 899-911.

3) Corcelli, A.; Lattanzio, V. M.; Mascolo, G.; Papadia, P.; Fanizzi, F. *J. Lipid Res.* **2002**, *43*, 132-140.

4) Frolov, V. A.; Shnyrova, A. V.; Zimmerberg, J. *Cold Spring Harb Perspect Biol.* **2011**, *3*, a004747.

5) Sparr, E.; Wadsten, P.; Kocherbitov, V.; Engstrom, S. *Biochim. Biophys. Acta.* **2004**, *1665*, 156-166.

6) Cullis, P. R.;de Kruijff, B. *Biochim. Biophys. Acta.* **1979**, *559*, 399-420.

7) Sparr, E.; Wadsten, P.; Kocherbitov, V.; Engstrom, S. *Biochim. Biophys. Acta.* **2004**, *1665*, 156-166.

8) Seelig, J.; Borle, F.; Cross, T. A. *Biochim. Biophys. Acta.* **1985**, *814*, 195-198.

9) Seelig, J. *Biochim. Biophys. Acta.* **1978**, *515*, 105-140.

10) (a) Andresen, T. L.; Jensen, S. S.; Madsen, R.; Jorgensen, K. *J. Med. Chem.* **2005**, *48*, 7305-7314; (b) Mikkilineni, A. B.; Kumar, P.; Abushanab, E. *J. Org. Chem.* **1988**, *53*, 6005-6009.

11) Lonnberg, H. *Org. Biomol. Chem.* **2011**, *9*, 1687-1703.

12) Ema, T.; Tanida, D.; Sakai, T. *Org. Lett.* **2006**, *8*, 3773-3775.

13) Stawinski, J.; Kraszewski, A. *Acc. Chem. Res.* **2002**, *35*, 952-960.

14) Kraszewski, A.;Stawinski, J. *Pure Appl. Chem.* **2007**, *79*, 2217-2227.

15) Lethu, S.; Matsuoka, S.; Murata, M. *Org. Lett.* **2014**, *16*, 844-847.

16) Steinbauer, B.; Mehnert, T.; Beyer, K. *Biophys. J.* **2003**, *85*, 1013-1024.

17) Salgado, G. F.; Struts, A. V.; Tanaka, K.; Fujioka, N.; Nakanishi, K.; Brown, M. F. *Biochemistry.* **2004**, *43*, 12819-12828.

18) Das, N.; Murray, D. T.; Cross, T. A. *Nat. Protoc.* **2013**, *8*, 2256-2270.

19) Oesterhelt, D.; Stoeckenius, W. *Methods Enzymol.* **1974**, *31*, 667-678.

Chapter 5

Conclusions

The thesis makes a research on developing novel phospholipid probes for exploring biomembrane functions by chemical synthesis. The behavior of these probes in model membranes has been studied by solid-state NMR techniques. There are three topics which are included in this thesis, and the following conclusions can be made:

1. In the development of membrane probes for a direct optical visualization of lipid rafts, three Raman probes bearing alkyne, diyne, and multiple C–D bonds on the polar head group of sphingomyelin (SM) have been synthesized and evaluated for their applicability to imaging experiments. One probe containing the diyne moiety on the polar head group was found to be the best candidate due to the strong and sharp Raman peak and high similarity in raft-like domain formation between the probe and natural SM. An important property of the probe is that it has a strong preference to partitioning into L_o phases revealed by solid-state ^2H NMR. Raman imaging in monolayer using the probe exhibited a "three phase" distribution of raft-like membranes, which provided a new insight into the raft formation mechanism.

2. To study lipid organization in raft like membranes at the molecular level, [C6-$^2H_2$] DOPC, a useful isotope probe, has been developed for solid-state ^2H NMR measurements. In this study, a highly efficient synthetic method for [C6-$^2H_2$] oleic acid, a key intermediate used for the synthesis of [C6-$^2H_2$] DOPC, has been established. In raft-like oriented bilayers, the newly synthesized probe shows clear L_o/L_d phase separation and characteristic phase behavior at various temperatures, and has been successfully utilized for the comparison of membrane properties between SM and dihydrosphingomyelin (DHSM) membranes. The probe may serve as a useful biochemical tool for investigating various L_o/L_d-co-existing systems.

3. A stereoselective synthesis of phosphatidylglycerophosphate methyl ester (PGP-Me) analogue has been accomplished, which demonstrates the usefulness and applicability of the H-phosphonate methodology for construction of lipid molecules containing a chiral glycerol bisphosphate moiety. A ^2H-labled PGP-Me analogue was synthesized and used as an isotope probe for a mesoscopic investigation of lipid–protein interactions in membranes. Solid-state ^{31}P NMR spectra suggested the formation of multiple phases using the analogue in bilayer preparation on glass plates. The interactions between delipidated bacteriorhodopsin (dbR) and lipids have

been successfully observed by ^{2}H NMR. The NMR result shows that a small change of content of dbR makes a significant change in behavior and morphology of lipid molecules. The optimal condition for reconstitution of dbR into liposomes has been found. Current study indicates that dbR can promote liposome formation under certain conditions. There are several type of commercial lipids with different polar heads, such as PC, PG, PE, PS, and PA, which have the similar side chain structure with the analogue. Thus, further physicochemical analytic result of the developed analogue would be useful for selectively evaluation of the importance of head group of PGP-Me in sustaining structural and functional integrity of protein in membranes.

Chapter 6

Experimental Section

General Information

Unless otherwise noted, all the chemicals and solvents were purchased from Nacalai Tesque, Sigma-Aldrich, TCI, and KANTO Chemicals Inc., and used without further purification. Thin layer chromatography (TLC) were Merck pre-coated silica gel 60 F-254 plates. TLC plates were visualized by UV irradiation (254 nm) or stained with phosphomolybdic acid in ethanol. Optical rotation was recorded on a JASCO P-1010 polarimeter. NMR spectra were collected with a JEOL ECA 400 (400 MHz) or JEOL ECA 500 (500 MHz) spectrometer, using the deuterated solvent as the lock. ^{31}P NMR chemical shifts are reported using triphenylphosphate (0.0485 M in $CDCl_3$) as external standard, referenced at -16.58 ppm. Chemical shifts were given in ppm (δ), coupling constants (*J*) in Hz. The following abbreviations were used to designate the multiplicities: s = singlet, d = doublet, t = triplet, q = quartet, quint = quintuplet, m = multiplet, br = broad. High resolution mass spectra (HRMS) were recorded on a LTQ-Orbitrap XL instrument.

Sample Preparation for NMR Measurements

For NMR samples used in Chapters 2 and 3:

Porcine brain SM was purchased from Avanti Polar Lipids and chol was purchased from Sigma-Aldrich. N-Stearoyl SM (SSM) was purified by HPLC (Cosmosil 5C18-AR-II column, 10 × 150 mm, Nacalai Tesque) from brain SM and used for ^{2}H NMR measurements. DHSM was prepared from SSM by hydrogenation using palladium as a catalyst. For oriented lipid multibilayers, 2 mg of total lipids were dissolved in *n*-PrOH/MeOH/$CHCl_3$ (70 μL, 4:1:1 v/v/v). The lipid solution was applied to 14 micro cover glasses (2 × 5 × 0.12 ~ 0.17 mm, Matsunami Glass Ind., Ltd), dried first in air and thereafter under high vacuum for 20 h. The slides were stacked in a culture dish and hydrated with K_2SO_4-saturated deuterium-depleted water at 40 °C for 3 days, resulting in a relative humidity of 96%. The stacked plates were transferred into an open-ended NMR tube (3 cm long, 4 mm o.d.) which was sealed in advance with a plastic stopper and epoxy glue at one end. After rehydration overnight at 40°C, the sample was fixed with another plastic stopper and sealed with epoxy glue. For unoriented samples, a mixture of lipids comprising 10.0 μmol of SM, 10.0 μmol of chol and 10.0 μmol of deuterated DOPC was dissolved in MeOH/$CHCl_3$ (1:1 v/v). After removing the solvent in vacuo for 20 h, the dried

membrane film was hydrated with 1 mL of distilled water and vigorously vortexed at 65 °C to make multilamellar vesicles. The sample was freeze−thawed three times, lyophilized and rehydrated with deuterium-depleted water to make 50% water (w/w). Then the mixture was again freeze−thawed ten times. The sample was transferred into a glass tube (5 × 26 mm), which was sealed with epoxy glue.

For NMR samples used in Chapter 4:

For oriented lipid multibilayers, 2 mg of total lipids were dissolved in MeOH/$CHCl_3$ (70 μL, 1:1 v/v). The lipid solution was applied to 14 micro cover glasses (2 × 5 × 0.12 ~ 0.17 mm, Matsunami Glass Ind., Ltd), dried first in air and thereafter under high vacuum for 20 h. The slides were stacked in a culture dish and hydrated with K_2SO_4-saturated deuterium-depleted water at 40°C for 9 days, resulting in a relative humidity of 96%. The stacked plates were transferred into an open-ended NMR tube (3 cm long, 4 mm o.d.) which was sealed in advance with a plastic stopper and epoxy glue at one end. After rehydration overnight at 40 °C, the sample was fixed with another plastic stopper and sealed with epoxy glue. For liposomal vesicles, 5.0 mg of the lipid was dissolved in MeOH/$CHCl_3$ (1:1 v/v). After removing the solvent in vacuo for 20 h, the dried membrane film was hydrated with 0.25 mL of distilled water and vigorously vortexed at 65 °C to make multilamellar vesicles. The sample was freeze−thawed six times, lyophilized, and rehydrated with deuterium-depleted water to make 60% water (w/w). Then the mixture was again freeze−thawed three times. The sample was transferred into the open-ended NMR tube (3 cm long, 4 mm o.d.) used above. After transferring, the tube was sealed with epoxy glue. For proteoliposomes, 5.0 mg of the lipid was dissolved in MeOH/$CHCl_3$ (1:1 v/v). After removing the solvent in vacuo for 20 h, the dried membrane film was hydrated with 0.5 mL of distilled water and vigorously vortexed at 65 °C to make multilamellar vesicles. The sample was freeze−thawed six times. Then dbR solution (5.57 mg/mL) was added in the dispersions which was vigorously vortexed. The sample was freeze−thawed, lyophilized, and rehydrated with deuterium-depleted water to make 60% water (w/w). Then the mixture was again freeze−thawed. The sample was transferred into the open-ended NMR tube (3 cm long, 4 mm o.d.). After transferring, the tube was sealed with epoxy glue.

^{2}H NMR Measurements

^{2}H NMR powder pattern spectra (Figure 3-3) were recorded on a 300 MHz CMX300 spectrometer

(Chemagnetics, Varian, Palo Alto, CA) with a 5 mm ^{2}H static probe (Otsuka Electronics, Osaka, Japan) using a quadrupolar echo sequence. The 90° pulse width was 2 μs, interpulse delay was 30 μs, and repetition rate was 0.5 s. The sweep width was 200 kHz, and the number of scans was around 100000. ^{2}H NMR spectra of oriented samples (Chapters 2, 3, and 4) and liposomal dispersion (Chapter 4) were acquired on a Bruker Ultrashield 400 MHz spectrometer with a Bruker 5 mm ^{2}H static probe using a quadrupolar echo sequence. The 90° pulse width was 5 μs, interpulse delay was 24 μs, and recycle delay was 0.5 s. The sweep width was 250 kHz, and the number of scans was 200000.

Solid-State ^{31}P NMR Measurements

^{31}P NMR spectra were recorded on a Bruker Ultrashield 400 MHz spectrometer. ^{31}P chemical shifts were referenced to 85% phosphoric acid.

DSC

The phase transition temperature of target molecule was measured by nanodifferential scanning calorimeter (Calorimetry Science Corp., UT). Lipid samples were prepared by following method: appropriate amounts (1-2 mg) of lipid dissolved in MeOH/$CHCl_3$ (1:4 v/v) were mixed in a glass vial. The solution was dried under a flow of nitrogen and then under high vacuum for at least 24 h. The resulting lipid film was dispersed into distilled and deionized water (0.5 mL) and incubated for 30 min at 65 °C with intermittent vortexing. 330 μL of the sample were used for DSC measurements with a scanning rate of 0.5 °C/min.

Raman Measurements

Monolayers of lipids were prepared on a computer-controlled Langmuir film balance (USI System, Fukuoka, Japan) calibrated using stearic acid (Sigma-Aldrich). The subphase, which consisted of distilled, freshly deionized water, was obtained using a Milli-Q System. The sample solution was prepared by mixing the appropriate amount of each lipid solution in a micro-vial. A total of 30 μL of lipid solution (1 mg/mL) was spread onto the aqueous subphase (100 × 290 mm^2) using a glass micropipette (Drummond Scientific Company, Pennsylvania, USA). After an initial delay period of 10 mins for evaporation of the organic solvents, the monolayers were compressed at a rate of 12 mm^2/s. Raman spectra of lipid monolayers were obtained by Raman microscopy

(Raman-11, Nanophoton) with a 532 nm excitation laser. The excitation laser was focused into a point at the sample with a water immersion objective lens (CFI Plan Apo IR 60XWI, Nikon Instruments). The exposure time was 6 s and the Raman measurement was performed 30 times per membrane. The laser power at the sample was 340 mW.

Preparation of PM

PM was prepared from cultured *Halobacterium salinarum* (strain R_1M_1) according to a standard method.[1,2] After resuspension of PM in 100 mM sodium phosphate buffer (pH 7.0), the concentration of bR were determined calorimetrically using the absorption coefficient ε = 63,000 $M^{-1}\cdot cm^{-1}$ at 570 nm of PM[3] and ε = 57,000 $M^{-1}\cdot cm^{-1}$ at 560 nm of dbR with Shimadzu UV-3150 (Kyoto, Japan).

Preparation of dbR

Delipidation of bR was performed with 3-[(3-cholamidopropyl)dimethylammonio]-2-hydroxy-1-propanesulfonate (CHAPS) and dodecyl-β-D- maltoside (DM) as described previously[4] with slight modifications as follows; PM (bR, 1 mg/mL) was incubated with 5% (w/v) CHAPS in 10 mM sodium phosphate buffer (pH 7.0) at room temperature for 48 h. The CHAPS-treated bR was then washed and incubated with 5% (w/v) DM in 10 mM sodium phosphate buffer (2 M NaCl pH 7.0) at room temperature for 48 h. The DM-treated bR was then washed, and dialysed against pure water, while being stirred with Bio-Beads at 4 °C for 1 day. The dbR was washed and resuspended in 10 mM sodium phosphate buffer (pH 7.0). The recovery of dbR was found to be ~ 95% according to the colorimetric method.

1) Oesterhelt, D.; Stoeckenius, W. *Methods Enzymol.* **1974**, *31*, 667-678.
2) Oesterhelt, D. *In Archaea: A Laboratory Manual. Halophiles.* DasSarma S, Robb FT, Place AR, Sowers KR, Schreier HJ, Fleischmann EM *et al.* (eds). Cold Spring Harbor, New York: Cold Spring Harbor Laboratory Press, **1995**, pp. 55–57.
3) Hartmann, R.; Oesterhelt, D. *Eur. J. Biochem.* **1977**, *77*, 325-335.
4) Seigneuret, M.; Neumann, J.M.; Rigaud, J. L. *J. Biol. Chem.* **1991**, *266*, 10066-10069.

Experimental Procedures and Compounds Data

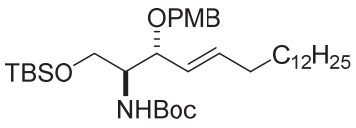

15

To a solution of **14** (500 mg, 0.97 mmol) in toluene (10 mL) was added *p*-methoxybenzyltrichloroacetimidate (0.24 mL, 1.16 mmol) and lanthanum triflate (87.9 mg, 0.15 mmol) at room temperature. After stirring at the same temperature for 30 min, the reaction mixture was washed with water. The combined organic layers were dried over $MgSO_4$, filtered and concentrated under reduced pressure. The residue was purified by flash column chromatography on silica gel (ethyl acetate/hexane = 1:10) to afford **15** (460.8 mg, 75%) as a colorless solid. ^{1}H NMR (500 MHz, $CDCl_3$): δ 0.03 (s, 3H); 0.04 (s, 3H); 0.87 (t, *J* = 6.4 Hz, 3H); 0.88 (s, 9H); 1.21-1.33 (m, 20H); 1.42 (s, 9H); 1.34-1.42 (m, 2H); 2.06 (apparent q, *J* = 7.0 Hz, 2H); 3.63 (dd, *J* = 9.0, 4.0 Hz, 1H); 3.70 (brm, 1H); 3.77-3.84 (m, 1H); 3.78 (s, 3H); 3.88 (dd, *J* = 10.0, 3.5 Hz, 1H); 4.23 (d, *J* = 11.0 Hz, 1H); 4.49 (d, *J* = 11.0 Hz, 1H); 4.73 (d, *J* = 9.5 Hz, 1H); 5.41 (dd, *J* = 15.5, 8.0 Hz, 1H); 5.65 (dt, *J* = 15.5, 7.0 Hz, 1H); 6.84 (d, *J* = 8.5 Hz, 2H); 7.21 (d, *J* = 9.0 Hz, 2H); ^{13}C NMR (125 MHz, $CDCl_3$): δ -5.34, 14.20, 18.35, 22.78, 26.00, 28.50, 29.32, 29.34, 29.45, 29.60, 29.74, 29.76, 29.79, 31.68, 32.02, 32.44, 54.83, 55.28, 61.78, 69.86, 78.94, 79.37, 113.79, 127.75, 129.36, 130.82, 136.50, 155.52, 159.12; HRMS (ESI) Calcd. for $C_{37}H_{68}NO_5Si$ $[M+H]^+$ 634.4861, found 634.4872.

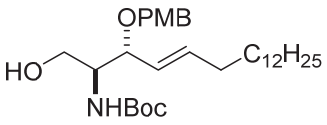

16

To a solution of **15** (200 mg, 0.32 mmol) in THF (5 mL) was added TBAF (0.47 mL, 0.47 mmol; 1.0 M solution in THF) at room temperature. After stirring at the same temperature for 1 h, the reaction mixture was concentrated. The residue was purified by flash column chromatography on silica gel (ethyl acetate/hexane = 1:10) to afford **16** (162.8 mg, 98%) as a white solid. ^{1}H NMR (400 MHz, $CDCl_3$): δ 0.87 (t, *J* = 6.4 Hz, 3H); 1.21-1.38 (m, 22H); 1.41 (s, 9H); 2.07 (apparent q, *J* = 6.8 Hz, 2H); 3.51-3.62 (m, 2H); 3.79 (s, 3H); 3.88-4.05 (m, 2H); 4.20 (d, *J* = 11.2 Hz, 1H);

4.52 (d, J = 11.2 Hz, 1H); 5.21 (d, J = 6.4 Hz, 1H); 5.40 (dd, J = 15.6, 8.0 Hz, 1H); 5.77 (dt, J = 15.6, 7.2 Hz, 1H); 6.85 (d, J = 8.8 Hz, 2H); 7.21 (d, J = 8.4 Hz, 2H); ^{13}C NMR (100 MHz, $CDCl_3$): δ 14.19, 22.77, 25.33, 28.44, 29.18, 29.25, 29.44, 29.54, 29.71, 29.76, 32.00, 32.42, 54.97, 55.33, 62.53, 68.05, 70.32, 79.50, 81.79, 113.98, 126.69, 129.48, 130.00, 136.85, 155.95, 159.37; HRMS (ESI) Calcd. for $C_{31}H_{53}NO_5Na$ $[M+Na]^+$ 542.3816, found 542.3826.

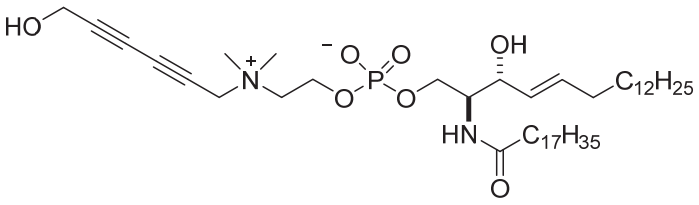

2

CuI (4.6 mg, 0.024 mmol), $NiCl_2 \cdot 6H_2O$ (1.0 mg, 4 μmol) and TMEDA (0.6 μL, 4 μmol) were added to THF (2 mL). The suspension was stirred for 5 min at room temperature. Then **1** (15 mg, 0.02 mmol) and propargyl alcohol (23.3 μL, 0.4 mmol) were added. The reaction mixture was stirred at room temperature under an air atmosphere. After completion of the reaction (~20 h), as evidenced by ^{1}H NMR of the crude reaction mixture, the solvent was evaporated under reduced pressure. The residue was washed with water and purified by flash column chromatography on silica gel (CH_2Cl_2/MeOH = 70:30 then CH_2Cl_2/MeOH/NH_4OH = 70:30:3) to afford **2** (6.4 mg, 40%) as a white solid. TLC: R_f: 0.18 (CH_2Cl_2/MeOH/NH_4OH = 70:30:3); ^{1}H NMR (500 MHz, CD_3OD): δ 0.88 (t, J = 7.5 Hz, 6H); 1.24-1.42 (m, 50H); 1.53-1.63 (m, 2H); 2.01 (q, J = 7.5 Hz, 2H); 2.13-2.20 (m, 2H); 3.24 (s, 6H); 3.70 (t, J = 5.5 Hz, 2H); 3.87-3.98 (m, 2H); 4.03 (t, J = 8.0 Hz, 1H); 4.06-4.13 (m, 1H); 4.27 (s, 2H); 4.25-4.30 (m, 2H); 4.56 (s, 2H); 5.43 (ddt, J = 15.5, 8.0, 1.5 Hz, 1H); 5.69 (dtd, J = 15.5, 7.0, 1.0 Hz, 1H); 7.90 (d, J = 9.0 Hz, 1H); ^{13}C NMR (125 MHz, CD_3OD): δ 13.11, 22.41, 25.85, 29.15, 29.18, 29.37, 29.44, 29.74, 31.75, 32.15, 36.05, 49.55, 50.86, 53.93, 55.79, 58.90, 64.22, 64.61, 65.64, 66.54, 71.22, 75.42, 81.27, 129.89, 133.82, 174.58; HRMS (ESI) Calcd. for $C_{46}H_{86}N_2O_7P$ $[M+H]^+$ 809.6167, found 809.6184.

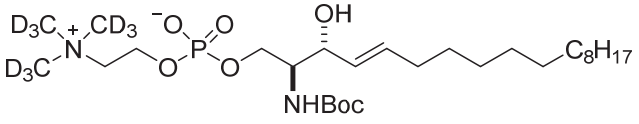

21

NaOH (352 mg, 8.8 mmol) was added to water (2 mL), to which was added $N(CD_3)_3 \cdot DCl$ (916 mg, 8.8 mmol, Cambridge Isotope Laboratories, Inc.) at 0 °C to afford 28% $N(CD_3)_3$ solution. To a solution of **20** (80 mg, 0.13 mmol) in MeOH (4 mL) was added 28% $N(CD_3)_3$ solution (2 mL). The reaction mixture was stirred at 50 °C for 6 h, and the solvents were then evaporated under reduced pressure. The residue was purified by flash column chromatography on silica gel (CH_2Cl_2/MeOH = 70:30 then CH_2Cl_2/MeOH/NH_4OH = 7:3:1) to afford **21** (30.4 mg, 40%) as a white solid. ^1H NMR (500 MHz, CD_3OD): δ 0.88 (t, *J* = 7.0 Hz, 3H); 1.27 (m, 20H); 1.35-1.44 (m, 2H); 1.41 (s, 9H); 2.01 (m, 2H); 3.55 (m, 1H); 3.61 (m, 2H); 3.94 (m, 1H); 4.00 (t, *J* = 8.0 Hz, 1H); 4.05 (m, 1H); 4.26 (m, 2H); 5.46 (dd, *J* = 15.5, 8.0 Hz, 1H); 5.70 (td, *J* = 15.5, 6.5 Hz, 1H); ^{13}C NMR (125 MHz, $CDCl_3$): δ 13.10, 22.20, 27.53, 29.03, 29.13, 29.35, 29.38, 29. 45, 31.73, 32.12, 55.36, 55.42, 59.05, 59.09, 64.76, 64.80, 65.87, 67.53, 71.66, 78.73, 129.75, 133.61, 156.66; HRMS (ESI) Calcd. for $C_{28}H_{49}D_9N_2O_7P$ $[M+H]^+$ 574.4541, found 574.4548.

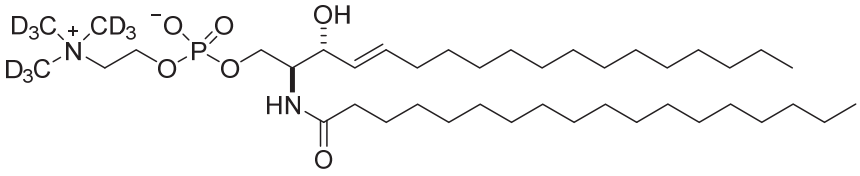

3

To a solution of **21** (27 mg, 0.047 mmol) in CH_2Cl_2 (1.2 mL) was added trifluoroacetic acid (0.24 mL) 0°C. After stirring at the same temperature for 1h, the reaction mixture was concentrated. The residue was diluted with THF (1.2 mL), and then triethylamine (40 μL, 0.28 mmol), DMAP (8.6 mg, 0.07 mmol) and *p*-nitrophenyl stearate (28.6 mg, 0.07 mmol) were added to the reaction mixture. After stirring at room temperature for 24 h, the residue was concentrated under reduced pressure and purified by flash column chromatography on silica gel (CH_2Cl_2/MeOH = 6:4 then CH_2Cl_2/MeOH/NH_4OH = 60:40:5) to afford **3** (20 mg, 58%) as a white solid. TLC: R_f: 0.13 (CH_2Cl_2/MeOH/NH_4OH = 60:40:5). ^1H NMR (500 MHz, CD_3OD): δ 0.88 (t, *J* = 7.0 Hz, 6H); 1.22-1.42 (m, 50H); 1.57 (m, 2H); 2.01 (q, *J* = 7.0 Hz, 2H); 2.16 (m, 2H); 3.60 (t, *J* = 4.5 Hz, 2H); 3.89-3.98 (m, 2H); 4.02 (t, *J* = 8.0 Hz, 1H); 4.09 (m, 1H); 4.26 (m, 2H); 5.42 (dd, *J* = 15.5, 8.0 Hz, 1H); 5.68 (td, *J* = 15.5, 6.5 Hz, 1H); ^{13}C NMR (125 MHz, $CDCl_3$): δ 13.12, 22.25, 25.59, 25.85, 28.99, 29.11, 29.14, 29.16, 29.19, 29.31, 29.38, 29.45, 29.50, 29.56, 31.76, 31.77, 32.16, 35.21, 36.05, 53.88, 53.94, 59.03, 59.07, 64.51, 64.55, 65.84, 65.85, 71.22, 129.92, 133.78, 174.55;

HRMS (ESI) Calcd. for $C_{41}H_{74}D_9N_2O_6PNa$ $[M+Na]^+$ 762.6484, found 779.6446.

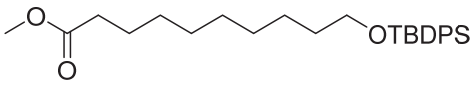

32

To a solution of methyl 10-hydroxydecanoate **31** (300 mg, 1.48 mmol) in THF (5 mL) were added imidazole (201 mg, 2.96 mmol) and *tert*-butyl(chloro)diphenylsilane (424 μL, 1.63 mmol) at 0°C. After stirring at room temperature for 2 h, the reaction mixture was concentrated under reduced pressure. The residue was purified by flash column chromatography on silica gel (ethyl acetate/hexane = 1:10) to afford **32** (640 mg, 98%) as a colorless oil. ^{1}H NMR (500 MHz, $CDCl_3$): δ 1.07 (s, 9H); 1.20-1.40 (m, 10H); 1.52-1.68 (m, 4H); 2.31 (t, J = 7.5 Hz, 2H); 3.66 (t, J = 6.5 Hz, 2H); 3.67 (s, 3H); 7.35-7.46 (m, 6H); 7.66-7.71 (m, 4H); ^{13}C NMR (125 MHz, $CDCl_3$): δ 19.33, 25.07, 25.85, 26.87, 26.98, 29.24, 29, 30, 29.40, 29.50, 32.67, 34.21, 51.52, 64.09, 127.66, 127.78, 129.36, 129.57, 129.69, 134.29, 135.45, 135. 62, 135.68, 174.40; HRMS (ESI) Calcd. for $C_{27}H_{40}O_3SiNa$ $[M+Na]^+$ 463.2639, found 463.2646.

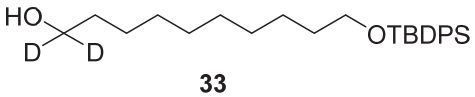

33

To a solution of $LiAlD_4$ (38 mg, 0.909 mmol) in THF (5 mL) at 0°C was added **32** (200mg, 0.454 mmol) in THF (1 mL) dropwise. After stirring at the same temperature for 2 h, the reaction mixture was quenched by ice water. The solvent was removed, and the residue was purified by flash column chromatography on silica gel (ethyl acetate/hexane = 1:3) to afford **33** (132 mg, 70%) as a colorless oil. ^{1}H NMR (500 MHz, $CDCl_3$): δ 1.04 (s, 9H); 1.21-1.39 (m, 12H); 1.51-1.59 (m, 4H); 3.65 (t, J = 6.5 Hz, 2H); 7.34-7.44 (m, 6H); 7.65-7.69 (m, 4H); ^{13}C NMR (125 MHz, $CDCl_3$): δ 19.32, 25.78, 25.85, 26.97, 29.44, 29.51, 29.62, 32.66, 32. 70, 64.10, 127.64, 129.55, 134.30, 135.67; HRMS (ESI) Calcd. for $C_{26}H_{38}D_2O_2SiNa$ $[M+Na]^+$ 437.2815, found 437.2822.

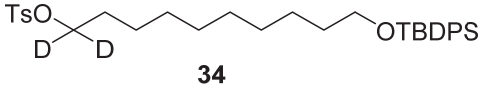

34

To a solution of **33** (36 mg, 0.087 mmol) in CH_2Cl_2 (5 mL) were added *p*-toluenesulfonyl chloride (24.8 mg, 0.13 mmol), triethylamine (29 μL, 0.209 mmol) and DMAP (7 mg, 0.05 mmol) at room

temperature. After stirring at the same temperature for 2 h, the solvent was removed. The residue was purified by flash column chromatography on silica gel (ethyl acetate/hexane = 1:3) to afford **34** (46.5 mg, 95%) as a colorless oil. ^{1}H NMR (500 MHz, $CDCl_3$): δ 1.04 (s, 9H); 1.15-1.35 (m, 12H); 1.50-1.58 (m, 2H); 1.59-1.63 (m, 2H); 2.44 (s, 3H); 3.64 (t, *J* = 6.5 Hz, 2H); 7.31-7.44 (m, 8H); 7.64-7.69 (m, 4H); 7.88 (d, *J* = 8.0 Hz, 2H); ^{13}C NMR (125 MHz, $CDCl_3$): δ 19.32, 21.72, 25.36, 25.83, 26.97, 28.69, 29.01, 29.41, 29.53, 32.65, 64.07, 127.65, 127.97, 129.56, 129,87, 133.40, 134.27, 135.66, 144.67; HRMS (ESI) Calcd. for $C_{33}H_{45}D_2O_4SSi$ $[M+H]^+$ 569.3084, found 569.3094.

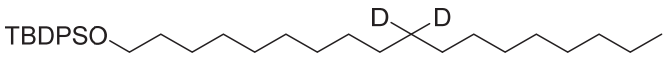

35

To a solution of **34** (70 mg, 0.123 mmol) in THF (2 mL) were added $CuCl_2$ (0.8 mg, 0.006 mmol) and 1-phenyl-1-propyne (3.0 μL, 0.025 mmol) at 0 °C. Afterward octylmagnesium bromide (123 μL, 0.246 mmol; 2.0 M in diethyl ether) was added in one portion. The ice bath was removed and the reaction mixture was stirred for 1 h. The solvent was evaporated and the residue was purified by flash column chromatography on silica gel (ethyl acetate/hexane = 1:20) to afford **35** (57 mg, 91%) as a colorless oil. ^{1}H NMR (500 MHz, $CDCl_3$): δ 0.89 (t, *J* = 7.5 Hz, 3H); 1.06 (s, 9H); 1.21-1.40 (m, 28H); 1.52-1.60 (m, 2H); 3.66 (t, *J* = 6.5 Hz, 2H); 7.35-7.44 (m, 6H); 7.65-7.70 (m, 4H); ^{13}C NMR (125 MHz, $CDCl_3$): δ 14.22, 19.32, 22.80, 25.88, 26.98, 29.47, 29.49, 29.60, 29.74, 29.76, 29.79, 29.82, 32.03, 32.69, 64.12, 127.65, 129.55, 134.31, 135.68; HRMS (ESI) Calcd. for $C_{34}H_{55}D_2OSi$ $[M+H]^+$ 511.4299, found 511.4304.

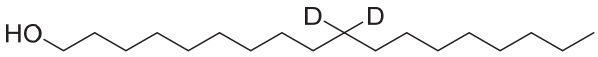

36

To a solution of **35** (30 mg, 0.058 mmol) in THF (0.5 mL) was added TBAF (58 μL, 0.116 mmol; 1.0 M in THF) at room temperature. After stirring at the same temperature for 2 h, the solvent was removed under reduced pressure. The residue was purified by flash column chromatography on silica gel (ethyl acetate/hexane = 1:3) to afford **36** (15.6 mg, 98%) as a white solid. ^{1}H NMR (400 MHz, $CDCl_3$): δ 0.87 (t, *J* = 7.2 Hz, 3H); 1.12-1.41 (m, 30H); 1.50-1.60 (m, 2H); 3.59-3.67 (m, 2H); ^{13}C NMR (125 MHz, $CDCl_3$): δ 14.20, 22.78, 25.83, 29.45, 29.53, 29.57, 29.71, 29.75, 29.80,

32.02, 32.91, 63.21; HRMS (ESI) Calcd. for $C_{18}H_{36}D_2ONa$ $[M+Na]^+$ 295.2940, found 295.2999.

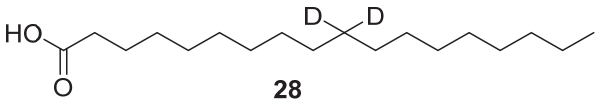

28

CrO_3 (100 mg, 1.0 mmol) was dissolved in water (0.3 mL) to which was added H_2SO_4 (0.1 mL) at 0°C to afford Jones' reagent. To a solution of **36** (15 mg, 0.05) in acetone (1 mL) was added the Jones' reagent (55 μL) and the mixture was stirred at room temperature for 10 mins. Isopropanol was added until the orange color disappeared and only a blue suspension remained. 1M HCl was then added to dissolve the blue-green solid and the mixture was extracted with ethyl acetate. The organic layers were combined and washed with brine, dried over $MgSO_4$, filtered and concentrated under reduced pressure. The residue was purified by flash column chromatography on silica gel (CH_2Cl_2/MeOH = 95/5) to afford **28** (11 mg, 70%) as a white solid. ^{1}H NMR (400 MHz, $CDCl_3$): δ 0.87 (t, *J* = 7.2 Hz, 3H); 1.16-1.42 (m, 28H); 1.57-1.68 (m, 2H); 2.34 (t, *J* = 7.6 Hz, 2H); ^{13}C NMR (100 MHz, $CDCl_3$): δ 14.20, 22.77, 24.76, 29.32, 29.44, 29.51, 29.55, 29.67, 29.74, 29.79, 32.01, 33.98, 179.37; HRMS (ESI) Calcd. for $C_{18}H_{33}D_2O_2$ $[M-H]^-$ 285.2757, found 285.2737.

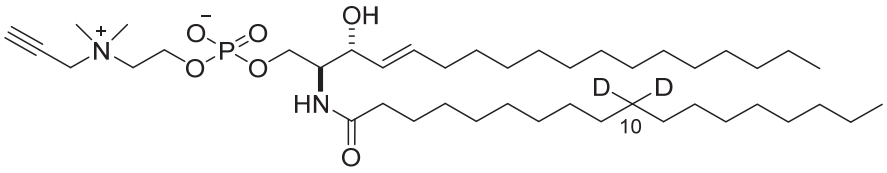

4

This compound was prepared according to the same procedure as described for **1**. ^{1}H NMR (500 MHz, CD_3OD): δ 0.88 (t, *J* = 7.0 Hz, 6H); 1.21-1.43 (m, 48H); 1.51-1.64 (m, 2H); 2.01 (q, *J* = 7.0 Hz, 2H); 2.13-2.21 (m, 2H); 3.26 (s, 6H); 3.53 (t, *J* = 2.5 Hz, 1H); 3.72 (t, *J* = 5.0 Hz, 2H); 3.88-3.98 (m, 2H); 4.02 (t, *J* = 8.0 Hz, 1H); 4.06-4.13 (m, 1H); 4.25-4.30 (m, 2H); 4.42 (d, *J* = 2.5 Hz, 2H); 5.43 (ddt, *J* = 15.5, 8.0, 1.5 Hz, 1H); 5.69 (dtd, *J* = 15.0, 7.0, 0.5 Hz, 1H); 7.90 (d, *J* = 9.0 Hz, 1H); ^{13}C NMR (125 MHz, CD_3OD): δ 13.15, 22.43, 25.86, 29.17, 29.20, 29.37, 29.46, 29.51, 29.54, 31.77, 31.78, 32.17, 36.05, 50.67, 53.87, 53.93, 55.12, 58.90, 58.94, 63.99, 64.05, 64.57, 64.61, 71.08, 71.21, 81.63, 129.93, 133.78, 174.54; HRMS (ESI) Calcd. for $C_{43}H_{83}D_2N_2O_6PNa$ $[M+Na]^+$ 779.6006, found 779.6016.

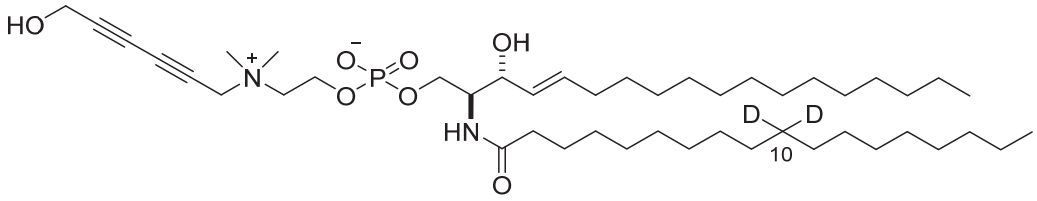

5

This compound was prepared according to the same procedure as described for **2**. ^{1}H NMR (500 MHz, CD_3OD): δ 0.88 (t, *J* = 7.5 Hz, 6H); 1.22-1.43 (m, 48H); 1.50-1.63 (m, 2H); 2.10 (q, *J* = 8.5 Hz, 2H); 2.13-2.20 (m, 2H); 3.25 (s, 6H); 3.71 (t, *J* = 5.0 Hz, 2H); 3.88-3.99 (m, 2H); 4.02 (t, *J* = 8.0 Hz, 1H); 4.06-4.12 (m, 1H); 4.27 (s, 2H); 4.21-4.34 (m, 2H); 4.56 (s, 2H); 5.43 (ddt, *J* = 15.0, 7.5, 1.2 Hz, 1H); 5.69 (dtd, *J* = 15.0, 7.0, 0.6 Hz, 1H); 7.90 (d, *J* = 9.0 Hz, 1H); ^{13}C NMR (125 MHz, CD_3OD): δ 13.16, 22.43, 25.87, 29.18, 29.21, 29.33, 29.47, 29.52, 29.55, 29.58, 31.77, 31.79, 32.18, 36.06, 49.56, 50.87, 53.87, 53.93, 55.80, 58.90, 59.94, 64.22, 64.28, 64.61, 64.65, 65.67, 66.56, 71.21, 75.43, 81.29, 129.93, 133.79, 174.54; HRMS (ESI) Calcd. for $C_{46}H_{83}D_2N_2O_7PNa$ $[M+Na]^+$ 833.6112, found 833.6124.

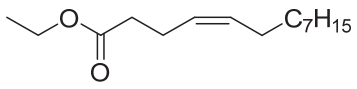

38

Triphenylphosphine (8.0g, 30.4 mmol) was added in dry toluene (20 mL) under argon atmosphere. Ethyl 4-bromobutanoate (2.0 g, 10.3 mmol) was added and the mixture was stirred at 120 °C for 24 h. After cooling down to room temperature, white solid was formed. The toluene was decanted off and the solid washed with hot toluene to give the crude phosphonium salt (4.2 g) which was dried under vacuum over P_2O_5 overnight and used without further purification. ^{1}H NMR (400 MHz, $CDCl_3$): δ 1.22 (t, *J* = 7.2 Hz, 3H); 1.91 (m, 2H); 2.90 (m, 2H); 4.04-4.16 (m, 4H); 7.64-7.71 (m, 6H); 7.74-7.80 (m, 3H); 7.85-7.93 (m, 6H). The phosphonium salt (4.1 g, 8.95 mmol) was dissolved in dry 1,3-Dimethyl-3,4,5,6-tetrahydro-2(1*H*)-pyrimidinone (30 mL) under argon and then dry THF (80 mL) was added. At -78°C, a 0.5M solution of potassium bis(trimethylsilyl)amide (17.9 mL, 8.95 mmol) was added dropwise over 15 min. The reaction mixture was stirred at -78°C for 1 h. Then nonanal (1.6 mL, 8.95 mmol) was added dropwise over 30 min. The reaction mixture was stirred at the same temperature for 2 h, and then allowed to come to room temperature over night while stirring. The reaction was quenched with water (20

mL) and extracted with EtOAc. The organic layers were combined and washed with brine, dried over $MgSO_4$, filtered and concentrated under reduced pressure. The residue was purified by flash column chromatography on silica gel (ethyl acetate/hexane = 1:7) to afford **38** (1.07 g, 50% for 2 steps) as a colorless oil. ^{1}H NMR (400 MHz, $CDCl_3$): δ 0.87 (t, *J* = 7.2 Hz, 3H); 1.20-1.38 (m, 15H); 2.02 (apparent q, *J* = 6.8 Hz, 2H); 2.28-2.38 (m, 4H); 4.13 (q, *J* = 7.2 Hz, 2H); 5.27-5.35 (m, 1H); 5.36-5.45 (m, 1H); ^{13}C NMR (100 MHz, $CDCl_3$): δ 14.18, 14.33, 22.75, 22.91, 27.28, 29.38, 29.59, 29.72, 31.97, 34.53, 60.37, 127.41, 131.63, 173.36.

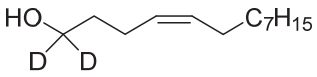

39

To a solution of $LiAlD_4$ (52 mg, 1.248 mmol) in THF (5 mL) at 0 °C was added **38** (150mg, 0.624 mmol) in THF (1.4 mL) dropwise. After stirring at the same temperature for 2 h, the reaction mixture was quenched by ice water. The solvent was removed, and the residue was purified by flash column chromatography on silica gel (ethyl acetate/hexane = 1:3) to afford **39** (100 mg, 80%) as a white solid. The total deuterium incorporation rate is > 95% determined by the residual signal of CH_2OH at 3.62 ppm. ^{1}H NMR (500 MHz, $CDCl_3$): 0.87 (t, *J* = 7.5 Hz, 3H); 1.20-1.38 (m, 12H); 1.61 (t, *J* = 7.5 Hz, 2H); 2.02 (apparent q, *J* = 6.5 Hz, 2H); 2.11 (apparent q, *J* = 6.5 Hz, 2H); 5.38 (m, 2H); ^{13}C NMR (125 MHz, $CDCl_3$): δ 14.19, 22.76, 23.64, 27.30, 29.41, 29.60, 29.80, 31.98, 32.55, 61.88, 62.05, 128.89, 130.93; HRMS Calcd. for $C_{13}H_{25}D_2O$ $[M+H]^+$ 201.2182, found 201.2201.

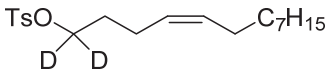

40

To a solution of **39** (80 mg, 0.4 mmol) in CH_2Cl_2 (10 mL) were added *p*-toluenesulfonyl chloride (91.5 mg, 0.48 mmol), triethylamine (134 μL, 0.96 mmol) and *N,N*-dimethyl-4-aminopyridine (9.8 mg, 0.08 mmol) at room temperature. After stirring at the same temperature for 1 h, the solvent was removed. The residue was purified by flash column chromatography on silica gel (ethyl acetate/hexane = 1:3) to afford **40** (139 mg, 98%) as a colorless semi-solid. The total deuterium incorporation rate is > 95% determined by the residual signal of CH_2OTs at 3.99 ppm. ^{1}H NMR (500 MHz, $CDCl_3$): δ 0.87 (t, *J* = 7.5 Hz, 3H); 1.21-1.32 (m, 12H); 1.67 (t, *J* = 7.5 Hz, 2H); 1.95

(apparent q, J = 7.0 Hz, 2H); 2.05 (apparent q, J = 7.5 Hz, 2H); 2.44 (s, 3H); 5.18-5.25 (m, 1H); 5.34-5.40 (m, 1H); 7.33 (d, J = 8.5 Hz, 2H); 7.78 (d, J = 8.0 Hz, 2H); ^{13}C NMR (125 MHz, $CDCl_3$): δ 14.19, 21.71, 22.76, 23.05, 27.27, 28.76, 29.38, 29.60, 29.69, 31.98, 69.52, 127.34, 127.95, 129.88, 131.80, 133.38, 144.71; HRMS Calcd. for $C_{20}H_{30}D_2O_3SNa$ $[M+Na]^+$ 377.2090, found 377.2123.

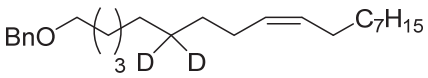

41

Formation of Grignard reagent: Under argon atmosphere, to a suspension of magnesium turnings (1.5 equiv) in THF (1.0 mL/mmol of substrate) containing 2–3 drops of 1,2-dibromoethane were added few drops of benzyloxypentyl bromide (1 equiv) in THF (0.5 mL/mmol of substrate). The mixture was heated until the reaction started, then the brominated compound was added drop by drop to maintain a non-assisted gentle reflux. After complete addition of the starting material, the mixture was heated under reflux for 1 h. The solution of Grignard reagent was cooled down and titrated prior to use. [3] To a solution of **40** (75 mg, 0.21 mmol) in THF (2 mL) were added $CuCl_2$ (1.4 mg, 0.01 mmol) and 1-phenyl-1-propyne (5.0 μL, 0.05 mmol) at 0°C under argon. Afterward the Grignard reagent (2.1 mL, 0.42 mmol; 0.2 M in THF) was added in one portion. The ice bath was removed and the reaction mixture was stirred for 1 h. The solvent was evaporated. The residue was purified by flash column chromatography on silica gel (ethyl acetate/hexane = 1:20) to afford **41** (68 mg, 90%) as a colorless semi-solid. ^{1}H NMR (400 MHz, $CDCl_3$): δ 0.87 (t, J = 7.2 Hz, 3H); 1.18-1.42 (m, 20H); 1.61 (m, 2H); 2.01 (m, 4H); 3.46 (t, J = 6.8 Hz, 2H); 4.49 (s, 2H); 5.34 (m, 2H); 7.23-7.37 (m, 5H); ^{13}C NMR (100 MHz, $CDCl_3$): δ 14.20, 22.77, 26.29, 27.24, 27.30, 29. 41, 29.50, 29.62, 29.64, 29.86, 31.99, 70.61, 72.94, 127.54, 127.69, 128.41, 129.96, 130.00, 138.82; HRMS Calcd. for $C_{25}H_{40}D_2ONa$ $[M+Na]^+$ 383.3253, found 383.3278.

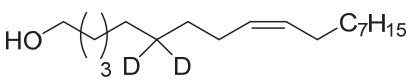

42

To a solution of **41** (80 mg, 0.22 mmol) in CH_2Cl_2 (10 mL) at -78 °C was added boron trichloride (0.44 mL, 1M in CH_2Cl_2). The reaction mixture was allowed to warm to room temperature, stirred

for 2 h, quenched with MeOH and diluted with water. The organic layer was washed with water, dried over $MgSO_4$, filtrated and concentrated under reduced pressure. The residue was purified by flash column chromatography on silica gel (ethyl acetate/hexane = 1:5) to afford **42** (55 mg, 95%) as a white solid. ^{1}H NMR (400 MHz, $CDCl_3$): δ 0.87 (t, *J* = 7.2 Hz, 3H); 1.20-1.40 (m, 20H); 1.55 (m, 2H); 2.00 (m, 4H); 3.62 (t, *J* = 6.4 Hz, 2H); 5.33 (m, 2H); ^{13}C NMR (100 MHz, $CDCl_3$): δ 14.19, 22.76, 25.82, 27.22, 27.29, 29.40, 29.44, 29.61, 29.85, 31.99, 32.89, 63.17, 129.91, 130.02; HRMS Calcd. for $C_{18}H_{34}D_2ONa$ $[M+Na]^+$ 293.2784, found 293.2814.

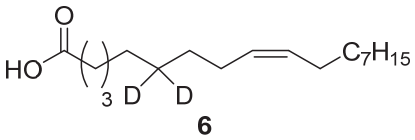

6

Preparation method for Jones' reagent: CrO_3 (100 mg, 1.0 mmol) was dissolved in water (0.3 mL) upon which was added H_2SO_4 (0.1 mL) at 0 °C. To a solution of **42** (40 mg, 0.15 mmol) in acetone (1 mL) was added the Jones' reagent (165 μL) and the mixture was stirred at room temperature for 10 min. Isopropanol was added until the orange color disappeared and only a blue suspension remained. 1M HCl was then added to dissolve the blue-green solid and the mixture was extracted with ethyl acetate. The organic layers were combined and washed with brine, dried over $MgSO_4$, filtered and concentrated under reduced pressure. The residue was purified by flash column chromatography on silica gel (CH_2Cl_2/MeOH = 95/5) to afford **6** (30.3 mg, 72%) as a white solid. ^{1}H NMR (400 MHz, $CDCl_3$): δ 0.87 (t, *J* = 7.2 Hz, 3H); 1.18-1.39 (m, 20H); 1.61 (m, 2H); 2.00 (m, 4H); 2.32 (t, *J* = 7.6 Hz, 2H); 5.33 (m, 2H); ^{13}C NMR (100 MHz, $CDCl_3$): δ 14.19, 22.76, 24.84, 27.20, 27.30, 28.35, 29.06, 29.12, 29.41, 29.61, 29.74, 29.85, 31.99, 34.18, 129.82, 130.08, 179.51; HRMS Calcd. for $C_{18}H_{31}D_2O_2$ $[M-H]^-$ 283.2601, found 283.2596.

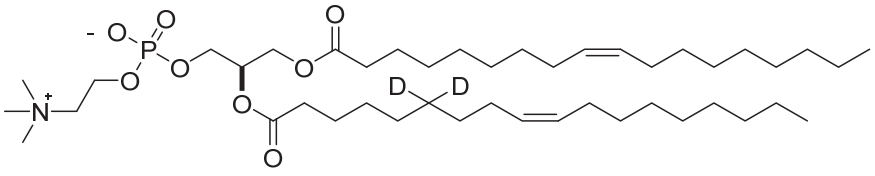

7

To a solution of 1-oleoyl-2-hdroxy-sn-glycero-3-phosphocholine (35 mg, 0.07 mmol, Avanti Polar Lipids) and **6** (25 mg, 0.09 mmol) in CH_2Cl_2 (1.3 mL) at room temperature were added 2-methyl-6-nitrobenzoic anhydride (116 mg, 0.34 mmol) and *N,N*-dimethyl-4-aminopyridine (82

mg, 0.67 mmol). After stirring at the same temperature for 16 h, the solvent was removed. The residue was purified by flash column chromatography on silica gel (CH_2Cl_2/MeOH/H_2O = 70:30:4) to afford **7** (31.7 mg, 60%) as a white solid. TLC: R_f: 0.3 (CH_2Cl_2/MeOH/ H_2O = 70:30:4). $[\alpha]^{23}_D$ +6.5 (*c* 0.001 ,$CHCl_3$/CH_3OH = 4:1); ^{1}H NMR (500 MHz, $CDCl_3$): δ 0.88 (t, *J* = 7.0 Hz, 6H); 1.21-1.39 (m, 38H); 1.58 (m, 4H); 2.10 (m, 8H); 2.31 (m, 4H); 3.21 (s, 9H); 3.62 (m, 2H); 3.98 (t, *J* = 6.5 Hz, 2H); 4.15 (dd, *J* = 6.5, 12.0 Hz, 1H); 4.25 (m, 2H); 4.42 (dd, *J* = 3.0, 12.0 Hz, 1H); 5.23 (m, 1H); 5.33 (m, 4H); ^{13}C NMR (100 MHz, $CDCl_3$): δ 13.17, 22.43, 24.69, 24.72, 26.85, 28.81, 28.83, 28.87, 29.05, 29.15, 29.31, 29.54, 31.76, 33.59, 33.76, 53.32, 53.36, 59.12, 59.16, 62.36, 63.52, 66.09, 70.42, 70.50,129.43, 129.59, 173.20, 173.49; HRMS Calcd. for $C_{44}H_{82}D_2NO_8PNa$ $[M+Na]^+$ 810.5952, found 810.6003.

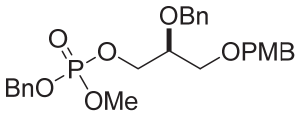

59

To a solution of **57** (730 mg, 2.4 mmol) and **46** (650 mg, 2.4 mmol) in CH_2Cl_2 (8 mL) was added 1H-tetrazole (169 mg, 2.4 mmol) at 0 °C. After stirring at room temperature for 1h, *t*-BuOOH (436 μL, 2.4 mmol, 5.5 M in nonane) was added at 0 °C. The reaction mixture was stirred at the same temperature for 1h. 1 mL of Na_2SO_3 (1M) was added in the mixture. After vigorous stirring for 10 min, the mixture was diluted with CH_2Cl_2 and washed with sat. Na_2CO_3. The organic layer was washed with water, dried over $MgSO_4$, filtrated and concentrated under reduced pressure. The residue was purified by flash column chromatography on silica gel (ethyl acetate/hexane = 2:5) to afford **59** (1.02 g, 87%) as a colorless oil. ^{1}H NMR (400 MHz, $CDCl_3$): δ 3.53 (dd, *J* = 2.8, 5.2 Hz, 2H); 3.68 (d, *J* = 11.2 Hz, 3H); 3.72-3.79 (m, 1H); 3.78 (s, 3H); 4.06-4.14 (m, 1H); 4.16-4.23 (m, 1H); 4.44 (d, *J* = 2.8 Hz, 2H); 4.58-4.67 (m, 2H); 5.03 (d, *J* = 8.0 Hz, 2H); 6.86 (dd, *J* = 0.8, 8.4 Hz, 2H); 7.19-7.73 (m, 12H); ^{13}C NMR (100 MHz, $CDCl_3$): δ 54.37, 54.40, 54.43, 54.45, 55.36, 67.07, 67.13, 68. 77, 69.37, 72.31, 73.21, 76.83, 77.15, 77.46, 113.86, 127.79, 127.88, 128.00, 128.45, 128.63, 128.68, 129.41, 135.91, 135.93, 135.97, 135.99, 138.20, 159.32; ^{31}P NMR (100 MHz, $CDCl_3$): δ 1.08; HRMS Calcd. for $C_{26}H_{31}O_7PNa$ $[M+Na]^+$ 509.1700, found 509.1703.

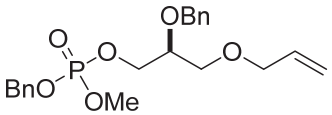

60

To a solution of **58** (480 mg, 2.2 mmol) and **46** (581 mg, 2.2 mmol) in CH_2Cl_2 (6 mL) was added 1H-tetrazole (147 mg, 2.2 mmol) at 0 °C. After stirring at room temperature for 1h, *t*-BuOOH (393 μL, 2.4 mmol, 5.5 M in nonane) was added at 0 °C. The reaction mixture was stirred at the same temperature for 1h. 1 mL of Na_2SO_3 (1M) was added in the mixture. After vigorous stirring for 10 min, the mixture was diluted with CH_2Cl_2 and washed with sat. Na_2CO_3. The organic layer was washed with water, dried over $MgSO_4$, filtrated and concentrated under reduced pressure. The residue was purified by flash column chromatography on silica gel (ethyl acetate/hexane = 2:5) to afford **60** (658 mg, 87%) as a colorless oil. ^{1}H NMR (500 MHz, $CDCl_3$): δ 3.53 (dd, J = 2.8, 5.2 Hz, 2H); 3.72 (d, J = 11.2 Hz, 3H); 3.73-3.78 (m, 1H); 3.94-4.00 (m, 2H); 4.06-4.13 (m, 1H); 4.16-4.23 (m, 1H); 4.62-4.69 (m, 2H); 5.05 (d, J = 8.4 Hz, 2H); 5.14-5.18 (m, 1H); 5.21-5.28 (m, 1H); 5.87 (m, 1H); 7.22-7.45 (m, 10H); ^{13}C NMR (125 MHz, $CDCl_3$): δ 54.54, 54.39, 54.41, 54.44, 67.05, 67.09, 69.12, 69.33, 69.38, 72.35, 72.46, 76.53, 76.55, 76.58, 76.61, 76.91, 77.16, 77.41, 117.22, 127.79, 127. 88, 128.00, 128.62, 128.68, 134.68, 134.57. 135.94, 138. 21; ^{31}P NMR (100 MHz, $CDCl_3$): δ 1.35; HRMS Calcd. for $C_{21}H_{27}O_6PNa$ $[M+Na]^+$ 429.1437, found 429.1439.

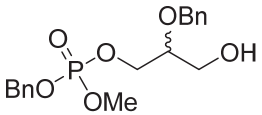

45

In the case of deprotection with DDQ; ^{1}H NMR (400 MHz, $CDCl_3$): δ 3.59-3.67 (m, 2H); 3.71 (d, J = 11.2 Hz, 1.8H); 3.72 (d, J = 11.2 Hz, 1.2H); 3.68-3.72 (m, 1H); 4.09-4.18 (m, 2H); 4.60 (ABq, 1.2H, $\Delta\delta_{AB}$ = 0.03, J_{AB} = 12.0 Hz); 4.62 (ABq, 1.8H, $\Delta\delta_{AB}$ = 0.03, J_{AB} = 12.0 Hz); 5.06 (d, J = 8.4 Hz, 1.2H); 3.72 (d, J = 8.4 Hz, 1.8H); 7.21-7.40 (m, 10H); ^{13}C NMR (100 MHz, $CDCl_3$): δ 54.50, 54.57, 61.11, 61.16, 65.82, 65.88, 69.59, 69.65, 72.25, 76.79, 77.11, 77.42, 77.61, 77.68, 127.92, 128.05, 128.07, 128.09, 128.60, 128.74, 135.74, 135.80, 137.87; ^{31}P NMR (100 MHz, $CDCl_3$): δ 1.58; HRMS Calcd. for $C_{18}H_{24}O_6PNa$ $[M+Na]^+$ 389.1124, found 389.1129.

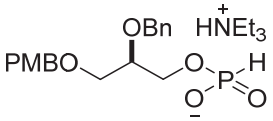

62

To a solution of **61** (186 mg, 0.62 mmol) in dry pyridine (1 mL) was added 2-chloro-4H-benzo[*d*][1,3,2]dioxaphosphinin-4-one (150 mg, 0.74 mmol) at 0 °C. After stirring at room temperature for 1h, $Et_3NH_2CO_3$ (2 ml, 1M) was added. The reaction mixture was stirred at the same temperature for 1h. After concentration, the residue was purified by flash column chromatography on silica gel (CH_2Cl_2/MeOH/Et_3N = 100:6:1) to afford **62** (244 mg, 85%) as a colorless oil. ^{1}H NMR (400 MHz, $CDCl_3$): δ 1.21 (t, *J* = 7.2 Hz, 9H); 2.93 (q, *J* = 7.2 Hz, 6H); 3.48-3.60 (m, 2H); 3.71-3.78 (m, 1H); 3.72 (s, 3H); 3.88-4.02 (m, 2H); 4.39 (s, 2H); 4.62 (ABq, 2H, $\Delta\delta_{AB}$ = 0.03, J_{AB} = 11.6 Hz); 6.78 (d, *J* = 8.4 Hz, 2H); 6.80 (d, *J* = 624 Hz, 1H); 7.14-7.30 (m, 7H); ^{13}C NMR (100 MHz, $CDCl_3$): δ 8.57, 45.54, 55.32, 63.34, 63.39, 70.04, 72.07, 73. 07, 76.94, 77.25, 77.58, 77.63, 77.71, 113.76, 127.46, 127.72, 128.28, 129.26, 130.48, 138.79, 159. 15; ^{31}P NMR (100 MHz, $CDCl_3$): δ 5.83; HRMS Calcd. for $C_{18}H_{22}O_6P$ [M-$HNEt_3^+$]$^-$ 365.1159, found 365.1151.

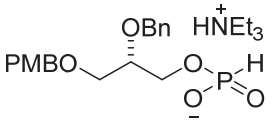

enantiomer of **62**

This compound was prepared by the same procedure as described for **62** using (S)-solketal. ^{1}H NMR (400 MHz, $CDCl_3$): δ 1.21 (t, *J* = 7.2 Hz, 9H); 2.93 (q, *J* = 7.2 Hz, 6H); 3.48-3.61 (m, 2H); 3.70-3.78 (m, 1H); 3.72 (s, 3H); 3.88-4.02 (m, 2H); 4.39 (s, 2H); 4.62 (ABq, 2H, $\Delta\delta_{AB}$ = 0.03, J_{AB} = 11.6 Hz); 6.78 (d, *J* = 8.4 Hz, 2H); 6.80 (d, *J* = 646 Hz, 1H); 7.14-7.31 (m, 7H); ^{13}C NMR (125 MHz, $CDCl_3$): δ 8.64, 45.78, 55.35, 63.86, 63. 90, 69.72, 72.19, 73.12, 76.86, 77.11, 77.37, 77.44, 113.82, 127.54, 127. 80, 128.34, 129.32, 130.44, 138.66, 159.21; ^{31}P NMR (100 MHz, $CDCl_3$): δ 5.83; HRMS Calcd. for $C_{18}H_{22}O_6P$ [M-$HNEt_3^+$]$^-$ 365.1159, found 365.1152.

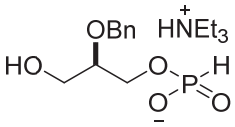

47

To a solution of **62** (53.6 mg, 0.11 mmol) in CH_2Cl_2 (1 mL) was added trifluoroacetic acid (0.2 mL) at 0 °C. After stirring at the same temperature for 1h, Et_3N (0.4 ml) was added slowly. After concentration, the residue was purified by flash column chromatography on silica gel (CH_2Cl_2/MeOH/Et_3N = 30:10:0.3) to afford **47** (31.8 mg, 80%) as a colorless oil. ^1H NMR (400 MHz, $CDCl_3$): δ 1.31 (t, J = 7.6 Hz, 9H); 3.03 (m, 6H); 3.60 (m, 1H); 3.66-3.78 (m, 2H); 4.03-4.10 (m, 2H); 4.60 (ABq, 2H, $\Delta\delta_{AB}$ = 0.03, J_{AB} = 12.0 Hz); 6.85 (d, J = 637 Hz, 1H); 7.21-7.35 (m, 5H); ^{13}C NMR (100 MHz, $CDCl_3$): δ 8.61, 45.63, 60.30, 61.48, 61.52, 71.61, 78.28, 127.75, 127.85, 128.45, 138.43; ^{31}P NMR (100 MHz, $CDCl_3$): δ 6.45; HRMS Calcd. for $C_{10}H_{14}O_5P$ [M-$HNEt_3^+$]$^-$ 245.0584, found 245.0578.

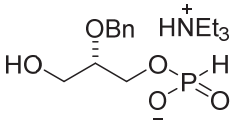

enantiomer of **47**

This compound was prepared by the same procedure as described for **47** using (S)-solketal. ^1H NMR (400 MHz, $CDCl_3$): δ 1.26 (t, J = 7.6 Hz, 9H); 3.00 (m, 6H); 3.58 (m, 1H); 3.65-3.75 (m, 2H); 4.03-4.08 (m, 2H); 4.59 (ABq, 2H, $\Delta\delta_{AB}$ = 0.03, J_{AB} = 12.0 Hz); 6.85 (d, J = 638 Hz, 1H); 7.20-7.35 (m, 5H); ^{13}C NMR (100 MHz, $CDCl_3$): δ 8.58, 45.65, 60.30, 61.70, 61.75, 71.62, 78.37, 127.72, 127.83, 128.42, 138.44; ^{31}P NMR (100 MHz, $CDCl_3$): δ 6.45; HRMS Calcd. for $C_{10}H_{14}O_5P$ [M-$HNEt_3^+$]$^-$ 245.0584, found 245.0578.

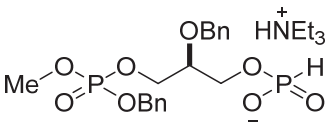

43

To a solution of **47** (70 mg, 0.2 mmol) and **46** (70 mg, 0.26 mmol) in CH_2Cl_2 (1 mL) was added 1H-tetrazole (18 mg, 0.26 mmol) at 0 °C. The mixture was stirred at room temperature for 1h. After stirring at room temperature for 1h, *t*-BuOOH (54 μL, 0.3 mmol, 5.5 M in nonane) was

added at 0 °C. The reaction mixture was stirred at the same temperature for 1h. 0.5 mL of Na_2SO_3 (1M) was added. After vigorous stirring for 10 min, the mixture was concentrated. The residue was purified by flash column chromatography on silica gel (CH_2Cl_2/MeOH/Et_3N = 100:6:1) to afford **43** (96 mg, 90%) as a colorless oil. ^{1}H NMR (400 MHz, $CDCl_3$): δ 1.18 (t, J = 7.6 Hz, 18H; $HNEt_3$ residue); 2.90 (m, 12H; $HNEt_3$ residue); 3.53 (md, J = 11.2 Hz, 3H); 3.64 (m, 1H); 3.78-3.86 (m, 2H); 3.92-4.02 (m, 1H); 4.04-4.12 (m, 1H); 4.59 (ABq, 2H, $\Delta\delta_{AB}$ = 0.03, J_{AB} = 11.6 Hz); 4.85-4.91 (m, 2H); 6.71 (d, J = 629 Hz, 1H); 7.06-7.22 (m, 10H); ^{13}C NMR (100 MHz, $CDCl_3$): δ 8.63, 45.74, 54.34, 54.39, 61.91, 61.96, 66.69, 66.74, 69.21, 69.26, 72.02, 76.61, 76.68, 76.74, 127.67, 127.71, 127.87, 128.31, 128.58, 135.72, 135.77, 137.98; ^{31}P NMR (100 MHz, $CDCl_3$): δ 0.80, 4.89; HRMS Calcd. for $C_{18}H_{23}O_8P_2$ $[M\text{-}HNEt_3^+]^-$ 429.0874, found 429.0870.

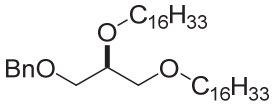

66

To a solution of **64** (209 mg, 1.15 mmol) in DMSO (10 mL) was added NaH (170 mg, 4.26 mmol, 60% in oil) at 0 °C. After stirring at the same temperature for 1h, **64** (2.19 g, 6.9 mmol) was added at 0 °C. The reaction mixture was stirred at room temperature for 20 h. The reaction was quenched with water at 0 °C. The mixture was diluted with EtOAc and washed with H_2O. The organic layer was washed with water, dried over $MgSO_4$, filtrated and concentrated under reduced pressure. The residue was purified by flash column chromatography on silica gel (ethyl acetate/hexane = 1:20) to afford **66** (404 mg, 56%) as a colorless oil. ^{1}H NMR (400 MHz, $CDCl_3$): δ 0.87 (t, J = 7.2 Hz, 6H); 1.20-1.36 (m, 52H); 1.49-1.60 (m, 4H); 3.37-3.62 (m, 9H); 4.54 (s, 2H); 7.24-7.35 (m, 5H); ^{13}C NMR (100 MHz, $CDCl_3$): δ 14.20, 22.78, 26.19, 26.21, 29.45, 29.60, 29.74, 29.79, 30.20, 32.01, 70.40, 70.70, 70.82, 71.75, 73.44, 78.01, 127.57, 127.66, 128.38, 138.54.

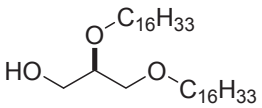

44

To a solution of **66** (205 mg, 0.33 mmol) in CH_2Cl_2 (1 mL) at -78 °C was added boron trichloride (0.66 mL, 1M in CH_2Cl_2). The reaction mixture was allowed to warm to room temperature, stirred

for 2 h, quenched with MeOH and diluted with water. The organic layer was washed with water, dried over $MgSO_4$, filtrated and concentrated under reduced pressure. The residue was purified by flash column chromatography on silica gel (ethyl acetate/hexane = 1:5) to afford **44** (40 mg, 60%) as a white solid. ^{1}H NMR (400 MHz, $CDCl_3$): δ 0.89 (t, *J* = 7.2 Hz, 6H); 1.19-1.36 (m, 52H); 1.50-1.60 (m, 4H); 3.39-3.75 (m, 9H).

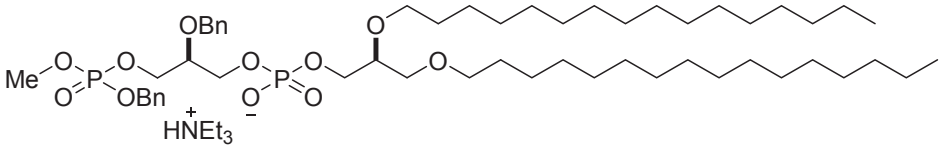

67

To a solution of **43** (92 mg, 0.173 mmol) and **44** (186 mg, 0.35 mmol) in dry pyridine (2 mL) at 0 °C was added pivaloyl chloride (64 μL, 0.52 mmol). The reaction mixture was stirred at room temperature for 1h. Then iodine (44 mg, 0.35 mmol) in pyridine/H_2O (1mL/50 μL) was added. The reaction mixture was stirred at the same temperature for 30 min. 1 mL of Na_2SO_3 (1M) was added. After stirring for 10 min, the mixture was diluted with water and washed with $CHCl_3$. The organic layer was combined, dried over $MgSO_4$, filtrated and concentrated under reduced pressure. The residue was purified by flash column chromatography on silica gel (CH_2Cl_2/MeOH/Et_3N = 100:6:1) to afford **67** (123 mg, 70%) as a colorless oil. ^{1}H NMR (400 MHz, $CDCl_3$): δ 0.85 (t, *J* = 7.2 Hz, 6H); 1.20-1.36 (m, 52H); 1.29 (t, *J* = 7.2 Hz, 15H; $HNEt_3$ residue); 1.43-1.54 (m, 4H); 3.01 (m, 10H; $HNEt_3$ residue); 3.32-3.44 (m, 3H); 3.46-3.60 (m, 4H); 3.65 (d, *J* = 11.2 Hz, 1.5H); 3.66 (d, *J* = 11.2 Hz, 1.5H); 3.78-3.91 (m, 3H); 3.93-4.02 (m, 2H); 4.07-4.16 (m, 1H); 4.21-4.28 (m, 1H); 4.63 (ABq, 2H, $\Delta\delta_{AB}$ = 0.03, J_{AB} = 11.6 Hz); 4.95-5.05 (m, 2H); 7.15-7.40 (m, 10H); ^{13}C NMR (100 MHz, $CDCl_3$): δ 8.61, 14.18, 22.75, 26.17, 26.20, 29.43, 29.63, 29.66, 29.78, 30.26, 31.99, 45,64, 54.35, 54.41, 63.59, 63.65, 65.12, 65.18, 67.28, 67.34, 69.23, 69.29, 70.63, 71.07, 71.72, 72.12, 78.07, 78.15, 127.60, 127.76, 127.95, 128.20, 128.33, 128.52, 128.61, 135.96, 136.01, 138.34; ^{31}P NMR (100 MHz, $CDCl_3$): δ 0.74, 1.01; HRMS Calcd. for $C_{53}H_{93}O_{11}P_2$ $[M\text{-}HNEt_3^+]^-$ 967.6199, found 967.6205.

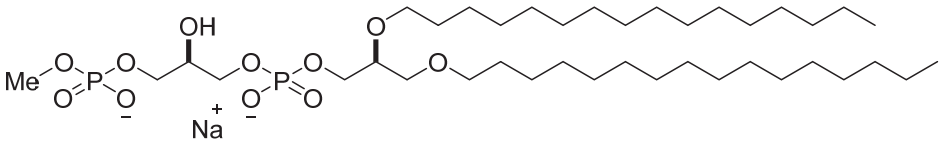

8

To a solution of **67** (100 mg, 0.09 mmol) in MeOH (2 mL) was added platinum oxide (21 mg, 0.09 mmol). The mixture was hydrogenated overnight at 1 atm of hydrogen gas. Platinum black was filtered. After concentration, the residue was purified by flash column chromatography on silica gel ($CHCl_3$/MeOH/H_2O = 65:20:3) to afford corresponding deprotected product in triethylamine salt form. The product was mixed with 1 mL of $NaClO_4$ solution (4 M). The mixture was stirred with a vortex mixer. After centrifugation the supernatant solution was removed, the precipitate was washed with distilled water, and dissolved in $CHCl_3$/MeOH (1:1). The solvent was concentrated to afford **8** (38 mg, 50%) in sodium salt form as a white solid. ^{1}H NMR (400 MHz, CD_3OD/$CDCl_3$ (4/3 v/v); using CD_3OD as the lock): δ 1.20 (t, *J* = 5.6 Hz, 6H); 1.52-1.70 (m, 52H); 1.83-1.92 (m, 4H); 3.72-3.84 (m, 3H); 3.87-3.99 (m, 4H); 3.93 (d, *J* = 10.5 Hz, 3H); 4.20-4.34 (m, 7H); ^{13}C NMR (125 MHz, CD_3OD/$CDCl_3$ (4/3 v/v)): δ 13.66, 22.57, 26.01, 26.07, 29.28, 29.47, 29.63, 29.94, 31.86, 52.40, 52.44, 64.88, 64.92, 65.35, 69.70, 70.44, 70.57, 71.67, 78.00; ^{31}P NMR (100 MHz, CD_3OD/$CDCl_3$ (4/3 v/v)): δ 1.74, 3.00; HRMS Calcd. for $C_{39}H_{80}O_{11}P_2Na$ $[M]^-$ 809.5079, found 809.5084.

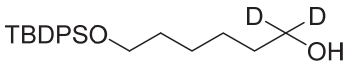

70

To a solution of $LiAlD_4$ (227 mg, 5.4 mmol) in THF (10 mL) at 0°C was added **69** (1.0 g, 2.7 mmol) in THF (1 mL) dropwise. After stirring at the same temperature for 2 h, the reaction mixture was quenched by ice water. The solvent was removed, and the residue was purified by flash column chromatography on silica gel (ethyl acetate/hexane = 1:3) to afford **70** (670 mg, 70%) as a colorless oil. ^{1}H NMR (400 MHz, $CDCl_3$): δ 1.04 (s, 9H); 1.28-1.42 (m, 4H); 1.49-1.61 (m, 4H); 3.65 (t, *J* = 6.4 Hz, 2H); 7.34-7.44 (m, 6H); 7.65-7.69 (m, 4H); ^{13}C NMR (100 MHz, $CDCl_3$): δ 19.31, 25.50, 25.68, 26.96, 32.58, 32.64, 63.93, 127.66, 129.59, 134.22, 135.66.

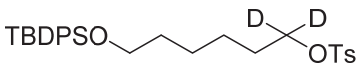

71

To a solution of **70** (340 mg, 0.95 mmol) in CH_2Cl_2 (2 mL) were added *p*-toluenesulfonyl chloride (272 mg, 1.42 mmol), triethylamine (318 μL, 2.28 mmol) and *N,N*-dimethyl-4-aminopyridine (580 mg, 4.75 mmol) at room temperature. After stirring at the same temperature for 1 h, the solvent was removed. The residue was purified by flash column chromatography on silica gel (ethyl acetate/hexane = 1:10) to afford **4** (462 mg, 95%) as a colorless semi-solid. ^{1}H NMR (400 MHz, $CDCl_3$): δ 1.03 (s, 9H); 1.21-1.32 (m, 4H); 1.45-1.52 (m, 2H); 1.56-1.63 (m, 2H); 2.42 (s, 3H); 3.60 (t, *J* = 6.4 Hz, 2H); 7.29-7.44 (m, 8H); 7.61-7.68 (m, 4H); 7.77 (d, *J* = 8.0 Hz, 2H).

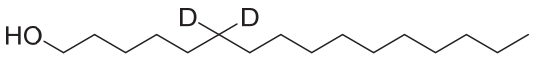

73

To a solution of **71** (600 mg, 1.17 mmol) in THF (20 mL) were added $CuCl_2$ (7.8 mg, 0.06 mmol) and 1-phenyl-1-propyne (29 μL, 0.23 mmol) at 0 °C under argon. Afterward the Grignard reagent (2.34 mL, 2.34 mmol; 1.0 M in diethyl ether) was added in one portion. The ice bath was removed and the reaction mixture was stirred for 1 h. The solvent was evaporated. The residue was purified by flash column chromatography on silica gel (ethyl acetate/hexane = 1:20) to afford crude **72** which was dissolved in THF (10 mL) and treated with tetrabutylammonium fluoride (2 mL, 1M in THF). After stirring at room temperature for 4 h, the solvent was removed. The residue was purified by flash column chromatography on silica gel (ethyl acetate/hexane = 1:5) to afford **73** (271 mg, 95%) as a white solid. ^{1}H NMR (400 MHz, $CDCl_3$): δ 0.87 (t, *J* = 6.8 Hz, 3H); 1.19-1.42 (m, 24H); 1.50-1.60 (m, 2H); 3.63 (t, *J* = 6.4 Hz, 2H).

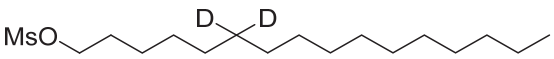

74

To a solution of **73** (3.0 g, 12.3 mmol) in pyridine/CH_2Cl_2 (13 mL/13 mL) was added methanesulfonyl chloride (1.05 mL, 13.4 mmol) at 0 °C. After stirring at the same temperature for 2 h, white solid was filtered. The solvent was removed to give **74** which was used directly for the next step without further purification. ^{1}H NMR (400 MHz, $CDCl_3$): δ 0.87 (t, *J* = 6.8 Hz, 3H);

1.18-1.44 (m, 24H); 1.70-1.82 (m, 2H); 2.99 (s, 3H); 4.21 (t, J = 6.4 Hz, 2H).

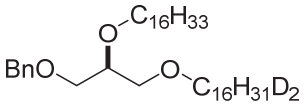

78

To a solution of **77** (512 mg, 1.3 mmol) in DMSO (10 mL) was added NaH (104 mg, 2.6 mmol, 60% in oil) at 0 °C. After stirring at the same temperature for 1 h, **74** (420 mg, 1.3 mmol) was added. The mixture was stirred at room temperature for 20 h. The reaction was quenched with water at 0 °C. The mixture was diluted with EtOAc and washed with H_2O. The organic layer was washed with water, dried over $MgSO_4$, filtrated and concentrated under reduced pressure. The residue was purified by flash column chromatography on silica gel (ethyl acetate/hexane = 1:20) to afford **78** (534 mg, 65%) as a colorless oil. ^{1}H NMR (400 MHz, $CDCl_3$): δ 0.87 (t, J = 7.2 Hz, 6H); 1.20-1.37 (m, 50H); 1.50-1.60 (m, 4H); 3.37-3.62 (m, 9H); 4.54 (s, 2H); 7.24-7.35 (m, 5H).

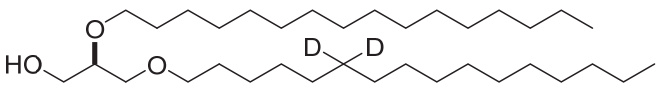

79

To a solution of **78** (460 mg, 0.73 mmol) in CH_2Cl_2 (10 mL) at -78 °C was added boron trichloride (1.09 mL, 1M in CH_2Cl_2). The reaction mixture was allowed to warm to room temperature, stirred for 2 h, quenched with MeOH and diluted with water. The organic layer was washed with water, dried over $MgSO_4$, filtrated and concentrated under reduced pressure. The residue was purified by flash column chromatography on silica gel (ethyl acetate/hexane = 1:5) to afford **79** (215 mg, 55%) as a white solid. ^{1}H NMR (400 MHz, $CDCl_3$): δ 0.89 (t, J = 7.2 Hz, 6H); 1.18-1.36 (m, 50H); 1.50-1.60 (m, 4H); 3.40-3.76 (m, 9H).

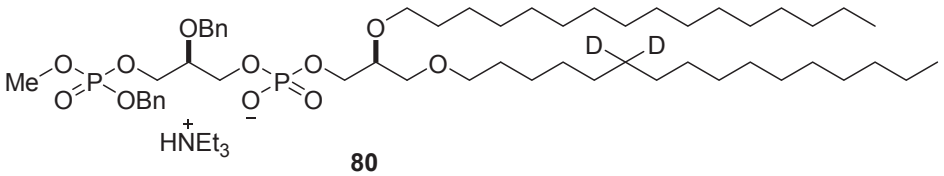

80

This compound was prepared in 68% yield over 2 steps as a colorless oil by following the same procedure as described for **67**. ^{1}H NMR (400 MHz, $CDCl_3$): δ 0.85 (t, J = 7.2 Hz, 6H); 1.20-1.36

(m, 50H); 1.29 (t, J = 7.2 Hz, 15H; $HNEt_3$ residue); 1.43-1.54 (m, 4H); 3.01 (m, 10H; $HNEt_3$ residue); 3.32-3.44 (m, 3H); 3.46-3.60 (m, 4H); 3.65 (d, J = 11.2 Hz, 1.5H); 3.66 (d, J = 11.2 Hz, 1.5H); 3.78-3.91 (m, 3H); 3.92-4.02 (m, 2H); 4.07-4.16 (m, 1H); 4.21-4.28 (m, 1H); 4.63 (ABq, 2H, $\Delta\delta_{AB}$ = 0.03, J_{AB} = 11.6 Hz); 4.95-5.05 (m, 2H); 7.15-7.39 (m, 10H); HRMS Calcd. for $C_{53}H_{91}D_2O_{11}P_2$ $[M\text{-}HNEt_3^+]^-$ 969.6324, found 969.6330.

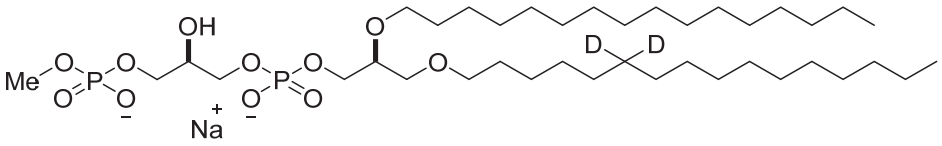

9

This compound was prepared in 46% yield over 2 steps as a white solid by following the same procedure as described for **8**. ^{1}H NMR (400 MHz, $CD_3OD/CDCl_3$ (4/3 v/v); using CD_3OD as the lock): δ 1.20 (t, J = 5.6 Hz, 6H); 1.52-1.71 (m, 50H); 1.82-1.92 (m, 4H); 3.72-3.84 (m, 3H); 3.87-3.99 (m, 4H); 3.93 (d, J = 10.5 Hz, 3H); 4.20-4.35 (m, 7H); HRMS Calcd. for $C_{39}H_{78}D_2O_{11}P_2Na$ $[M]^-$ 811.5205, found 811.5212.

Acknowledgement

I would like to express my sincerest appreciation to my advisor Prof. Michio Murata, who has provided me with tremendous support and insightful and valuable guidance in my Ph.D. work. Meanwhile, I would like to thank you for creating the perfect environment in ERATO lab in which I have performed my studies.

I am very grateful to Dr. Fuminori Sato not only for his great support in my academic work, but also for giving me many help in living. He is a great person with wisdom and a warm heart. I would like to thank Prof. Shigeru Matsuoka and Prof. Nobuaki Matsumori for providing guidance and insightful discussions. I would like to express my gratitude to Dr. Shinya Hanashima and Dr. Hiroshi Tsuchikawa for their contributions.

I would like to acknowledge our collaborators, Prof. Mikiko Sodeoka (RIKEN), Prof. Katsumasa Fujita (Department of Applied Physics, Osaka Univ.), Dr. Jun Ando (RIKEN), and Dr. Kosuke Dodo (RIKEN) for their great assistance.

I extend my appreciation to the reviewers of my thesis work, Prof. Hironobu Hojo and Prof. Koichi Fukase, for correcting the manuscript and providing constructive comments.

I would like to offer my thanks to the members of ERATO group, Dr. Yuichi Umegawa, Dr. Sébastien Lethu, Dr. Masanao Kinoshita, Dr. Toshiaki Hara, Dr. Satoshi Kawatake, and Ms. Kaori Oshimo for their friendship, and the help they have given me and the work they did.

I would like to thank Ms. Misaki Yofu and Ms. Saori Ichino for the kind help and patience.

My time at Osaka University was made enjoyable and memorable due to the many members in our lab, and I would like to express my thanks to: Mr. Hajime Shibata, Mr. Rafael Atillo Espiritu, Mr. Tomokazu Yasuda, Mr. Yasuo Nakagawa, Ms. Yue Huang, Ms. Kimberly Cornelio, Ms. Yeung Clarisse Francesca, Mr. MD. Imran Hossain, Ms. Haruka Saiki, Mr. Yuya Tanaka, Mr. Yoshifumi Yasukawa, Mr. Misa Takada, Mr. Tatsuru Hayashi, Ms. Mami Monji, and Mr. Takumi Nankaku.

Finally, a special thanks to my mother, father, and sister. Words cannot express how thankful I am for their sacrifices and continuous and unconditional support in my life. I would like express deep appreciation to my loving wife Ping for being with me in Japan and for her faithful support and selfless love.

NMR Spectra

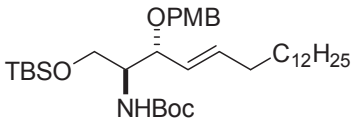

15

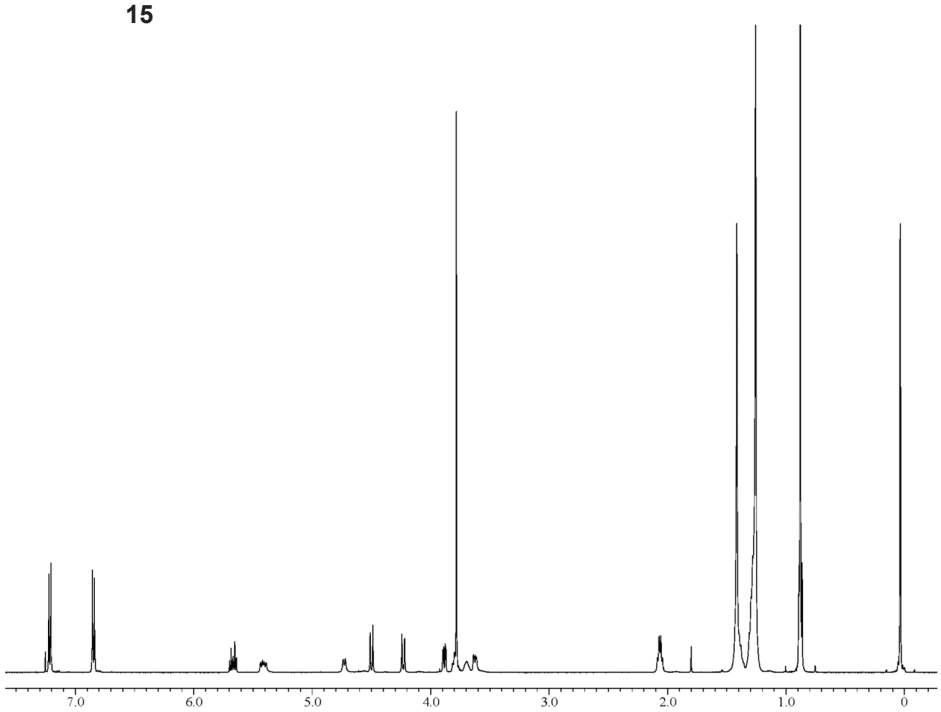

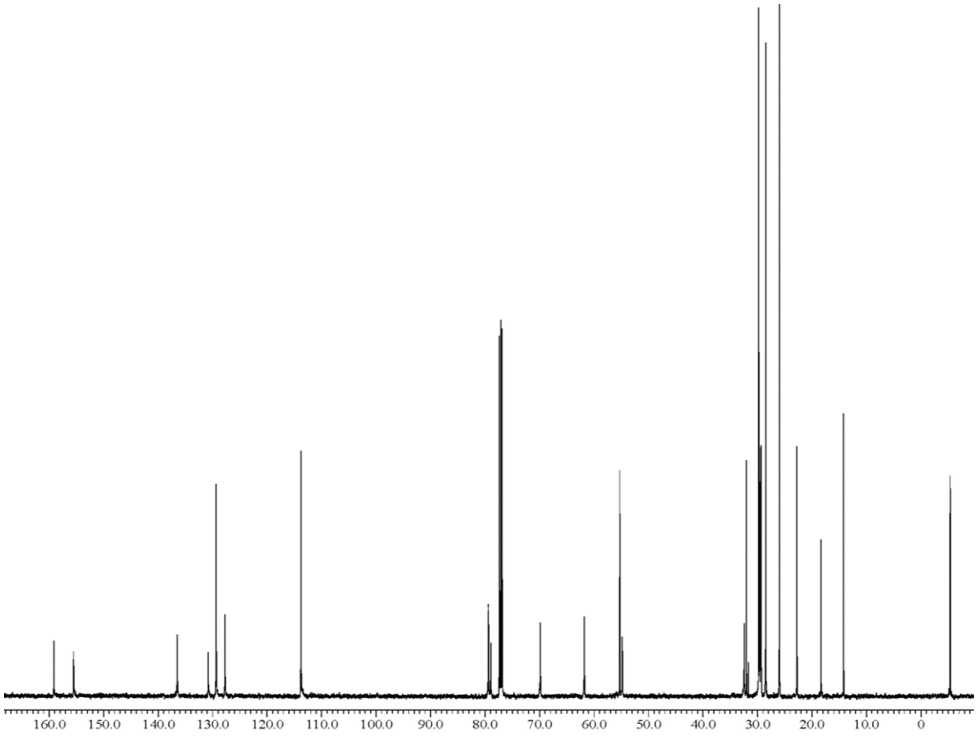

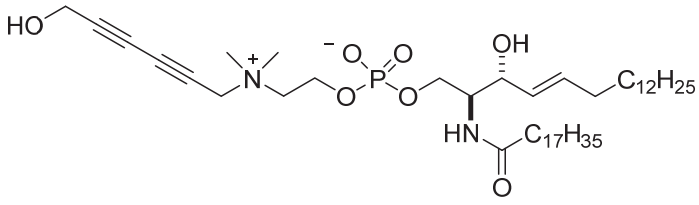
HO
N
O
P
O
O
O
OH
$C_{12}H_{25}$
HN
$C_{17}H_{35}$
O

2

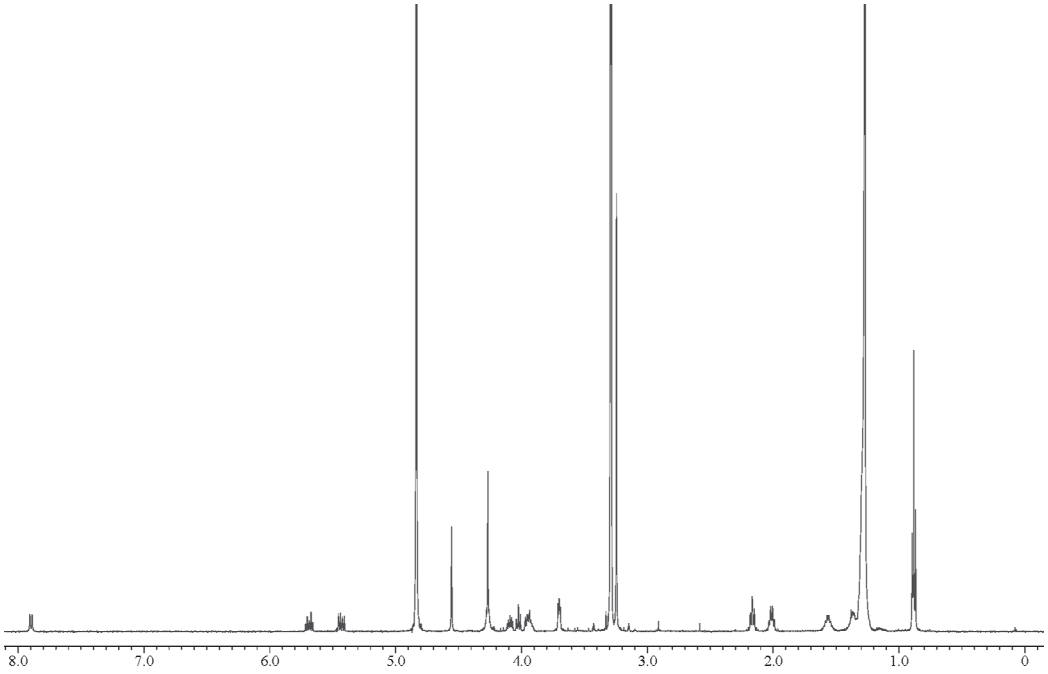
8.0
7.0
6.0
5.0
4.0
3.0
2.0
1.0
0

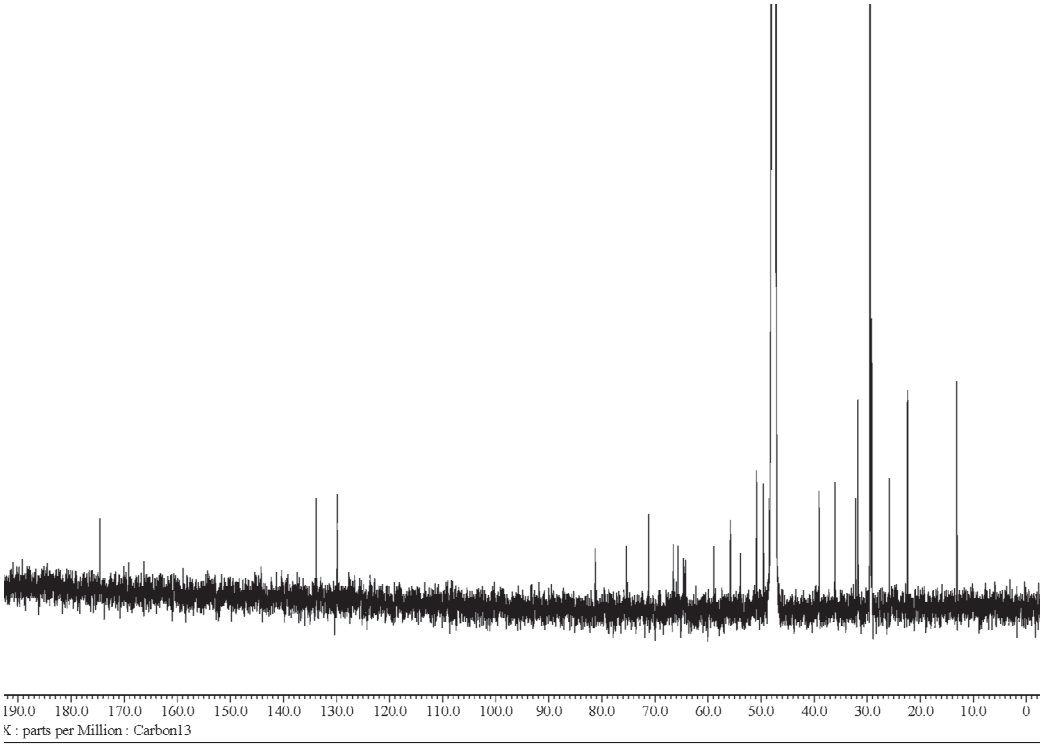
190.0 180.0 170.0 160.0 150.0 140.0 130.0 120.0 110.0 100.0 90.0 80.0 70.0 60.0 50.0 40.0 30.0 20.0 10.0 0
X : parts per Million : Carbon13

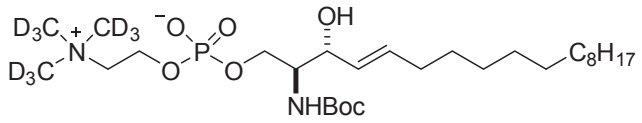
D3C
CD3
D3C
N
+
O
P
O
O
O
OH
NHBoc
C8H17

21

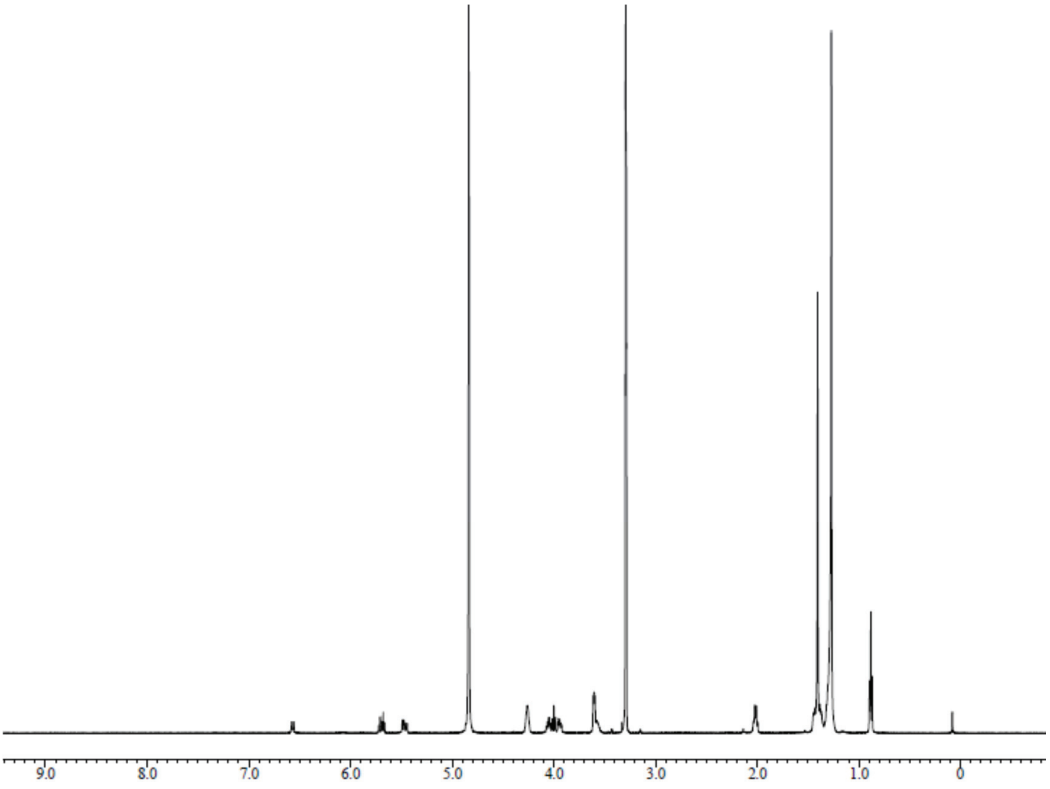
9.0
8.0
7.0
6.0
5.0
4.0
3.0
2.0
1.0
0

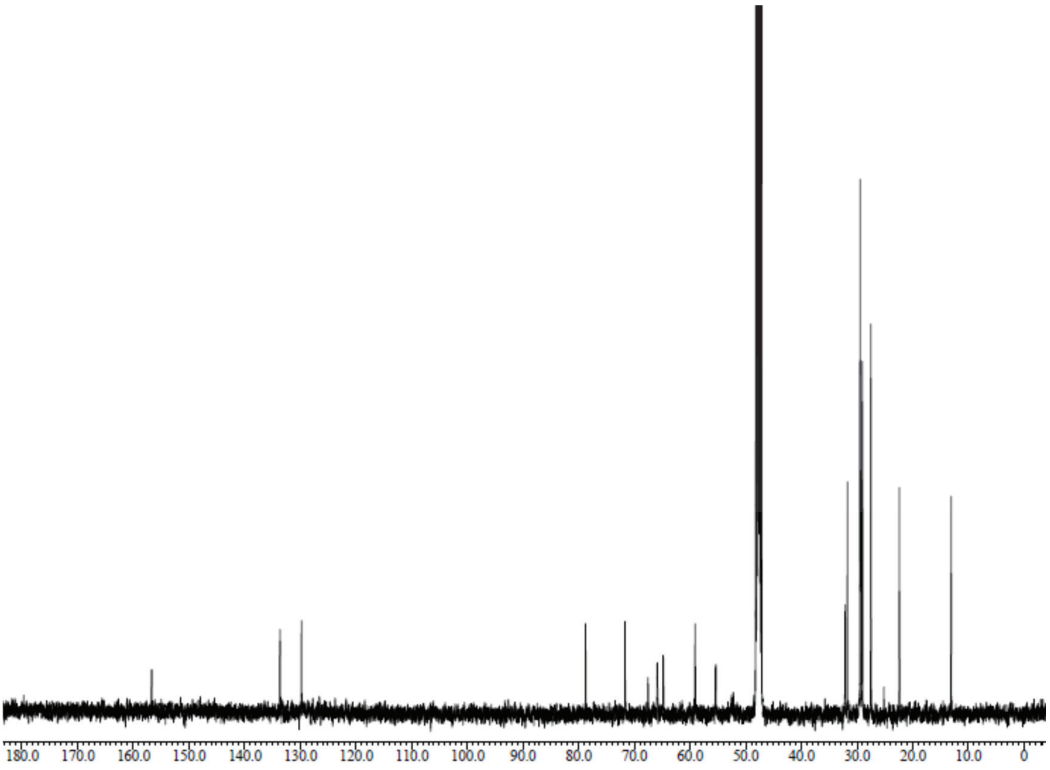
180.0
170.0
160.0
150.0
140.0
130.0
120.0
110.0
100.0
90.0
80.0
70.0
60.0
50.0
40.0
30.0
20.0
10.0
0

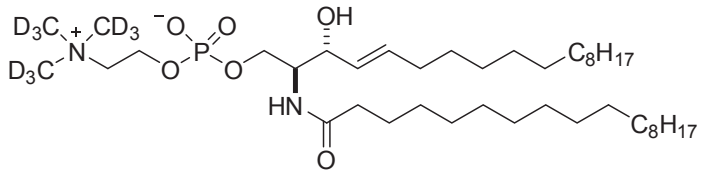
D3C
CD3
D3C
N
O
P
O
O
OH
C8H17
HN
C8H17
O

3

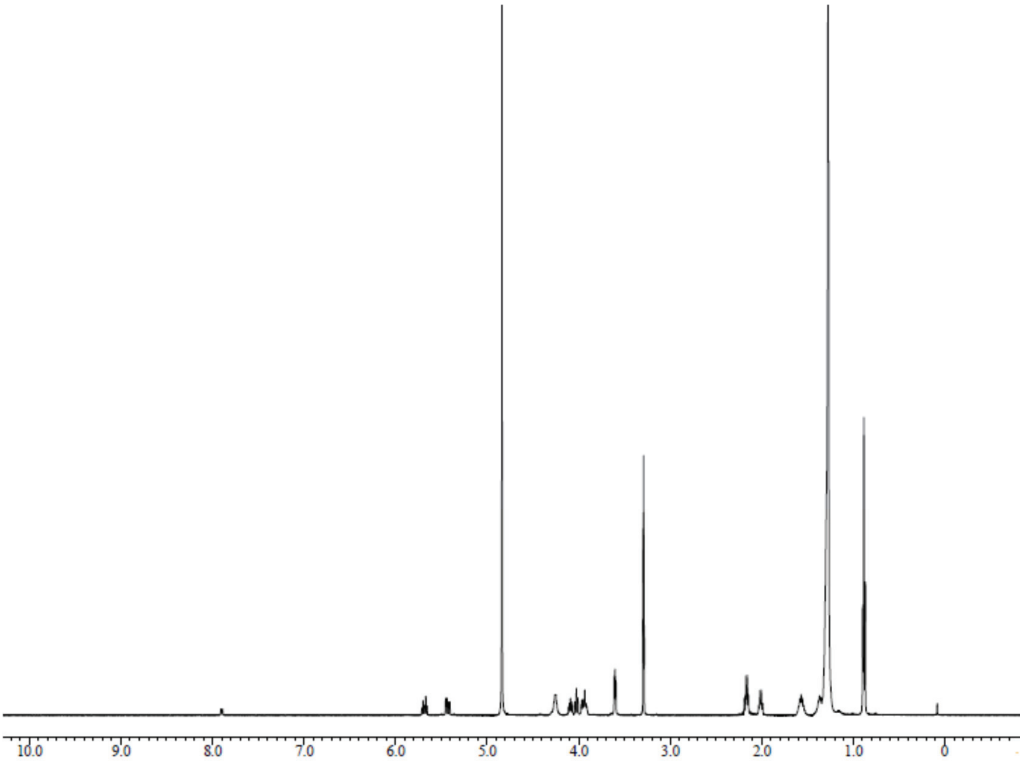
10.0
9.0
8.0
7.0
6.0
5.0
4.0
3.0
2.0
1.0
0

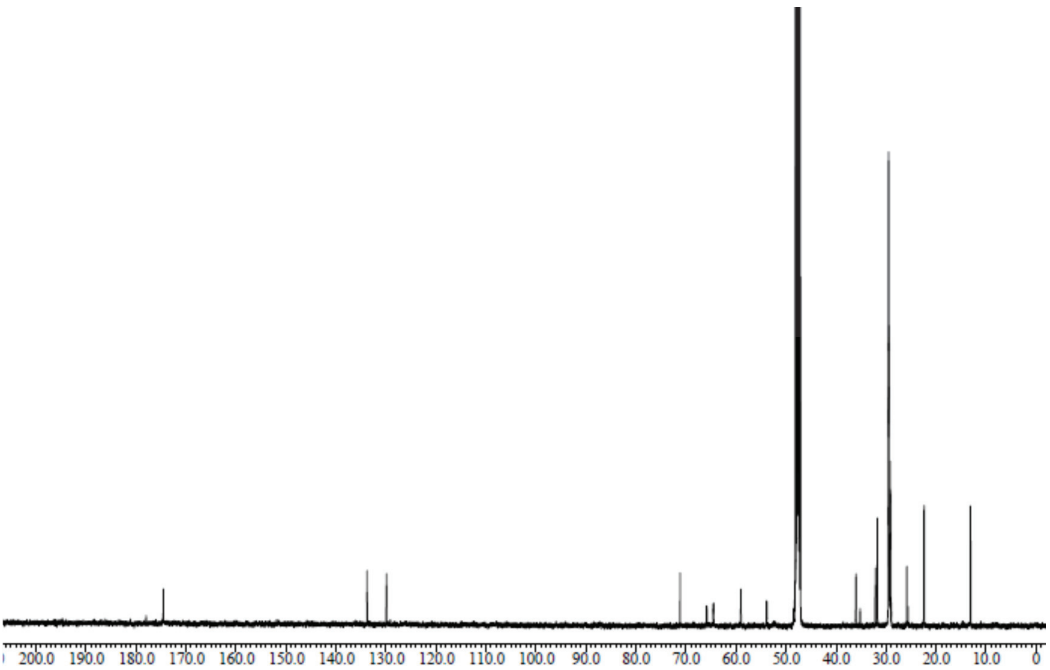
200.0
190.0
180.0
170.0
160.0
150.0
140.0
130.0
120.0
110.0
100.0
90.0
80.0
70.0
60.0
50.0
40.0
30.0
20.0
10.0
0

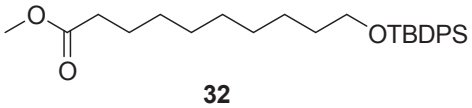
O
O
OTBDPS

32

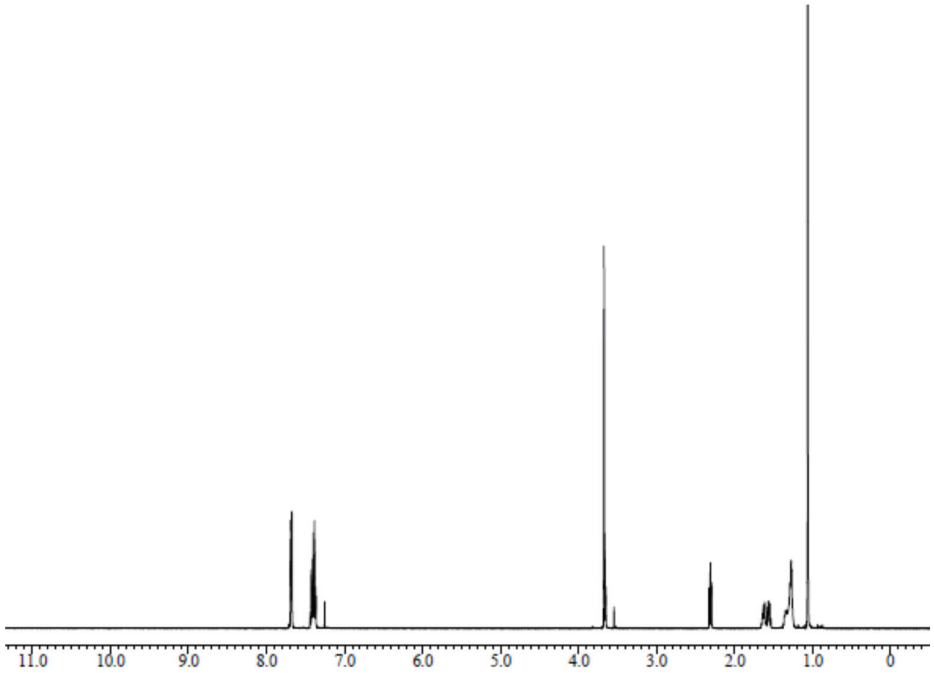
11.0
10.0
9.0
8.0
7.0
6.0
5.0
4.0
3.0
2.0
1.0
0

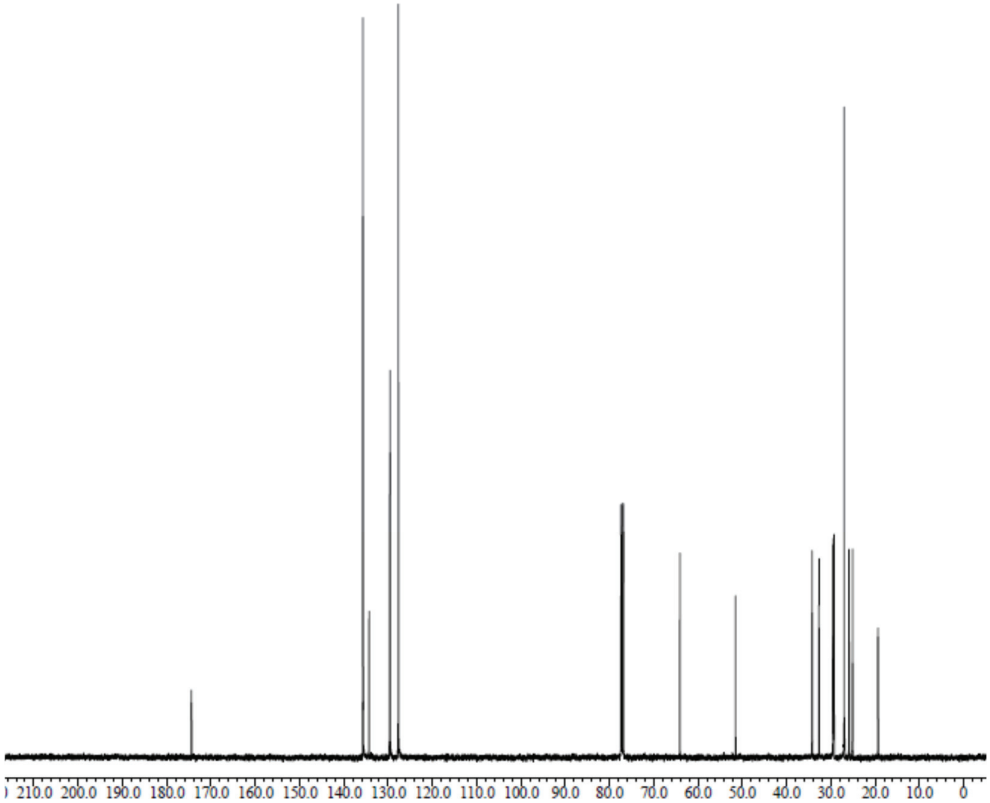
210.0
200.0
190.0
180.0
170.0
160.0
150.0
140.0
130.0
120.0
110.0
100.0
90.0
80.0
70.0
60.0
50.0
40.0
30.0
20.0
10.0
0

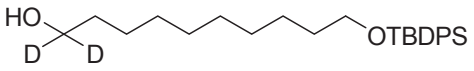
HO
D
D
OTBDPS

33

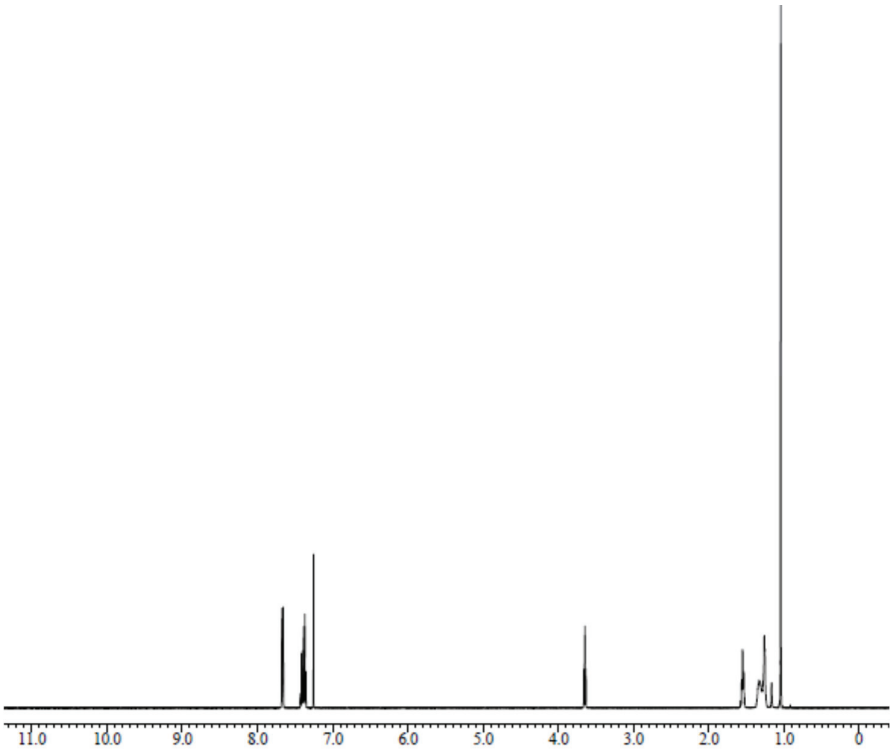
11.0
10.0
9.0
8.0
7.0
6.0
5.0
4.0
3.0
2.0
1.0
0

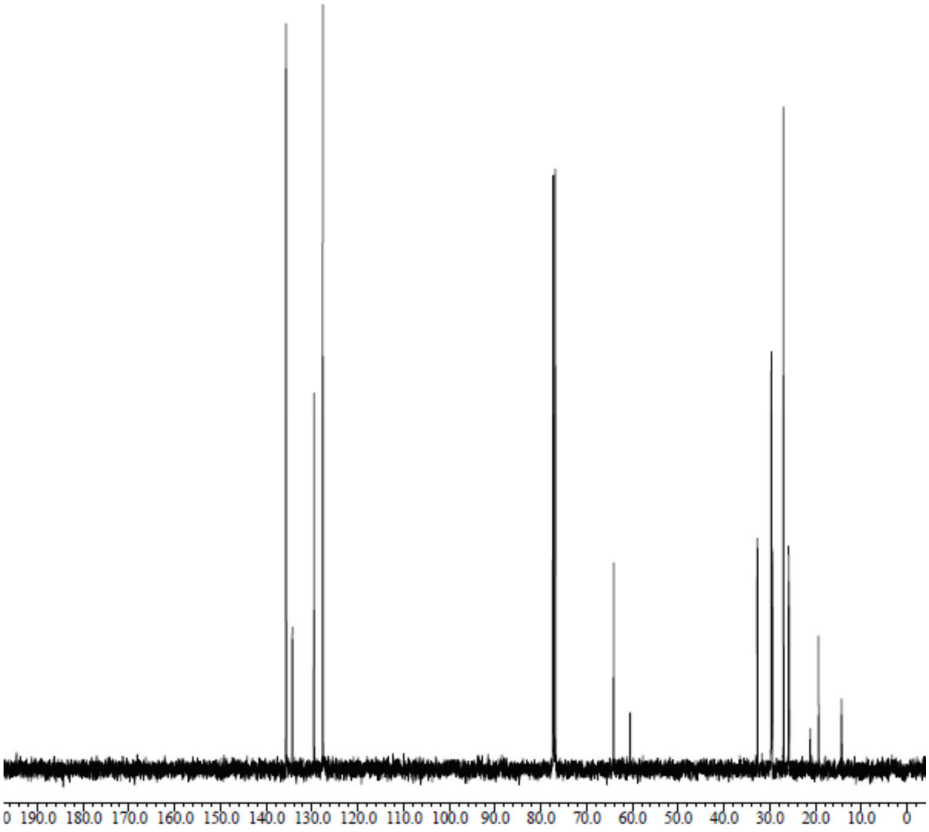
0 190.0 180.0 170.0 160.0 150.0 140.0 130.0 120.0 110.0 100.0 90.0 80.0 70.0 60.0 50.0 40.0 30.0 20.0 10.0 0

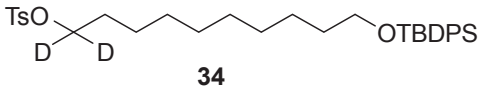
TsO
D
D
OTBDPS

34

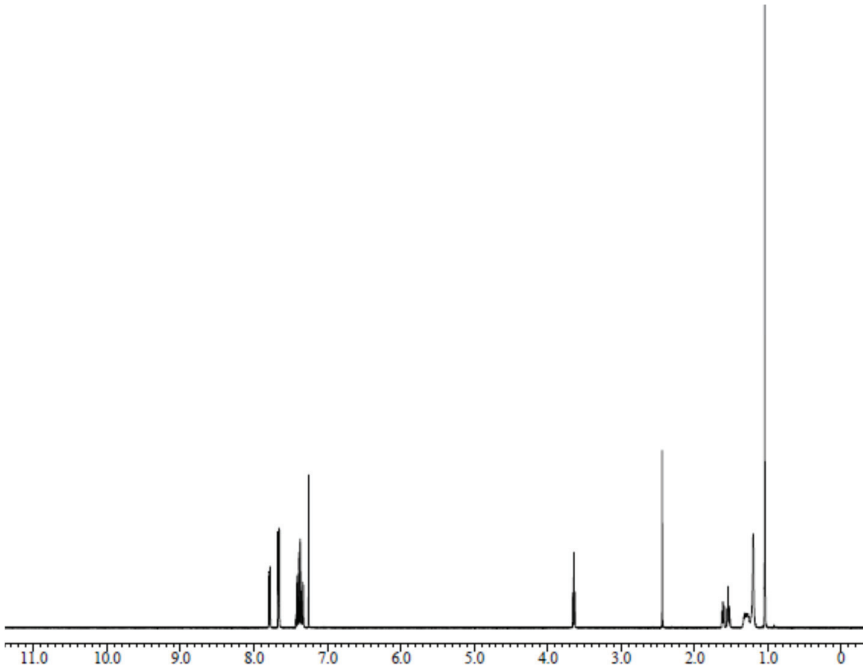
11.0
10.0
9.0
8.0
7.0
6.0
5.0
4.0
3.0
2.0
1.0
0

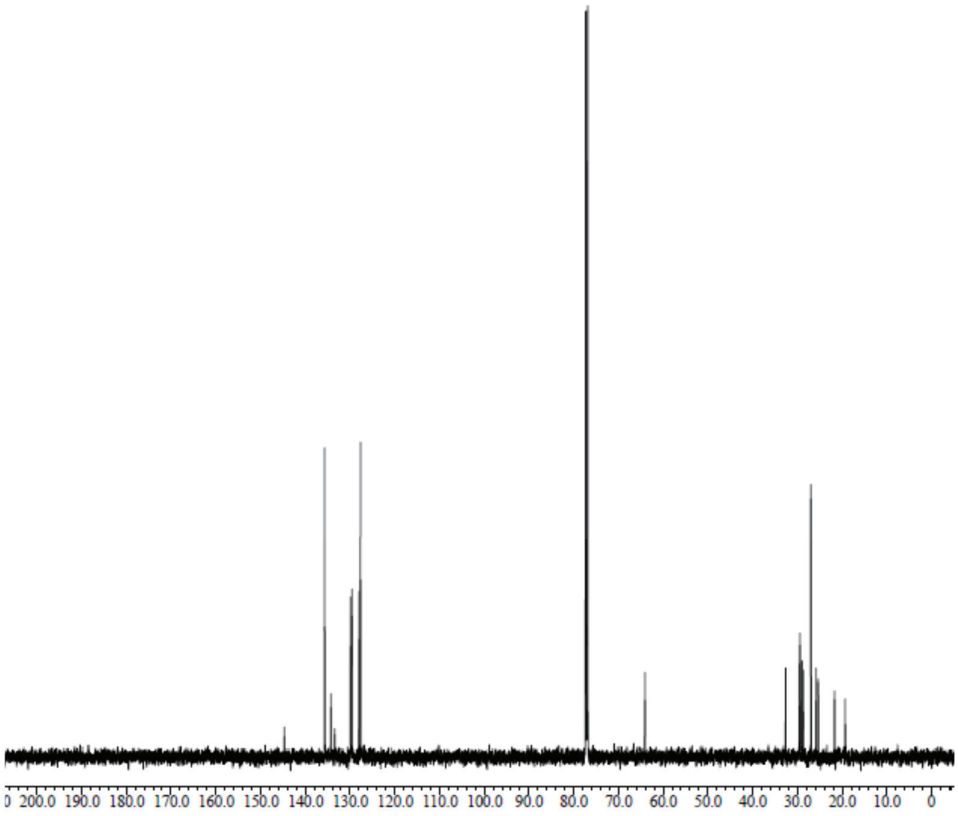
200.0
190.0
180.0
170.0
160.0
150.0
140.0
130.0
120.0
110.0
100.0
90.0
80.0
70.0
60.0
50.0
40.0
30.0
20.0
10.0
0

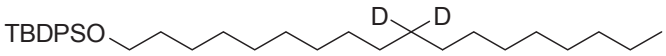
TBDPSO
D
D

35

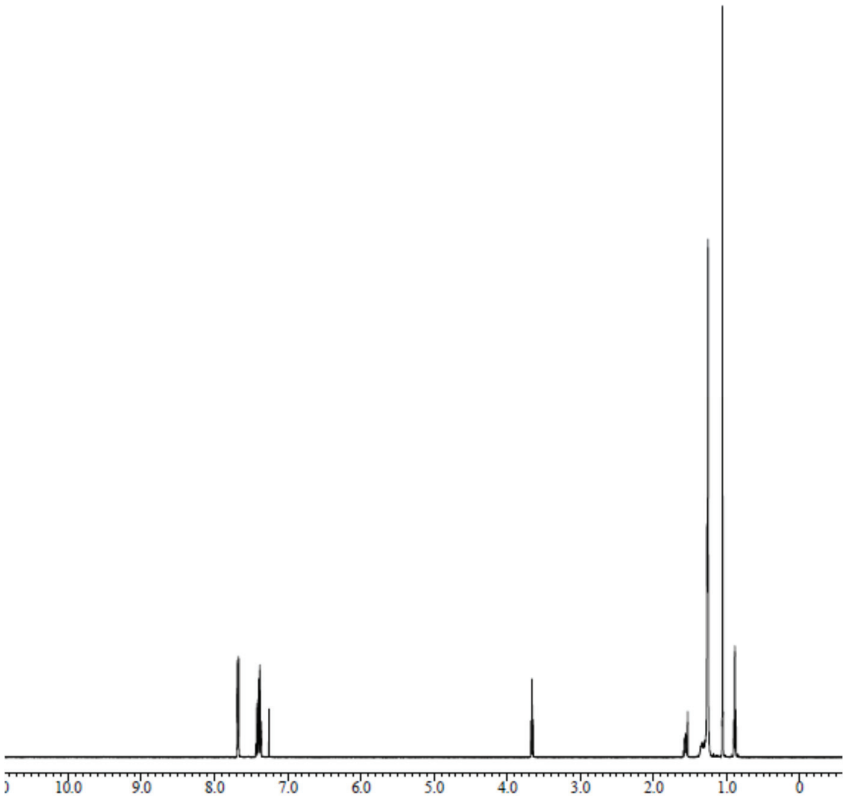
10.0
9.0
8.0
7.0
6.0
5.0
4.0
3.0
2.0
1.0
0

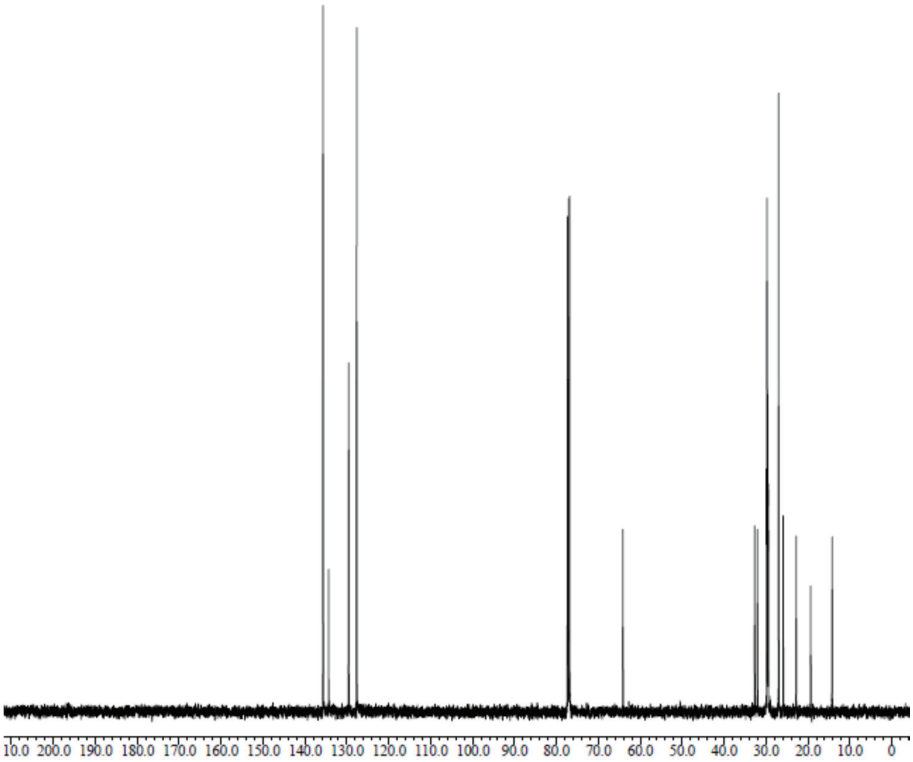
10.0 200.0 190.0 180.0 170.0 160.0 150.0 140.0 130.0 120.0 110.0 100.0 90.0 80.0 70.0 60.0 50.0 40.0 30.0 20.0 10.0 0

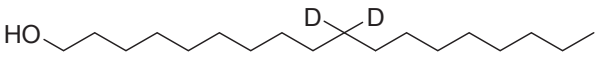
HO
D
D

36

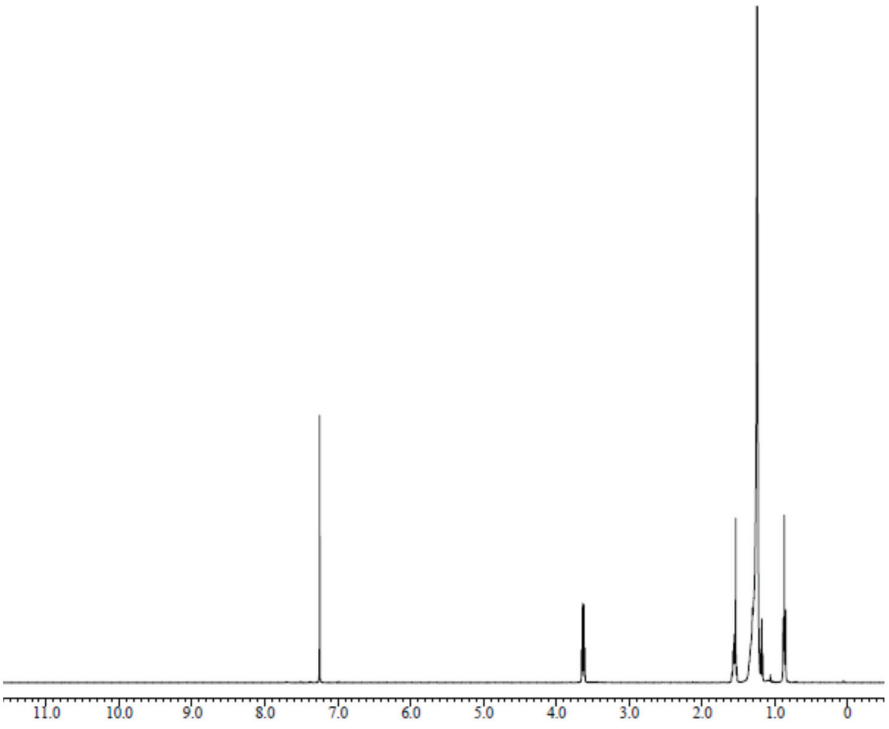
11.0
10.0
9.0
8.0
7.0
6.0
5.0
4.0
3.0
2.0
1.0
0

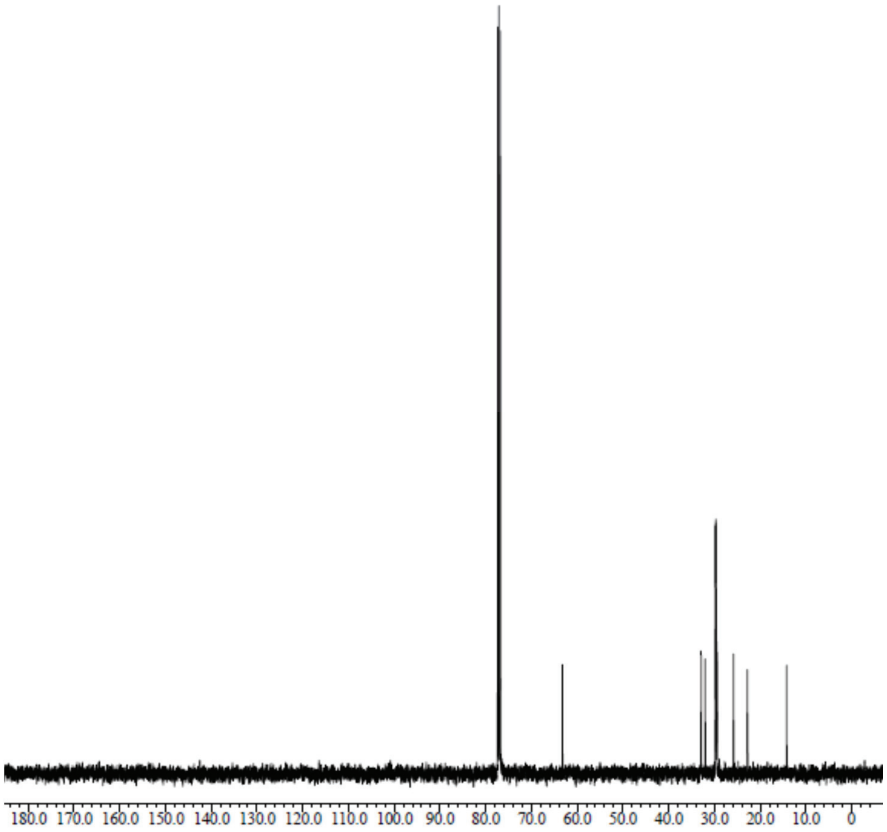
180.0
170.0
160.0
150.0
140.0
130.0
120.0
110.0
100.0
90.0
80.0
70.0
60.0
50.0
40.0
30.0
20.0
10.0
0

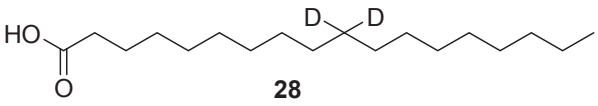
HO
O
D
D

28

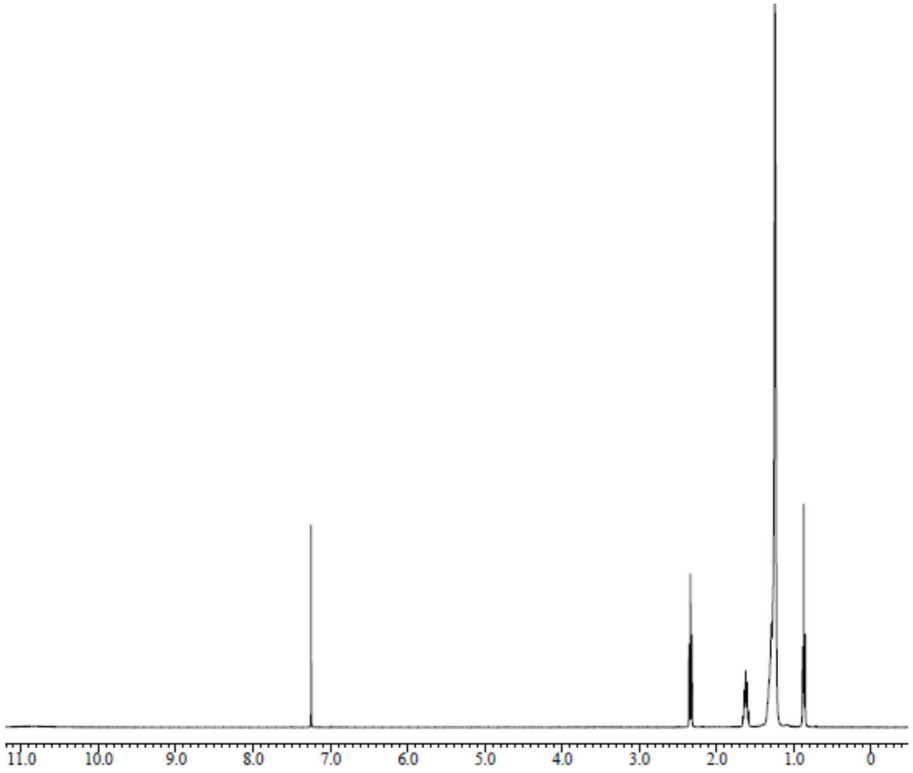
11.0
10.0
9.0
8.0
7.0
6.0
5.0
4.0
3.0
2.0
1.0
0

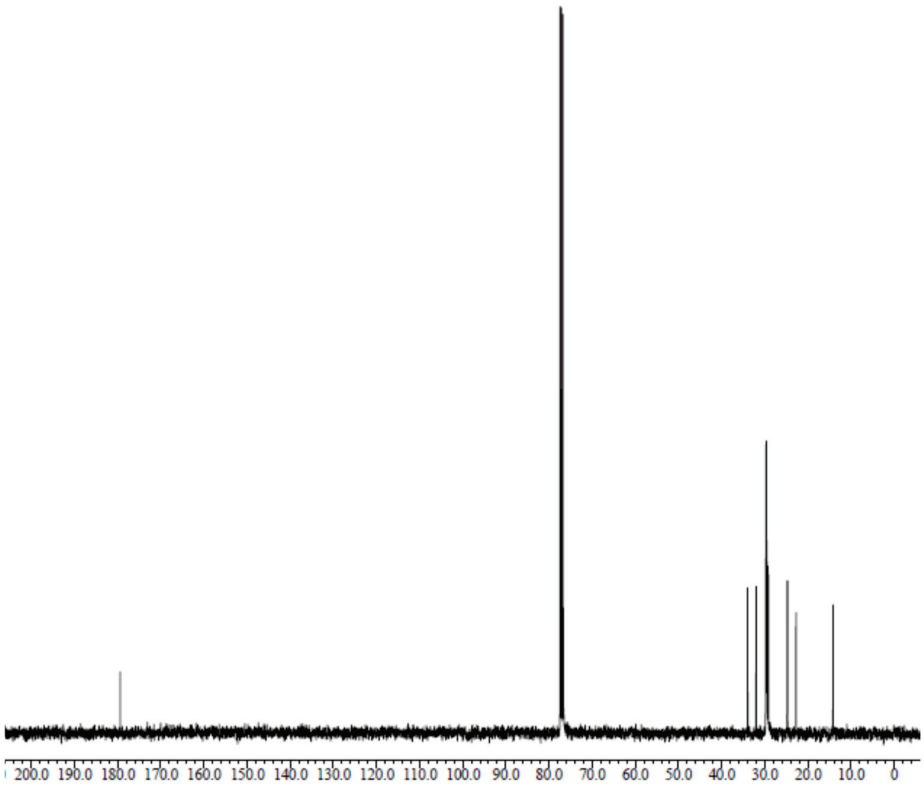
200.0
190.0
180.0
170.0
160.0
150.0
140.0
130.0
120.0
110.0
100.0
90.0
80.0
70.0
60.0
50.0
40.0
30.0
20.0
10.0
0

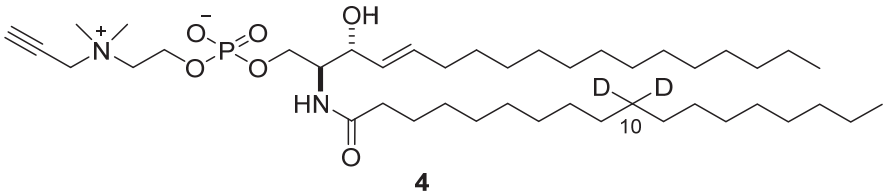
OH
HN
O
D
D
10

4

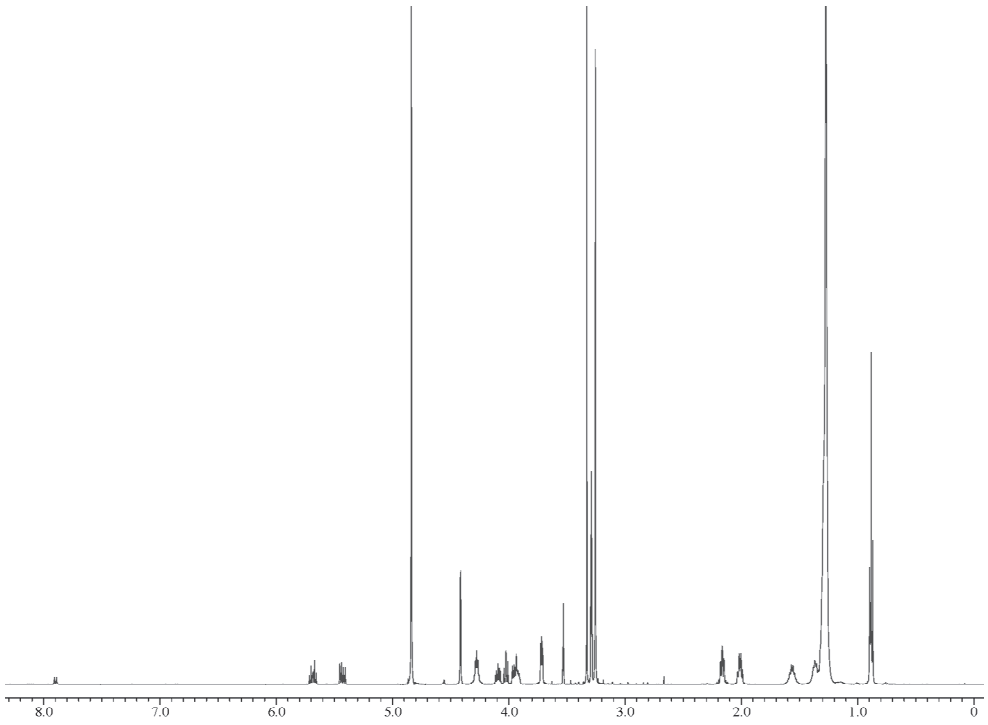
8.0
7.0
6.0
5.0
4.0
3.0
2.0
1.0
0

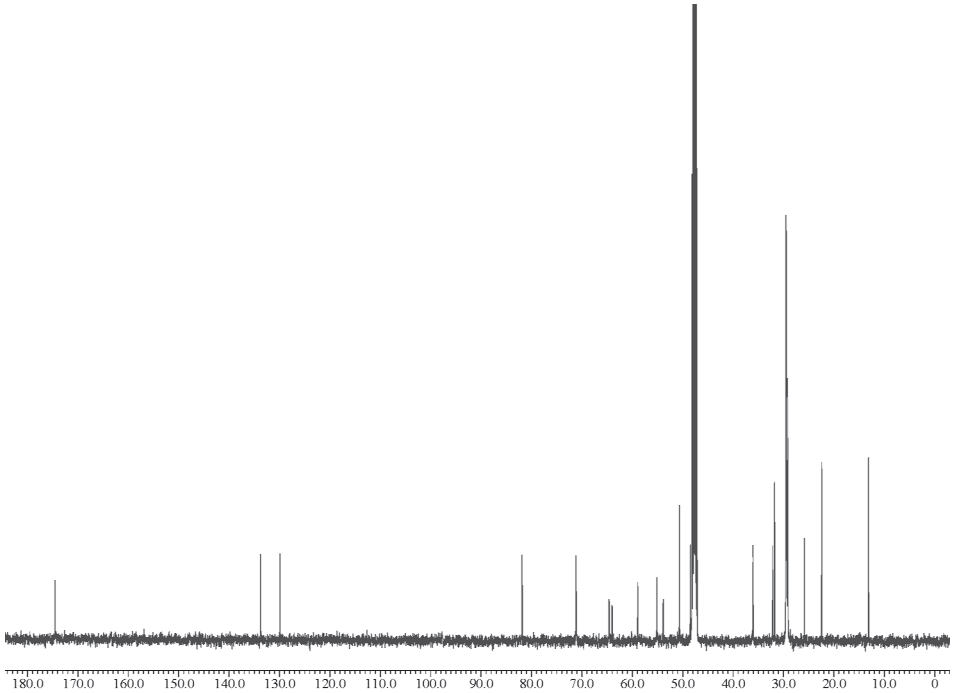
180.0
170.0
160.0
150.0
140.0
130.0
120.0
110.0
100.0
90.0
80.0
70.0
60.0
50.0
40.0
30.0
20.0
10.0
0

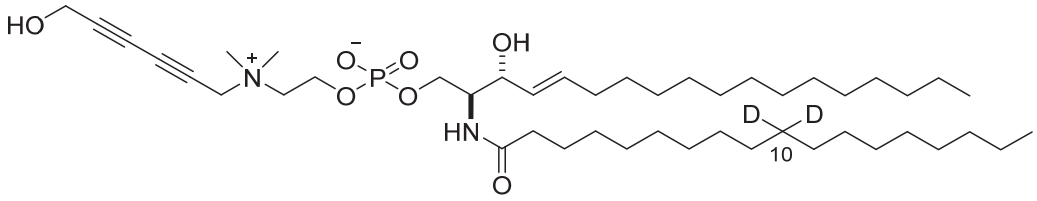
HO
N
O
P
O
O
O
OH
HN
O
D
D
10

5

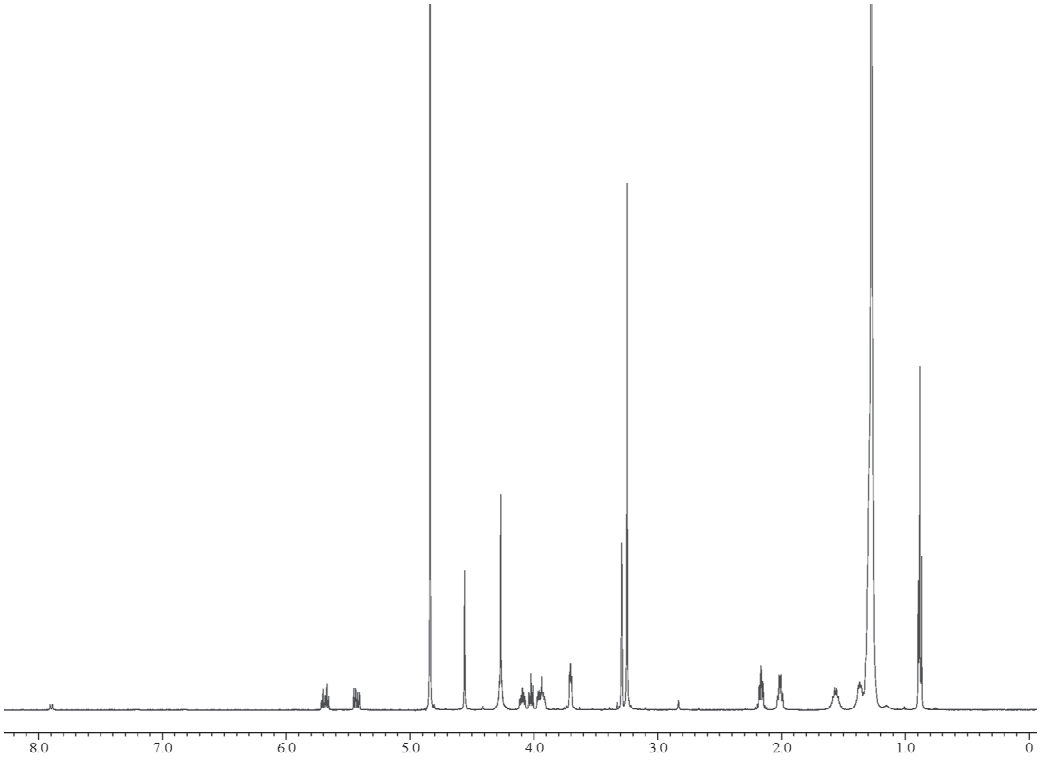
8.0
7.0
6.0
5.0
4.0
3.0
2.0
1.0
0

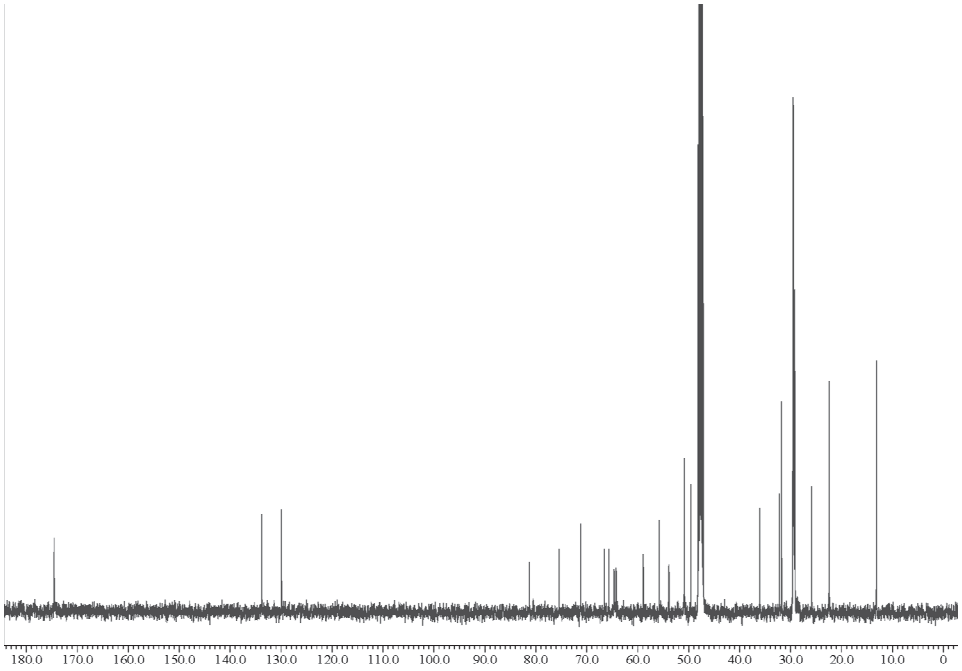
180.0
170.0
160.0
150.0
140.0
130.0
120.0
110.0
100.0
90.0
80.0
70.0
60.0
50.0
40.0
30.0
20.0
10.0
0

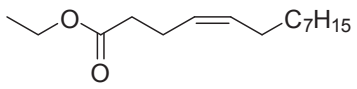
O
O
C7H15

38

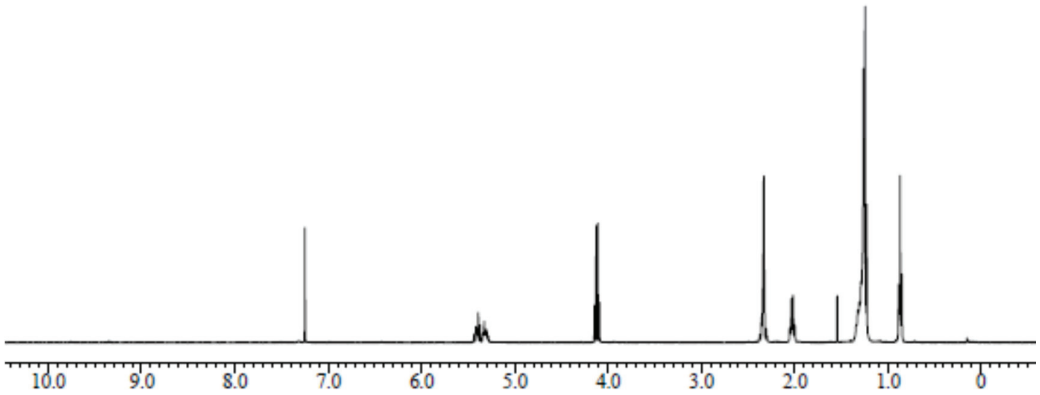
10.0
9.0
8.0
7.0
6.0
5.0
4.0
3.0
2.0
1.0
0

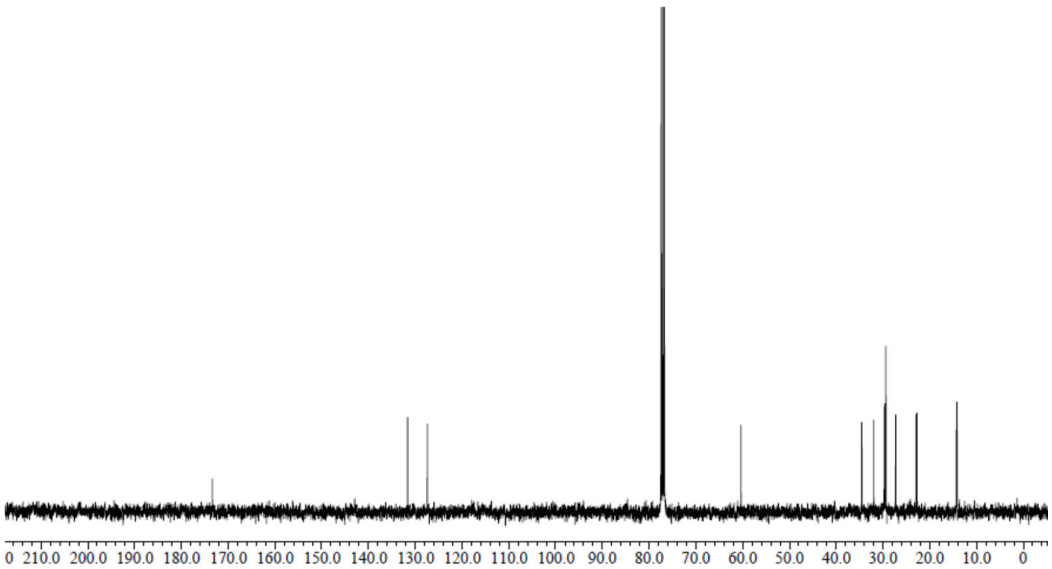
0 210.0 200.0 190.0 180.0 170.0 160.0 150.0 140.0 130.0 120.0 110.0 100.0 90.0 80.0 70.0 60.0 50.0 40.0 30.0 20.0 10.0 0

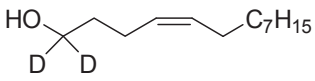
HO
D
D
C7H15

39

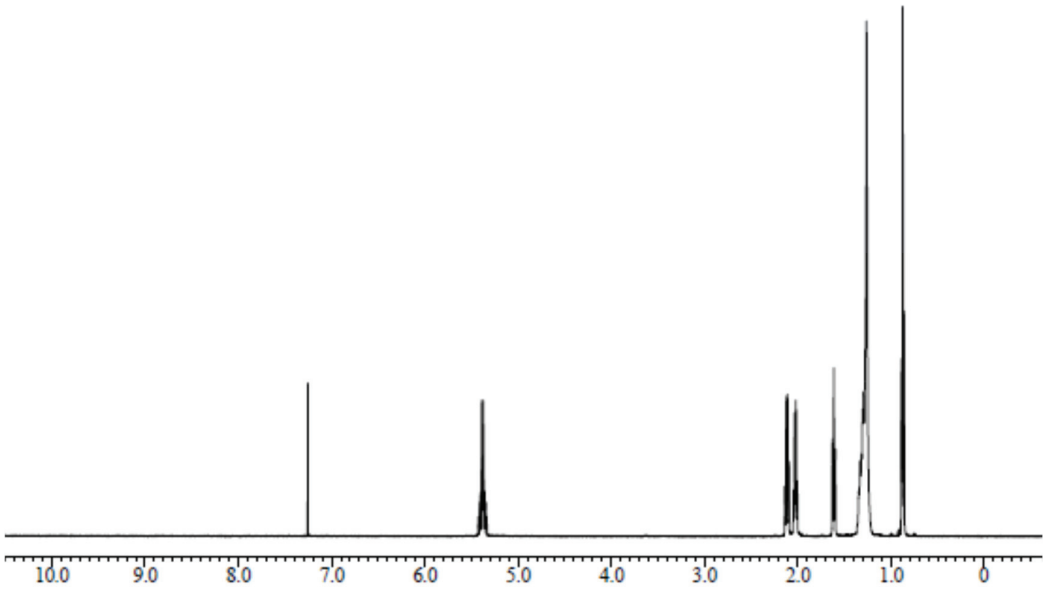
10.0
9.0
8.0
7.0
6.0
5.0
4.0
3.0
2.0
1.0
0

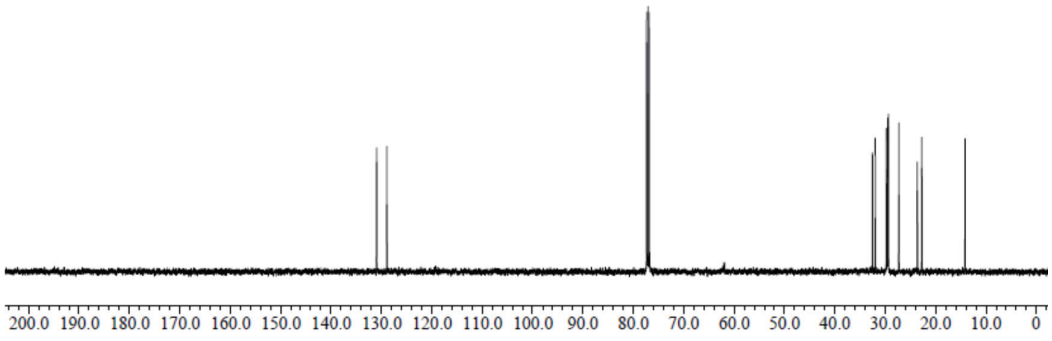
200.0 190.0 180.0 170.0 160.0 150.0 140.0 130.0 120.0 110.0 100.0 90.0 80.0 70.0 60.0 50.0 40.0 30.0 20.0 10.0 0

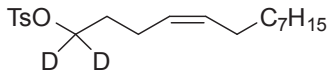
TsO
D
D
C7H15

40

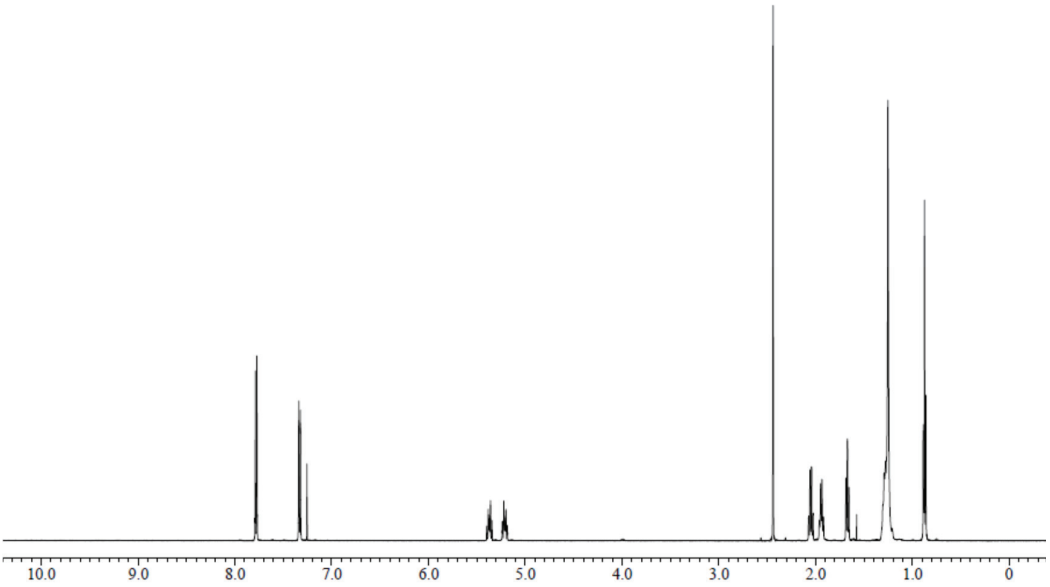
10.0
9.0
8.0
7.0
6.0
5.0
4.0
3.0
2.0
1.0
0

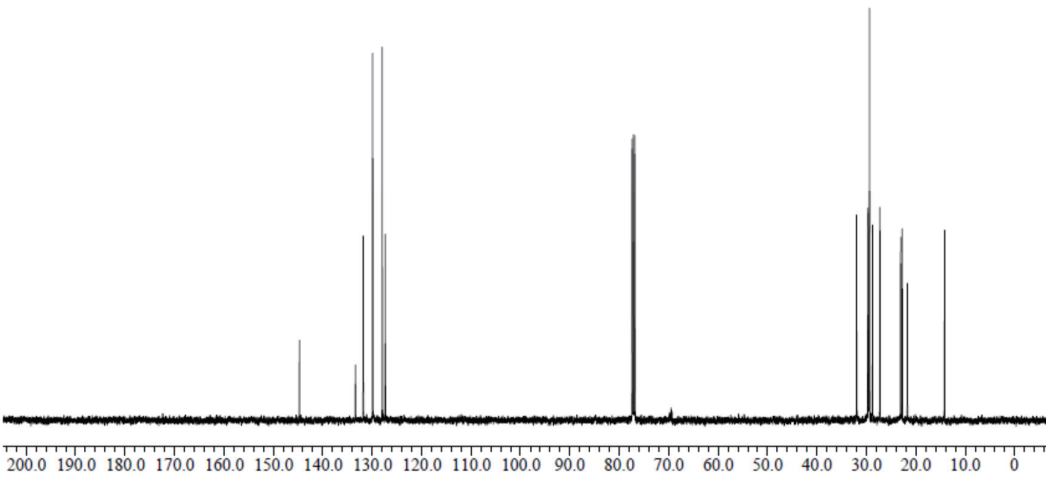
200.0 190.0 180.0 170.0 160.0 150.0 140.0 130.0 120.0 110.0 100.0 90.0 80.0 70.0 60.0 50.0 40.0 30.0 20.0 10.0 0

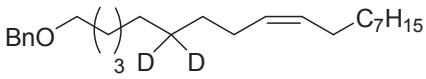
BnO
3
D
D
C7H15

41

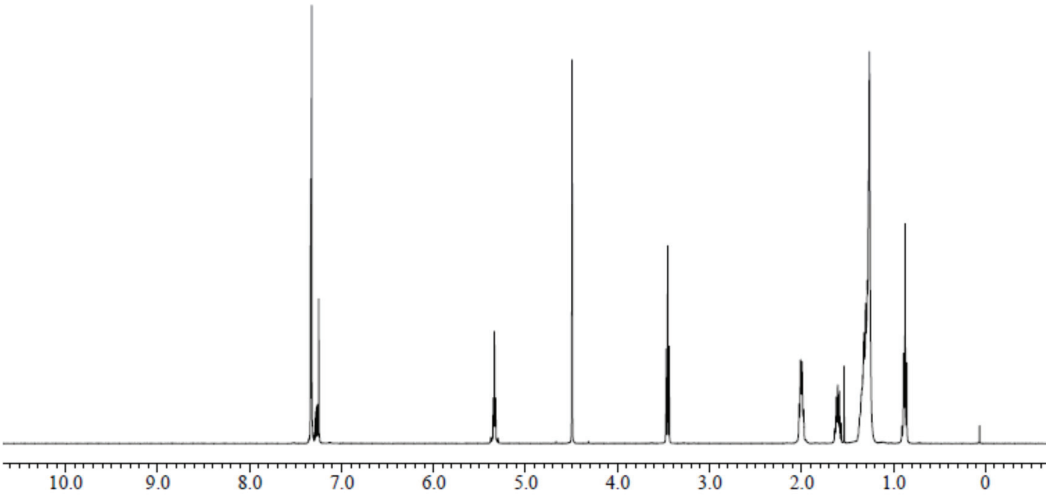
10.0
9.0
8.0
7.0
6.0
5.0
4.0
3.0
2.0
1.0
0

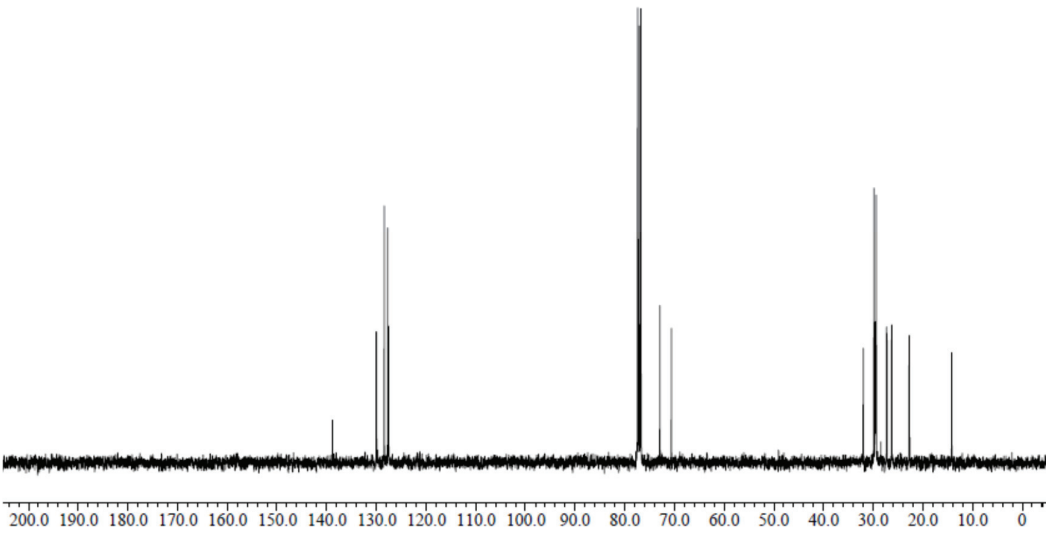
200.0 190.0 180.0 170.0 160.0 150.0 140.0 130.0 120.0 110.0 100.0 90.0 80.0 70.0 60.0 50.0 40.0 30.0 20.0 10.0 0

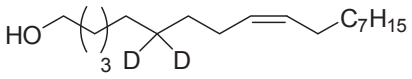
HO
3
D
D
C7H15

42

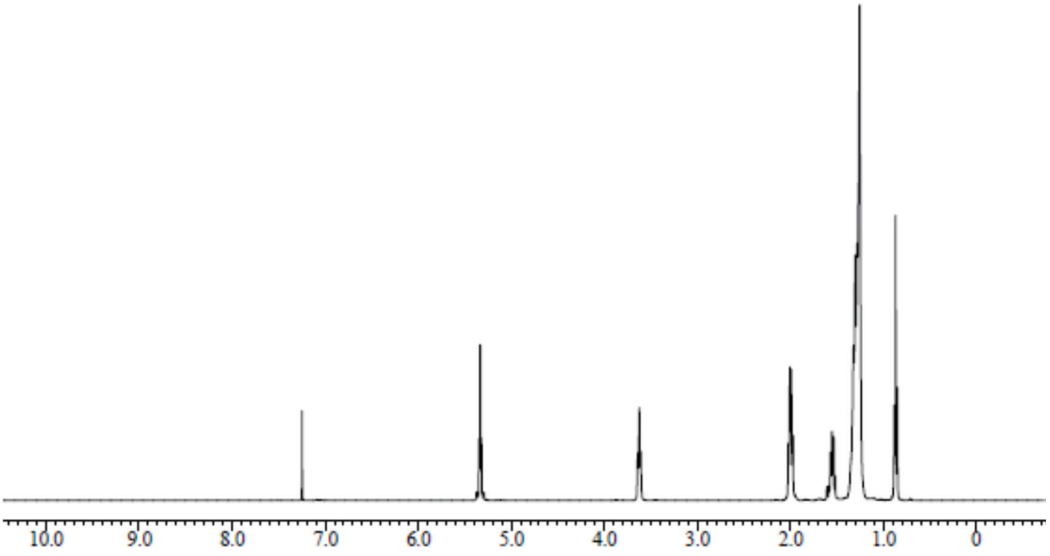
10.0
9.0
8.0
7.0
6.0
5.0
4.0
3.0
2.0
1.0
0

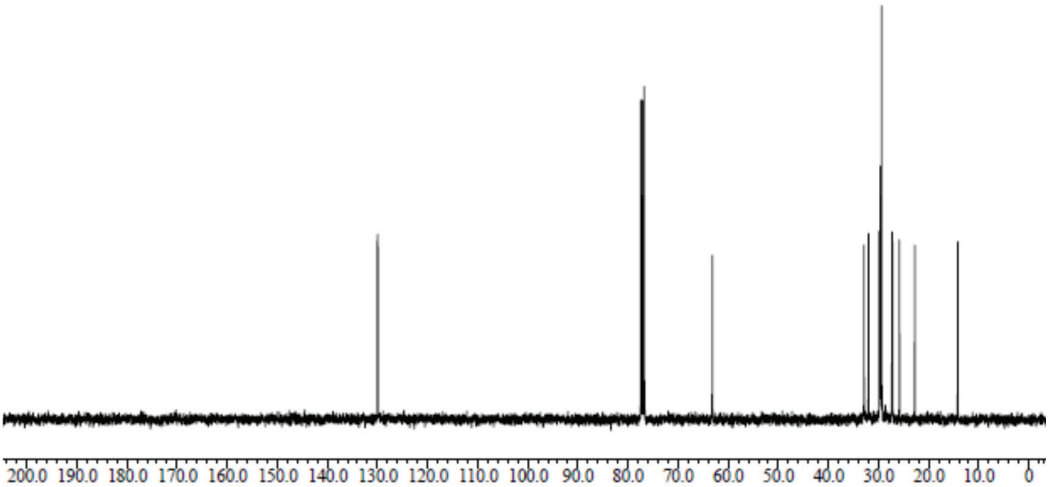
200.0 190.0 180.0 170.0 160.0 150.0 140.0 130.0 120.0 110.0 100.0 90.0 80.0 70.0 60.0 50.0 40.0 30.0 20.0 10.0 0

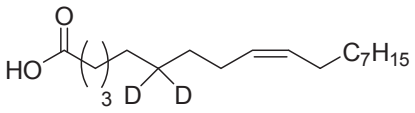
O
HO
3
D
D
C7H15

6

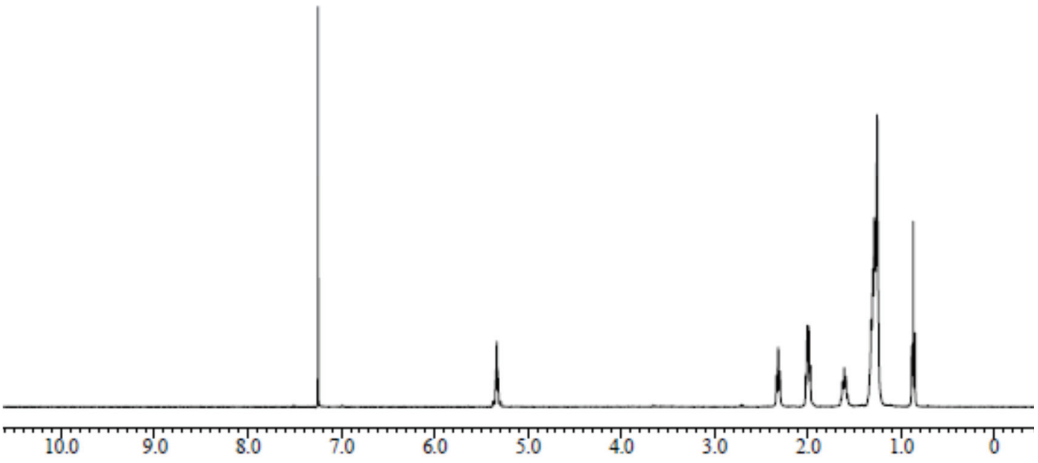
10.0
9.0
8.0
7.0
6.0
5.0
4.0
3.0
2.0
1.0
0

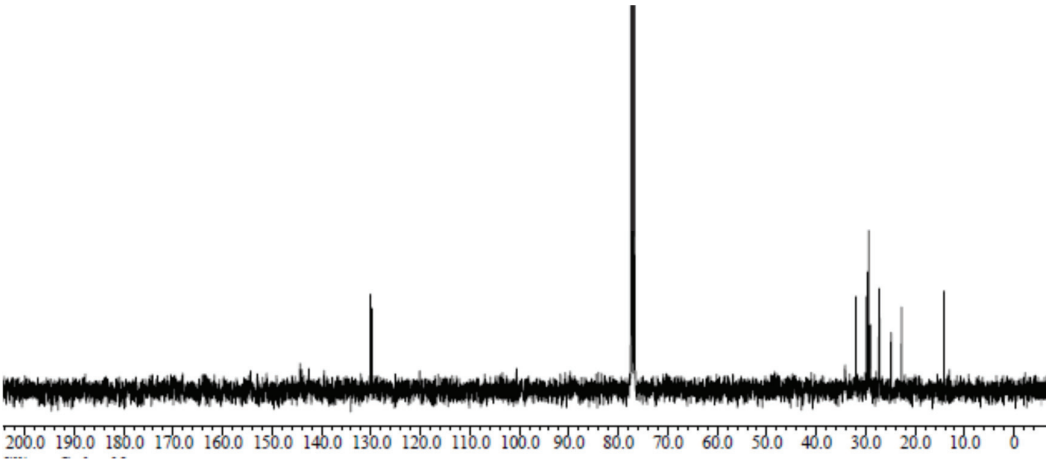
200.0 190.0 180.0 170.0 160.0 150.0 140.0 130.0 120.0 110.0 100.0 90.0 80.0 70.0 60.0 50.0 40.0 30.0 20.0 10.0 0

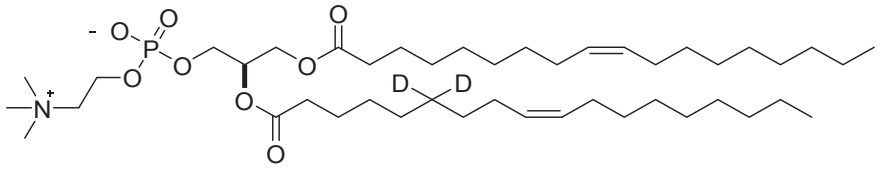
O
O
P
O
O
O
O
O
O
D
D
N+

7

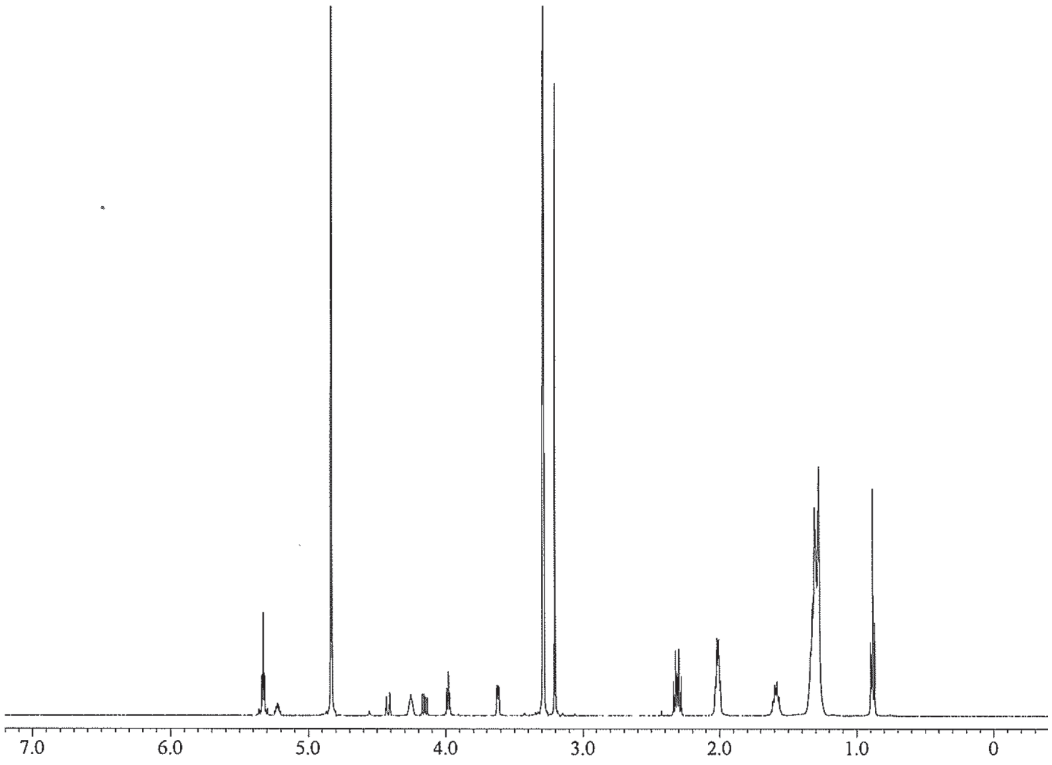
7.0
6.0
5.0
4.0
3.0
2.0
1.0
0

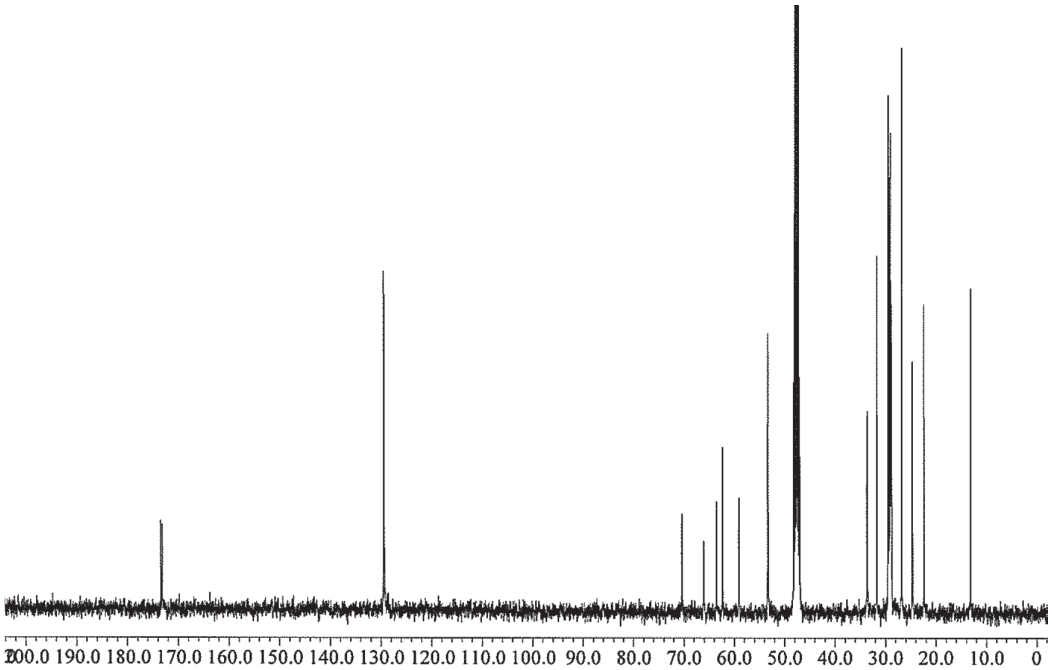
200.0 190.0 180.0 170.0 160.0 150.0 140.0 130.0 120.0 110.0 100.0 90.0 80.0 70.0 60.0 50.0 40.0 30.0 20.0 10.0 0

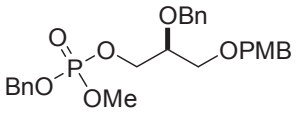
OBn
O
O
OPMB
P
BnO
OMe

59

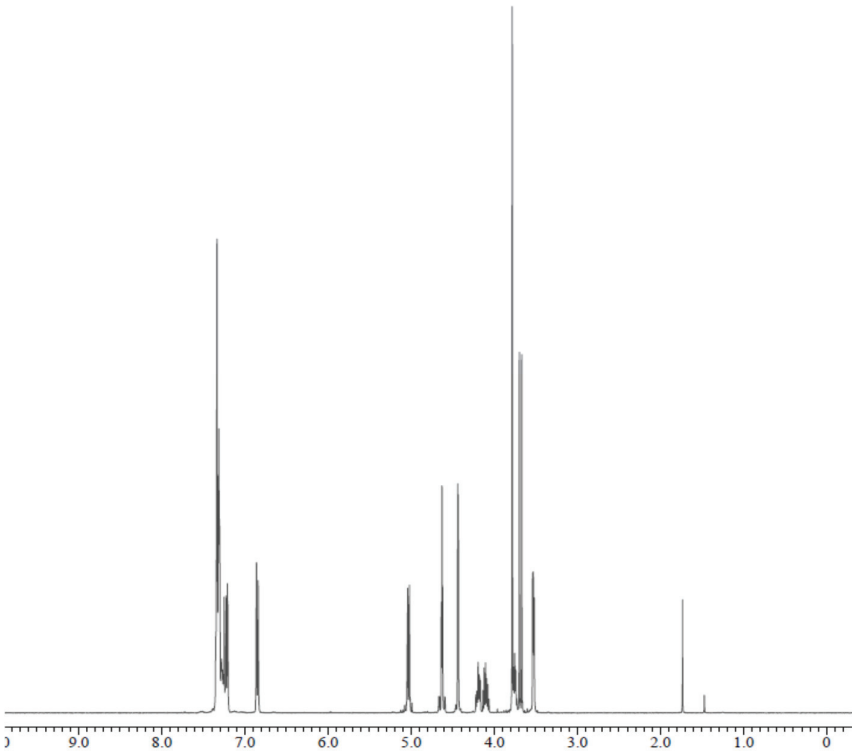
9.0
8.0
7.0
6.0
5.0
4.0
3.0
2.0
1.0
0

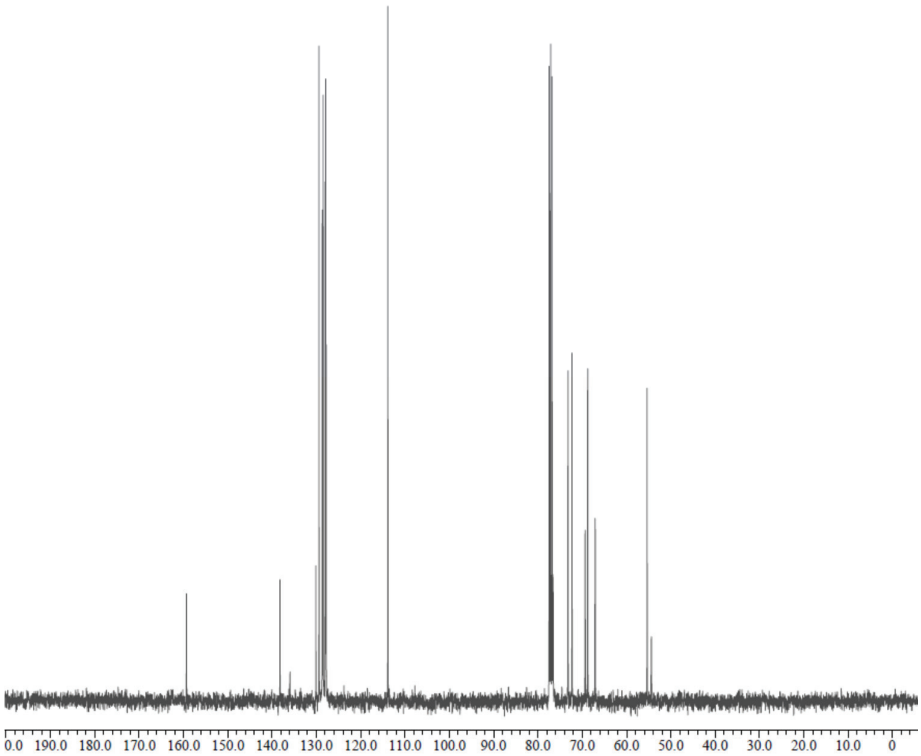
190.0
180.0
170.0
160.0
150.0
140.0
130.0
120.0
110.0
100.0
90.0
80.0
70.0
60.0
50.0
40.0
30.0
20.0
10.0
0

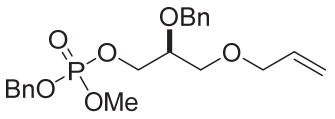
OBn
O
P
O
O
BnO
OMe

60

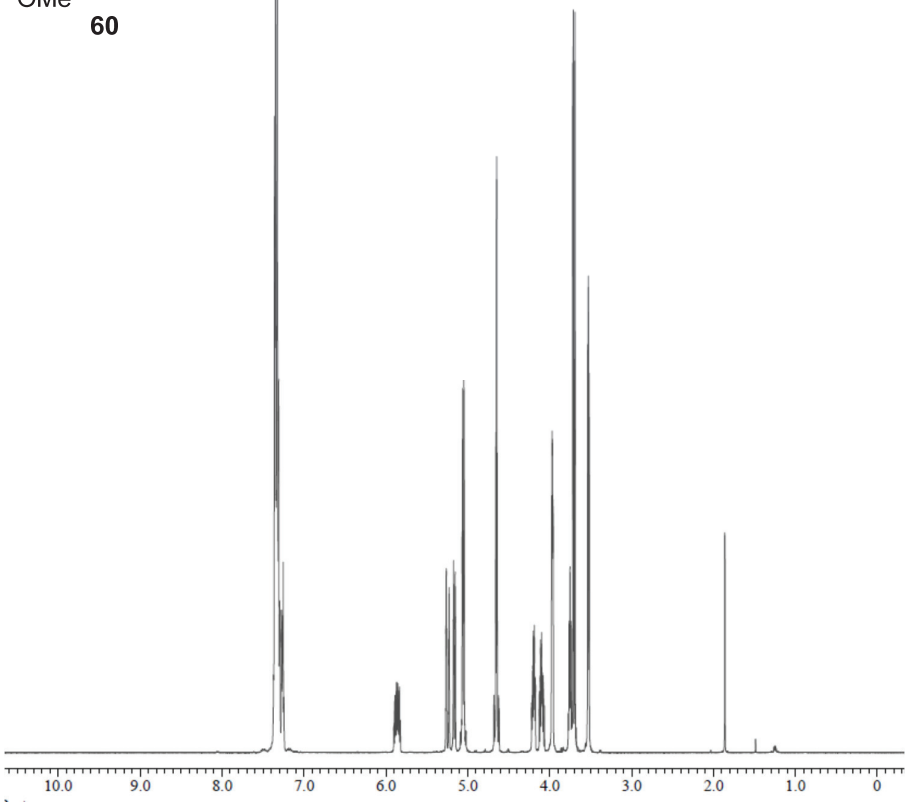
10.0
9.0
8.0
7.0
6.0
5.0
4.0
3.0
2.0
1.0
0

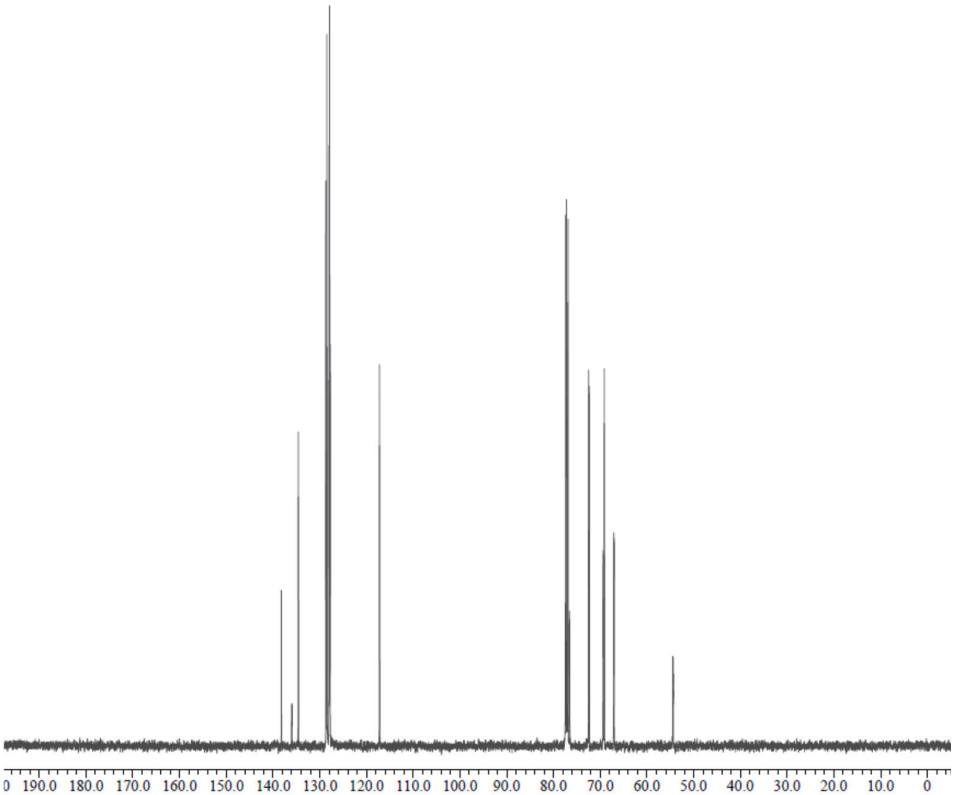
0
190.0
180.0
170.0
160.0
150.0
140.0
130.0
120.0
110.0
100.0
90.0
80.0
70.0
60.0
50.0
40.0
30.0
20.0
10.0
0

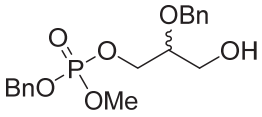
OBn
O
O
OH
P
BnO
OMe

45

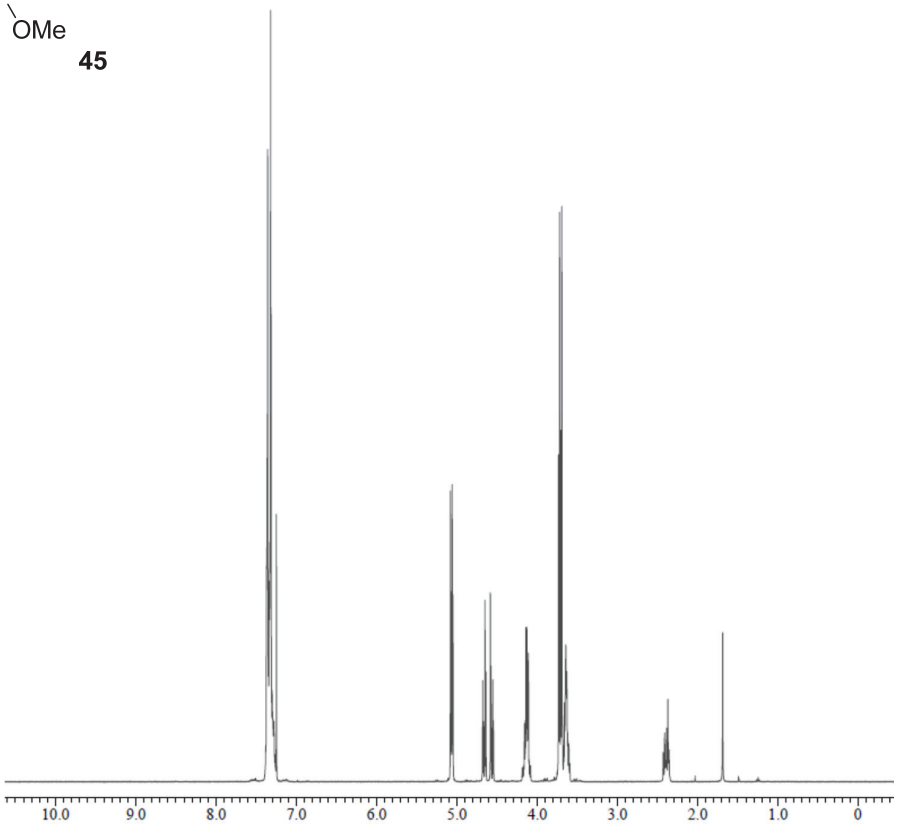
10.0
9.0
8.0
7.0
6.0
5.0
4.0
3.0
2.0
1.0
0

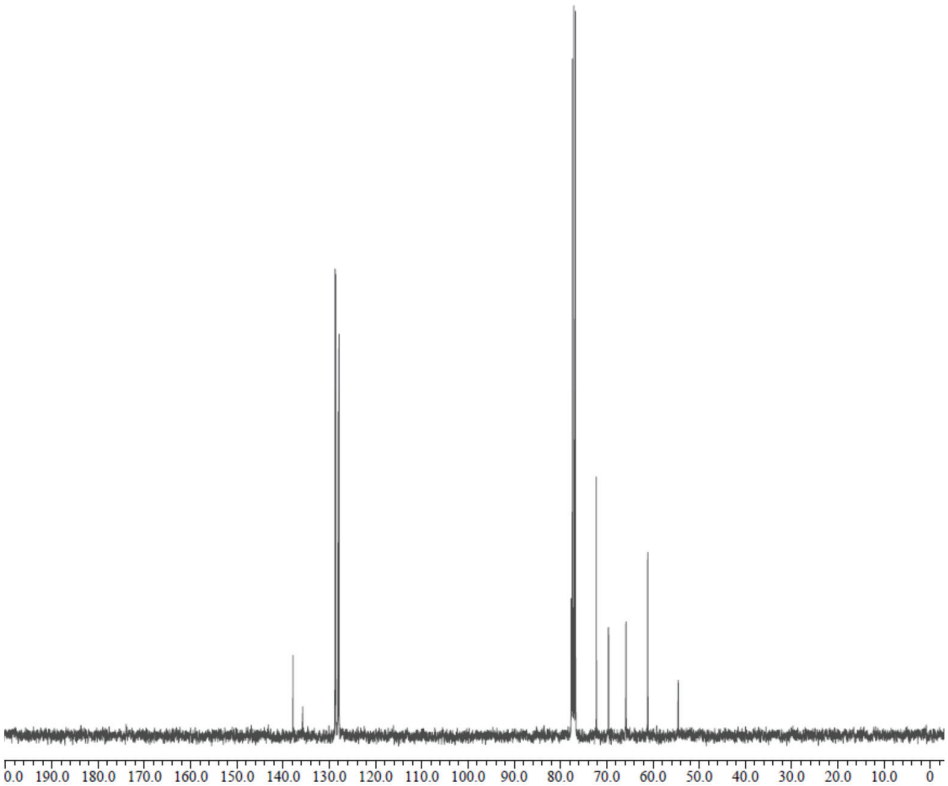
0.0
190.0
180.0
170.0
160.0
150.0
140.0
130.0
120.0
110.0
100.0
90.0
80.0
70.0
60.0
50.0
40.0
30.0
20.0
10.0
0

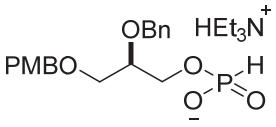
OBn
HEt3N+
PMBO
O
P
H
O
O−

62

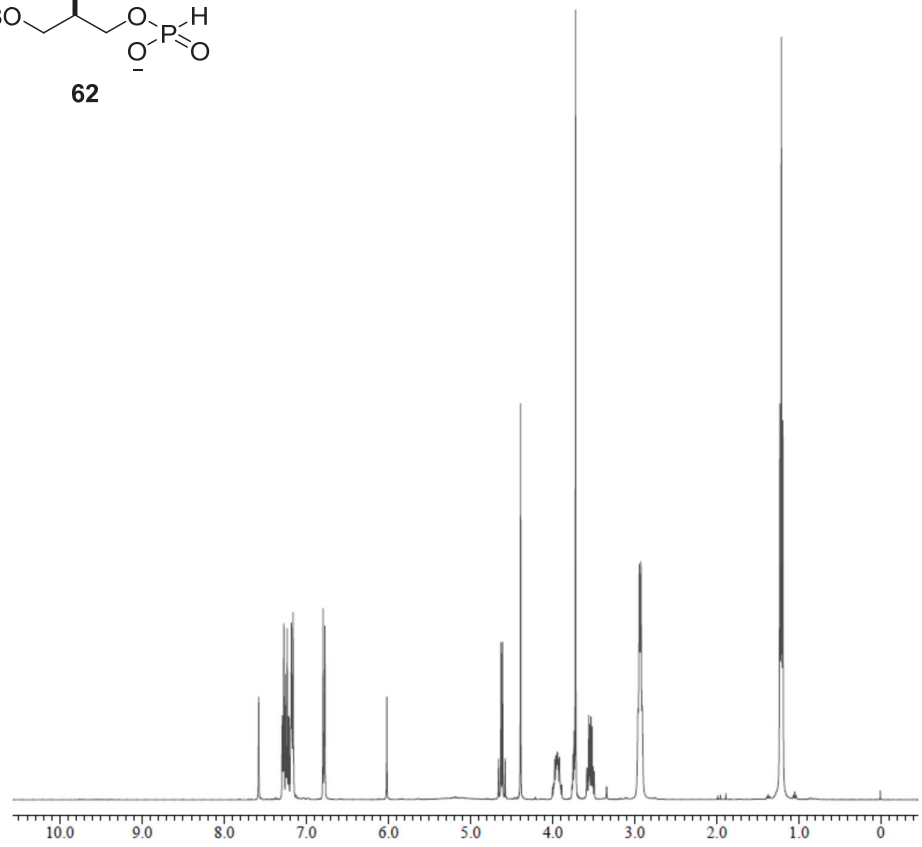
10.0
9.0
8.0
7.0
6.0
5.0
4.0
3.0
2.0
1.0
0

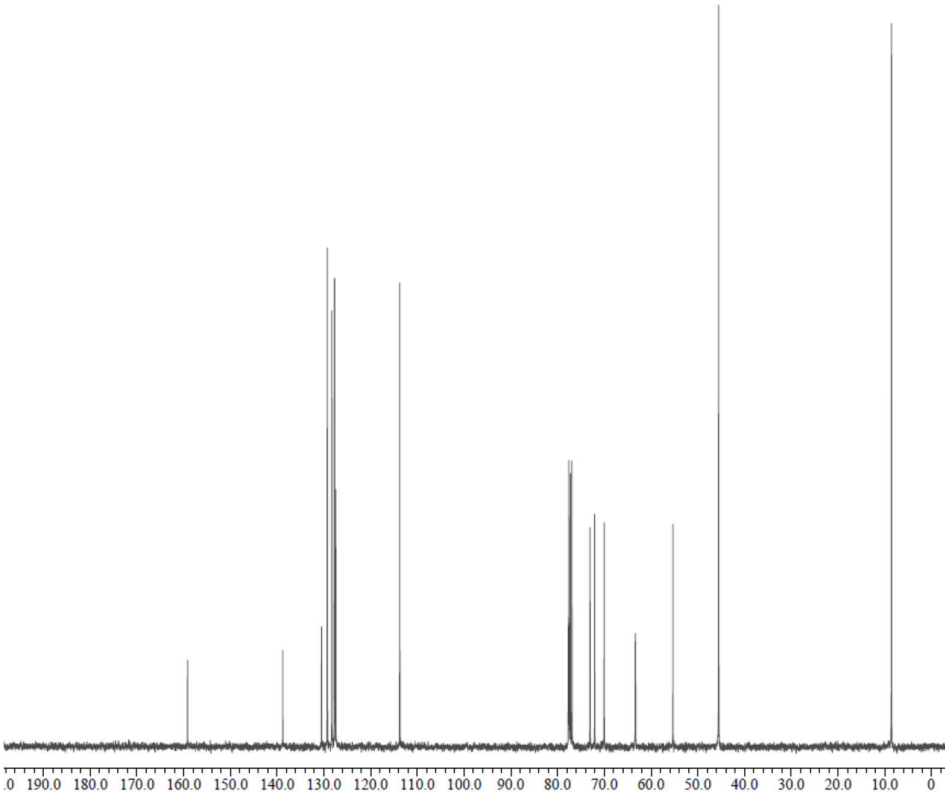
190.0
180.0
170.0
160.0
150.0
140.0
130.0
120.0
110.0
100.0
90.0
80.0
70.0
60.0
50.0
40.0
30.0
20.0
10.0
0

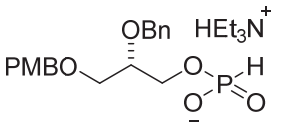

enantiomer of **62**

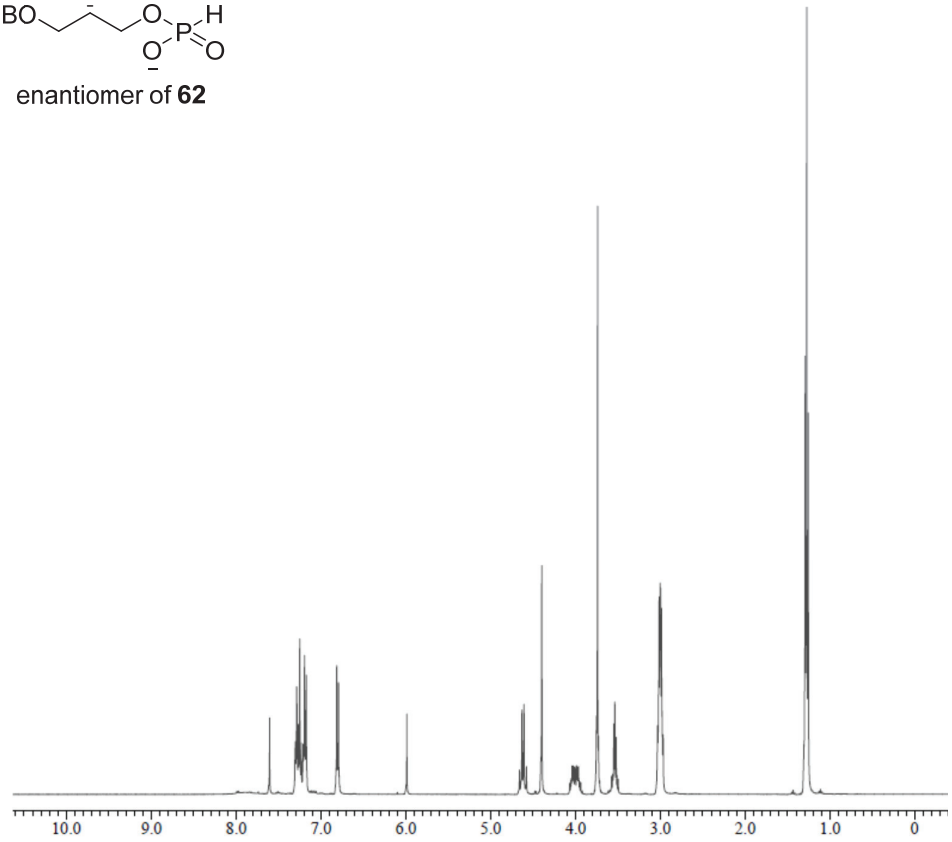

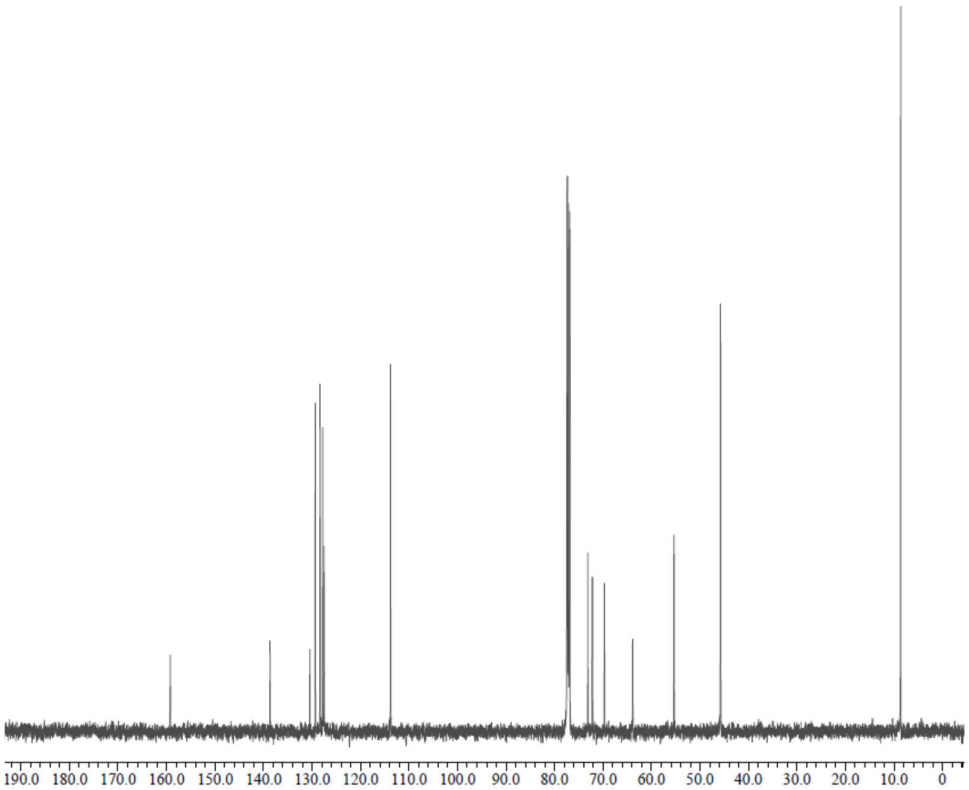

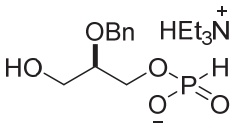
OBn
HEt3N+
HO
O
P
H
O
O-

47

10.0
9.0
8.0
7.0
6.0
5.0
4.0
3.0
2.0
1.0
0

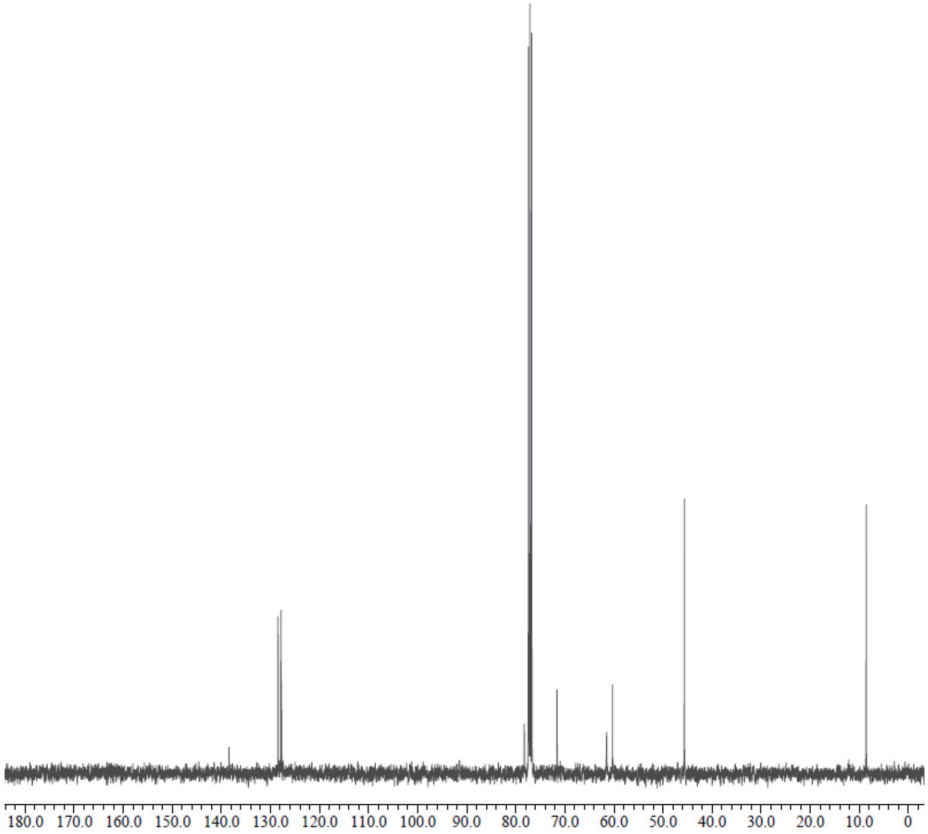
180.0
170.0
160.0
150.0
140.0
130.0
120.0
110.0
100.0
90.0
80.0
70.0
60.0
50.0
40.0
30.0
20.0
10.0
0

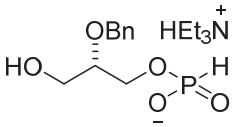

enantiomer of **47**

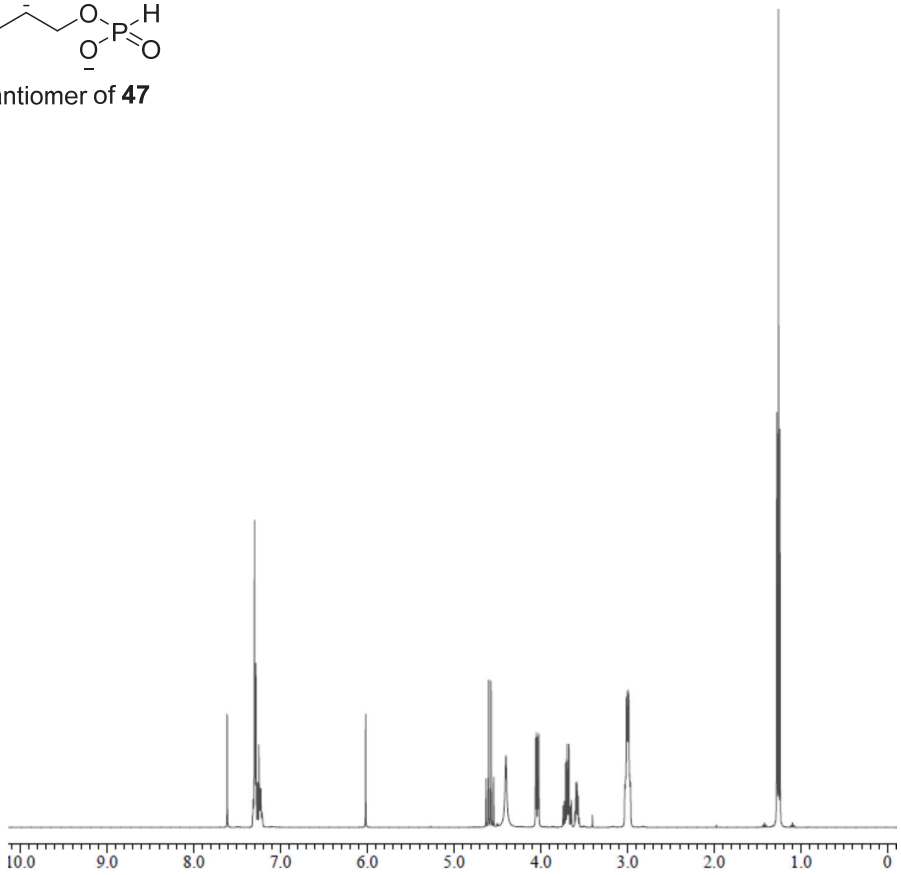

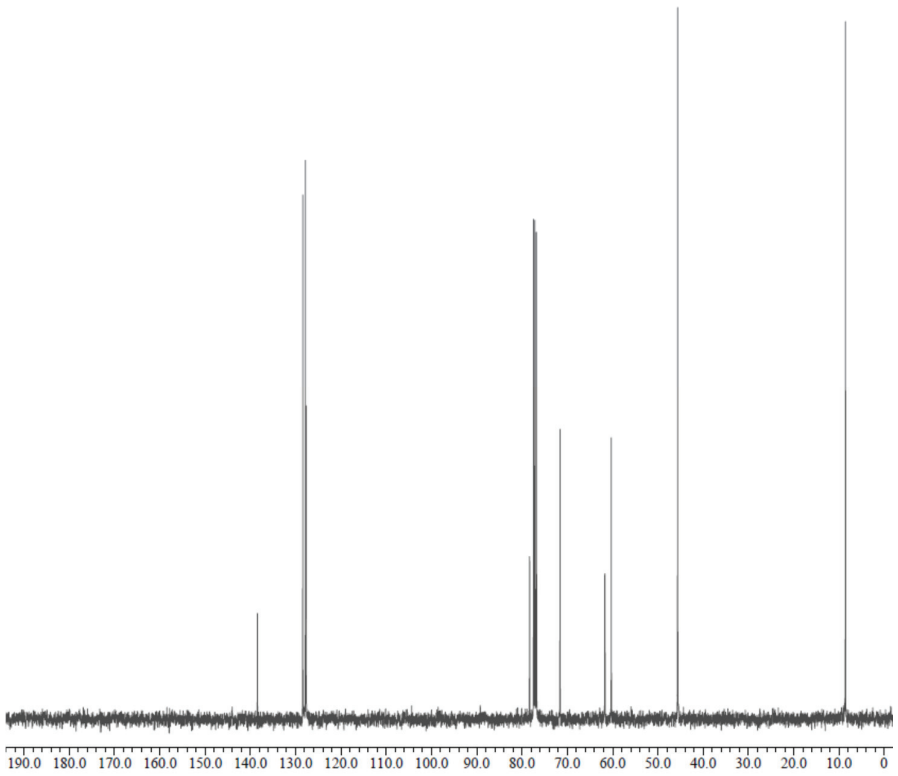

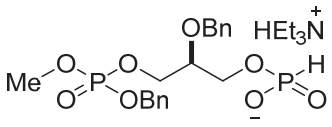
OBn
HEt3N
Me
O
P
O
OBn
O
P
H
O
O

43

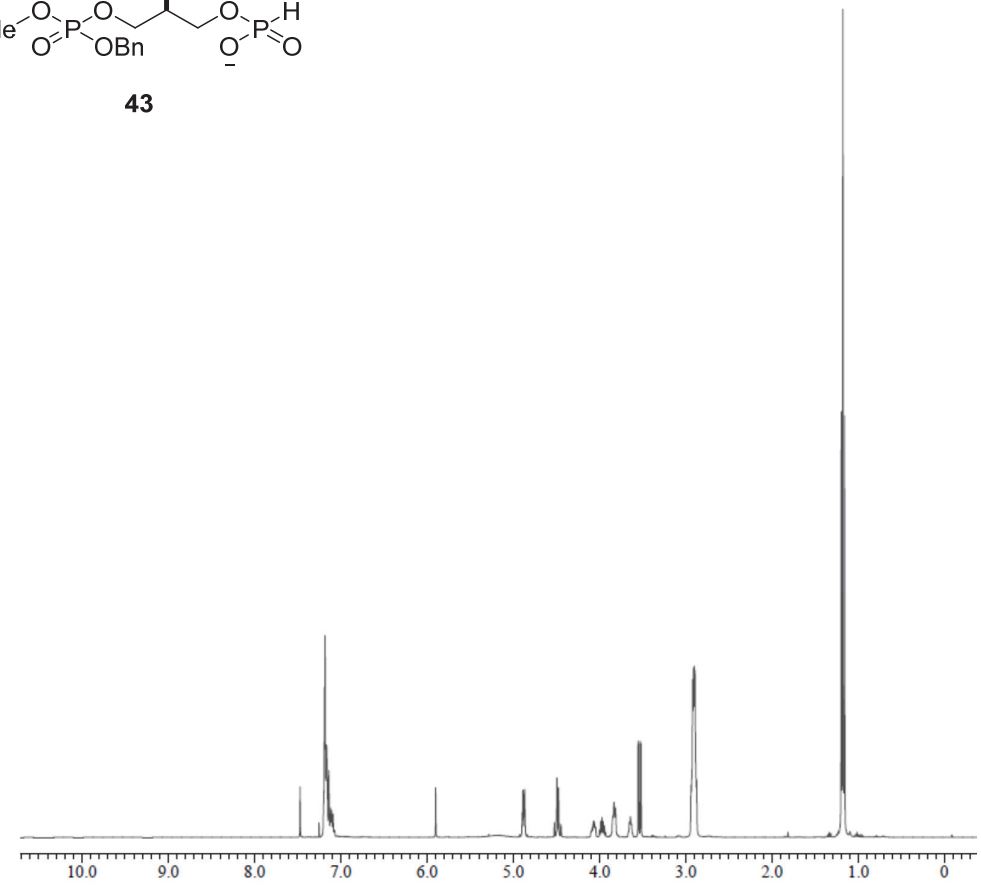
10.0
9.0
8.0
7.0
6.0
5.0
4.0
3.0
2.0
1.0
0

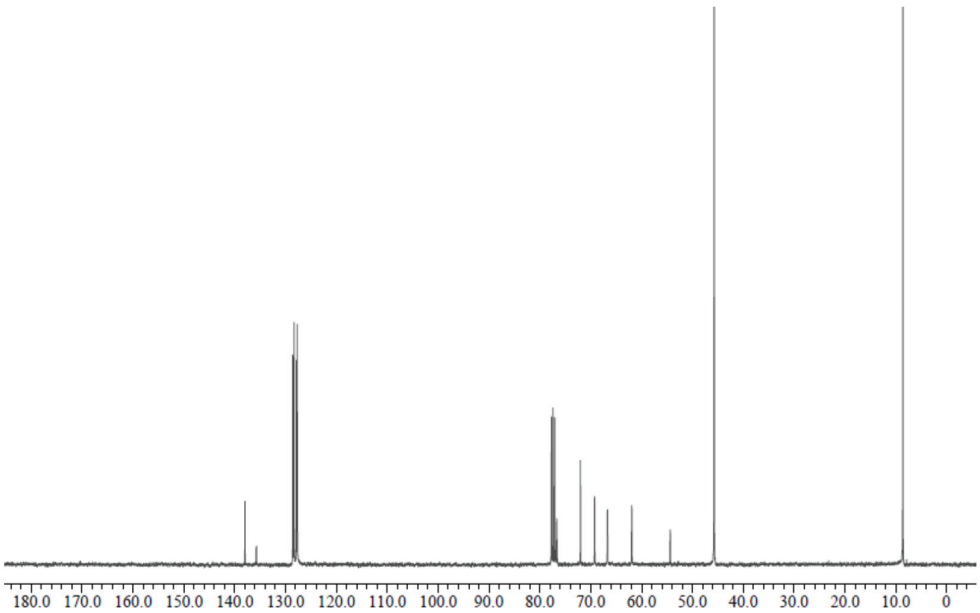
180.0
170.0
160.0
150.0
140.0
130.0
120.0
110.0
100.0
90.0
80.0
70.0
60.0
50.0
40.0
30.0
20.0
10.0
0

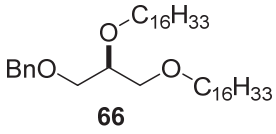
O
C16H33
BnO
O
C16H33

66

10.0
9.0
8.0
7.0
6.0
5.0
4.0
3.0
2.0
1.0
0

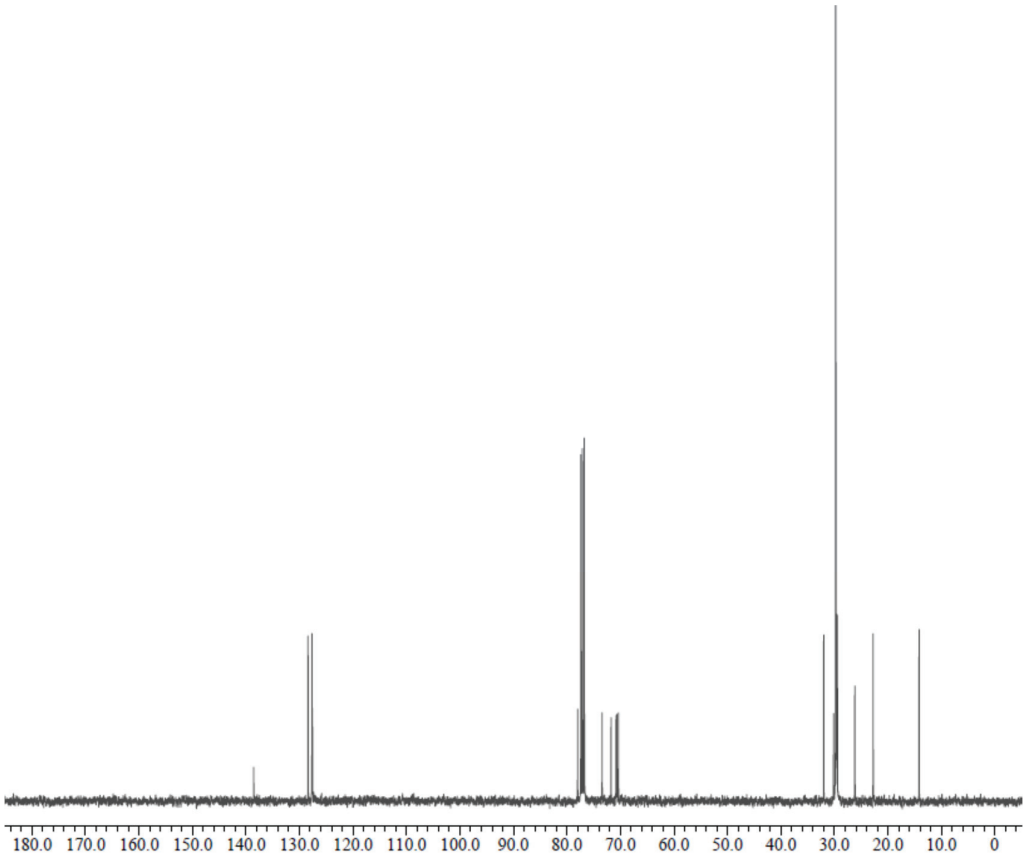
180.0
170.0
160.0
150.0
140.0
130.0
120.0
110.0
100.0
90.0
80.0
70.0
60.0
50.0
40.0
30.0
20.0
10.0
0

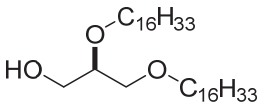
O
$C_{16}H_{33}$
HO
O
$C_{16}H_{33}$

44

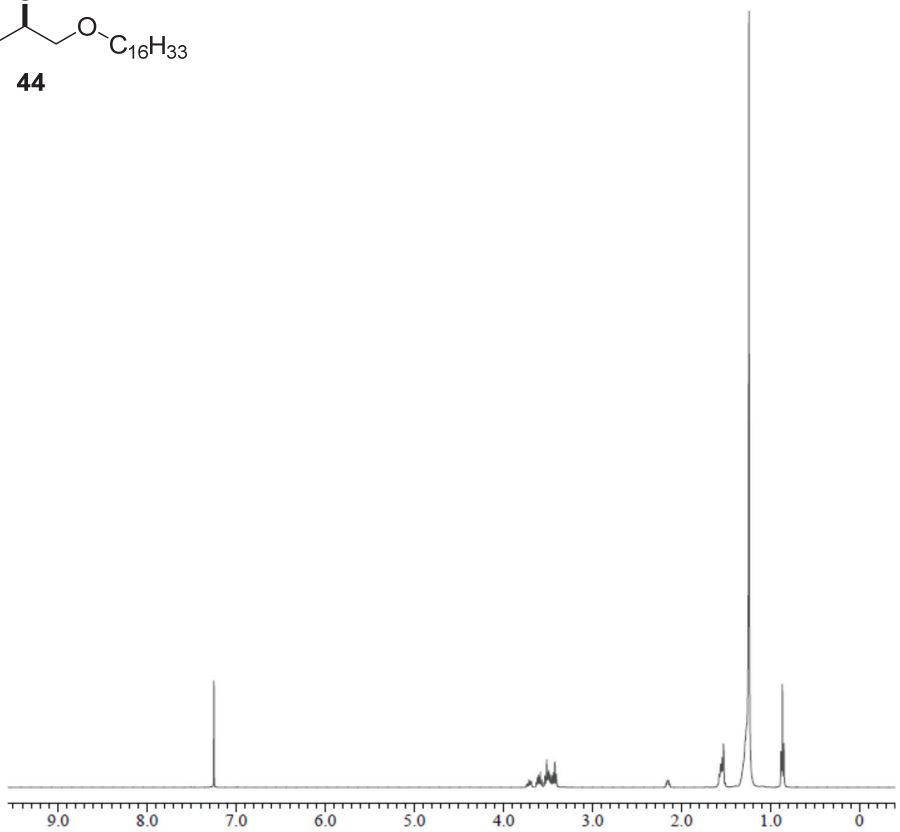
9.0
8.0
7.0
6.0
5.0
4.0
3.0
2.0
1.0
0

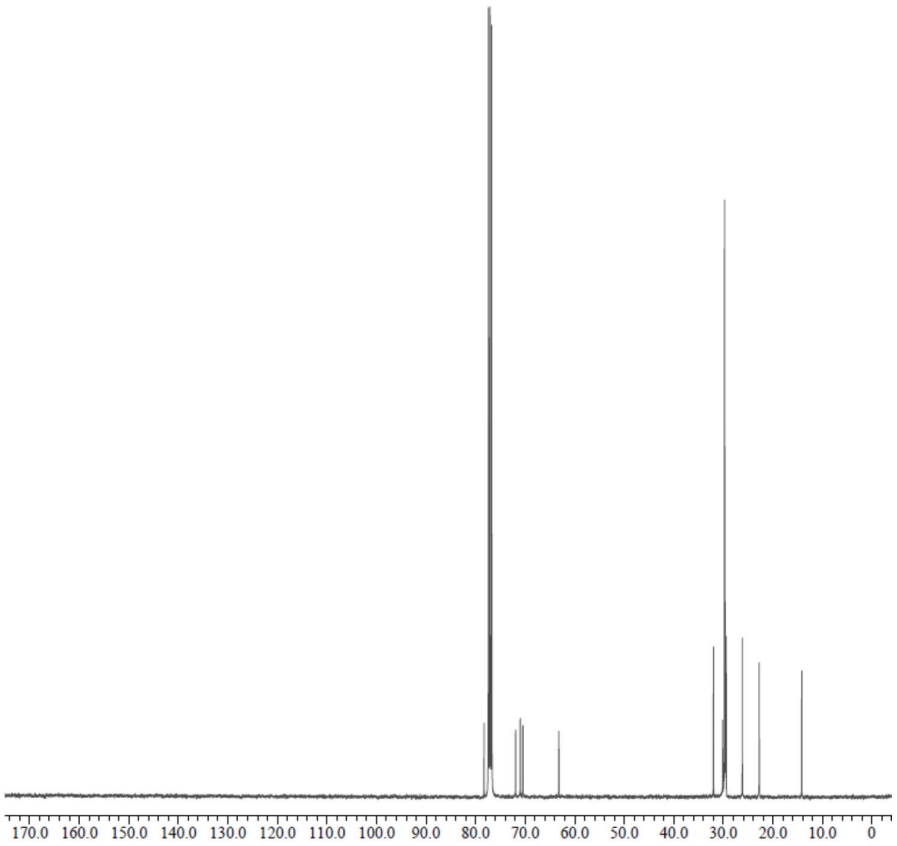
170.0
160.0
150.0
140.0
130.0
120.0
110.0
100.0
90.0
80.0
70.0
60.0
50.0
40.0
30.0
20.0
10.0
0

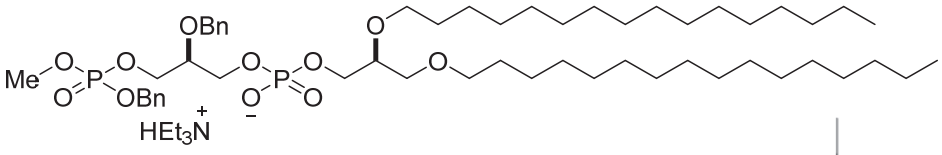
OBn
O
Me
O
P
O
O
OBn
O
O
P
O
O
O
HEt3N
+
−

67

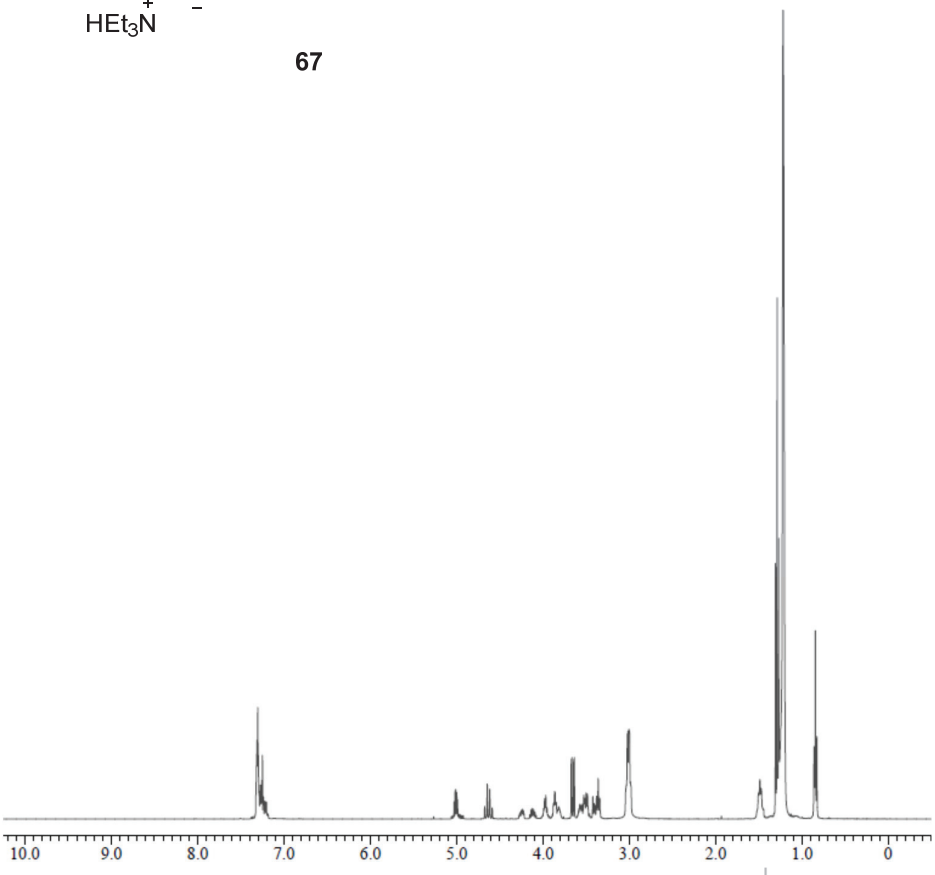
10.0
9.0
8.0
7.0
6.0
5.0
4.0
3.0
2.0
1.0
0

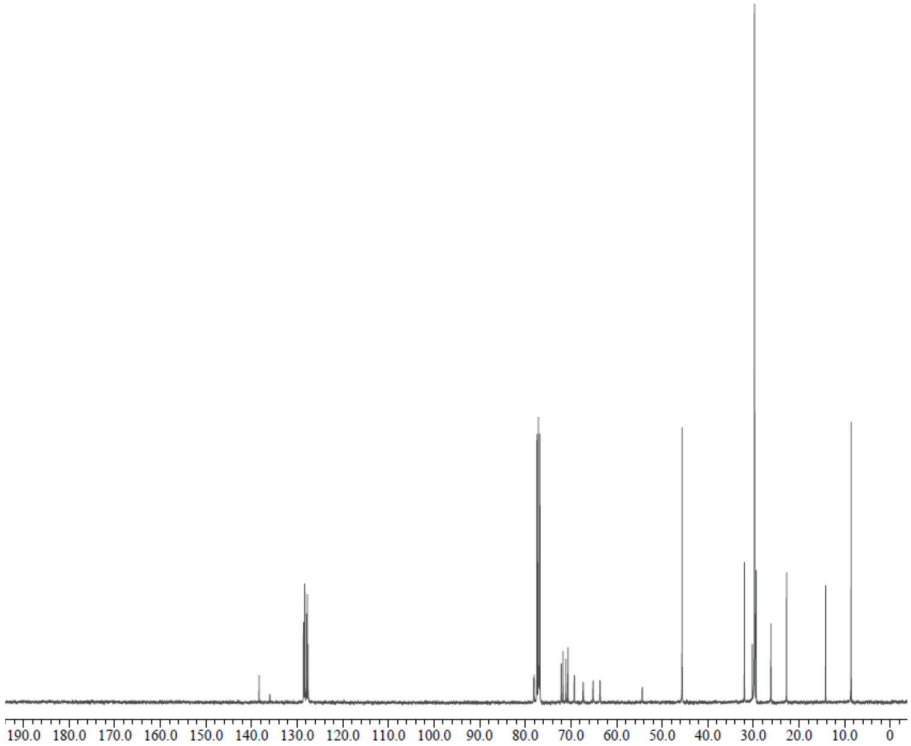
190.0
180.0
170.0
160.0
150.0
140.0
130.0
120.0
110.0
100.0
90.0
80.0
70.0
60.0
50.0
40.0
30.0
20.0
10.0
0

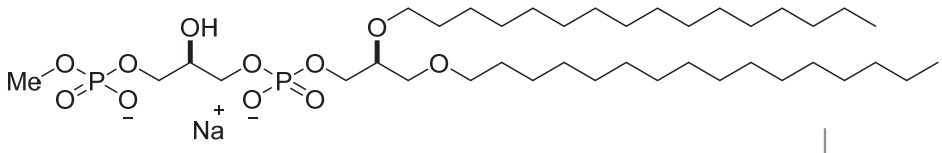
OH
O
Me
O
P
O
O
O
O
P
O
O
O
O
Na
+
−
−

8

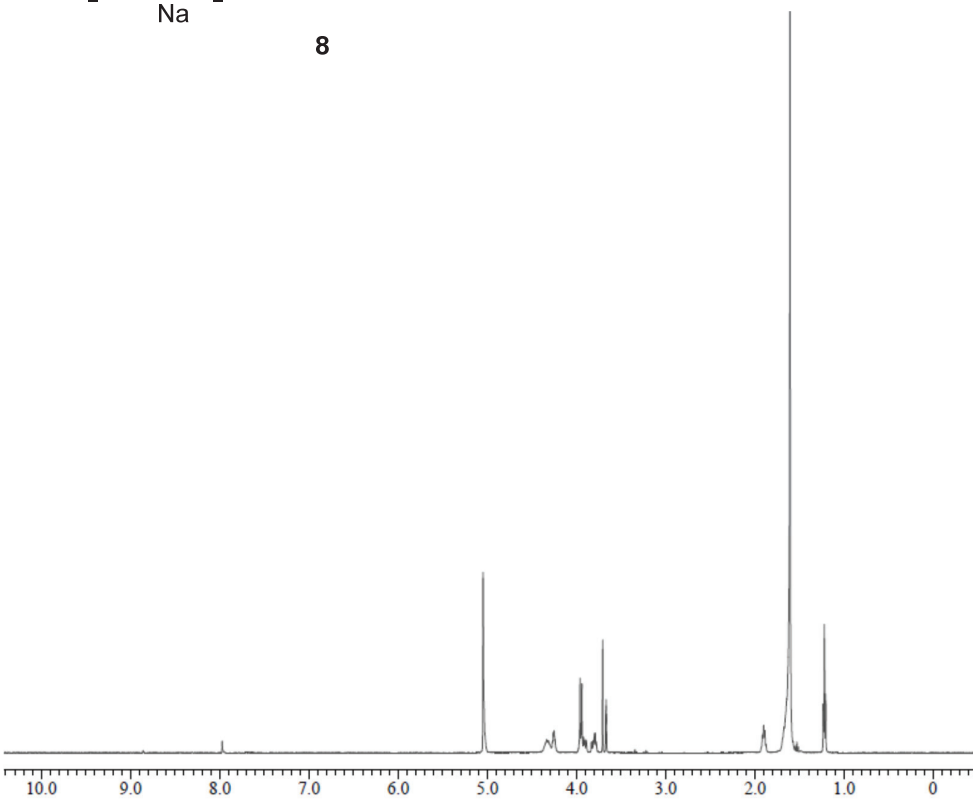
10.0
9.0
8.0
7.0
6.0
5.0
4.0
3.0
2.0
1.0
0

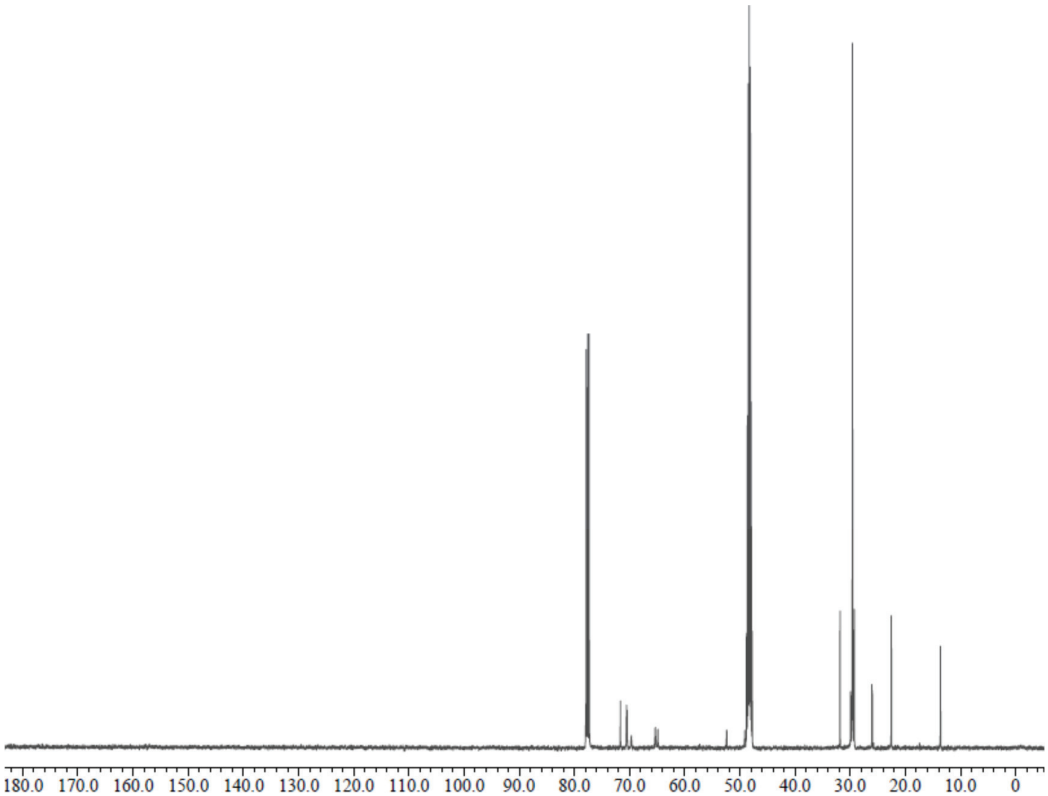
180.0
170.0
160.0
150.0
140.0
130.0
120.0
110.0
100.0
90.0
80.0
70.0
60.0
50.0
40.0
30.0
20.0
10.0
0

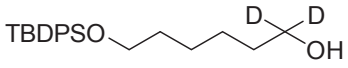
TBDPSO
D
D
OH

70

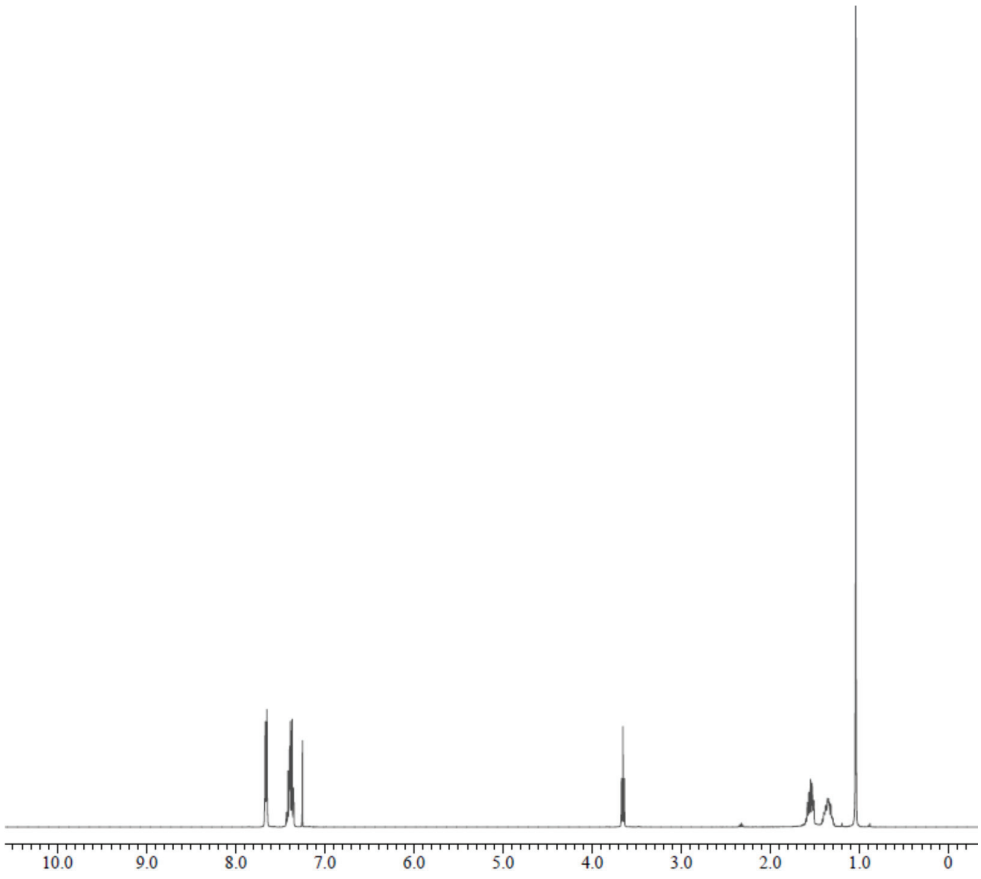
10.0
9.0
8.0
7.0
6.0
5.0
4.0
3.0
2.0
1.0
0

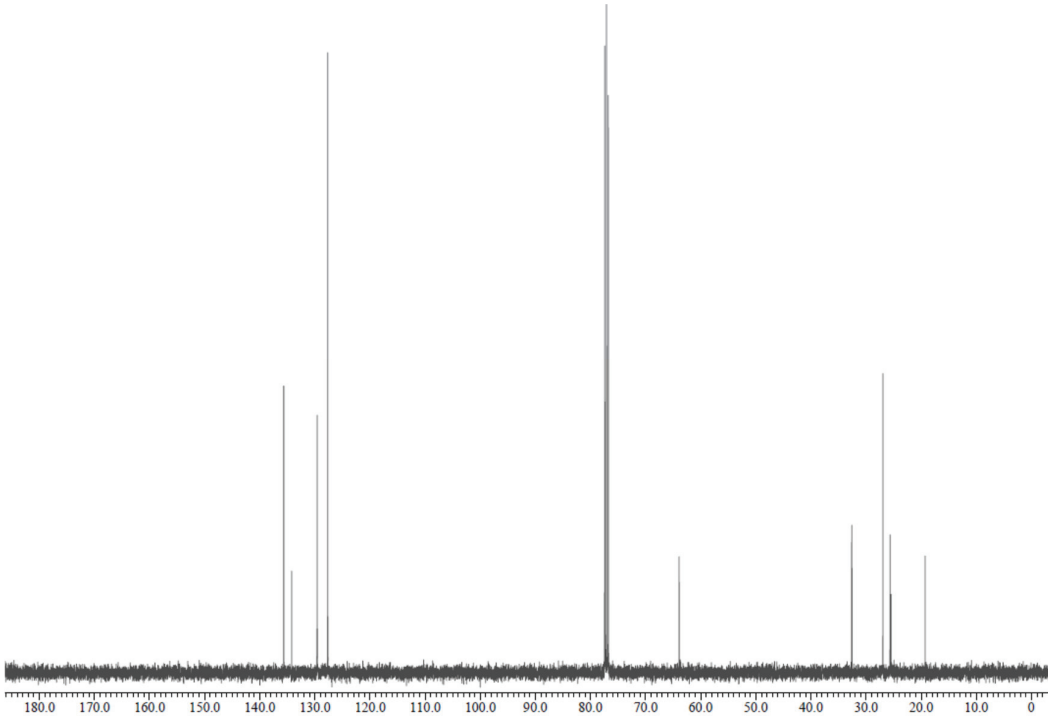
180.0
170.0
160.0
150.0
140.0
130.0
120.0
110.0
100.0
90.0
80.0
70.0
60.0
50.0
40.0
30.0
20.0
10.0
0

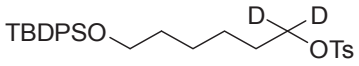
TBDPSO
D
D
OTs

71

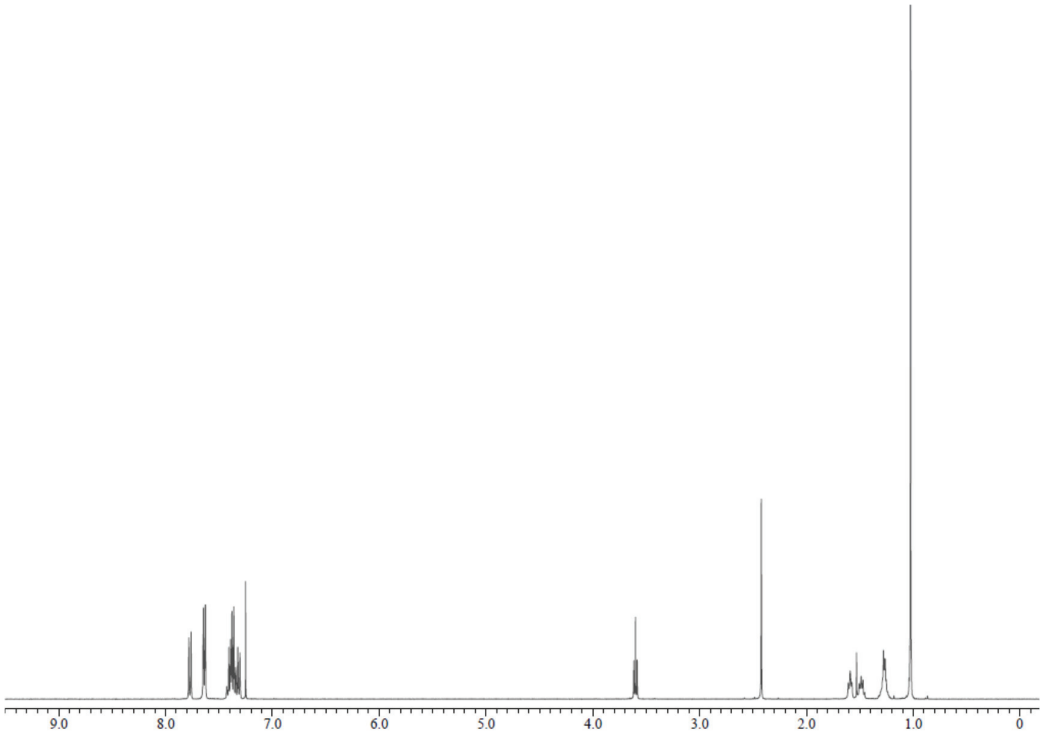
9.0
8.0
7.0
6.0
5.0
4.0
3.0
2.0
1.0
0

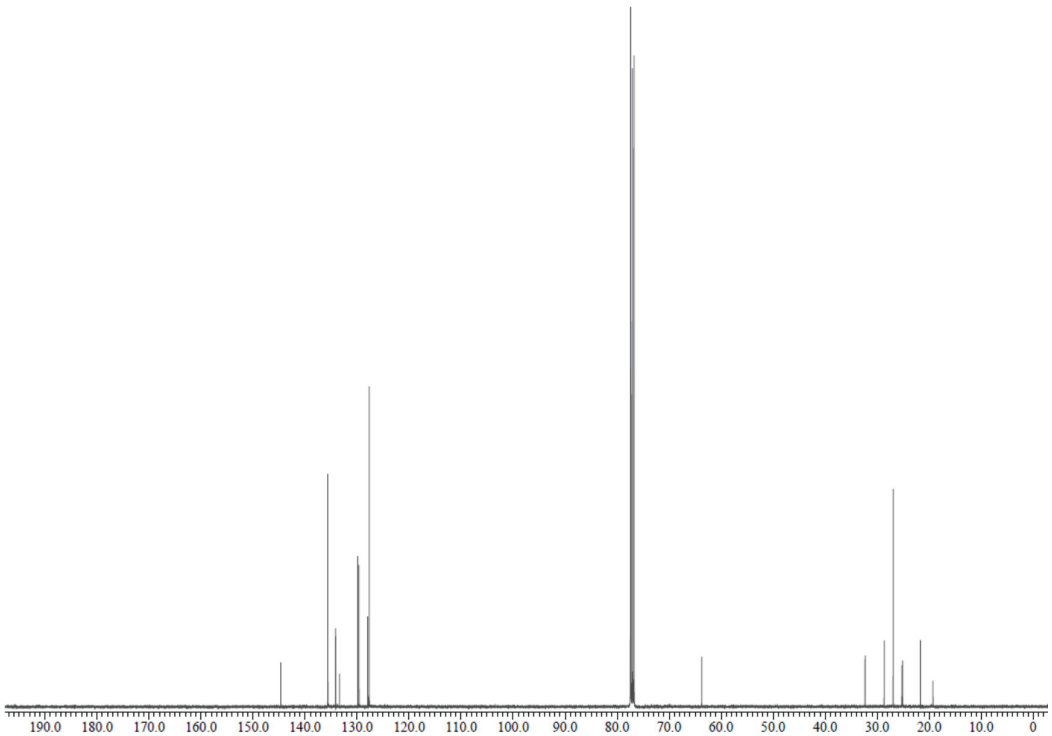
190.0
180.0
170.0
160.0
150.0
140.0
130.0
120.0
110.0
100.0
90.0
80.0
70.0
60.0
50.0
40.0
30.0
20.0
10.0
0

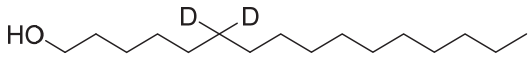
HO
D
D

73

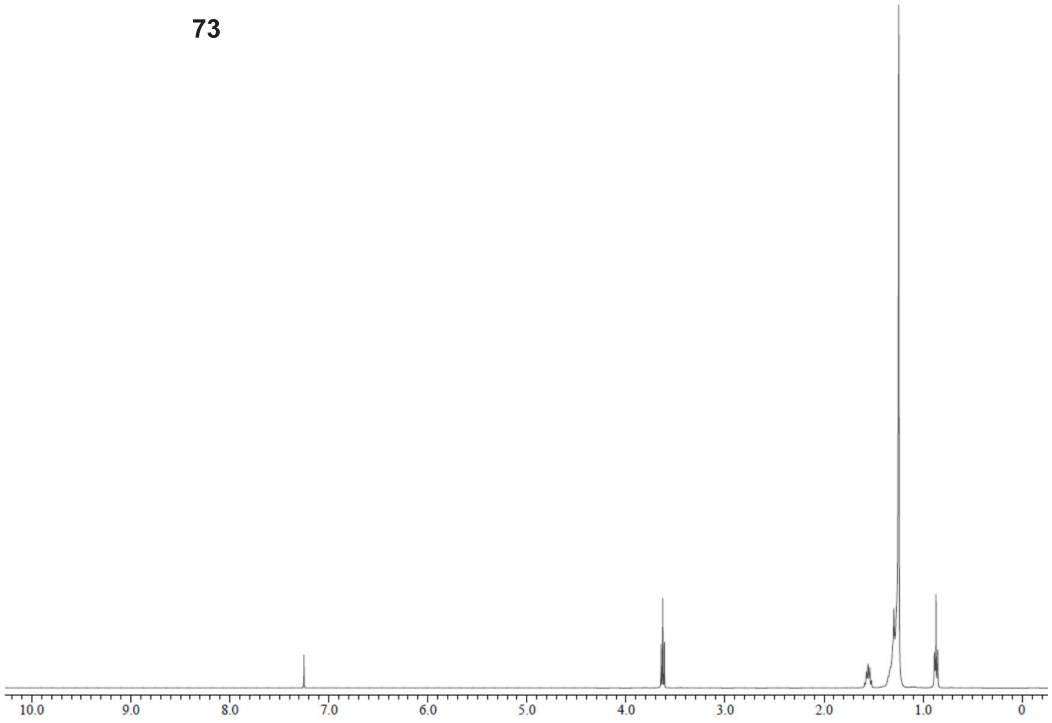
10.0
9.0
8.0
7.0
6.0
5.0
4.0
3.0
2.0
1.0
0

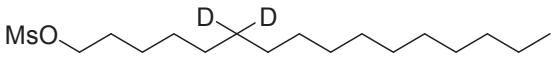
MsO
D
D

74

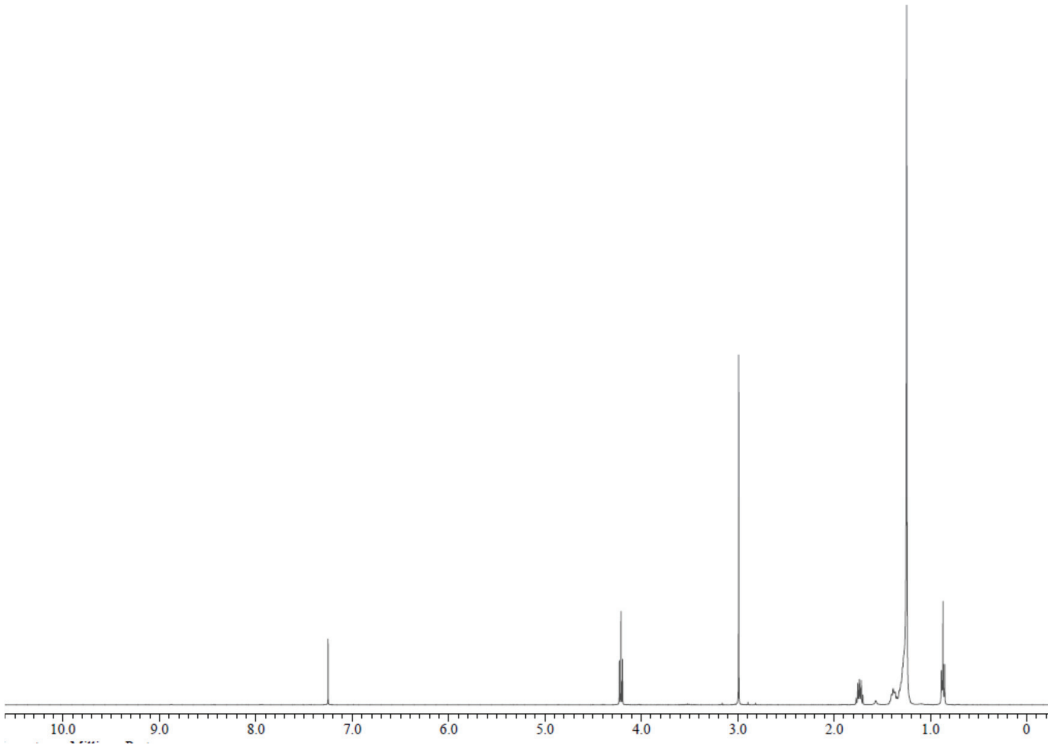
10.0
9.0
8.0
7.0
6.0
5.0
4.0
3.0
2.0
1.0
0

Publications

1. Phosphatidylcholine Bearing 6,6-Dideuterated Oleic Acid: A Useful Solid-State ^{2}H NMR Probe for Investigating Membrane Properties. Cui J.; Lethu S.; Yasuda T.; Matsuoka S.; Matsumori N.; Sato F.; Murata M. *Bioorg. Med. Chem. Lett.* **2015**, 25, 203-206.
2. Sphingomyelin Distribution in Lipid Rafts of Artificial Monolayer Membranes Visualized by Raman Microscopy. Ando, J.; Kinoshita, M.; Cui, J.; Yamakoshi, H.; Dodo, K.; Fujita, K.; Murata, M.; Sodeoka, M. **2015** (submitted)
3. Raman-Tagged Sphingomyelin that Closely Mimics Original Raft-Forming Behavior. Cui, J.; Ando, J.; Kinoshita, M.; Sato F.; Sodeoka, M.; Murata, M. (to be submitted)